Synthesis and characterization of chitosan oligomers for biomedical applications

Amani Moussa

N°d'ordre NNT : 2019LYSE1120

THESE de DOCTORAT DE L'UNIVERSITE DE LYON

Opérée au sein de

L'Université Claude Bernard Lyon 1

ED34 : Ecole Doctorale Matériaux de Lyon

Spécialité de doctorat :

Discipline : Chimie et physico-chimie des polymères

Soutenue à huis clos le 09/09/2019, par :

Amani MOUSSA

Synthèse et caractérisation d'oligomères de chitosane pour applications biomédicales

---

Synthesis and characterization of chitosan oligomers for biomedical applications

Devant le jury composé de :

M. Ghislain DAVID, Maitre de confèrences, ENSCM, Montpellier	Rapporteur
Mme Jessica KWOK, University Academic Fellow, University of Leeds, Leeds	Rapporteure
M. Didier PIN, Professeur, Vetagro Sup, Lyon	Examinateur
M. Thierry DELAIR, Professeur, UCBL, Lyon	Examinateur
Mme Caroline PROUILLAC, Maitre de conférences, Vetagro Sup, Lyon	Examinatrice
Mme Isabelle ROYAUD, Professeure, IJL, Nancy	Examinatrice
M. Laurent DAVID, Professeur, UCBL, Lyon	Directeur de thèse
M. Stéphane TROMBOTTO, Maitre de confèrences, UCBL, Lyon	Co-Directeur de thèse
Mme Paula NUNES DE OLIVEIRA, Chercheur, UCBL, Lyon	Inviteé

Université Claude Bernard – LYON 1

Président de l'Université	M. Frédéric FLEURY
Président du Conseil Académique	M. Hamda BEN HADID
Vice-Président du Conseil d'Administration	M. Didier REVEL
Vice-Président du Conseil des Etudes et de la Vie Universitaire	M. Philippe CHEVALLIER
Vice-Président de la Commission de Recherche	
Directeur Général des Services	M. Damien VERHAEGHE

COMPOSANTES SANTE

Faculté de Médecine Lyon-Est – Claude Bernard	Doyen : M. Gilles RODE
Faculté de Médecine et Maïeutique Lyon Sud Charles. Mérieux	Doyenne : Mme Carole BURILLON
UFR d'Odontologie	Doyenne : Mme Dominique SEUX
Institut des Sciences Pharmaceutiques et Biologiques	Directrice : Mme Christine VINCIGUERRA
Institut des Sciences et Techniques de la Réadaptation	Directeur : M. Xavier PERROT
Département de Formation et Centre de Recherche en Biologie Humaine	Directrice : Mme Anne-Marie SCHOTT

COMPOSANTES & DEPARTEMENTS DE SCIENCES & TECHNOLOGIE

UFR Biosciences	Directrice : Mme Kathrin GIESELER
Département Génie Electrique et des Procédés (GEP)	Directrice : Mme Rosaria FERRIGNO
Département Informatique	Directeur : M. Behzad SHARIAT
Département Mécanique	Directeur M. Marc BUFFAT
UFR - Faculté des Sciences	Administrateur provisoire : M. Bruno ANDRIOLETTI
UFR (STAPS)	Directeur : M. Yannick VANPOULLE
Observatoire de Lyon	Directrice : Mme Isabelle DANIEL
Ecole Polytechnique Universitaire Lyon 1	Directeur : Emmanuel PERRIN
Ecole Supérieure de Chimie, Physique, Electronique (CPE Lyon)	Directeur : Gérard PIGNAULT
Institut Universitaire de Technologie de Lyon 1	Directeur : M. Christophe VITON
Institut de Science Financière et d'Assurances	Directeur : M. Nicolas LEBOISNE
ESPE	Administrateur Provisoire : M. Pierre CHAREYRON

Acknowledgments

This thesis work took place within the Laboratory of Polymer Materials Engineering (IMP@Lyon1 UMR 5223) at the University Claude Bernard Lyon 1. This work was supervised by Pr. Laurent David and Dr. Stéphane Trombotto in collaboration with the School of Biomedical Sciences at the University of Leeds, with Dr. Jessica Kwok; the Cell-Environment Interaction team (ICE) at VetAgro-Sup (Campus vétérinaire de Lyon at the University of Lyon), with Pr. Didier Pin, Nadège Milhaud and Dr. Caroline Prouillac. These three years of research were achieved thanks to funding from the Bill & Melinda Gates foundation and the ANR (French National Agency for Research).

First I want to thanks Pr. Laurent David my thesis director, for the confidence he gave me by trusting me with this work, his critical thinking and especially his good mood.

My warm thanks are also directed to my co-supervisor, Dr. Stéphane Trombotto. Thank you for always being there when needed. I learned alot from you during these years. Your patience your encouragement and your trust have been very precious to me.

I am very honored and grateful to Dr. Jessica Kwok university academic fellow at the school of Biomedical Sciences, University of Leeds and Dr. Ghislain David maître de conférences of Université Ecole Nationale Supérieure de Chimie de Montpellier ENSCM for examining and being members of the thesis jury.

Part of the work presented in this thesis is the result of collaboration between IMP@Lyon 1 and the School of Biomedical Sciences at the University of Leeds, with Dr. Jessica Kwok. Again I want to thank Dr. Jessica Kwok for welcoming me to her laboratory. Defintly this stay was fruitfull from the wide knowledge that I gained during the team meeting every week and our constant discussion. Special thanks to Stuart Dickens and Ashleigh Goodenough for their help to explore the British culture and ofcourse for all the tea biscuits break that we had. Also a seconde collaboration was with the Cell-Environment Interaction team (ICE) at VetAgro-Sup (Campus vétérinaire de Lyon at the University of Lyon), with Pr. Didier Pin, Nadège Milhaud and Dr. Caroline Prouillac. Thanks to Pr. Didier Pin for accepting to be the president of the jury and to Dr. Caroline Prouillac for her participation in the thesis jury. Also I want to thank Pr. Thierry delair, Pr. Isabelle royaud and each member of the jury for their time and skills to judge this work.

With regard to the technical aspect, I would particularly like to express my thanks to Dr. Catherine ladaviere for MALDI-TOF MS analyses, Agnès crepet for SEC analyses, Anne baudoun for NMR analyses and Dr. Paula nunes de oliveira for synthesis of COS coated Fe_3O_4 at the department of Physics, Maringá State University Brazil.

I sincerely thank all the staff of the laboratory for all these moments shared with good humor: Florian, Sylvie, Nadia, Sabine, Olivier ... During these years at IMP, I had the chance to meet great people who have become true friends: Thibaut was my best french professor and my partner with the laymone (Orange) break. All these moments helped to destress, smile and to improve my French. Renaud best lab partner always present to help with his smile and big heart. Anthony habibi your sense of humor and the picnic moments out in the sun :p are all unforgettable. As I always tell you “I am waiting for your visit in Lebanon”. Anais, Pierre, Florian.V, Mo, Melanie, Yann, Christophe, Imed, Micheal, Sylvain, Keven, Nico, Gautier, Margarita, Luisa, Noemie, Clementine, Anatole, Raphael, Sarah, Claire, Orianne, Laura, Dimitry, Cyrielle, Amira, Iman, Asma, Huber, Chloe, Yoanh, Lea, Mathieu, Clement, Clemence, Mathilde S, Laurent, Bryan, Soline, Alice G, Maxime, Jimmy, Yinquanyi, Thomas, Maud, Florian, Antoine, Kilian, Busra, Lina, Amar, Josian and Jihane. You were my second family in Lyon! To the new PhD students and Internships, thanks for their kindness and support to finish with the best. Office colleagues 425! "Besancon", I will never forget the pleasant moments we shared together: Manon, Mathilde, Benjamin, Walid and André, I love you all!

Finally, I would like to thank my family. My lovely mom who was supporting me from far away and taking care of me with homemade delicious food that she sent me from Lebanon. My father who trusted me and gave me the freedom to pursue my education and travel on my own despite the traditional rules. My sisters who were always there for me for advice and moral support. They gave me confidence in myself in moments of doubt. I love the three of you. My youngest brothers who were my childhood friends. I thank them for their never ending love. My cutest nephew, 7 years old Jean and my lovely niece, 4 years old Joud. I hope by the time you grow up and read this, you will be pursuing your dreams just like I did. Finally, to my grandmother Sharifa and my aunt Siham, you are both a blessing in my life. I want you to know that my love for you is extraordinary.

<< I was taught that the way of progress was neither swift nor easy >>

Marie Curie

To my family and to all those who mean a lot to me

Summary

Chitooligosaccharides (COS) classically present several biological properties such as anti-microbial, anti-tumor and anti-fungal activity. In this work, we used COS for widely different applications, such as tissue engeneering of neuronal cells (blocking of perineuronal net formation), the complexation of iron cations (Fe^{2+} and Fe^{3+}) for the synthesis of supermagnatic particle and finally for the development of advanced functional COS-based conjugates. In this partnership studies, we worked on the elaboration of controlled structure chitooligosaccharides in order to decipher their physico-chemical or biological properties. Further modification of chitooligosaccharides was performed in this thesis in two ways: modification *via* amine *N*-substitution and the modification *via* the 2,5-anhydro-D-mannofuranose (amf) aldehyde group located at the reducing end of chitooligosaccharides. The first COS types consist in the nitrous depolymerization followed by *N*-acetylation in order to (partly) control both the mean degree of *N*-acetylation and the degree of polymerization. The second consist in the synthesis of new COS-based building blocks functionalized at their reducing end by reductive amination and oximation with different clickable chemical groups (*i.e.* alkyne, alkene, azide, thiol, and hydrazide). Depending on the targeted functionalized COS, different analysis techniques were carried out to fully characterize such as NMR spectroscopy, MALDI-TOF mass spectrometry, HPLC-chromotography, RAMAN spectroscopy and SEC chromatography. Specific chitooligosaccharides were studied in the objective to use them to modulate the perineuronal net of neurons, and the establishment of synaptic connections. We also showed that water soluble COS permit the precipitation of supramagnetic Fe_3O_4 nanoparticles with a COS coating and succeded in decreasing their toxicity. Finally we have shown that COS-based building blocks could be useful intermediates for the development of advanced functional COS-based conjugates such as COS-*b*-PEG diblock copolymers.

Résumé

Les chitooligosaccharides (COS) présentent des propriétés biologiques intéressantes telles que l'activité antimicrobienne, antifongique et antitumorale. Dans ce travail, nous avons utilisé les COS pour des applications très diverses, telles que l'ingénierie des cellules neuronales (blocage de la formation du réseau périneuronal), la complexation des cations Fe^{2+} et Fe^{3+} pour la synthèse de particules supermagnatiques et enfin pour le développement de conjugués fonctionnels à base de COS. Dans le cadre de ces études en partenariat, nous avons travaillé sur l'élaboration de chitooligosaccharides à structure contrôlée afin d'étudier leurs propriétés physico-chimiques ou biologiques. Des modifications de chitooligosaccharides ont été effectuées dans ce travail de deux façons: la modification par *N*-substitution et la modification par le groupe aldéhyde du résidu 2,5-anhydro-D-mannofuranose (amf) à l'extrémité réductrice des chitooligosaccharides. Les premiers types de COS consistent en la désamination suivie d'une réaction de *N*-réacétylation afin de contrôler (partiellement) à la fois le degré moyen d'acétylation et le degré moyen de polymérisation. La seconde stratégie consiste en la synthèse de nouveaux COS fonctionnalisés à leur extrémité réductrice par amination réductrice et oximation avec différents groupes chimiques cliquables (c'est-à-dire alcyne, alcène, azide, thiol et hydrazide). En fonction des COS fonctionnalisé ciblé, différentes techniques d'analyse ont été réalisées pour analyser pleinement leurs caractéristiques structurales telles que la spectroscopie RMN, la spectrométrie de masse MALDI-TOF, la chromatographie HPLC, la spectroscopie RAMAN et la chromatographie SEC. Des structures chimiques spécifiques de chitooligosaccharides modifiés ont été étudiées dans le but de les utiliser pour moduler le réseau périneural de neurones et l'établissement de connexions synaptiques. Nous avons également montré que les COS solubles permettent la précipitation des nanoparticules supramagnétiques de Fe_3O_4 avec un revêtement COS en les rendant moins toxiques. Enfin, les COS fonctionnalisés à leur extrémité réductrice pourraient être des intermédiaires utiles pour le développement de nouveaux conjugués fonctionnels à base de chitosane.

Contents

Abbreviations

A

AcOH: Acetic acid

AE-COS: aminoethyl-chitooligosaccharides

AgOTf: Silver triflate

AIBN: Azobisisobutyronitrile

B

Bn: Benzyl

$BF_3.Et_2O$: Boron trifluoride diethyl etherate

Bu_3SnH: Tributyltin hydride

Bu_4NF: Tetrabutylammonium fluoride

C

CCOS: Carboxylated COS

CCl_3CN: Trichloroacetonitrile

CH_2Cl_2: Dichloromethane

CH_3CN: Acetonitrile

COS: Chitooligosaccharides

$CuI.P(OEt)_3$: Iodocopper;Triethyl Phosphite

CSA: Chlorosulfonic acid

D

DA: Degree of *N*-acetylation

DABITIC: 4-dimethylaminoazobenzene-4'-isothiocyanate

DBU: 1,8-Diazabicyclo(5.4.0)undec-7-ene

DMSO: Dimethyl sulfoxide

DMF: N, N-Dimethylformamide

DP: Degree of polymerization

E

EDANS: Fluorophore 5-(2-aminoethyl) amino-1-naphthalene-sulfonic acid

F

FRET: Fluorescence resonance energy transfer

G

GlcN: D-glucosamine

GlcNAc: *N*-acetyl-D-glucosamine

H

$Hg(CN)_2$: Mercury(II) cyanide

L

$LiOH/H_2O$: Lithium hydroxide monohydrate

M

MeOH: Methanol

N

NaOMe: Sodium methoxide

NaH: Sodium hydride

$(NH_4)_2Ce(NO_3)_6$: Ammonium cerium(IV) nitrate

$NH_2NH_2.H_2O$: Hydrazine hydrate solution

P

Pd/C: Palladium on carbon

p-TolSCl: *p*-Toluenesulfonyl Chloride

p-TsOH*: p*-Toluenesulfonic acid

S

SCOS: Sulfated COS

T

TBAF: Tetra-*n*-butylammonium fluoride

TBAI: Tetrabutylammonium iodide

TBDMS: tert-Butyldimethylsilyl

tBuOk: potassium tert-butoxide

TES: Triethylsilane

TFA: Trifluoroacetic acid

THF: Tetrahydrofuran

TMSOTf: Trimethylsilyl trifluoromethanesulfonate

General introduction

Chitosan is a linear copolymer consisting of 2-acetamido-2-deoxy-D-glucopyranose (GlcNAc) and 2-amino-2-deoxy-D-glucopyranose (GlcN) units linked by a β-(1→4) glycosidic bond. It is mainly obtained by *N*-deacetylation of chitin, the most abundant polysaccharide in biomass after cellulose. Chitosan is a biocompatible biodegradable and bioactive biopolymer. In view of these important biological properties it is envisioned in many applications in the biomedical, agricultural, food industry, cosmetics ... Chitosan, however, has some limitations in its applications because of its low solubility in physiological conditions, its high molar masses and its high viscosity. Chitooligosaccharides that are prepared from chitin or chitosan either chemically or enzymatically, have lower molar mass and higher water solubility. Chitooligosaccharides could also have specific biological properties, but as degradation products, may explain the bioactivity of chitosan in the form of gels, fibers, films or sponges used as implants. The establishment of a structure – biological activity relationship is therefore essential for the development of this family of compounds [1].

The objective of this work is the synthesis of chitooligosaccharides with well control of structural parameters to obtain well-defined chemical structures. This strategy offers to relate their biological activity with chemical structure, exploring the structure of COS by the chemical modification *via* amine *N*-substitution and by modification *via* the reducing end. This thesis consist of four chapters showing collaborative work with the School of Biomedical Sciences at the University of Leeds and with VetAgro-Sup Campus vétérinaire de Lyon at the University of Lyon.

The first chapter of the manuscript deals with the bibliographic study. The first part briefly describes the difference between chitin, chitosan and chitooligosaccharides. Then, the interests of chitooligosaccharides will be evidenced by the study of their properties and applications. In a third part, we will describe the methods for the preparation of chitooligosaccharides existing to date, as well as their limits concerning the obtaining of a 'well-defined' structure. Finally, we will focus on the chemical modification of chitooligosaccharides and their effect on enhancing the biological properties of

chitooligosaccharides. This bibliographic research summarizes the pathways we have followed to reach our goals.

The second chapter entitled "Synthesis and characterization of well-defined chitooligosaccharides structures » will detail the strategies we have chosen for the synthesis and characterization of various structurally defined chitooligosaccharides, in terms of their degrees of polymerization and *N*-acytelation.

The third chapter, entitled "Applications of well-defined and characterized chitooligosaccharides in biology and material science" is divided into different parts showing the:

- Toxicity of synthesized chitooligosaccharides with different degree of polymerization and *N*-acetylation
- Screening for the use of well controlled chitooligosaccharides for an application in nervous tissue regeneration: cytotoxicity analyses.
- In situ synthesis of Fe_3O_4 nanoparticles coated by chitooligosaccharides, characterization and toxicity evaluation for biomedical, in the form of a publication. .

Finally, ***the fourth chapter*** will present the chemical modification of chitooligosaccharides at the reducing end. It is structured in publication form.

- Reducing-end 'clickable' functionalizations of chitosan oligomers for the synthesis of chitosan-based diblock copolymers.

Chapter I

Bibliography study

1. Introduction

1.1. Chitin, Chitosan and Chitooligosaccharides

Chitin was first discovered by the French pharmacist and chemist Professor Henri Braconnot in 1811. Chitosan was discovered later in 1823, as it was first observed by Auguste Odier, another French scientist. Odier observed that the compound of chitin could be manipulated through chemical and temperature treatments and become soluble. This new compound was later named "chitosan".

Chitin is the most abundant polysaccharide in biomass after cellulose. It is a linear copolymer consisting of D-glucosamine (GlcN) and *N*-acetyl-D-glucosamine (GlcNAc) units linked by a β-(1→4) glycosidic linkage. Chitin is present in cuticles or exoskeletons of arthropods (crustaceans, insects, arachnids) as well as in the endoskeleton of cephalopods (squid, cuttlefish). It is also present in the cell walls and the extracellular matrix of most fungi, certain yeasts and algae. Chitosan is also a linear copolymer consisting of D -glucosamine (GlcN) and *N*-acetyl-D-glucopyranose (GlcNAc) units linked by a β-(1→4) bond. It is found naturally in the cell wall of certain microorganisms (fungi, bacteria, yeasts and algae) and the cuticle of insects, but in relatively small quantities [2]. At the industrial level, it is mainly produced by *N*-deacetylation of chitin. Chitin and chitosan have the same chemical structure described in Figure 1 and differ only in the mean fraction of the acetylated units along the polymer chain, called the degree of *N*-acetylation (DA).

Nevertheless, the "limit" between chitin and chitosan is more strictly established from the physico-chemical differences (*i.e.* mainly results from the solubility of chitosan in acidic aqueous media and the insolubility of chitin in aqueous solvents). It is frequently but erroneously published that below a critical DA < 50-60 %, the polysaccharide is called chitosan [3, 4] whereas homogeneous reacetylation of chitosan yields soluble 'statistical' copolymer up to 74.5 % [5].

Chitosan is not soluble in water at neutral or alkaline pH due to the presence of strong intermolecular hydrogen bonding and hydrophobic interactions between polymer chains. However, the protonation of the amines moieties in diluted acidic aqueous solution ensures

the chitosan solubility thanks to repulsive electrostatic interactions that counter-balance pre-existing H-bonds and hydrophobic interactions, but mainly a favored solvation through the protonated sites. Chitosan is the only naturally occurring cationic polysaccharide at acidic pH and its pKa ranges from 6.3 to 6.7 when the DA increases from 0 to 60 % [5, 6]. The solubility of chitosan thus highly depends on the DA. Moreover, the physico-chemical properties of chitosan also vary with its structural parameters such as its molar mass and the distribution of acetylated and non-acetylated residues along the polymer backbone [2]. The nature of the acid used for solubilization can also have an influence [7]. To conclude, there is a profound need to fully characterize the intrinsic parameters of the chitosans used to be able to understand their behavior in solution.

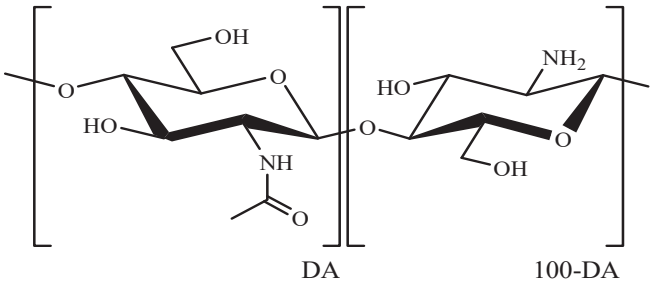

Figure 1: Chemical structure of chitin and chitosan $(GlcNAc)_{DA}(GlcN)_{100-DA}$ defining the degree of *N*-acetylation (DA).

Chitooligosaccharides (COS) are oligomers prepared from chitin or chitosan either chemically or enzymatically. Chitooligosaccharides with degrees of polymerization (DP) <20 and thus an average molar mass less than 3900 g/mol are called chitin/chitosan oligomers, chitooligomers, or chitooligosaccharides [1].

Over the past decades, chitosan has received increasing attention as a functional biopolymer due to its biocompatibility, biodegradability and numerous biological activities [8]. Chitosan and their derivatives have been proposed for applications including gene and drug delivery, tissue repair, water purification, food additive and cosmetics [8]. However many applications of chitosan are often limited by its high viscosity in dilute aqueous acid solutions or its poor solubility at neutral pH conditions. Consequently, an increasing interest has been shown to chitooligosaccharides. COS are water-soluble in a large pH range, they have low-toxicity and

exhibit several additional biological properties compared to their parent structures chitosan, including anti-microbial, anti-tumor and anti-fungal activity, as well as immuno-enhancing effects on animals [9]. COS have also been shown to elicit protective responses in various plants and possess antimicrobial activities against a wide spectrum of phytopathogens [10].

Many studies have therefore focused on chitooligosaccharides, *i.e*. lower molar mass molecules to overcome the above-mentioned problems encountered with the polymer, while hoping to maintain an interesting bioactivity. We will first detail the potential of chitooligosaccharides by describing the main biological properties highlighted by several studies, as well as the potential applications that result from them. In a second part, we will examine the different methods existing to date to prepare chitooligosaccharides and finally in the third part, we will discuss several methods to modify chitooligosaccharides.

2. Interest of chitooligosaccharides

2.1. Biological Properties

Unlike chitosan, chitooligosaccharides show a better water solubility and a lower viscosity in aqueous solutions [11]. Their low viscosity and greater solubility at neutral pH have attracted the interest of many researchers. A safety assessment study of oral exposure to chitooligosaccharides concluded that the maximum tolerated dose in mice was greater than 10g/kg/day, no genetic mutation or abnormal symptoms or mortality were observed [12]. Similarly, absence of toxic effects by COS (0.050–1.0 mg/mL) at 24h was also reported on human and mouse leukocyte cell lines [13]. In addition, De Assi *et al*. [14] team studied the cytotoxicity of COS on human tumor cell lines (HepG2 and HeLa) and mouse normal (embryonic 3T3) cells. Their results showed a high proliferative activity on normal 3T3 cells when they used COS (0.5 and 1.0 mg/ml). They showed that COS exert a pronounced proliferative effect on HeLa cells but not on HepG2.

2.1.1. Antimicrobial activity

Much research has been conducted on the study of the antimicrobial properties of chitooligosaccharides [15, 16]. Several structural factors have been reported to contribute to the antimicrobial activity: molar mass (M_W), the degree of *N*-acetylation (DA) as well as

environmental effects (pH, temperature, ionic force, etc.). Wang *et al*. [17] showed that the antimicrobial activity of chitooligosaccharides increases with decreasing degrees of *N*-acetylation and polymerization. Chitooligosaccharides with a mean degree of *N*-acetylation of 10% and degree of polymerization 4 are the most active to inhibit the growth of several bacteria (*E. coli, S. aureus, S. lactis* and *B. subtilis*).

In contrast, Ueno *et al*. [18] have shown that chitooligosaccharides with a 50% *N*-acetylation degree and a molar mass of less than 2 200 g/mol (DP 12) are not able to suppress microbial growth while chitooligosaccharides of the same degree of *N*-acetylation but with a molar mass of 5 500 g/mol (DP 30) significantly decreases it. The microbial growth is even practically eliminated at a molar mass of 9 300 g/mol (DP 51). The authors also determined the minimal concentration suppressing bacterial growth for each of these chitooligosaccharides. These minimum concentrations are respectively 0.004% and 0.032% for the chitooligosaccharides of molar masses of 9 300 g/mol and 5 500 g/mol while in the case of a chitooligosaccharides of 2 200 g/mol even at a concentration of 0.5%, no antimicrobial activity is observed. These results suggest that the antimicrobial activity of chitooligosaccharides is largely impacted (increases) with the degree of polymerization.

Furthermore, it has been shown that environmental effects (pH, temperature, salinity, etc.) play a significant role in the antimicrobial activity [19]. Li *et al*. [20] investigated the antibacterial activity against *Staphylococcus aureus* by studying the effect of the oligomer size and the pH without mentioning the influence of DA. In their study, different degrees of polymerization of COS were used ranging from DP 2 till 12. Their results show that the antibacterial activity of COS required a minimum size of DP 5 and again the inhibitory effect increased with increasing DP. Lower pH value could enhance the antibacterial activity of COS, since the solubility and protonation state may depend of the pH. The COS with DP > 12 showed a minimum inhibitory concentration (MIC) value of 62.5 mg/mL at pH 6.0, while the MIC value increased to 500 and 1 000 mg/mL at pH 6.5 and 7.0, respectively.

The antimicrobial activity of chitooligosaccharides leads to contradictory results concerning the evolution of this activity according to the structural parameters. In addition to the type of microorganism, this property seems to be impacted by environmental conditions such as pH, neighboring components of the culture medium and its structural parameters such as molar

mass, degree of deacetylation, polymerization, derivative form, its concentration, and original source [21]. All these parameters impact the solubility of chitosan that, in it-self, could result in a modulation of biological activity. Moreover, it has been suggested, that the amine moieties present in the structure of chitooligosaccharides could interact with negatively charged carboxylic acid groups of proteins or lipids present on the surface of bacteria. This results in the formation of polyelectrolyte complexes [22, 23] creating an impermeable layer and slowing the metabolic activity of the bacteria by blocking the transfer of nutrients through the cell wall. Chitooligosaccharides could also alter the membrane permeability of microbial cells, thus preventing cell transfection [24].

2.1.2. Anti-fungal activity

Some studies have shown that chitooligosaccharides have antifungal activity, this activity being influenced by the degree of polymerization and *N*-acetylation. Oliveira *et al*. [25] studied the influence of the degree of polymerization on growth inhibition of several phytopathogens. Mixtures of oligosaccharides were used in this study. The first includes DP 2–DP 7 main components, the second DP 2–DP 10 and the third contain oligomers of DP 6–DP 7 all with 0 % degree of *N*-acetylation. Their results show that small chitooligosaccharides of DP ≤ 7 (the first mixture), are not inhibitory to any of the fungi. On the other hand, higher DP chitooligosaccharides (in the second and the third mixture) show initially inhibitory effects on *alternaria alternata*, *Rhizopus stolonifer* and *Botrytis cinerea*. Kendra *et al*. [26] studied the antifungal activity of COS at very low degrees of polymerization. They show an increase in antifungal activity with the increase in DP from monomer to dimer of glucosamine. The antifungal activity of chitooligosaccharides is therefore related to the polycationic character. This property would allow them to react with negatively charged groups of fungi membranes, hence antifungal activity. The inhibition mechanism of chitooligosaccharides against fungi is similar to that previously described for antimicrobial activity. The formation of polyelectrolyte complexes between chitooligosaccharides and negative charges on the surface of cells would directly interfere with fungal growth. As a result, the antifungal activity of chitooligosaccharides would depend on the distribution of charges along the oligomeric chain and would vary depending on the degrees of *N*-acetylation and polymerization [27].

2.1.3. Antitumor activity/ anticancer activity

Several teams were interested in studying the antitumor activity of chitooligosaccharides [28-33]. Suzuki *et al*. [31] showed that chitohexasaccharides $(GlcN)_6$ and $(GlcNAc)_6$ inhibit the growth of S180 (sarcoma 180) and MM46 (mouse mammary 46) tumors implanted in mice. Intravenous injection of 100 mg/kg/day of $(GlcNAc)_6$ seven days after tumor implantation results in inhibition of growth of S180 and MM46 tumors by 83% and 85%, respectively. The injection of chitooligosaccharides $(GlcN)_6$ inhibits the growth of the same tumors respectively by 55 and 93%. $(GlcN)_6$ and $(GlcNAc)_6$ have the same degree of polymerization, but the change in the degree of *N*-acetylation results in different inhibition rates. It was hypothesized that a strong electronic charge is an important factor for the antitumor activity of COS. Nevertheless, several studies on different tumors have confirmed that neutral chitooligosaccharides $(GlcNAc)_6$ have also a strong antitumor activity [30]. Several studies have been conducted on the effect of chitooligosaccharides of different structure on antitumor activity. For example, Jeon *et al*. [34] studied the activity of chitooligosaccharides with a degree of *N*-acetylation of 0% and degrees of polymerization of less than 9, between 9 and 34 or greater than 34 on the inhibition of tumors S180 and U14 (Uterine cervix carcimona No. 14) implanted in mice. The mixture of chitooligosaccharides with degrees of polymerization ranging from 9 to 34 has greater antitumor activity than mixtures of degrees of polymerization of less than 9 or greater than 34. In addition to that, a recent study by Zou *et al*. [33] studied the activity of chitooligosaccharides with a sharp range of degree of polymerization of 2-6 as an anti-tumor drug. The results show that COS can suppress the growth of HCT116 cells *in vitro* and *in vivo*, and inhibit the growth rate of tumor weight up to 85%. According to the different investigation carried out, the impact of DP of COS seems to be less important, since most DP have shown significant and similar effects. Therefore, a mixtures of COS instead of purified COS could be used which will help to reduce the cost of production of the drug. The anti-tumor activities of COS ascertained their potential for the treatment of cancer, however, further investigations are necessary as many aspects are still unclear and not defined properly such as the correlation between physicochemical properties of COS and anti-tumor activity.

2.1.4. Eliciting activity

Elicitors are substances capable, under certain conditions, of stimulating the natural defense mechanisms of plants. These natural defenses would be directed either against bio aggressors (disease, pest) or against abiotic stresses such as those caused by frost or drought [35]. The term elicitor originally referred to molecules capable of inducing the synthesis and accumulation of phyto-alexin in plant cells [36] but it is now used for molecules stimulating any plant defense mechanism [35, 37]. For about fifteen years, the eliciting activity of chitooligosaccharides has been extensively studied as plant defense elicitors. Many studies reported the positive effects of COS for activation of plant defense [35, 38-41]. Hadwiger *et al*. [38] investigated the ability of chitooligosaccharides $(GlcN)_4$, $(GlcN)_6$ and $(GlcN)_8$ to inhibit the growth of fungal pathogens in pea. While the first two show no eliciting activity, the chitooctosaccharide $(GlcN)_8$ turns out to be a very effective elicitor.

Cabrera *et al*. [41] investigated the influence of degrees of polymerization and *N*-acetylation on defense activation in a culture of *Arabidopsis thaliana cells*. Chitooligosaccharides with degrees of polymerization of 5 to 9 with a degree of *N*-acetylation of 0% have a higher eliciting activity than chitooligosaccharides of the same degree of *N*-acetylation but with degrees of polymerization between 3 and 6. After an *N*-acetylation of these chitooligosaccharides, the authors observed a maximal elicitation activity for a degree of *N*-acetylation of 65%. Beyond this value, the activity decreases. Vander *et al*. [42] confirmed the influence of the degree of *N*-acetylation on the eliciting activity of chitooligosaccharides. GlcN oligomers with degrees of polymerization ranging from 5 to 7 do not show any eliciting activity when they are injected into the leaves of *Triticum aestivum L*., whereas GlcNAc oligomers with degrees of polymerization greater than 7 are active.

2.1.5. Other biological activities

Other works have described hypertensivity, antioxidant, anti-inflammatory, immunostimulatory and antiviral activities for chitooligosaccharides. Such studies are briefly summarized below.

a) Hypertensivity activity

Angiotensin I converting enzyme (ACE) plays an important role in regulating blood pressure in mammals. Researches on chitooligosaccharides have identified their potential to inhibit ACE activity. Park *et al*.[43] studied the effect of partially *N*-acetylated chitooligomers, at DA 10, 25, and 50%, with a different molar masses (5 000−10 000 g/mol), (1 000−5 000 g/mol) and (below 1 000 g/mol) on ACE activity. Their result show that all acetylated COS exhibit ACE inhibitory activity. However, Chitooligosaccharides with 50% degree of *N*-acetylation exhibited the highest ACE inhibitory activity; with IC_{50} value 1.22 ± 0.13 mg/mL. The IC_{50} value was defined as the concentration of inhibitor required to inhibit 50% of the ACE inhibitory activity. Park *et al*. show that this activity was dependent on DA and has no significant differences when using different molar masses.

b) Antioxidant activity

In recent years, reactive oxygen species (ROS) and free radicals play an important role in many diseases such as cancer [44]. The superoxide anion radical (O^{2-}) and hydroxyl radical (·OH) are very unstable and react rapidly with the other groups or substances in the body, leading to cell or tissue injury. It has been shown that chitooligosaccharides possess anti-free radical and antioxidant potency [45]. These activities of chitooligosaccharides are significantly related to their degree of polymerization (DP) and degree of *N*-acetylation (DA) [46]. Chen *et al*. [47] reported that $(GlcN)_2$ and $(GlcN)_3$ had stronger antioxidant activity than those chitooligosaccharides with higher DP. Also Li *et al.* [48] demonstrated the antioxidant activity of chitooligosaccharides with different DP (3,4,5,6,7,10). The antioxidant was investigated, including hydroxyl and superoxide radical scavenging activity. The antioxidant activity of chitooligomers was significantly related to its DP. The chitooligomers with low DP showed better effect of scavenging hydroxyl radical and reducing power than that with high DP.

Dos Santos *et al.* [49] studied the antioxidant activity of chitosan polymers DP 190 with different degrees of *N*-acetylation (DA 1-69%), and chitooligosaccharides ($3 < DP < 8$) of different DA (0-91%). Their results show that chitosan polymers of high DA (60 and 69%) and chitooligosaccharides of high DA (78 and 91%) have higher antioxidant level then their couterparts at lower DA. The authors concluded that antioxidant activity was strongly dependent on the degree of *N*-acetylation of the chitosan oligo-and polymers, with highly acetylated chitosans being most active. A confirmation of this hypothesis by Li *et al.*[46],

were the antioxidant activities of chitotrioses and its partially *N*-acetylated varieties were investigated. Chitotrioses with high degree of *N*-acetylation displayed greater antioxidant activity, illustrating that the DA has a major role in the antioxidant activity of COS.

c) Anti-inflammatory activity

Several studies have reported the anti-inflammatory activities of COS [50-53]. Liang *et al.* [51] reported the anti-inflammatory activity of enzymatically synthesized COS of two series S1 ($8 < DP < 16$) and S2 ($DP < 8$). Their result show that the anti-NO (NO is an extremely reactive free radical species that involved in numbers of pathological and physical processes [54]) was higher for S2 than for S1 at a concentration of 100 mg/mL showing that with low DP, COS have a greater anti-inflammatory activities. The interest of the use of low molar mass oligosaccharides was also studied by Vo *et al.*[52]. Their study shows that LMW COS has a greater effect in preventing histamine release and the production of proinflammatory cytokines including IL-1β, IL-4, IL-6, IL-8 and IL-13 in basophils. However, the impact of DA was not mentioned.

d) Immunostimulatory activity

The immune system plays an important role in eradicating foreign pathogenic substances and micro-organisms from the body. Recent studies have revealed the potential of COS as immunostimulant. Mei *et al*. [55] evaluated the effect of COS on cyclophosphamide (Cy)-induced immunosuppression. In their study they used COS sample with a degree of polymerization 4–11 and degree of *N*-acetylation 8%. Thymus (A lymphoid organ, which produces T-lymphocytes for the immune system) and spleen (An abdominal organ, involved in the production and removal of blood cells, thus forming part of the immune system) indices, delayed-type hypersensitivity (DTH) reaction, macrophage phagocytosis, and certain enzyme activities were significantly higher in mice treated with COS and Cy than in mice treated with Cy alone. Also Zhang *et al*. [56] showed that COS with polymerization degree of 3–8 possesses potent immune-stimulating properties by activating the Toll Like Receptor4 (TLR4) on macrophages.

e) Antiviral activity

Some research has highlighted an antiviral activity of chitooligosaccharides [57, 58]. It has been shown that as the degree of polymerization decreases, the antiviral activity is lower. On the other hand, as the degree of *N*-acetylation decreases, the antiviral activity is improved. It has therefore been suggested that the antiviral activity would be directly related to the presence of positive charges on the amine functions present in the chitooligosaccharides and would depend on the degrees of *N*-acetylation and polymerization. The mechanism of antiviral activity is not well understood, but one possible explanation could be that the positive charges of the amine groups would activate the immune and defense systems in plants and animals [59].

2.2. Applications of Chitooligosaccharides

Thanks to their interesting biological properties described above, chitooligosaccharides are likely to be used in many fields such as medicine and pharmacy [60] (protective effects against bacterial infections, antitumor agents, cholesterol lowering, acceleration of absorption calcium), agriculture [61], the food industry [62] (antimicrobial agents, preservatives), cosmetics [63, 64].

Thanks to their antimicrobial properties, chitooligosaccharides can find applications in the field of food preservation. A mixture of chitooligosaccharides with a degree of *N*-acetylation of 0% and degrees of polymerization varying from 1 to 8 makes it possible to improve the preservation of milk [65]. A patent discloses a solution of chitooligosaccharides with a degree of *N*-acetylation of 0% and a molar mass of less than 3 000 g/mol (DP <18) used as a protective film to improve the preservation of fish fillets [66].

The antimicrobial properties of chitooligosaccharides can also be exploited by the textile industry. Thus, two chitooligosaccharides having a degree of *N*-acetylation of 0% and respective degrees of polymerization of 3 and 10 have been incorporated in cotton fabrics [67, 68]. After 50 washes, tissues containing 2.4% chitooligosaccharides are able to maintain a 95% reduction in bacteria for DP 3 and 100% for DP 10. In addition, these fabrics withstand the wear and tear of washings. Chitooligosaccharides can also be of interest in the pharmaceutical and biomedical fields. Chitooligosaccharides with degrees of polymerization ranging from 1 to 30 are for example added to gels or creams to improve the vectorization of

drugs [69] [70]. The use of chitooligosaccharides in chewing gums [71] or toothpastes [72] would limit tooth decay through their antimicrobial properties.

2.3. Conclusion on the interest of chitooligosaccharides

Many studies have been conducted to determine the bioactivity of chitooligosaccharides. The results indicate that these compounds have numerous biological activities such as antimicrobial, antitumor, antifungal, antiviral, and antioxidant activities….. It appears that these biological properties depend on the length of the oligosaccharide chain or degree of polymerization (DP), as well as the number of *N*-acetyl-D-glucosamine units or degree of *N*-acetylation (DA). Although most of the work highlights the variation of the studied activity according to these two structural parameters, no constitutive law has been determined, since possibly, there is a constitutive law for every studied biological effect. However to simplify, Figure 2 show in general which chitooligosaccharides structures are actually responsible for biological activity.

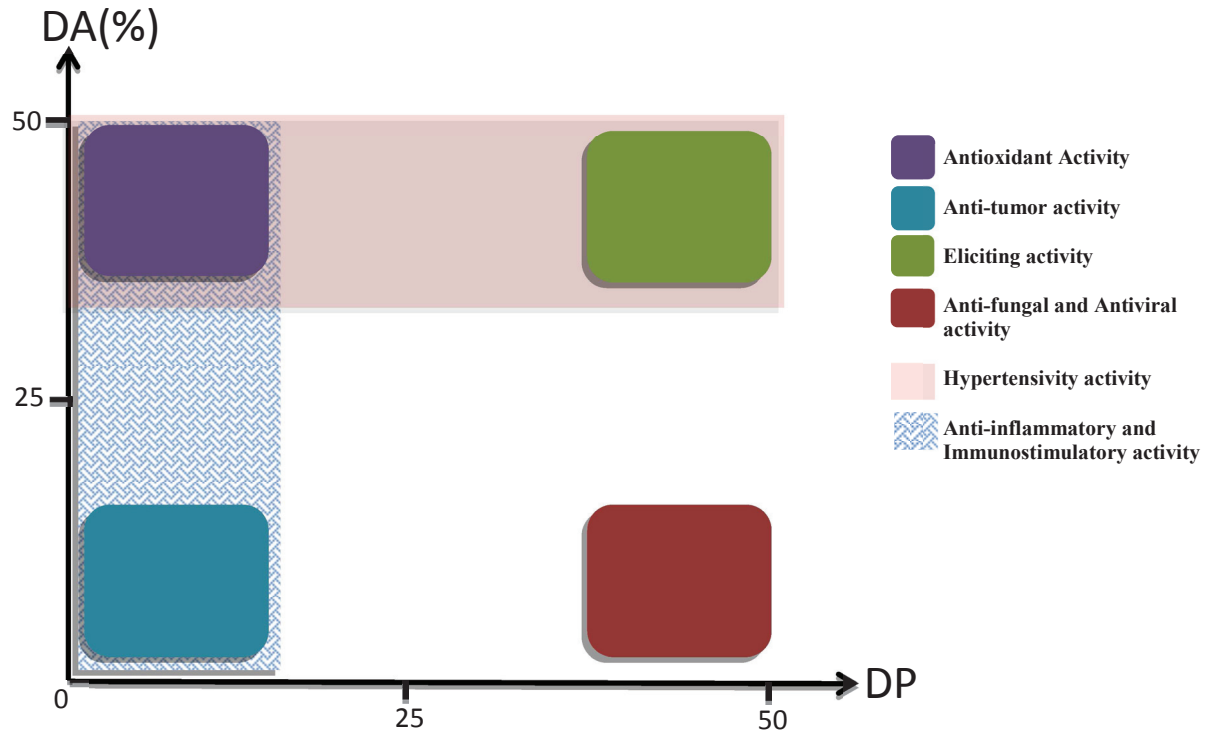

Figure 2: General relation between structural parameters (DP, DA) of chitooligosaccharide and their various biological activities.

It should be noted that most of the work related to the bioactivity of chitooligosaccharides has mainly been conducted with mixtures characterized at best by their average degrees of polymerization and average DA. Under these conditions, it is difficult to determine which oligosaccharide structures are actually responsible for the biological activity. In order to overcome this disadvantage, it is essential to obtain chitooligosaccharides with perfectly (or better) defined and characterized structures. In this context, several methods for the preparation of chitooligosaccharides have been developed.

3. Preparation methods of chitooligosaccharides

The development of efficient methods for their preparation of COS has been of great interest for many years. Two main production strategies have been developed: one by depolymerization of chitin and chitosan and the other by synthesis. Both methods can be performed according to chemical or enzymatic processes.

3.1. Preparation by depolymerization of chitin and chitosan

Several methods allow cleaving the glycosidic bonds of chitin and chitosan, thus leading to chitooligosaccharide mixes. This route was the first explored because chitin and chitosan are easily accessible and abundant. The main depolymerization methods of chitin and chitosan use chemical or enzymatic processes. Some physical methods have also been reported.

3.1.1. Chemical methods

3.1.1.1. Acid hydrolysis

The "classical" chemical method for obtaining the oligomers of chitin and chitosan from the polymer is acid hydrolysis [73, 74]. Indeed, like all polysaccharides, chitosan and chitin can be hydrolyzed. The glycosidic bond is relatively unstable when it is placed in acidic aqueous solutions. The glycosidic bonds cleave during hydrolysis, this leads to a decrease in molar masses. The hydrolysis mechanism described in Figure 3 involves in a first step the protonation of the oxygen atom of the glycosidic bond. The limiting step of this mechanism corresponds to the rupture of the bond between the exocyclic oxygen atom and the anomeric carbon. The resulting structure is a cyclic oxocarbenium ion, which then reacts with a water molecule to form the reducing end sugar.

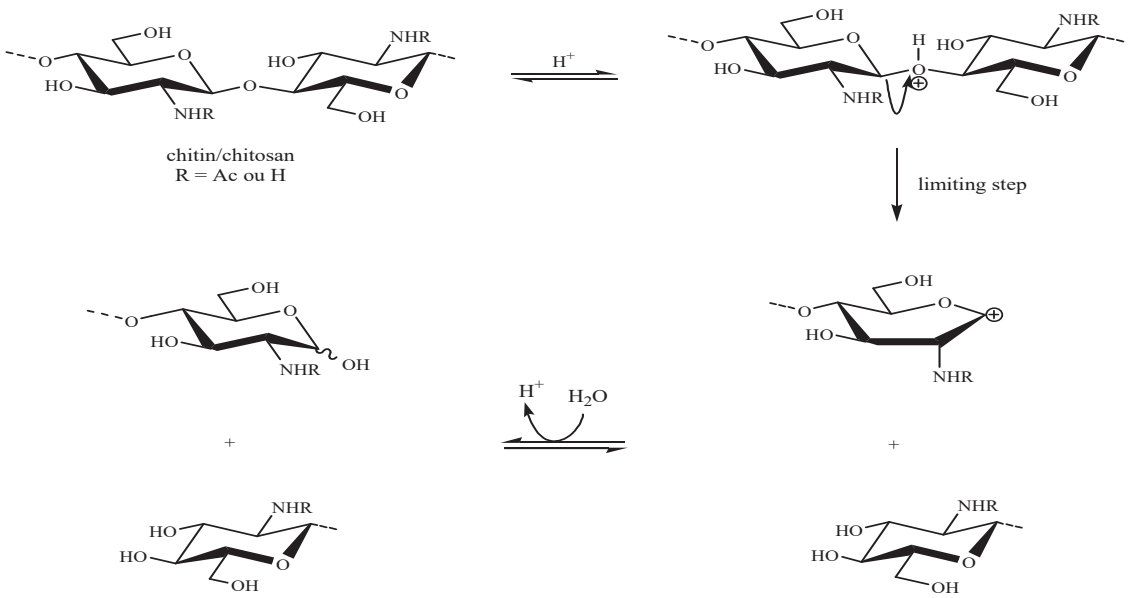

Figure 3: Schematic illustration of the proposed reaction mechanisms for the acid-catalysed hydrolysis of chitin and chitosan [74].

Since chitosan is soluble in acidic aqueous media, this reaction can take place in a homogeneous medium. Hydrolysis can also be performed in solid state (heterogeneous conditions) to selectively degrade the amorphous phase in order to produce chitosan fibrils after washing the chitooligosaccharides [73]. On the other hand, the acid hydrolysis of chitin systematically occurs under heterogeneous conditions since the latter is not soluble in acidic aqueous media. The first preparation of chitosan oligomers was made by Horowitz *et al*. in 1957 [75]. In this study, the authors have shown that the time of hydrolysis is decisive for the size of the chitooligosaccharides formed. They showed that chitosan having a degree of *N*-acetylation of 0% was hydrolyzed in 4N hydrochloric acid, at 53°C for 48 h. Oligomers of D-glucosamine was obtained with polymerization degrees varying from 1 to 6, DP 1 and 2 being the majority. After 72 hours of hydrolysis, only the monosaccharide D-glucosamine is isolated. On the other hand, if the hydrolysis is shorter, a mixture of chitooligosaccharides consisting essentially of degrees of polymerization ranging from 4 to 6 is recovered. In addition to the reaction time, the effectiveness of the hydrolysis also depends on the acid concentration, acid nature, the temperature or the degree of *N*-acetylation of chitosan.

To go a step further, Trombotto *et al*. [76] have reported a method for chemical preparation of partially deacetylated COS from fully deacetylated high molar mass chitosan. The starting

chitosan was partially depolymerized using HCl to produce fully deacetylated oligomers that were fractionated by selective precipitation and ultrafiltration to yield a mixture of DP 2–DP 12. The oligomers were then partly *N*-acetylated using stoichiometric amounts of acetic anhydride to reach the decided DA. By this way, COS fractions of DP 2–DP12 were successfully prepared. However, the drawback of this method, as for the enzymatic preparation of COS, is the heterogeneity of the prepared COS.

Another study by Domard and Cartier [77] have shown that D-glucosamine oligomers with degrees of polymerization up to 40 can easily be obtained by hydrolysis of a totally deacetylated chitosan in 12 M hydrochloric acid at 72°C for 90 minutes. Then, oligomers up to degree of polymerization 15 are separated by size exclusion chromatography with acetic acid / ammonium acetate buffer solution as eluent. The acid hydrolysis of chitin and chitosan by aqueous HCl is a straighfoward method. This is an inexpensive process but, the reaction conditions are harsh and may result in chemical modification of the glucosidic ring. Another disadvantage is that this method leads to either complete depolymerization or a large polydispersity. To overcome these problems, other methods of preparation have been studied and other acids have been used to hydrolyze chitosan such as phosphoric acid [78, 79], hydrogen fluoride [80] acetolysis [81], lactic acid [82] and nitrous deamination[83].

3.1.1.2. Acetolysis

Acetolysis is defined as the breakdown of an organic compound using either acetic acid or acetic anhydride. Inaba *et al*. [81] used chitin as a starting material for acetolysis. The glycosidic bond is cleaved by the reaction of acetic anhydride in sulfuric acid that leads to the formation of both per-*O*-acetylated and per-*N*-acetylchitooligosaccharides (Figure 4) with good yields and high reproducibility.

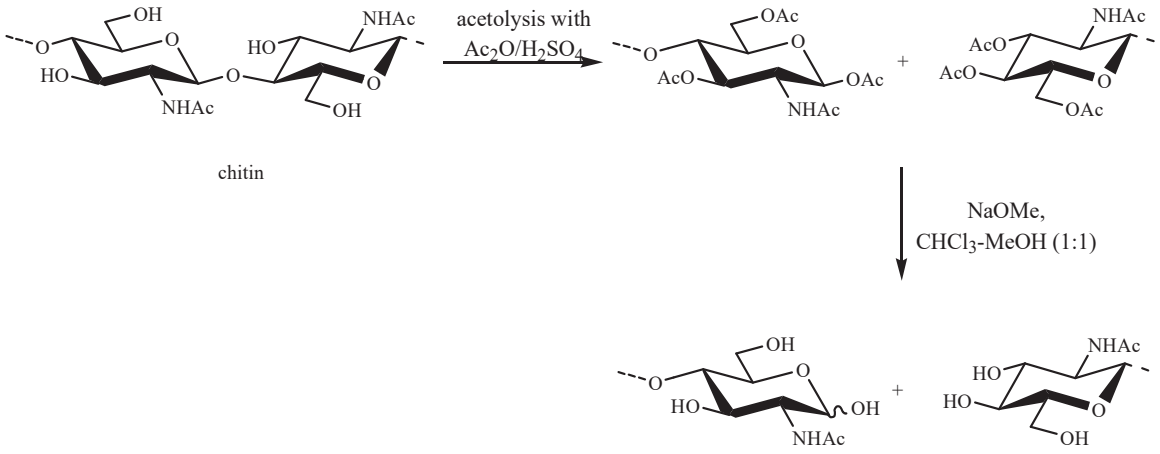

Figure 4: Schematic illustration of the proposed reaction mechanisms for the acetolysis of chitin [81].

The authors studied the influence of the reaction time at 55°C on the acetolysis yield of chitin and observed the best results after three hours of acetolysis. They obtained a mixture of peracetylated chitooligosaccharides which they then separated on a Sephadex LH-20 chromatographic column. The *O*-deacetylation was carried out in the presence of sodium methanolate in a chloroform-methanol mixture that yields chitooligosaccharides with different degrees of polymerization 2, 3 and 4.

3.1.1.3. Fluorohydrolysis

Defaye *et al* [84] noted that the fluorohydrolysis of chitin in anhydrous hydrogen fluoride led to the formation of chitooligosaccharides in quantitative yields (Figure 5). The reaction conditions (time, temperature) can be modified to optimize the preparation of specific chitooligosaccharides containing from 2 to 9 residues. In addition, since chitin is soluble in hydrogen fluoride, the fluorohydrolysis is carried out under homogeneous conditions.

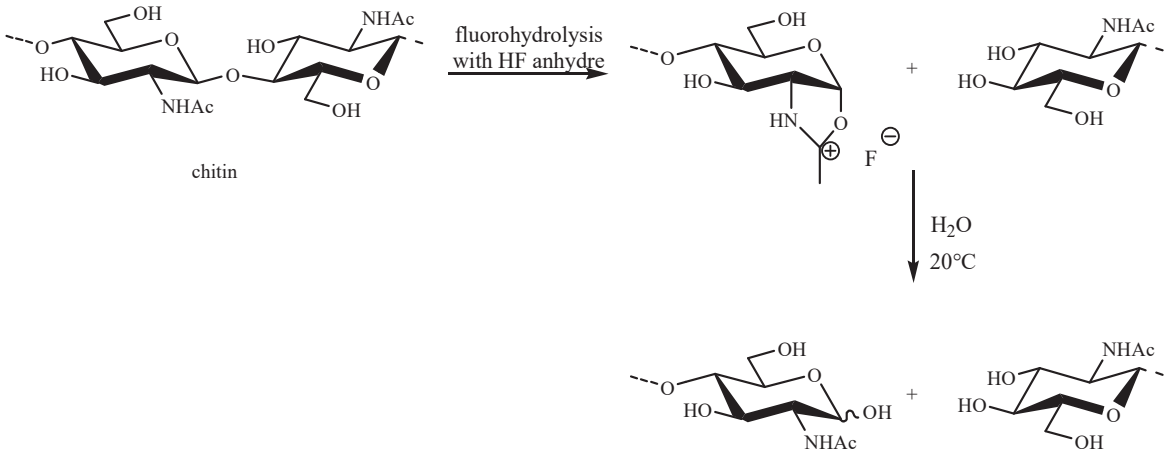

Figure 5: Fluorohydrolysis reaction of chitin [84].

After half an hour of reaction at 20°C, chitin is not hydrolyzed, whereas after one hour, it is partially cleaved. Further hydrolysis during 24 hours of reaction leads to complete cleavage. Interestingly, after 4 hours of fluorohydrolysis, the predominant product is GlcNAc-GlcNAc dimer. By this method, a mixture of chitooligosaccharides with degrees of polymerization ranging from 2 to 10 and with a degree of *N*-acetylation of 100% (since the starting chitin is fully acetylated) is obtained. This mixture was then separated on a Bio-Gel P-4 preparative column to yield the chitooligosaccharides with yields of 37% (DP 2), 23% (DP 3), 10% (DP 4), 5% (DP 5), 4.6% (DP 6), 3% (DP 7), 2.2% (DP 8), 1.6% (DP 9) and 1% (DP 10). The same team then fluorohydrolyzed chitosan under the same conditions as those described for chitin [80]. The dissolution of chitosan in hydrogen fluoride is slower, but the reaction is nevertheless carried out in homogeneous conditions. Fluorohydrolysis of chitosan leads to chitooligosaccharides having a fluorine atom in α-configuration at the anomeric position of the reducing end [80]. The products are isolated by precipitation with ether and then the action of perchloric acid at 60°C allows the formation of chitooligosaccharides with an hydroxyl group in the anomeric position (Figure 6).

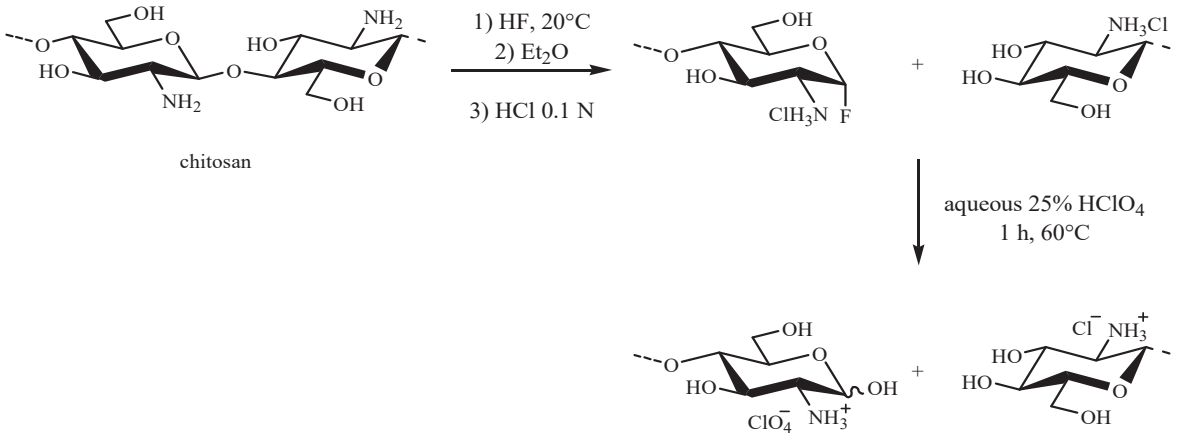

Figure 6: Fluorhydrolysis reaction of chitosan [80].

Thus, in contrast to the mechanism described in Figure 5 for the fluorohydrolysis of chitin, in the case of chitosan, a fluoride is formed in the anomeric position. The mixture of chitooligosaccharides obtained after the fluorohydrolysis of chitosan and treatment with $HCLO_4$ were separated on a Bio-Gel P-4 chromatographic column and the yields were 3.0% (DP 2), 9.9% (DP 3), 14.3% (DP 4), 15.9% (DP 5), 15.4% (DP 6), 12.0% (DP 7), 8.8% (DP 8), 4.7% (DP 9), 3.0% (DP 10) and 1.0% (DP 11).

3.1.1.4. Nitrous deamination

Several teams have studied the formation of chitooligosaccharides by nitrous deamination of chitosan [11, 83, 85-88]. The depolymerization of chitosan by nitrous acid (HNO_2) is a homogeneous reaction in which the number of cleaved glycosidic bonds is stoichiometric to the amount of nitrous acid used [11] (Figure 7a). With regard to the reaction mechanism, it has been found to be specific in the sense that HNO_2 attacks the amino group of GlcN but does not attack GlcNAc untis. Specifically, a diazonium ion is first formed on a D-glucosamine unit and then decomposes to give a carbocation. The latter undergoes nucleophilic addition of endocyclic oxygen, leading to a 2,5-anhydro-D-mannofuranose structure as a new chain end [88], as shown in

Figure 7b. The terminal chitooligosaccharides of newly formed chitooligosaccharides molecules are unstable and decompose with time leading to the formation of 5-hydroxymethylfurfural (HMF) as shown in Figure 8. Standard protocol generally include

additional post-treatment of the reaction mixture containing sodium borohydride ($NaBH_4$) which is able to reduce the aldehyde (-CHO) group of the terminal 2,5-anhydro-D-mannofuranose to (-CH_2OH) [1, 83].

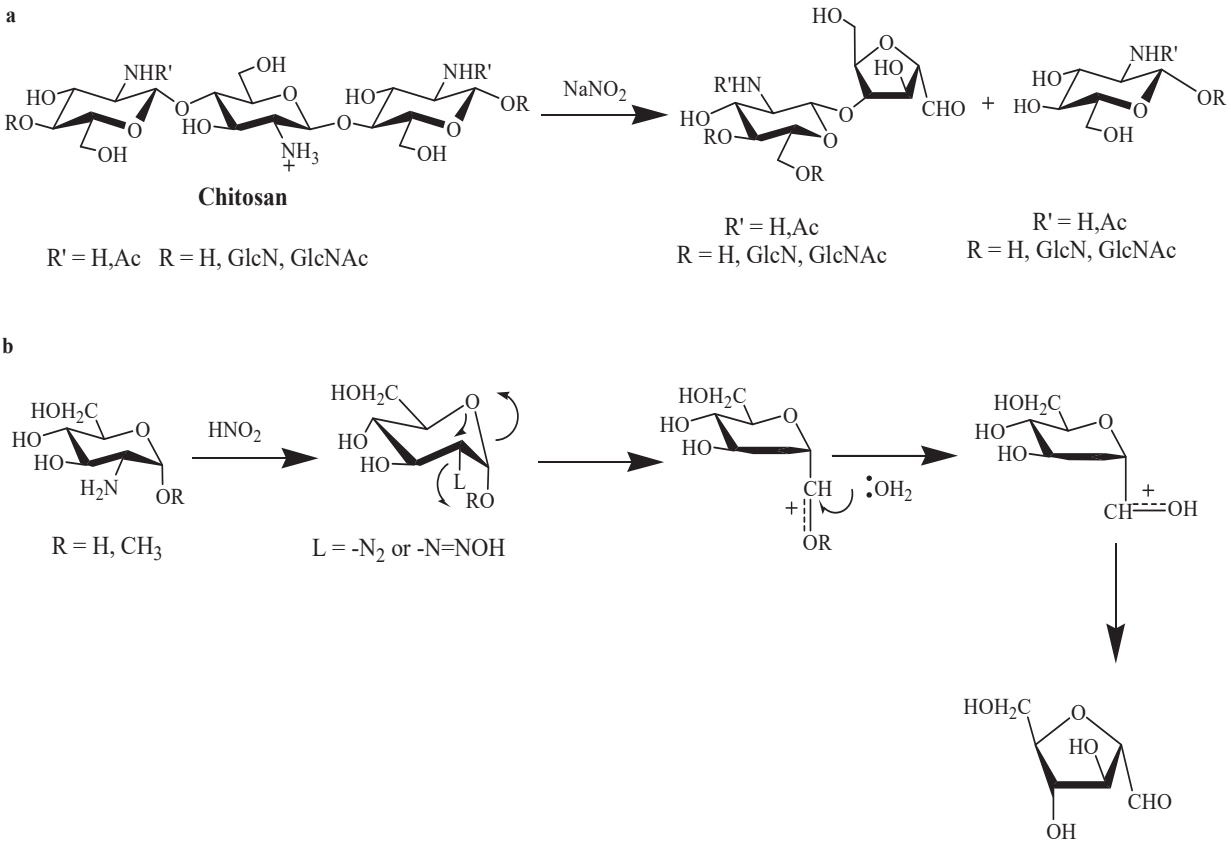

Figure 7: (a) Depolymerisation of chitosan by nitrous acid. The reaction forms 2,5-anhydro- D-mannose-reducing end. (b) Mechanism of nitrous deamination of amino sugars [1].

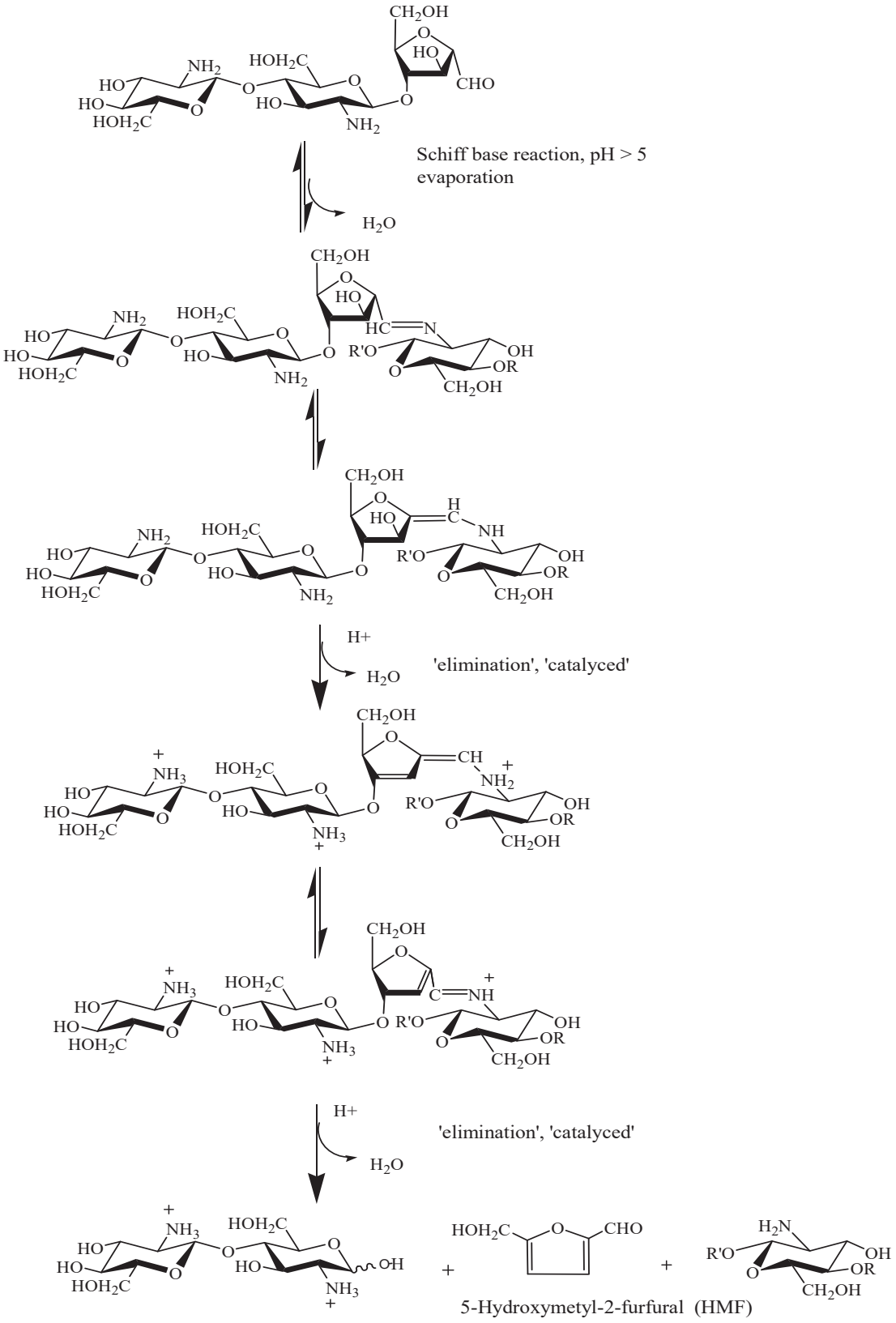

Figure 8: Proposed mechanism of the Schiff base reaction facilitating the elimination of water leading to the formation of HMF and chain cleavage [83].

3.1.2. Oxido-reductive depolymerization

Chitooligosaccharides were also synthesized by radical depolymerization using several oxydoreduction methods involving persulfate [1] and hydrogen peroxide [89, 90]. Xia *et al*. [89] described the production of chitooligosaccharides by using hydrogen peroxide under the catalysis of phosphotungstic acid in homogeneous phase. Experimental results showed that the optimum concentration of phosphotungstic acid was around 0.1% (w/v). This optimum concentration helped to increasing the depolymerization kinetics of chitosan. Chitosan of DA 6.5% and molar mass of $410x10^3$ g/mol was dissolved in 1% (v/v) aqueous acetic acid (HAc) solution. H_2O_2 2% (v/v), and phosphotungstic acid 0.1% (w/v) were added at 65°C for 40 min. COS of DP 2-9 were successfully produced with a yield of 92.3% (w/w). In addition, Chang *et al*. [90] reported the degradation of chitin and chitosan by using low concentration hydrogen peroxide leading to the production of COS DP 1-10 at 80°C. They showed that the production of COS using this method is much faster in comparison with enzymatic methods (discussed below) and ultrasonic depolymerization.

Mouray *et al*. [1] propsed a general mechanism for the degradation of chitosan by persulfate free radical. Persulfate is thermally dissociated into anionic radicals. The anionic radicals are attracted by the cationic amino group in chitosan. The anionic radical attacks the C4 carbon of glucosamine and transfers the radical to the C4 carbon by substituting the hydrogen atom. The presence of free radical at C4 carbon eventually results in the breakage of the glycosidic C–O–C bond in the chitosan main chain. In practice, an acidic solution of chitosan is reacted with potassium persulfate at 70°C (Figure 9).

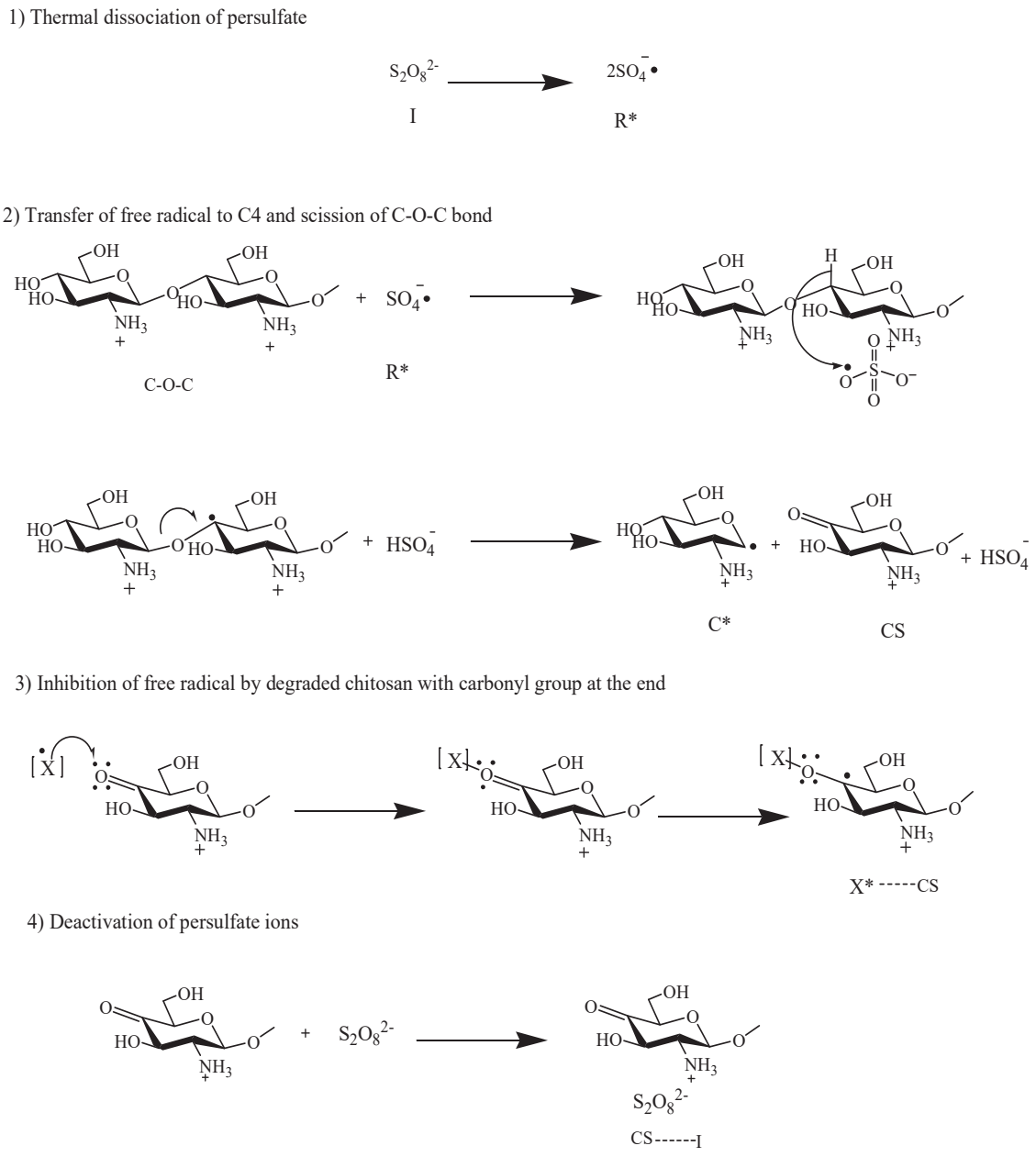

Figure 9: Proposed degradation mechanism of chitosan by persulfate free radical [1].

Chitooligosaccharides can be prepared from chitin and chitosan by chemical hydrolysis using different acids and reactive species. However, chemical hydrolysis has some drawbacks in a commercialization context, due to the development of toxic compounds, higher risk associated to pollution. Thus, enzymatic hydrolysis has been considered as eco-friendly alternative methods of degradation due to the safety and non-toxicity of these methods [91].

3.1.3. Enzymatic depolymerization

The sequence of acetylated and non-acetylated residues along the chitosan chain plays an important role during enzymatic hydrolysis. Indeed, chitin and chitosan have four types of glycosidic bonds:

- 1 bond between two acetylated units (A-A)
- 1 bond between an acetylated unit and a deacetylated unit (A-D)
- 1 bond between a deacetylated unit and an acetylated unit (D-A)
- 1 bond between two deacetylated units (D-D)

Depending on their specificity, the enzymes will selectively cleave a type of glycosidic bond. The specificity of enzymatic cleavage extends in fact over short sequences of a few residues. Chitinases cleave the glycosidic bond between two *N*-acetyl-D-glucosamine units while chitosanases cleave the glycosidic bond between two D-glucosamine units.

3.1.3.1. Enzymatic depolymerization by chitinases

Chitinases are present in bacteria, fungi, plants and insects but are absent in most mammals except cows, goats and sheep [92]. Most chitinases isolated from bacteria are used to obtain *N*-acetyl chitooligosaccharides with a degree of polymerization around two. In addition chitinases act on partially *N*-acetylated chitosan by recognizing GlcNAc residues in the chitosan sequence [93]. Chitinases have been used in several studies to obtain chitooligosaccharides by enzymatic hydrolysis [94-97]. Lang-Wang *et al*. [95] showed that chitooligosaccharides with DP 4–9 range can be produced by enzymatic degradation of chitosan with degree of *N*-acetylation 40% by using chitinases extracted and purified from *Bacillus cereus TKU027*. Tanabe *et al*. [97] described the production of dimer $(GlcNAc)_2$ and trimer $(GlcNAc)_3$ with the hydrolysis of chitin by chitinases. The chitinase purified from *streptomyces griseus HUT* hydrolyzed partially *N*-acetylated chitosan with DA 54% and then was separated by CM-Sephadex C-25 column chromatograph. Thanks to MALDI-TOF mass spectrometry the hetero-chitooligosaccharides with GlcNAc at the reducing end were detected, confirming the selectivity and specificty of chitinases enzyme. Mitsutomi *et al*. [96] isolated chitinase *Bacillus circulans* specifically hydrolyzing the *N*-acetyl-β-D-glucosamine bonds in a chitosan of 50% *N*-acetylation degree to form hetero-chitooligosaccharides of degrees of polymerization 2 and 3 mainly and carrying a GlcNAc unit on the reducing part.

3.1.3.2. Enzymatic depolymerization by chitosanases

Chitosanases cleaves D-D glycosidic bonds which have been generally recognised as enzymes that specifically attack chitosan but not chitin. Chitosanases are found in bacteria, fungi and plants [98, 99]. Chitosanases are classified into three distinct subclasses. Subclass I chitosanases split both D–D and A–D linkages. Subclass II chitosanases can cleave only D–D linkages. On the other hand, subclass III chitosanases split both D–D and D–A [100]. However, since chitosanases cleave D-D glycosidic bonds, they are more effective on chitosans with a low degree of *N*-acetylation [100, 101]. Chitosanases are also distinguished from chitinases by their smaller molar mass [99]. They can be divided into two categories (exo and endo types) according to their mode of action during enzymatic hydrolysis. Exo-chitosanases will release D-glucosamine residues from the non-reducing end of chitosan and its oligomers. Concerning endo-chitosanases, they will provide a mixture of chitooligosaccharides mainly containing dimers and trimers. Monaghan *et al*. [102] were the first to record the existence of chitosanase hydrolyzing chitosan but not allowing cleaving the glycosidic bonds of a chitin having a degree of *N*-acetylation of 100%. Since then, endo-chitosanases have often been used to prepare chitooligosaccharides by enzymatic hydrolysis of chitosan [59, 99, 103].

Although many chitinases and chitosanases from microorganisms have been developed, they are produced as recombinant proteins and they are frequently too expensive to be used industrially. This is why other enzymes have been studied for industrial use at lower cost.

3.1.3.3. Enzymatic depolymerization by lysozymes

Like chitinases, lysozymes can degrade β-(1→4) bonds between *N*-acetyl-D-glucosamine units to produce chitooligosaccharides. They specifically cleave glycosidic bonds of type A-A [93, 104, 105]. The hydrolytic action of a lysozyme is different depending on its source [104, 105]. Nordtveit *et al*. studied the effect of lysozyme degradation rate of chitosan with degree of *N*-acetylation from 12 to 60 % for lysozyme originating from human milk and hen egg white. Their result shows that the degradation rate of chitosan by lysozyme is independent of both ionic strength and pH. However the human lysozyme degradation rate was much higher than the hen lysozyme. As for the influence of the DA, it was shown a higher degradation rate with higher DA. The DA effect was confirmed by Verheul *et al*.

[106] who studied the influence of the degree of *N*-acetylation ranging from 11 to 55% on the enzymatic degradation rate. Their result show that lysozymes from hen-egg white activity was highly dependent on the DA and polymers with the highest DA showed the strongest decrease in molar mass.

The use of lysozyme is an alternative to the use of chitinases. The hydrolytic activity of other enzymes such as glycanases, proteases, lipases or tannases has also been studied.

3.1.3.4. Enzymatic depolymerization by other enzymes

Chitooligosaccharides was prepared by depolymerizing chitosan using different commercial enzymes. Below some enzymes will be discussed in details (cellulase, hemicellulose and lipase).

Zhang *et al*. used chitosan of 24% degree of *N*-acetylation that was depolymerized by a mixture of cellulase, alpha amylase, and protease for the fabrication of oligosaccharides [107]. Also Xie et al.[108] prepared chitooligosaccharides from depolymerization of chitosan having 20% degree of *N*-acetylation by the cellulase of *Aspergillus niger*, followed by separation fractionation using acetone–water. This method was successful in the production of chitooligosaccharides with DP values less than 11 in good yield.

Qin *et al.* [109] prepared three mixtures of chitooligosaccharides from a chitosan of high molar mass with a degree of *N*-acetylation of 20% by the hydrolytic action of an hemicellulase. The first fraction of chitooligosaccharides corresponds to an average degree of polymerization of 106 and a degree of *N*-acetylation of 14.0%. The yield obtained is 12.2%. The second fraction obtained with a yield of 6.8% contains chitooligosaccharides of degree of polymerization 58 with a degree of *N*-acetylation of 28.5%. Finally, the third fraction obtained with a yield of 81.0% consists of chitooligosaccharides of average degree of polymerization 8 and a degree of *N*-acetylation of 42.1%.

Muzzarelli *et al*. [110] hydrolyzed chitosan having average molar mass of 700 000 g/mol by a lipase enzyme isolated from wheat germ subtilis at 25°C using enzyme concentrations of $4.5x10^{-3}$ to $9x10^{-1}$ g/L to obtain a mixture of chitooligosaccharides and short chains with average molar mass of 13 000 g/mol (DP~75). The same authors [111] studied the depolymerization of chitosan but using papain enzyme. Chitosans with average molar mass in

the range 400×10^3 to 700×10^3 g/mol could be easily depolymerized to highly polydisperse chitosans. Their study was focused for medical and biotechnological applications. A general summary is illustraed in Figure 10.

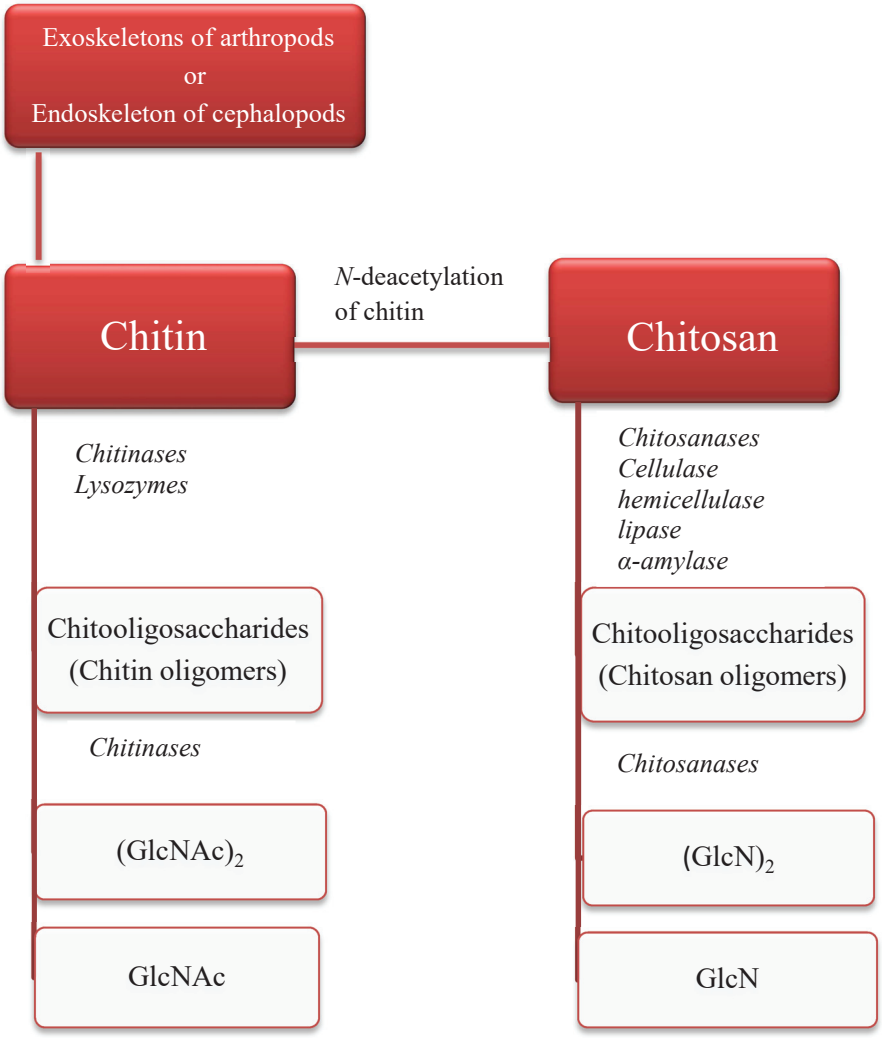

Figure 10: Summary of the different enzymes used for the depolymerization of chitin and chitosan and the synthesis of chitooligosaccharides of different degrees of polymerization and *N*-acetylation.

Enzymatic methods offer advantages such as mild reaction conditions, high specificity, no glucose ring modifications, and mass production of chitooligosaccharides with commercial enzymes. However they are still too expensive to be used industrially and require a systematic purification of the resulting products due to the presence of additives used to

initiate the reactions and the presence of the enzyme. Other physical methods have been developed to prepare chitooligosaccharides by degradation of chitin and chitosan.

3.1.4. Physical depolymerization

In order to overcome the problems encountered in chemical and enzymatic degradation of chitin and chitosan, physical methods such as gamma irradiation [112, 113], microwave [114], and ultrasonic treatments have been performed.

3.1.4.1. Gamma irradiation

The study of Tahtat *et al*. discussed the use of a Co60 gamma source for the depolymerizaion of chitosans in the form of a solid powder and in aqueous solution, with doses ranging from 10 to 500 kGy. Chitosan with *N*-acetylation degrees of 30, 18 and 10% and with different molar masses showed that depending on the radiation dose it is possible to produce chitooligosaccharides of controlled mean molar mass, according to Charlesby-Pinner Equation 1[115].

Equation 1: $$\left(\frac{1}{Mn} - \frac{1}{Mn0}\right) = G \times D$$

Mn: is the number average molar mass of chitosan, deduced from viscosity measurements
Mn_0: is the number average molar mass of the starting chitosan
D: is the irradiation dose (kGy)
G: is the radiation depolymerization yield
Due to the method used (capillary viscometry method) to determine Mn, the dispersity was not evaluated.

These irradiation method induce random chain scission, and the mean DA of COS will be mainly the DA of the parent polymer, since the DA is not changed after irradiation [116]. It is found that irradiation in solution is more efficient than irradiation in the solid state of chitosan [115, 116]. Mean DPn in the range from 40 to 250 were obtained.

Choi *et al*. [113] obtained chitooligosaccharides with degrees of polymerization varying from 2 to 6 from a chitosan having a low degree of *N*-acetylation of 0% irradiated with gamma-

rays Co60 with doses ranging from 2 to 200 kGy. From a practical point of view, an irradiation dose of 100 kGy is sufficient to degrade chitosan and obtain chitooligosaccharides with degrees of polymerization varying from 2 to 4 with the best yields.

These methods induce chemical degradation with the formation of carbonyl groups and color change. Such chemical degradation may be detrimental to preserve the biological properties of chitosan and chitooligosaccharides.

3.1.4.2. Ultrasonic irradiation

Sonication, another physical method, makes it possible to obtain chitooligosaccharides by degradation of the polymer. This technique degrades chitosan by providing the necessary mechanical energy to break the glycosidic bonds. The control of molar mass of the chitooligosaccharides is affected by several factors such as the degree of *N*-acetylation, the molar mass of the starting chitosan and environmental parameters such as the power of the ultrasonic wave, the temperature of the solution, the pH or the ionic strength [117, 118] and sonication time.

Chen *et al*. [117] studied ultrasonic treatment at a power of 220 watts for periods ranging from 1.5 hour to 48 hours at 60°C on chitosan solutions at polymer concentration C_p=1% in a 0.2 M acetic acid / 0.1 M sodium acetate mixture. These authors observed that the molar mass of a chitosan having a degree of *N*-acetylation of 37% decreases rapidly after 1.5h of reaction (from 650 000 to 160 000 g/mol) then the reaction slows down until reaching a molar mass limit (120 000 g/mol, DP 680). On the other hand, the same treatment on a chitosan having a degree of *N*-acetylation of 26% and a molar mass of 410 000 g/mol led to a slight decrease in the molar mass during the first twelve hours (310 000 g/mol) and the latter drops to 100 000 g/mol over the next 12 hours. The authors also noted that the dispersity of chitosan gradually decreases during sonication. This value decreases from 6.5 to 2.7 after 48 hours sonication of chitosan 37% DA and from 4.8 to 2.5 during 48 hours in the case of 26% DA chitosan. Thus, the formation of oligosaccharides requires long sonication times and/or high sonication power.

Popa-Nita *et al*. [118] proposed two mechanism during ultrasonic depolymerization of commercial chitosan in solution, with high initial DP 1720; DA 1.5%, and a dispersity index

Ip=1.6. The polymer was dissolved at pH 4.5 in acetic acid aqueous solutions. Different ultrasound generators were used (Sonics Vibra Cell -Fisher Scientific Bioblock, France- and Lixea formulator type B); different sonications frequencies (20kHz, 39 kHz), different sonication (electrical) powers (285 W and 100 W) and different probe diameters were tested.

When a small probe (diam 3mm) was used, a rapid decrease of the degree of polymerization is observed with a lowering of dispersity. At a sonication time close to 360 min, a value of DPw ~200 and Ip=1.1, was obtained. The first mechanism thus yields monodisperse short chains. It was modeled according to Equation 2.

Equation 2: $$\left(\frac{1}{DP_n(t)} - \frac{1}{DP_n(0)}\right) = n^0(1 - e^{-kt})$$

When a large sonotrode probe was used, after 6 h, the treatment successfully resulted in oligosaccharides of DPn ~25. This leads to the production of short polymer chains and oligomers of high dispersity. This second experimental conditions were modeled with the addition of two depolymerization mechanisms as shown in Equation 3.

Equation 3: $$\left(\frac{1}{DP_n(t)} - \frac{1}{DP_n(0)}\right) = n_1^0(1 - e^{-K_1 t}) + n_2^0(1 - e^{-K_2 t})$$

As a conclusion, several routes have therefore been developed to prepare chitooligosaccharides by depolymerization of chitin or chitosan. These techniques use chemical, enzymatic or physical methods. None of them allows controlling precisely the size distribution and the architecture of the produced chitooligosaccharides. Thus, the obtaining of identical COS collections would requires the development of sophisticated separation processes for the control of the DP and the DA, and hypothetically the sequence of the oligosaccharide. Synthesis is another alternative for the preparation of chitooligosaccharides to overcome these problems. Again, two cases are to be distinguished: enzymatic synthesis and chemical synthesis.

3.2.Preparation of chitooligosaccharides by synthesis

3.2.1. Enzymatic synthesis

Enzymatic syntheses have also been developed to modify chitooligosaccharides in a controllable manner. Tokuyasu *et al*.[119] thus prepared partially deacetylated chitooligosaccharides using chitin deacetylase from *Colletotrichum lindemuthianumi*. This enzyme was used to produce the fully deacetylated trimers $(GlcN)_3$ and tetramers $(GlcN)_4$ from fully acetylated trimers and tetramers. The same enzyme was also used to selectively deacetylates the GlcNAc residue at the non-reducing end of the GlcNAc-GlcNAc dimer to exclusively give GlcNAc-GlcN. [120]. True synthesis of oligosaccharides and oligosaccharide conjugates is possible by biotechnology techniques, still for a limited set of COS or COS derivatives [121, 122]. Since the problem of extraction/purification is a challenge, an alternative is to combine chemical and enzymatic syntheses ('chemo-enzymatic pathways'), yielding chitooligosaccharide derivatives [123]. An other example is to synthesize the hexa- and heptamers $(GlcNAc)_6$ and $(GlcNAc)_7$ from the tetra- and pentamers $(GlcNAc)_4$ and $(GlcNAc)_5$ by exploiting the transferase activity of a chitinase isolated from *Nocardia orientalis IFO 12806* [124]. Both chitinase and lysozyme have transglycosylation activity (transfer of a sugar residue to a pre-existing COS). Akiyama *et al*. [40] synthesized chitooligosaccharides using a transglycosylation reaction catalyzed by chicken egg white lysozyme (Figure 11). They chose *N,N′,N″*-tri (monochloro) acetylchitotriose and *N,N′,N″*-triacetylchitotriose as starting substrates to obtain different COS with DP 4-12.

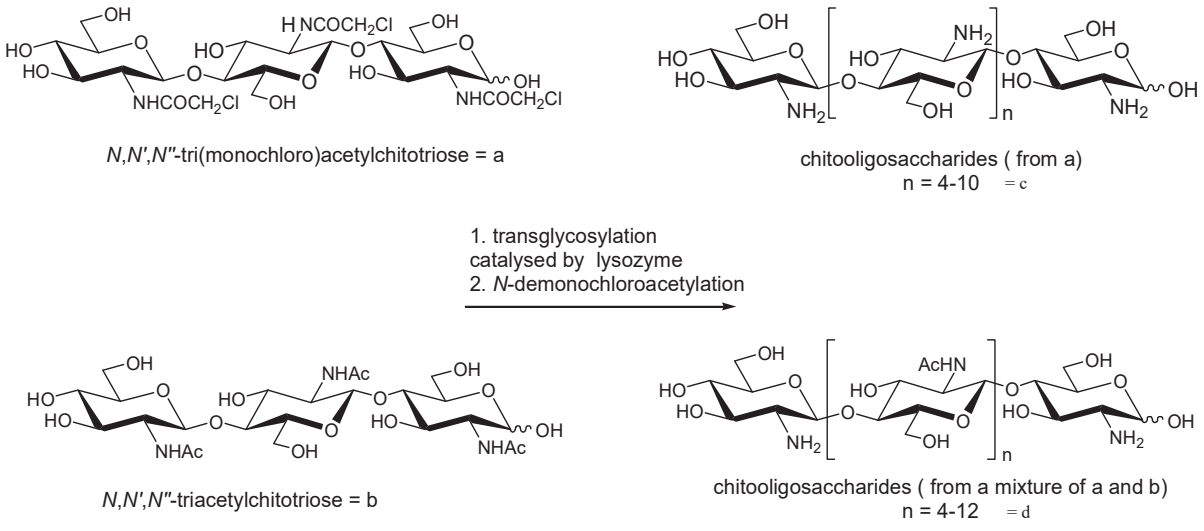

Figure 11: Chemo-enzymatic synthesis of chitooligosaccharides [40].

The action of lysozyme from chicken egg white on *N,N′,N″*-tri(monochloro)acetylchitotriose results in a mixture of fully deacetylated chitooligosaccharides (c) with degrees of polymerization ranging from 4 to 10 with a yield of 33.2%.

A mixture of *N,N′,N″*-tri (monochloro) acetylchitotriose and *N,N′,N″*-triacetylchitotriose reacts under the same conditions and allows the authors to obtain a mixture of chitooligosaccharides (d) of degrees of polymerization between 4 and 12 with *N*-acetylation degrees of 23 to 76% depending on the proportion of each of the two starting materials. These chitooligosaccharides are obtained with a yield of 21.3%. The structure of these oligosaccharides is partly controlled with deacetylated units at both ends of the oligosaccharide, and acetylated residues inside. Further purification could yield monodisperse collections of this small family of COS.

As above-mentioned, some chitooligosaccharides were prepared by enzymatic synthesis. This way allows the (partial) control of the structural parameters, but at the cost of many efforts concerning the isolation and the purification of the enzymes. In addition, the yields obtained are low. As an alternative to enzymatic techniques, chemical syntheses of chitooligosaccharides have also been studied.

3.2.2. Chemical synthesis

Most of the chemical synthesis are limited to the elaboration of homo-oligosaccharides of GlcNAc or GlcN units, [125-129] and only a few of them deal with the preparation of hetero-COS composed of both GlcN and GlcNAc units [130, 131].

3.2.2.1. Chemical synthesis of homo-chitooligosaccharides

Chitooligosaccharides are part of the structure of some *N*-glycoproteins [132]. The latter contain chitobioses. In order to synthesize them, several chemical syntheses of protected chitobioses have been carried out [125-129]. The first study from 1973 when Schmitt *et al*. [127] synthesized per-*O*-acetylated GlcNAc-GlcNAc dimer (see structure 6) according the synthesis pathway described on Figure 12.

a) Chemical synthesis of homo chitooligosaccharides with GlcNAc units

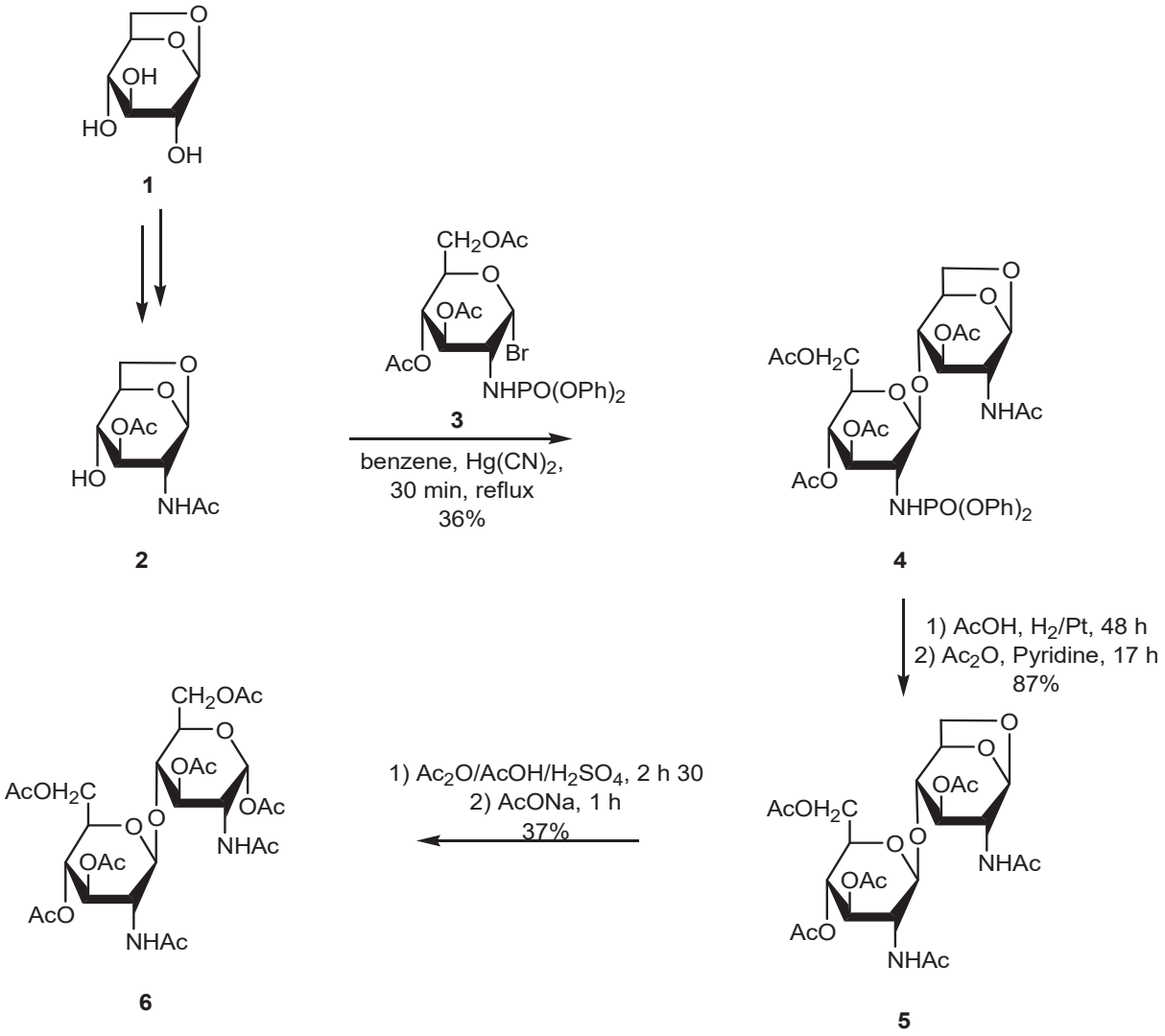

Figure 12: First chemical synthesis of per-*O*-acetylated GlcNAc-GlcNAc chitobiose [127].

In this synthesis, the final product **6** is first prepared in several steps from 1,6-Anhydro-β-D-glucopyranose **1**. Condensation of 3,4,6-Tri-*O*-acetyl-2-deoxy-2-diphenoxyphosphorylamino-α-D-glucopyranosyl bromide **3** with compound **2** in anhydrous benzene in the presence of mercuric cyanide led to disaccharide **4** in 30 min with a yield of 36%. The product **4** is then catalytically hydrogenated. This step resulting in partial deacetylation, the disaccharide is acetylated under standard conditions. The acetylated compound is obtained in 87% yield for both steps and is then acetolysed in an acetic anhydride / acetic acid / concentrated sulfuric acid mixture for 2h30 before addition of sodium acetate. The chitodisaccharide **6** is obtained with a yield of 37% for the last two steps.

In the literature, a chemical synthesis of deprotected chitobiose was reported by Nashed *et al*. [128]. GlcNAc-GlcNAc dimer **11** is obtained according to the procedure described in Figure 13.

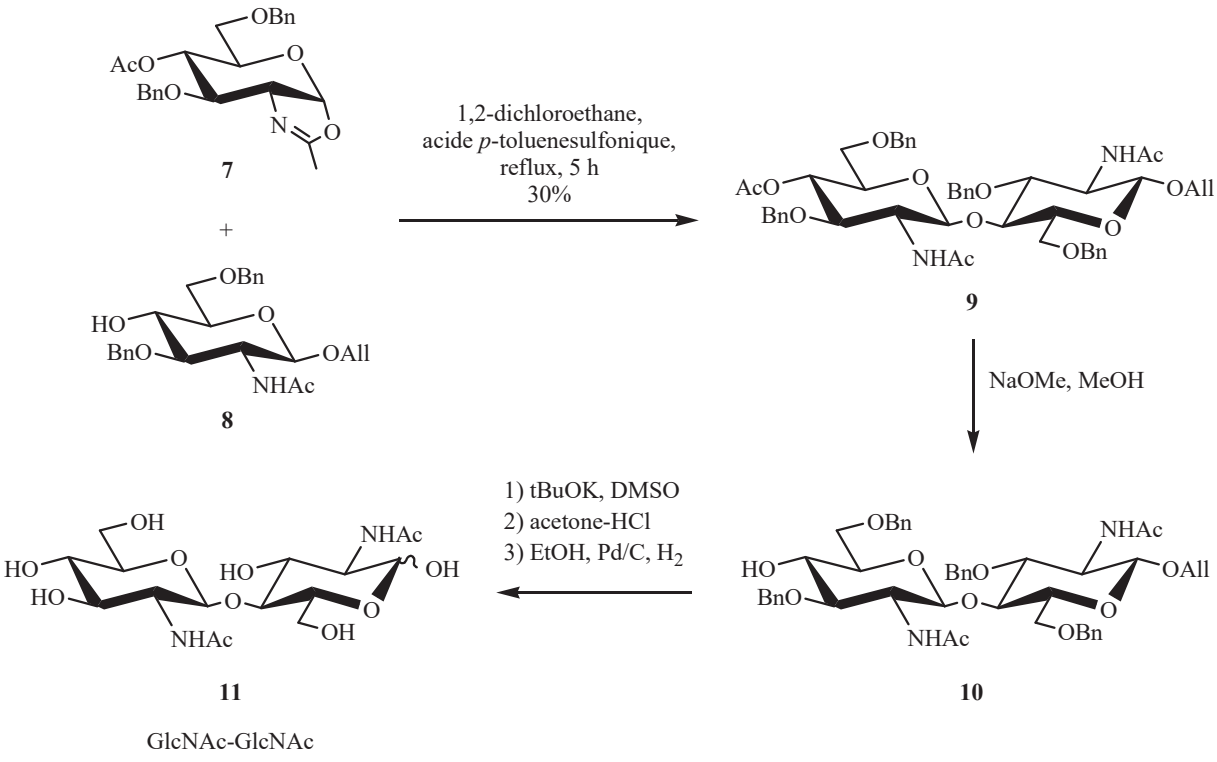

Figure 13: Chemical synthesis of GlcNAc-GlcNAc chitobiose [128].

The coupling reaction between oxazoline **7** and the glycoside 1-*O*-allyl **8** at reflux for 5 h in 1,2-dichloroethane, catalyzed by para-toluenesulphonic acid, leads to the disaccharide **9** with a yield of 37%. The compound **9** is first *O*-deacetylated quantitatively under standard conditions (sodium methanolate in methanol) to give the product **10**, then the allyl group is isomerized by potassium tert-butoxide in DMSO. The resulting 1-propenyl glycoside was hydrolyzed in an acetone/HCl mixture, followed by hydrogenolysis to obtain the chitodisaccharide GlcNAc-GlcNAc **11**.

Aly *et al*. synthesized a fully *N*-acetyl tetrasaccharide according to the protocol described in Figure 14 [125].

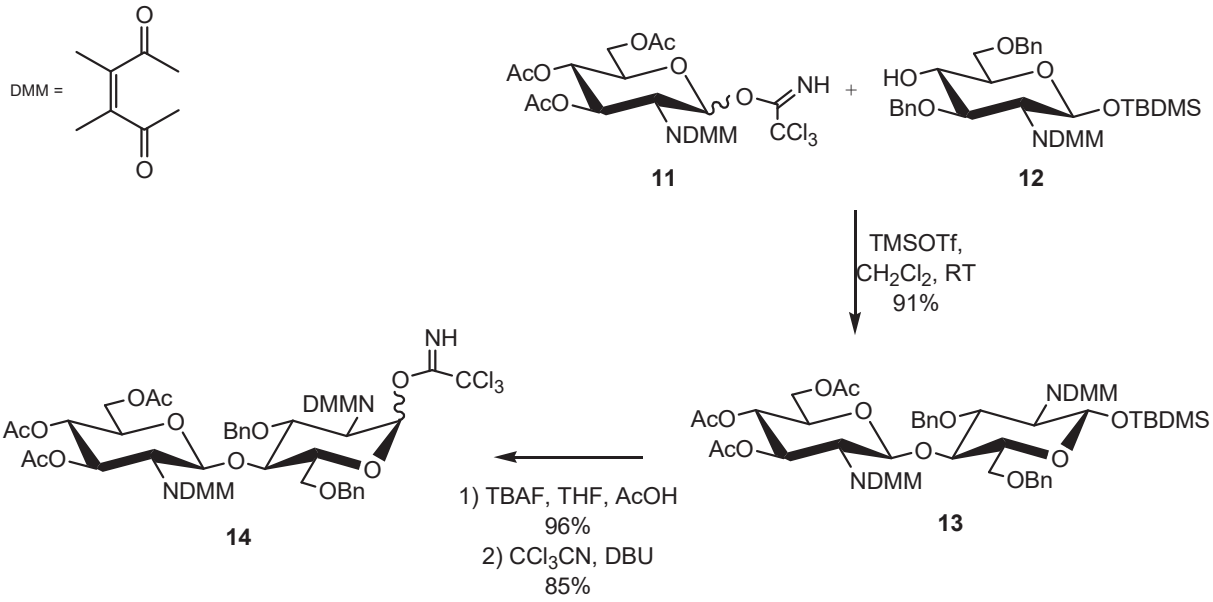

Figure 14: Preparation of intermediate 14[125].

The glycosylation of tert-Butyldimethylsilyl 3,6-di-*O*-benzyl-2-dimethylmaleimido-β- D-glucopyranoside **12** with 3,4,6-Tri-*O*-acetyl-2-dimethylmaleimido-D-glucopyranosyl trichloroacetimidate **11** in dichloromethane in the presence of trimethylsilyl trifluoromethanesulfonate leads to disaccharide **13** with a yield of 91%. The anomeric alcohol of compound **13** is desilylated in 96% yield by TBAF and acetic acid in THF. The resulting hemiacetal reacts with trichloroacetonitrile in the presence of DBU to yield the disaccharide **14** in 85% yield (Figure 14). The treatment of tert-butyldimethylsilyl 3,6-di-*O*-benzyl-2-dimethylmaleimido-β-D-glucopyranoside **12** with phenoxyacetyl chloride, followed by desilylation of the anomeric alcohol with TBAF, followed by the reaction of the resulting hemiacetal with CCl_3CN in the presence of DBU, leads to compound **15** with an overall yield of 57% as described in Figure 15.

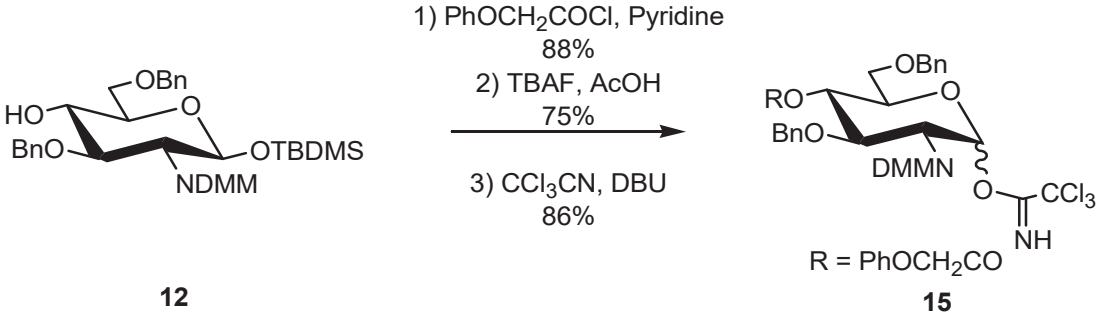

12 **15**

Figure 15: Preparation of intermediate 15 [125].

TMSOTf catalyzed glycosylation of imidate **15** with 3,6-Di-*O*-benzyl-2-deoxy-2-dimethylmaleimido-1-*O*-tert-butyldimethylsilyl-β-D-glucopyranoside **12** in acetonitrile makes it possible to obtain the disaccharide **16** with a yield of 71% (Figure 16). Product **16** can be deacylated with sodium methanolate in methanol to yield compound **17** in 74% yield.

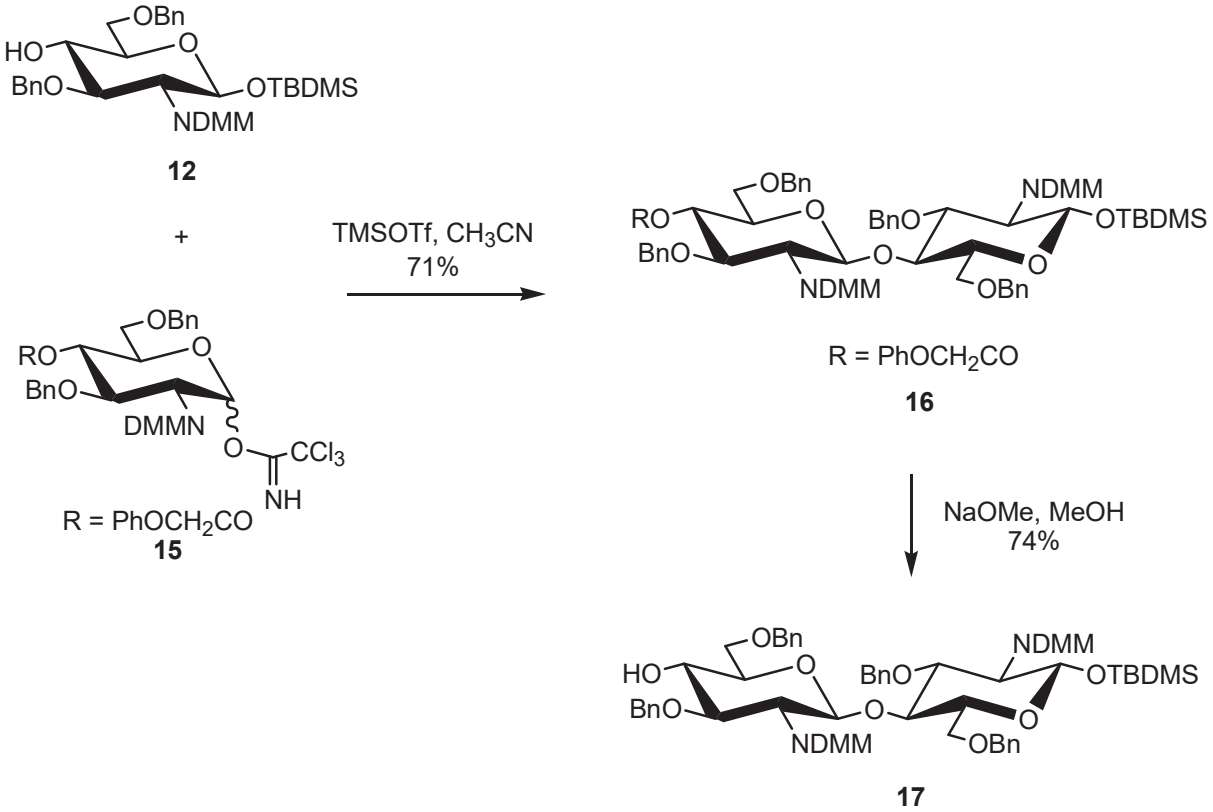

Figure 16: Preparation of intermediate 17 [125].

Glycosylation between the disaccharide **14** obtained according to Figure 14 and disaccharide **17** obtained according to Figure 16 in acetonitrile in the presence of TMSOTf leads to tetrasaccharide **18** in a yield of 74% (Figure 17). Compound **18** is then completely deprotected in several steps to yield the chitotetrasaccharide **19**.

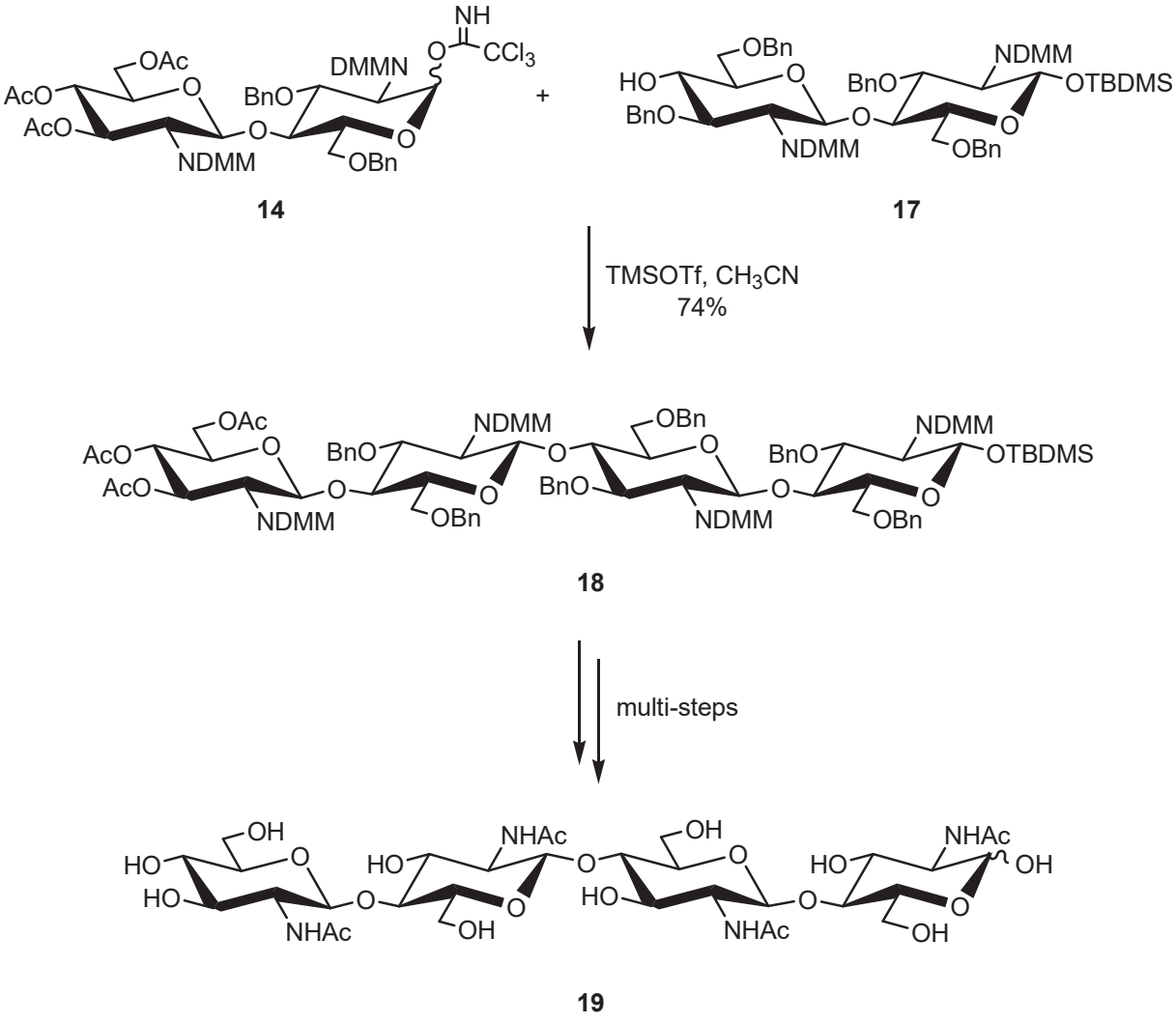

Figure 17: Chemical synthesis of per-*N*-acetylated chitotetrasaccharide 19 $(GlcNAc)_4$ [125].

b) Chemical synthesis of homo chitooligosaccharides with GlcN units

Kuyama *et al*. [126] developed a stereocontrolled synthesis of a chitododecasaccharide detailed in Figure 18 and Figure 19. First, Kuyama *et al*. described the synthesis of dimers **23**

and **24** from monosaccharide derivatives **20** and **21** (Figure 18). After that, the team described the synthesis of chitododecasaccharide **31** (Figure 19).

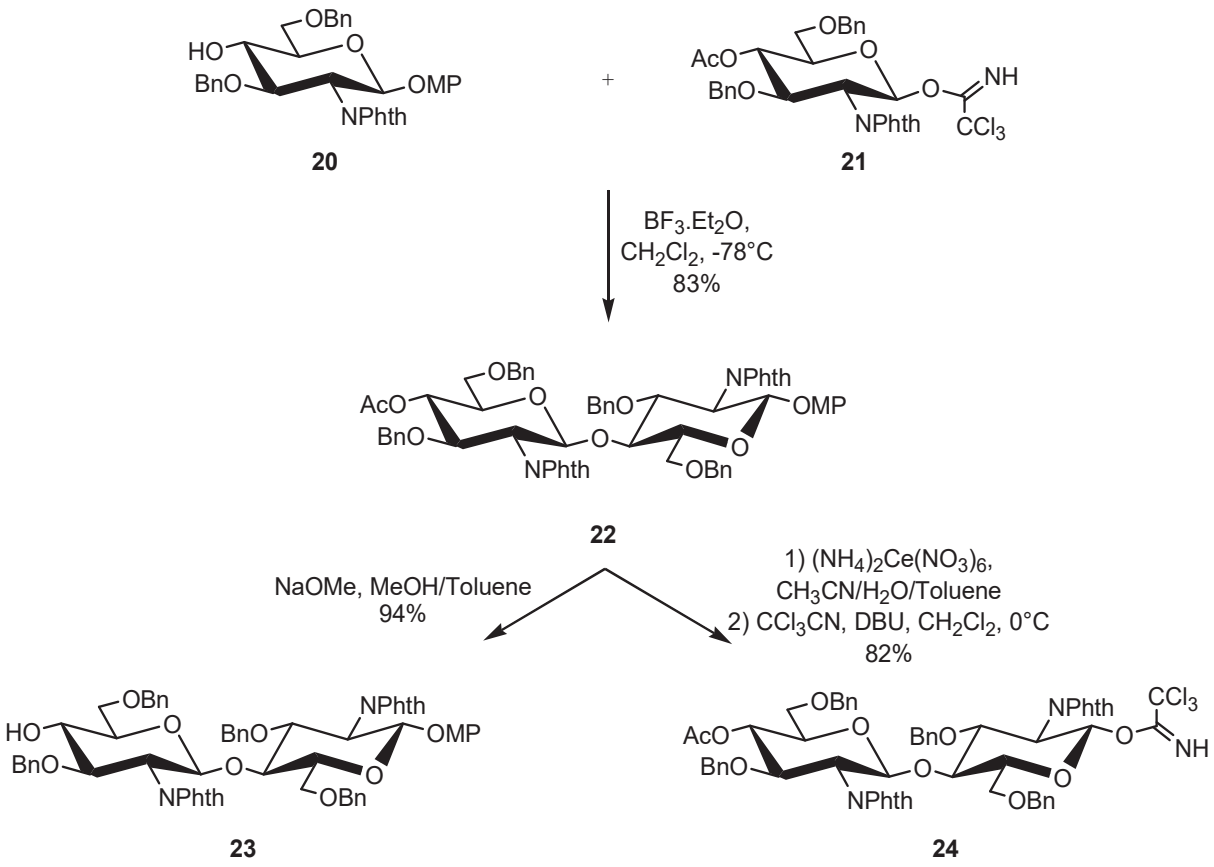

Figure 18: Chemical synthesis of two disaccharides intermediates 23 and 24 [126].

The glycosylation reaction of the two monosaccharides **20** and **21** in the presence of $BF_3.Et_2O$ in dichloromethane at -78°C leads to chitodisaccharide **22** with a yield of 83%. On the one hand, saponification of **22** conducted in the presence of sodium methanolate in methanol / toluene gave the product **23** in 94% yield. On the other hand, the deprotection of the anomeric alcohol of chitodisaccharide **22** by ammonium nitrate and cerium (IV), followed by the reaction of the hemiacetal obtained with CCl_3CN in the presence of DBU in dichloromethane at 0°C leads to compound **24** with a yield of 82%.

The coupling reaction in dichloromethane in the presence of $BF_3.Et_2O$ at -78°C between the previously synthesized compounds **23** and **24** leads to chitotetrasaccharide **27** in 75% yield

(Figure 19). Product **27** is deacetylated at the 4-position by reaction in LiOH / H_2O_2 / THF at 0°C to give compound **28** in quantitative yield. Then, the chitotetrasaccharide **28** is coupled with the disaccharide **24** in a mixture of dichloromethane/toluene in the presence of $BF_3.Et_2O$ at -78°C to form the chitohexasaccharide **29** with a yield of 62%. The acetyl group in the 4-position of the compound **29** is cleaved according to the same protocol as in the previous step and a new coupling with the disaccharide **24** leads to the chitooctosaccharide. The authors proceed as follows until the protected chitododecasaccharide is obtained. The latter is deprotected in two steps to lead to the target chitododecasaccharide **31** by the action of hydrazine in methanol at reflux and then by hydrogenolysis with an overall deprotection efficiency of 85%.

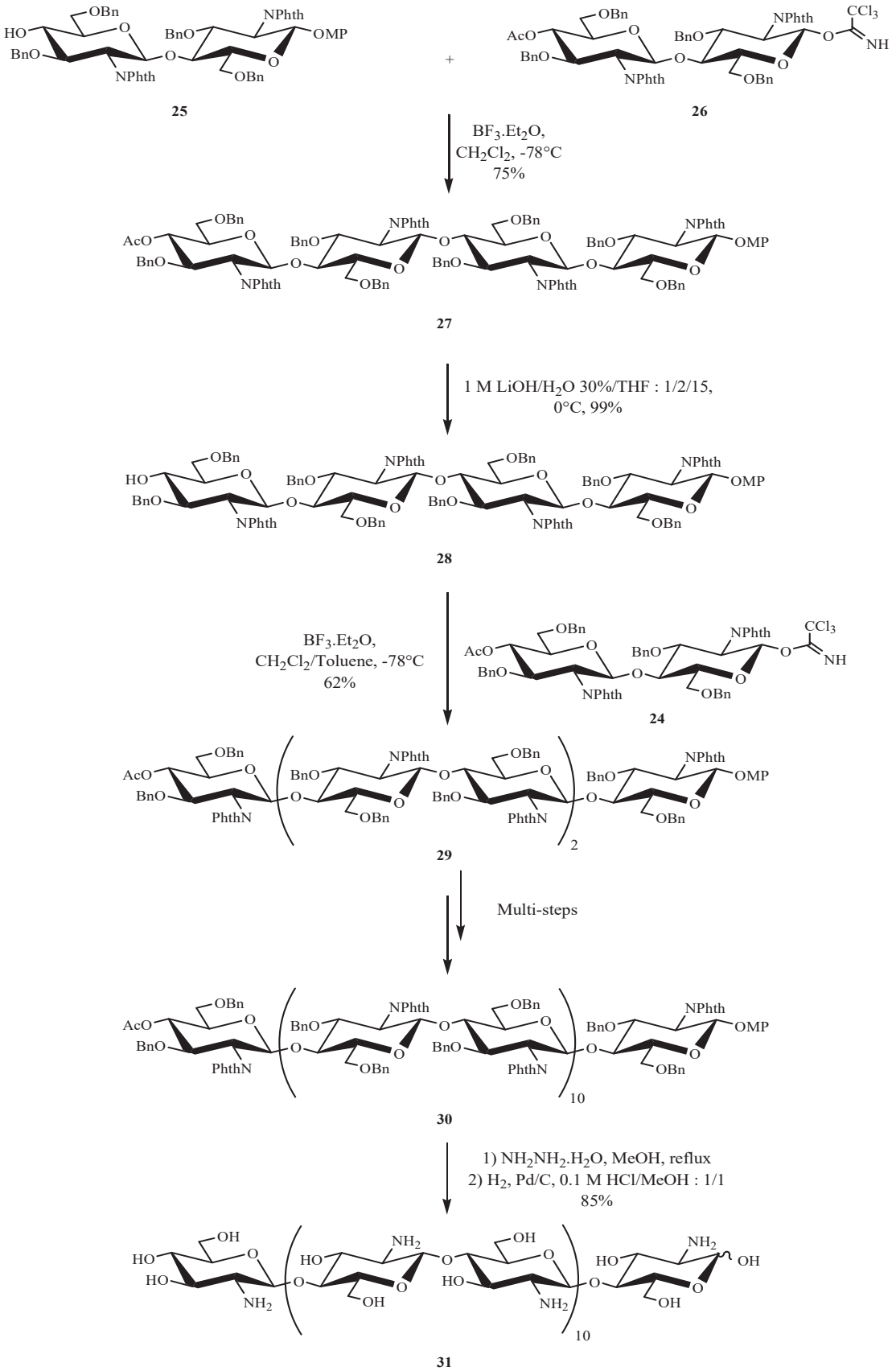

Figure 19: Chemical synthesis of chitododecasaccharide 31 $(GlcN)_{10}$ [126].

Huang *et al*. [129] developed a new "one-pot" glycosylation method for the synthesis of chitotetraose $(GlcN)_4$. The monosaccharides **32**, **33** and **34** described in Figure 20 are synthesized and serve as building blocks for the synthesis of the protected chitotetrasaccharide **35** (Figure 20). Reaction conditions are detailed in Figure 21.

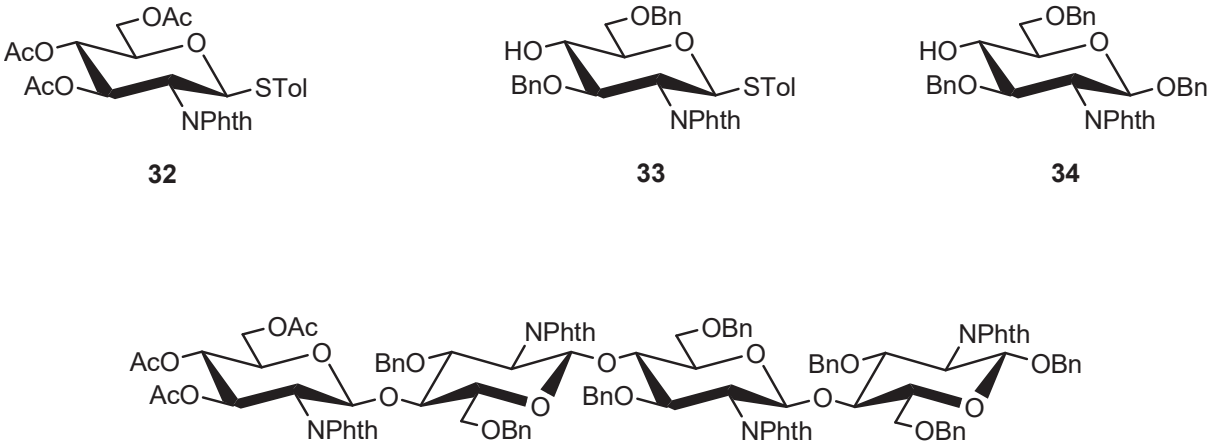

Figure 20: Chemical structures of building block 32-35 used for the synthesis of chitotetraose $(GlcN)_4$.

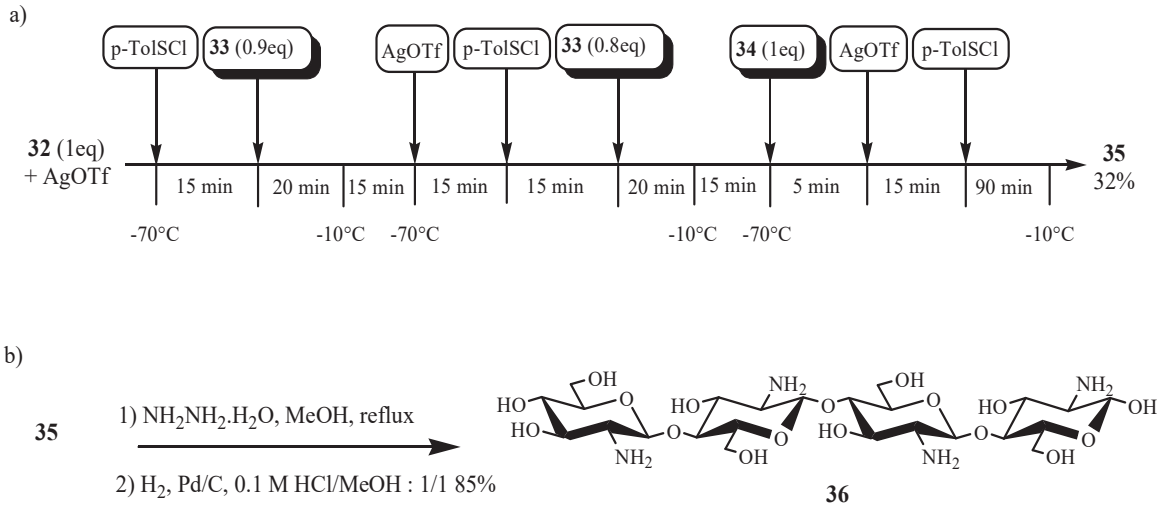

Figure 21: a) Reaction conditions for the synthesis of protected chitotetraose 35 b) Deprotection conditions for the synthesis of chitotetraose [36].

3.2.2.2. Chemical synthesis of hetero-chitooligosaccharides

Kawada *et al.*[131] reported the total synthesis of two hetero-COS, the disaccharide GlcN–GlcNAc and the tetrasaccharide $(GlcN–GlcNAc)_2$, using both phthalimido and azido groups for the protection of the free amino groups, as illustrated in Figure 22.

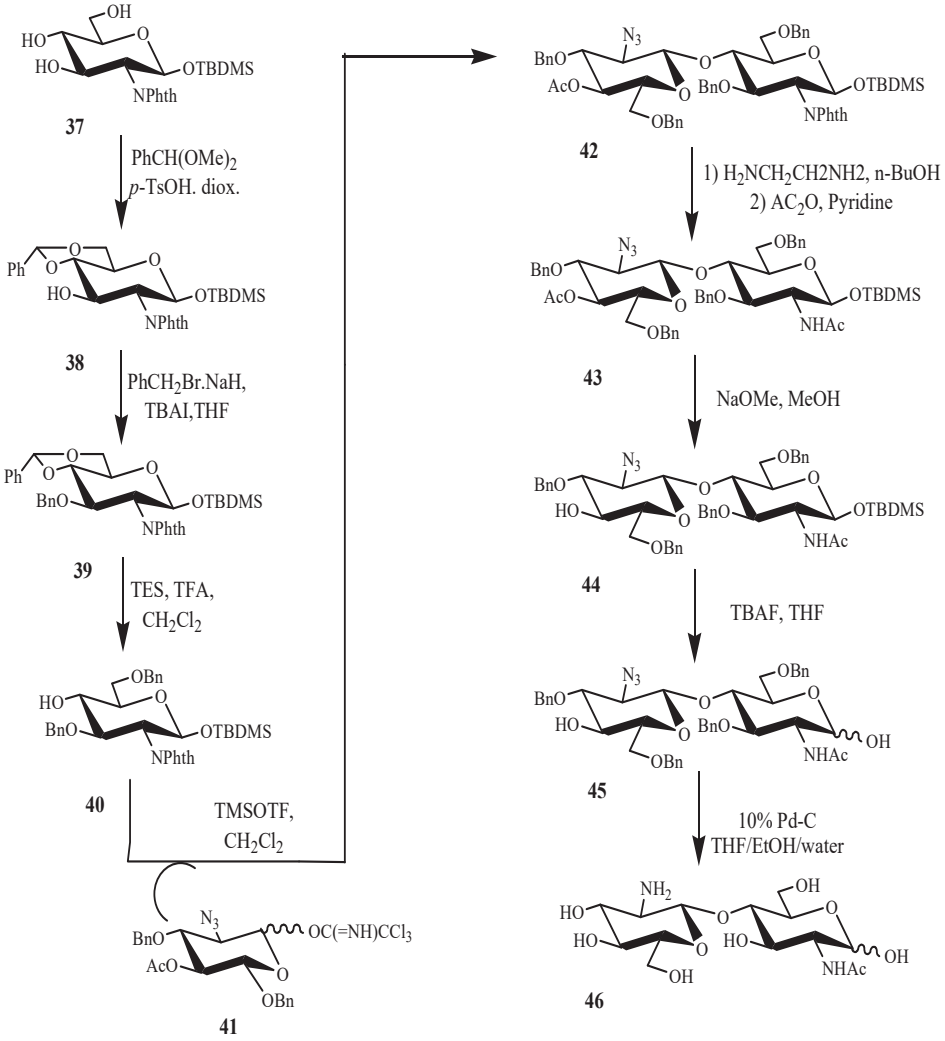

Figure 22: The synthetic route for the preparation of the repeating unit GlcN-GlcNAc dimer [131].

Moreover, the synthetic strategy developed by Issaree [133] and Barroca-Aubry *et al.*[134] allowed the synthesis of both homo- and hetro chitooligosaccharides. Issaree's thesis work [133] was based on the synthesis of homo- and hetero-chitobioses and hetero-chitotetraoses.

In this work dimethylmaleoyl and phthaloyl groups were used for protection of the amines. The donor was activated as the trichloroacetimide in order to form the β-linkages. Glycosylation in the presence of trimethylsilyl trifluoromethanesulfonate, followed by *N*- and *O*-deprotection furnished chitobioses and chitotetraoses in good yields. In addition to that, Barroca-Aubry *et al*. [134] described the synthesis of four well defined chitodisaccharides. The synthesis was carried out according to a strategy that paves the way to the elaboration of various homo- and hetero-chitooligosaccharides, with perfect control of the number and the position of GlcN and GlcNAc units along the oligomer chain Figure 23. This was performed by the use of N-trichloroacetyl (TCA) and N-benzyloxycarbonyl (Z) as C-2 protecting groups for acetamido and free amino groups, respectively. First, the assembly of well-defined COS requires the preparation of differentially protected glucosamine-based monosaccharide building blocks (Figure 23).

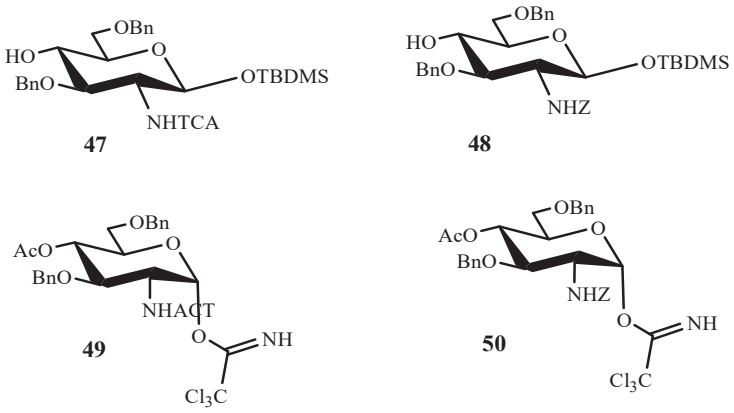

Figure 23: Protected glucosamine-based monosaccharide building blocks.

Each monosaccharide building block was used as a GlcNAc/GlcN acceptor (**47** and **48**, respectively) or a GlcNAc/GlcN donor (**49** and **50**, respectively) with a minimum number of transformation steps from the commercial D-glucosamine hydrochloride (Figure 24).

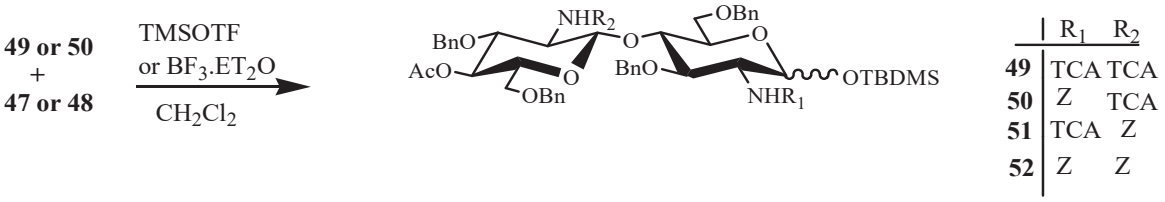

	R_1	R_2
49	TCA	TCA
50	Z	TCA
51	TCA	Z
52	Z	Z

Figure 24: Preparation of protected chitodisaccharides 49, 50, 51 and 52.

After the assembly of the oligosaccharide skeleton under perfect control, the next step consist in the complete deprotection of protected chitodisaccharides to afford four targeted chitodisaccharides **61**, **62**, **63** and **64** (Figure 25).

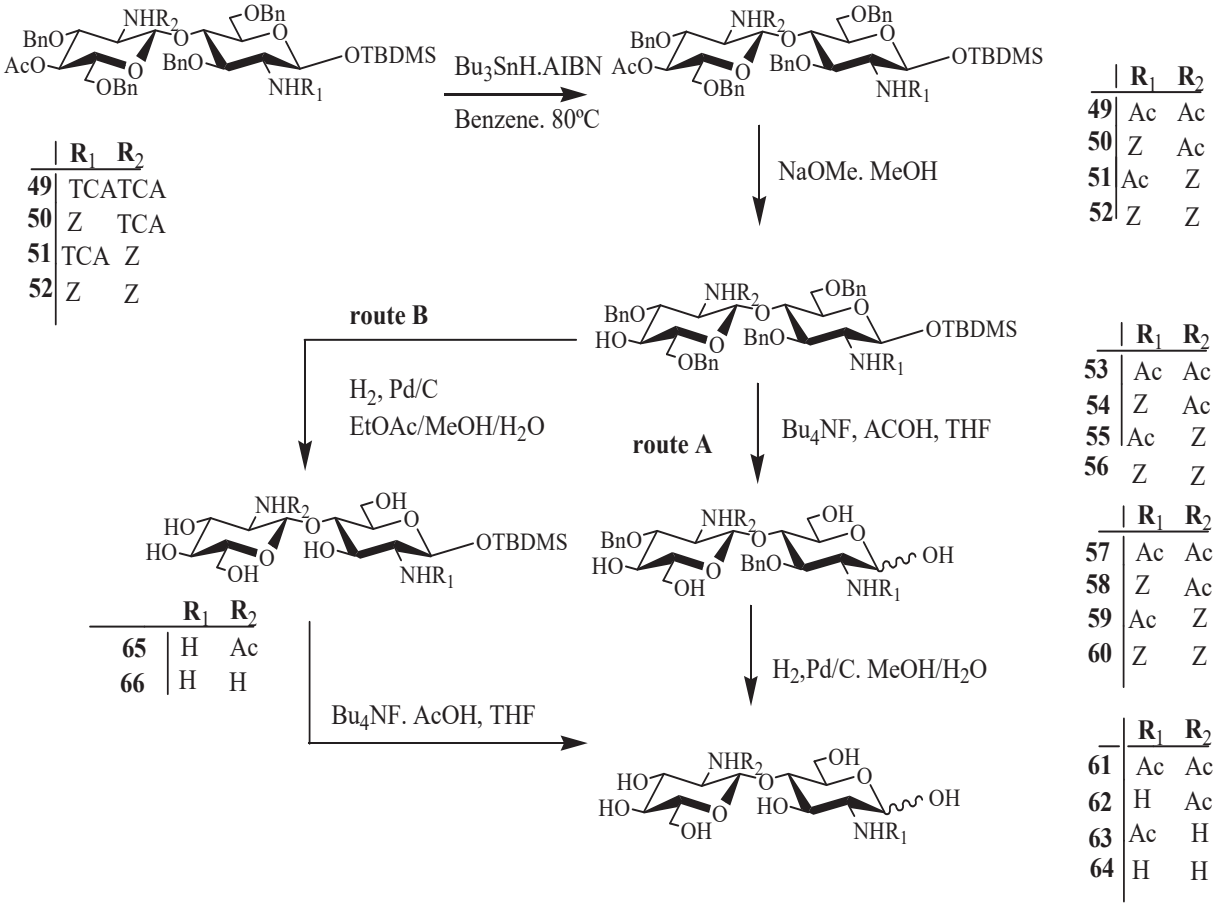

	R_1	R_2
49	TCA	TCA
50	Z	TCA
51	TCA	Z
52	Z	Z

	R_1	R_2
49	Ac	Ac
50	Z	Ac
51	Ac	Z
52	Z	Z

	R_1	R_2
53	Ac	Ac
54	Z	Ac
55	Ac	Z
56	Z	Z

	R_1	R_2
57	Ac	Ac
58	Z	Ac
59	Ac	Z
60	Z	Z

	R_1	R_2
65	H	Ac
66	H	H

	R_1	R_2
61	Ac	Ac
62	H	Ac
63	Ac	H
64	H	H

Figure 25: Deprotection reaction pathways leading to chitodisaccharides 61, 62, 63 and 64.

Barroca-Aubry *et al.* also demonstrated the synthesis of larger size COS. This was performed by converting any protected chitooligosaccharides previously synthesized into new donors or acceptors with a minimum number of reaction steps (Figure 26).

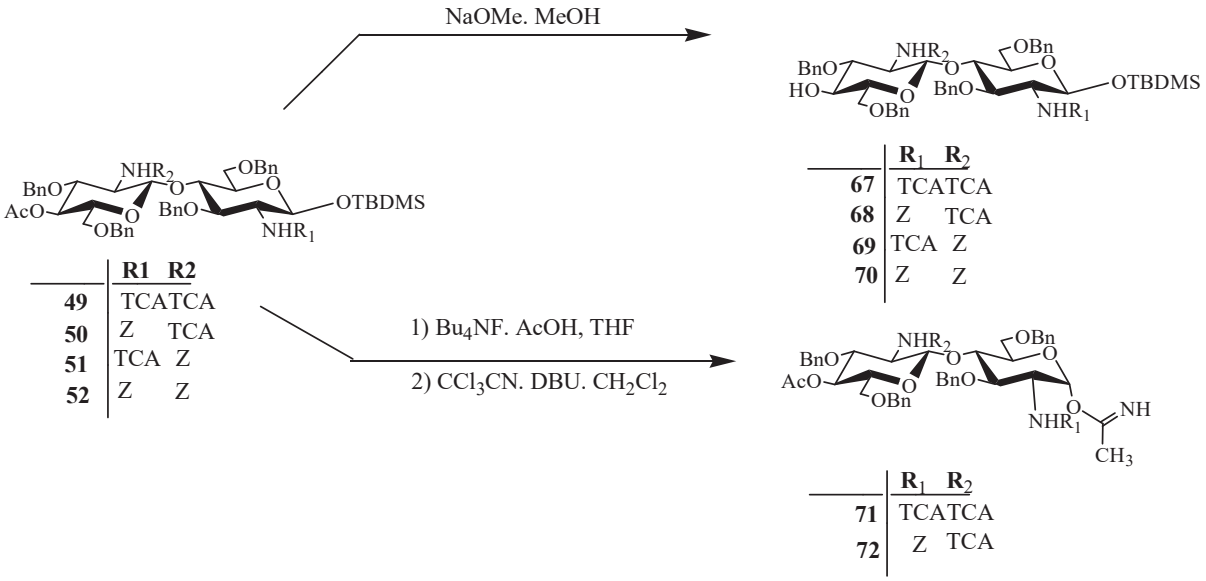

Figure 26: Chemical conversions of protected chitodisaccharides into new acceptors (67, 68, 69 and 70) and donors (71 and 72).

In order to test the synthetic route for the well-defined COS elaboration, disaccharide **67** was used to synthesis a trisaccharide (Figure 27).

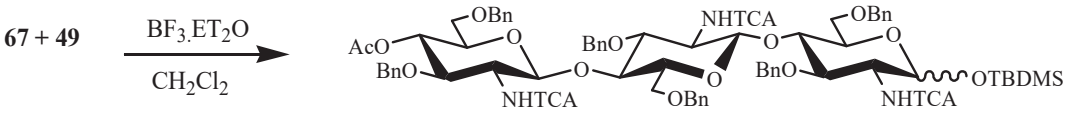

73

Figure 27: Synthesis of the protected chitotrisaccharide 73.

3.3.Conclusion for the preparation of chitosan oligomers

Several methods are reported in the literature to prepare chitooligosaccharides. They can be grouped in two large parts: firstly the preparation by depolymerization of chitin and chitosan, and secondly by chemical or enzymatic synthesis. Methods of depolymerization of chitin or

chitosan can be carried out chemically, enzymatically or physically. They have the advantage of starting from an easily accessible product and allow chitooligosaccharides to be obtained rapidly and in a few steps. Chemical methods for depolymerizing chitin and chitosan such as acid hydrolysis, acetolysis, fluorohydrolysis or nitrous deamination result most of the time in random cleavage of the glycosidic bond. Although under certain conditions it is possible to improve the control of the molar mass of chitooligosaccharides obtained (nitrous deamination method by adjusting the amount of nitrous acid). For other methods, generally it is very difficult to control the degree of polymerization and mixtures of chitooligosaccharides with relatively wide dispersity are always obtained. Chromatographic methods make it possible to separate the chitooligosaccharides but these techniques require a lot of time and the yields obtained are very low. In addition, unless a starting *N*-acetylation degree of 0 or 100% is achieved, it is not possible to obtain a controlled degree of *N*-acetylation after cleavage. An average degree of *N*-acetylation can nevertheless be easily determined by NMR analysis. Compared to chemical depolymerization, the enzymatic depolymerization of chitin and chitosan has the advantage of producing chitooligosaccharides with a better control of the value of DP and more rapidly under milder reaction conditions. This path also makes it possible to perform specific cleavages. In contrast, the preparation of enzyme as the purification of the product requires heavy work and this process is not easily adaptable at the industrial level. It is also a costly method, although more affordable enzymes have shown their ability to cleave glycosidic linkages between the D-glucosamine and *N*-acetyl-D-glucosamine units. The third depolymerization pathway for chitin and chitosan involves physical techniques such as gamma irradiation or sonication. By adapting the experimental parameters it is possible to determine the degree of polymerization of the chitooligosaccharides obtained. On the other hand, the degree of *N*-acetylation still cannot be controlled.

The chitooligosaccharides can be prepared by the reverse path, which is to say by synthesis. Two pathways have been studied: enzymatic and chemical. Unlike depolymerization, synthesis allows control of the degrees of polymerization and *N*-acetylation. As regards the enzymatic synthesis, the control of these parameters requires a very important work of isolation and purification of the enzymes to obtain a very low yield. The cost of such a path can be very important. Many examples of preparation of chitooligosaccharides by chemical synthesis are reported. This is the method of choice for preparing chitooligosaccharides with

controlled degrees of polymerization and *N*-acetylation. But these syntheses requires multiple protection and deprotection steps and most methods existing today are time consuming and require extensive use of organic solvents and lead in most cases to homo-chitooligosaccharides. This is why it is not considered as a routine procedure.

4. Preparation methods for the reacetylation of chitooligosaccharides

As mentioned before, chitosan is the only naturally occurring cationic polysaccharide at acidic pH and its pKa ranges from 6.3 to 6.7 when the DA increases from 0 to 60 %. [5, 6]. The solubility of chitosan highly depends on the DA. Thus, finding methods to acetylate chitooligosaccharides are important, in particular in the objective to control the degree of *N*-acetylation and ideally the *N*-acetylation sequence. Two main methods were used to acetylate chitooligosaccharides, the chemical method and enzymetic method.

4.1.Chemical *N*-acetylation of chitooligosaccharides

The *N*-acetylation reaction was first discovered by Hirano and Yamaguchi in 1976 [135], who described the way to partially acetylate chitosan gels. This study was updated by others for the *N*-acetylation of chitooligosaccharides [46, 76, 136, 137]. Such as, Trombotto *et al*. [76] described the production of a homogeneous series of well-defined chitooligosaccharides varying in DA from 0 to 90%. This was achieved by dissolving GlcN oligomer mixture in methanol/water (50:50, v/v) followed by the addition of a fresh acetic anhydride in a stoichiometric amount to reach the desired DA. This method was also applied to acetylate chitopentaose $(GlcN)_5$ to produce $(GlcNAc)_4(GlcN)_1$, ajusting the solvent ratio methanol/water to (90:10, v/v) by Abla *et al*. [138]. In addtion to that, Abla *et al*. tested the influence of the acytelation by using three different acetylating agents, acetic anhydride, acetyl chloride and pentafluorophenyl acetate (PFPA). Their results show that the best *N*-acetylation efficiency was found with acetic anhydride. This specificity is due to the low stability of acetyl chloride and PFPA in aqueous medium that leads to their hydrolysis before reacting with amino groups of chitopentaose, leading to a very low *N*-acetylation degree.

4.2.Enzymatic *N*-acetylation of chitooligosaccharides

Tokuyasu *et al*. studied the preparation of partially acetylated chitooligosaccharides by using a chitin deacetylase [119, 120, 139]. In their study, the team found that the chitin deacetylase from *Colletotrichum lindemuthianum* can serve as an acetylating agent in the presence of 3.0 M sodium acetate [119]. In details, Tokuyasu *et al*. described the preparation of $(GlcNAc)_3(GlcN)_1$ from the *N*-acetylation of $(GlcN)_4$ by using a chitin deacetylase from *Colletotrichum lindemuthianum* ATCC 56676 [139]. This was performed by dissolving $(GlcN)_4$ in 3.0 M sodium acetate (pH 7.0) followed by the addition of a purified chitin deacetylase. The reaction mixture was incubated at 37°C for 16 h and at the end, the reaction mixture was purified again by cation-exchange column chromatography. Following the same protocol, this team also reported the *N*-acetylation of $(GlcN)_2$ to produce (GlcNAc)(GlcN) [119]. On the other hand, the enzyme chitin deacetylase was also used by several teams to hydrolyze the acetamido group in the *N*-acetylglucosamine units of chitin, thus generating glucosamine units and acetic acid (deacetylation of chitin) [140-143]. In order to increase the efficiency of the enzymatic deacetylation for the production of chitosans, chitins were "modified" either physically or chemically [142]. Thus, Win *et al*. [143] reported the enzymatic deacetylation of chitin using chitin deacetylase isolated from *Absidia coerulea*. In details, chitin with DA 90% and molecular weight of 2×10^5 was dissolved in 100 ml methanol with 83% calcium chloride dihydrate and 2% glucose (w/v). A very fine suspension of chitin called superfine (SF) chitin was obtained by drop wise addition of methanol. Then SF chitin was treated with 18% formic acid for 2hr at room tempreture then incubated with 0.15 AU purified *Absidia coerulea* chitin deacetylase at a pH 4.0 and at 50°C in a shaking incubator (150 rpm). In this way chitin (DA 90%) was deacetylated by the enzyme into chitosan with DA of 10%. However, the formic acid treatment reduces the molecular weight of the polymeric chain from 2×10^5 in chitin to 1.2×10^4 in the chitosan product. A major draw-back in chitin deacetylases was and still to simplify the harsh chemical conversion process of chitin into chitosan, which more or less not environmentally friendly. Such deacetylated chitins may not be 'randomly' deacetylated and contain a fingerprint of the used deacetylase, that can be studied from the structure of the COS obtained by enzymatic depolymerization [144]. This field is in strong development.

4.3.Conclusion for the *N*-acetylation of chitooligosaccharides

Two methods were reported for the *N*-acetylation of chitooligosaccharides, the enzymatic method and the chemical method. The chemical method was used widly due to facilty and low cost of this method, whereas, the enzymetic method has advantageous characteristics yielding unique compounds such as GlcN-GlcNAc. It allows a regioselective *N*-acetylation that is hard to achieve by chemical *N*-acetylation. However it is a costly method, and is not easily adaptable at the industrial level.

5. Other chemical modifications of chitooligosaccharides

New or improved properties of COS can be obtained by grafting various functional groups to COS backbone due to the existence of reactive hydroxyl and amino groups. Recently, importance has been given to synthesize functionalized COS by chemical modifications with the aim to improve the bioactivities of COS, while keeping intact the basic chemical properties. More studies could be found dealing with the synthesis of modified COS via *N*-substitution, less often through *O*-substitution and rarely through the aldehyde function of reducing-end units.

5.1.Modifications via *N*-substitution

N-substitution modifications result from a reaction with the amino groups of COS. Several studies investigated this type of modification, for example, conjugation of COS with phenolic compounds, sulfation, carboxylation and quaternary ammonium group gained an interest in the medicinal applications. Below are some examples.

Conjugation of COS with phenolic compounds, gained an interest in the medicinal applications. Phenolic acid have the ability to donate H-atom, which will enhance the antioxidant activity of conjugated COS. Eom *et al.* [145] conjugated phenolic acids to COS via amide coupling reaction. They used eight different kinds of phenolic acids with different substitution groups such as, hydroxybenzoic acid, p-coumaric acid, protocatechuic acid, caffeic acid, vanillic acid, ferulic acid, syringic acid and sinapicic acid. Synthesized conjugated oligomers were characterized by UV, FT-IR and ^{1}H NMR spectroscopy. Phenolic acid conjugated chitooligosaccharides showed similar UV spectrum due to the absorption of

aromatic ring present on them, indicating that phenolic acids were conjugated onto the COS successfully. Likely, the synthesis of gallic acid conjugated COS was also reported by Vo *et al*. [50] and Ngo *et al*. [146]. COS (3-5 kg/mol) was conjugated to gallic acid that leads to enhancement of antioxidant and anti-inflammatory properties (Figure 28).

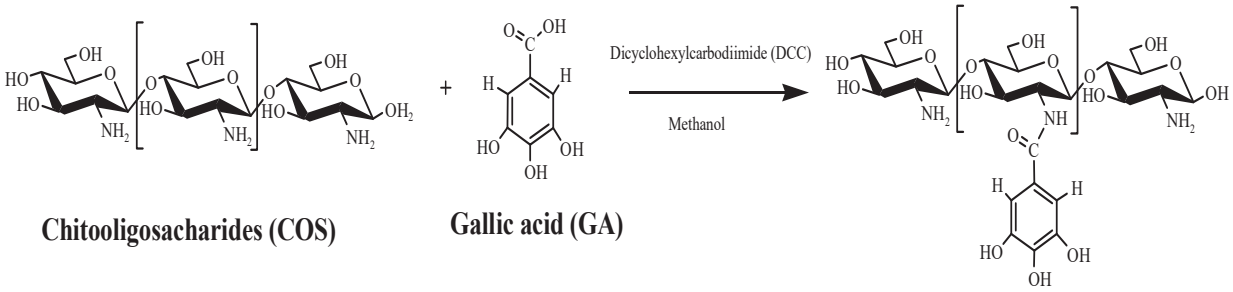

Figure 28: Synthesis of gallate-chitooligosaccharides [50].

On the other hand, the synthesis of sulfated COS has attracted much attention in biomedical field due to their antimicrobial, antiHIV-1, and heavy metal complexation activity. *Je et al.*[147] studied the inhibition of modified COS by prolyl endopeptidase (PEP) which digests small peptide-like hormones and neuroactive peptides that would cause neurodegenerative disorders. For that, Je *et al*. team performed the sulfation reaction by the addition of anhydrous sodium carbonate and trimethylamine-sulfur trioxide to COS at 65°C for 12h. Sulfated COS (SCOS) were obtained in over 90% yields as white and water-soluble with degree of substitution of 0.76. In this study different molar masses of COS and degree of *N*-acetylation (DA; 10%, 25%, and 50%) were used to synthesize SCOS (Figure 29). Their results show that the 50% degree of *N*-acetylation SCOS (50-SCOS) exhibit higher inhibitory activities against PEP compared to other degree of *N*-acetylation. In parallel when comparing the different molar mases for 50-SCOS (50-SCOS I, 5 000–10 000 g/mol; 50-SCOS II, 1 000–5 000 g/mol; 50-SCOS III, below 1 000 g/mol), 50-SCOS II possessed the highest inhibitory activity with an IC_{50} value close to 0.38 mg/ml. Another way to synthesize sulfated COS was proposed by Lu *et al*. [148]. This was performed by using chlorosulfuric acid/pyridine method to obtain COS with different degree of substitution 0.8 and 1.9 having a molar mass of 8.0–10 $\times 10^3$ g/mol. Their results show that the antioxidant properties of SCOS hold great potential for the oxidative diseases treatment. This study also suggested that

increased degree of substitution could contribute to enhance the defense mechanisms against H_2O_2-induced oxidative damage in MIN6 cells.

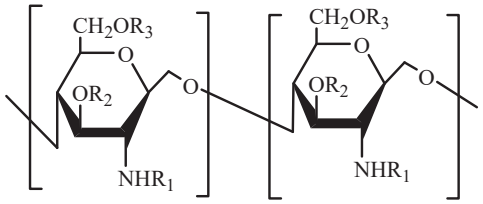

R_1= $COCH_3$ or SO_3H **R_2= H or SO_3H** **R_3= H or SO_3H**

Figure 29: Chemical structure of sulfated chitooligosaccharides synthesized by Lu *et al*.[148].

In addition to above functionalizations, carboxylated COS (CCOS) has also attracted attention. Rajapakse *et al*.[13] used succinic anhydride to synthesize carboxylated COS. In their study, COS of DA 27 % and molar mass $6.0–7.0\times10^3$ g/mol were used to accomplish this coupling by adding methanol to a solution of COS in 10% acetic acid. Then different amounts of succinic anhydride dissolved in acetone was added dropwise at room temperature for 1 h, to obtain CCOS with different substitution degrees of $–COCH_2CH_2COO^-$ groups (Figure 30). The substitution degree were assessed as 0.36 (CCOS-1), 0.69 (CCOS-2) and 0.89 (CCOS-3). Rajapakse *et al*. results show that CCOS exerted a dose-dependent inhibitory effect on MMP-9 in human fibrosarcoma cell line (HT1080). They also observed that reduction in MMP-9 expression was due to downregulation of MMP-9 transcription that was mediated via inhibition of AP-1 (activator protein-1) and this inhibition of MMP-9 expression led to inhibition of tumor invasiveness.

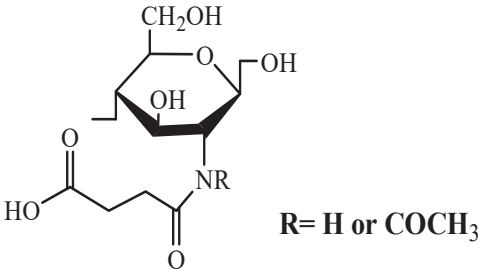

R= H or $COCH_3$

Figure 30: Chemical structure of carboxylated chitooligosaccharides [13].

In addition to the above mentioned studies, Trinh *et al.* [149] synthesized 4 hydroxybenzyl-COS (HB-COS) by mixing COS of molar mass 1.0–3.0×10^3 g/mol (DP 6-20) with 4-hydroxybenzaldehyde in water/ethanol mixture with 1% acetic acid to form Schiff base. These mixed compounds of various DP and substitution degree were evaluated their anti-inflammatory activity in Chang liver cells lines. Their results indicate that HB-COS can contribute to the suppression of inflammatory responses in Chang liver cells lines and might be a potential candidate for novel inhibitor of hepatodegenerative diseases (Figure 31).

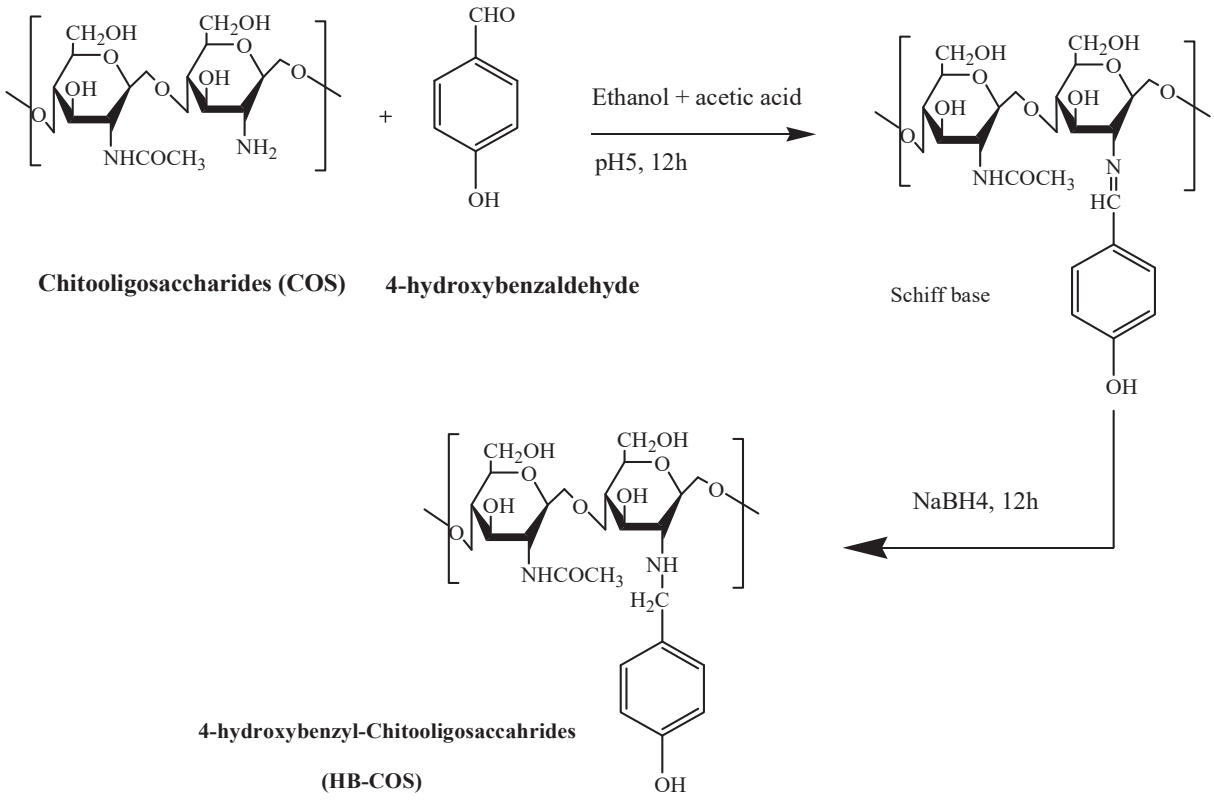

Figure 31: Chemical modifications of chitooligosaccharides with 4-hydroxybenzaldehyde [149].

Also, Kim *et al.* [23] were interested in the introduction of a quaternary ammonium group to COS of DA 13% and composed of dimer 2.31 mol%, trimer 12.53%, tetramer 15.11%, pentamer 13.59%, hexamer 8.86%, heptamer 6.46%, octamer 8.87%, nonamer or higher 32.27 mol%. This was done by coupling of glycidyl trimethylammonium chloride (GTMAC) to COS in aqueous solution. In details the reaction was performed under nitrogen purging at

70°C for 3–24 h then poured into acetone/ethanol (50/50, v/v) mixture to obtain the precipitate (COS-GTMAC) (Figure 32). At the end the product is filtrated, washed with acetone several times and dried at room temperature. Their result showed that antimicrobial activity of the COS was considerably enhanced by the introduction of quaternary ammonium functionality.

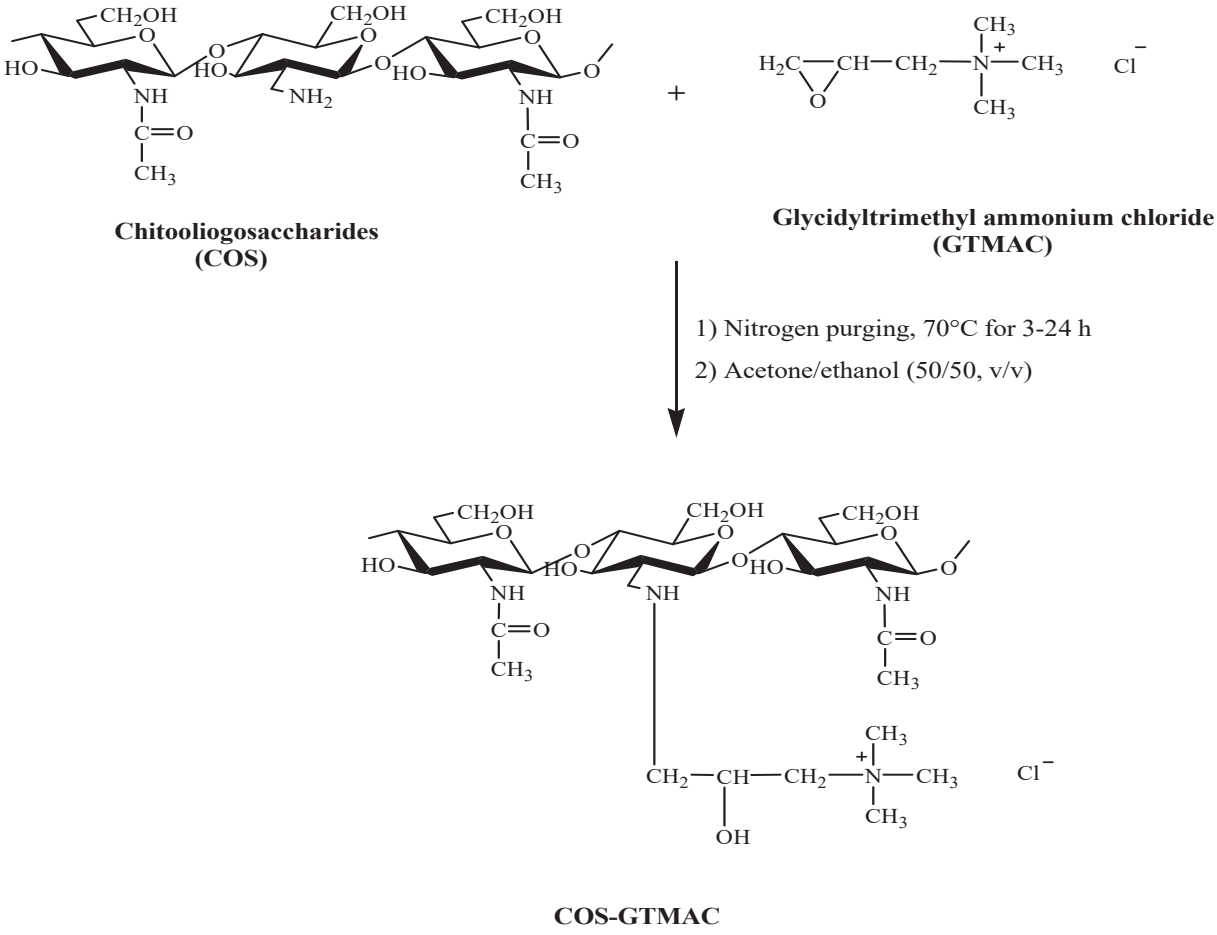

Figure 32: Synthesis of COS-GTMAC from glycidyl trimethylammonium [23].

Finally, Marzaioli *et al*.[150] produced glucosamine oligomers with the amino functions transformed into azido groups in order to be used lately for click chemistry reactions. In their study they depolymerized chitin in aqueous HCl solution having *N*-acetylation degree 90% and molar mass of 612 kg/mol to obtain chitooligosaccharides of mean DP 5. After, these oligomers were dissolved in 0.5 M AcOH/AcONa buffer and reduced by the addition of $NaBH_4$ at room temperature overnight. Then it was chemically modified. This was performed

by solubilizing the glucosamine oligomers in 1M phosphate buffer together with $CuSO_4 \cdot 5H_2O$ and imidazole-1-sulfonyl azide hydrochloride. The mixture was stirred at room temperature for 3h. The obtained structures are as shown in Figure 33.

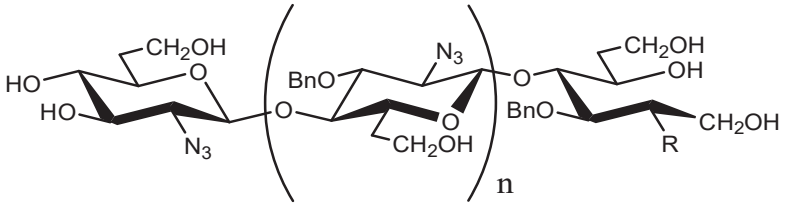

1: n = 0, R= N_3
2: n = 1, R= NH_2
3: n = 1, R= NHAc
4: n = 1, R= N_3
5: n = 2, R= NH_2
6: n = 2, R= NHAc
7: n = 2, R= N_3
8: n = 3, R= N_3
9: n = 4, R= N_3

Figure 33: Structure of the different azide glucosamine oligomers.

5.2.Modifications via *O*-substitution

O-substitution reactions imply bonding of small molecules or polymers on the hydroxyl groups of COS. The modified COS can have new properties with sustaining its cationic oligomer electrolyte character.

Ngo *et al*. [151] investigated the inhibitory effects of aminoethyl-chitooligosaccharides (AE-COS) on oxidative stress in mouse macrophages (RAW 264.7 cells). Chitooligosaccharides with Mw 800–3 000 g/mol (DP 4-20) and degree of *N*-acetylation DA 10%, was dissolved in an aqueous 3.0 M (20 ml) 2-chlorethylamino hydrochloride and stirred at 40°C. NaOH (3.0 M, 20 ml) was added to the reaction mixture drop wise, with continuously stirring for 48h the reaction is shown in Figure 34. Then, the solution was filtered using a filter paper. Subsequently, the reaction mixture was acidified with 0.1N HCl, and dialyzed against water for 2 days. The product was freeze dried to give AE-COS.

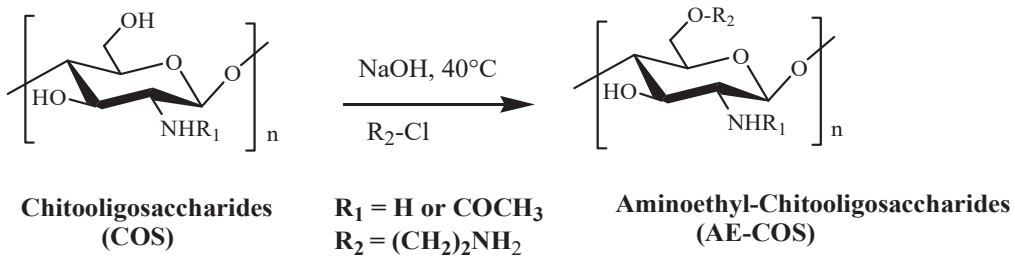

Figure 34: Synthesis pathway of aminoethyl-chitooligosaccharides (AE-COS) [151].

Ngo *et al*. have performed two other studies in which they described the importance of AE-COS [152] [153]. The first [152] aim to investigate in more details the inhibitory effects mechanism of AE-COS on oxidative stress in mouse macrophages (RAW 264.7 cells). Their result suggest that AE-COS acts as a potential free radical scavenger in RAW 264.7 cells. As for the second study [153] The aim was to investigate the antioxidant and anti-inflammatory activities of AE-COS in murine microglial cells (BV-2). They showed that AE-COS possess potential antioxidant and anti-inflammatory activities in brain microglia and could be a useful in therapeutic agent for the treatment of neuroinflammatory diseases. Important point to mention that in both studies the synthesis of AE-COS was performed following the same protocol as described in Figure 34.

5.3.Modifications via the aldehyde group at the reducing-end unit

a) Modifications via masked aldehyde

This type of modification deals with the masked aldehyde that is formed during equilibration reaction of reducing end of COS with water [154]. In an interesting study, Guerry *et al*. [154], described several syntheses. First they focused on the synthesis of chitooligosaccharides conjugates by incorporation of a functional group (alkyne) through reductive amination at the reducing end (Figure 35). This was done by dissolving chitooligosaccharides with a DP 5 in an aqueous ammonium acetate buffer. Then, propargylamine (2.5 mmol) and 2-azidoethylamine (0.25 mmol) respectively for product **74** and **75** along with aniline (0.25 mmol) were dissolved in aqueous ammonium acetate buffer (50 mM, pH 5.0). The mixture was stirred for 5 min at room temperature, and sodium cyanoborohydride (160 mg, 2.5 mmol) was added. The solution was stirred for 4 days at 40°C (Figure 35). As for the synthesis of product **76**, chitooligosaccharides and 4-

propargyloxyaniline were dissolved in acetate buffer at room temperature, after 5 min sodium cyanoborohydride was added and the solution was stirred for 4 days at 40°C (Figure 35).

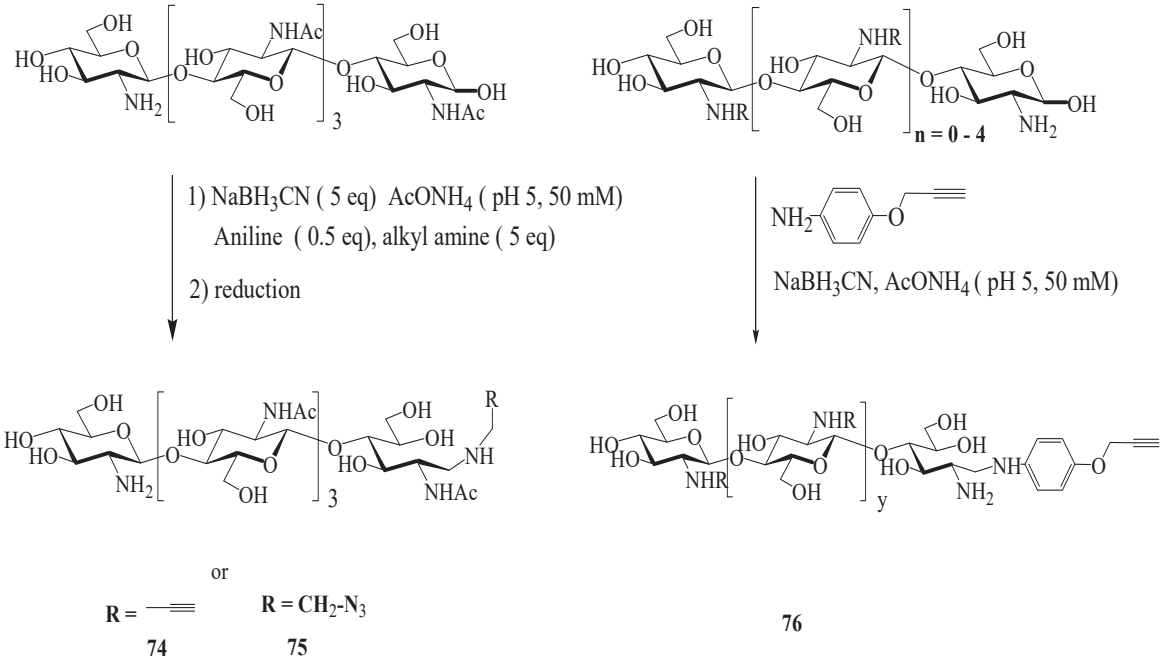

Figure 35: 1) Synthetic pathway of chitopentaose−Alkyne Conjugate 2 or 3 by aniline – mediated reductive amination of tera-*N*-acetyl-chitopentaose, 2) Reductive amination of chitosan oligosaccharides with alkyne-modified aniline.

In the second part of synthesis, the reactivity of these conjugates (**74** and **76**) is studied for the synthesis of COS based copolymers. For that, two reactions have been performed. The first one deals with the preparation of chitopentaose-based FRET probe from product **74** and the second deals with the preparation of poly (caprolactone)-*graft*-COS from product **76**. All reaction conditions are detailed in Figure 36.

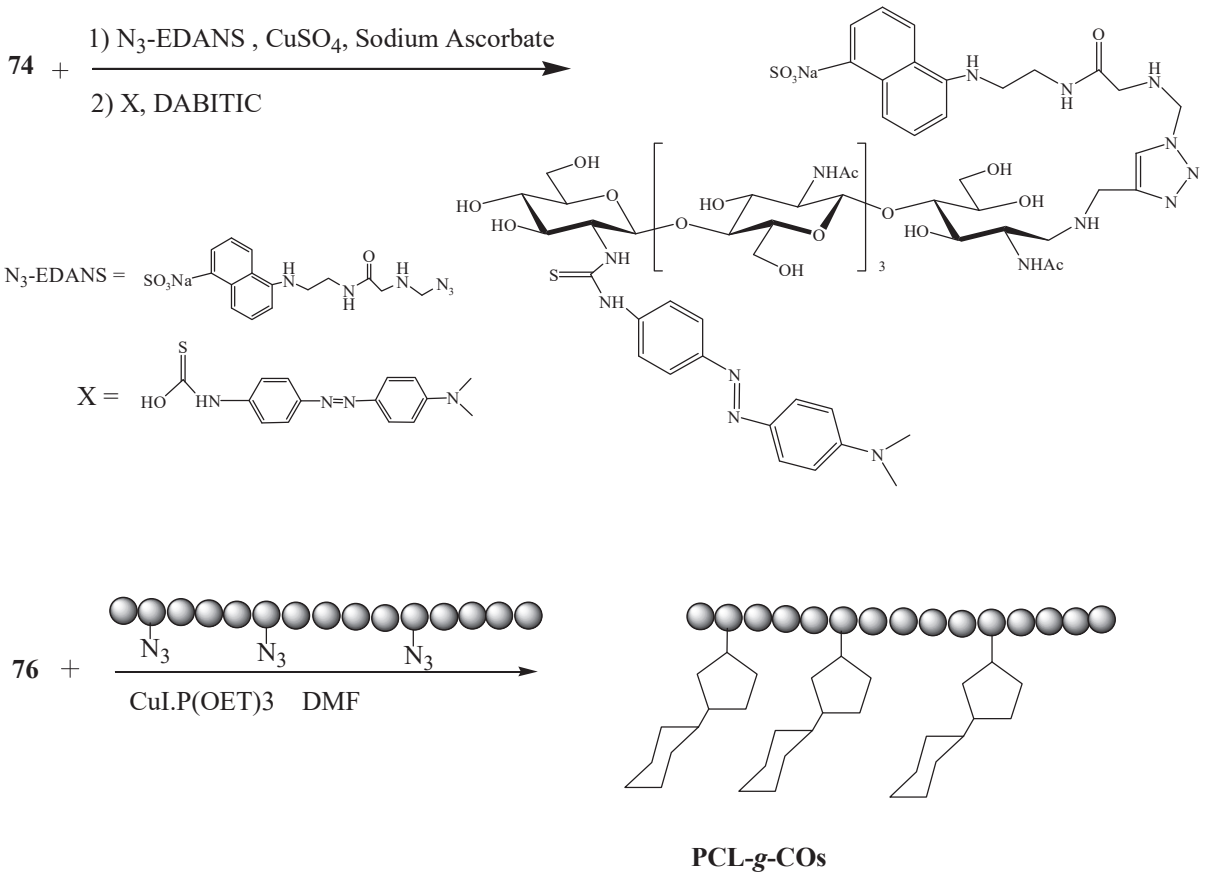

Figure 36: 1) Synthesis of chitopentaose-based FRET probe from 74 2) Preparation of Poly(Caprolactone)-graft-COS Copolymer by click conjugation from 76 [154].

b) Modifications via the aldehyde moiety of 2,5-anhydro-D-mannofuranose unit

These types of modifications using the aldehyde group that is formed after the nitrous acid depolymerization of COS. The obtained COS bears an aldehyde group at their reducing end. Previous studies were performed in relation with these types of modifications [155-157] including studies already published by our team [158-160].

In 2015, Pickenhahn *et al.* [156] developed thioacetylation of COS end groups for nanoparticle gene delivery systems. This was performed in several steps. First COS was formed using nitrous acid depolymerization of a chitosan with DA of 8% and Mw = 200 kg/mol, to a mean molar mass of 1 kg/mol to give equilibrium forms **77** and aldehyde-hydrated or gem-diol form in water **78**. Second the COS aldehyde react directly with a thiol-bearing model molecule (b-mercaptoethanol and 3-mercaptopropionic acid, BME and MPA

respectively) to form a hemithioacetal intermediate (**79**). Finally, by a schiff base formation where the equilibrium displacement occurs by water removal, the hemithioacetal can be stabilized into the corresponding thioacetal (**80**) by freeze-drying (Figure 37).

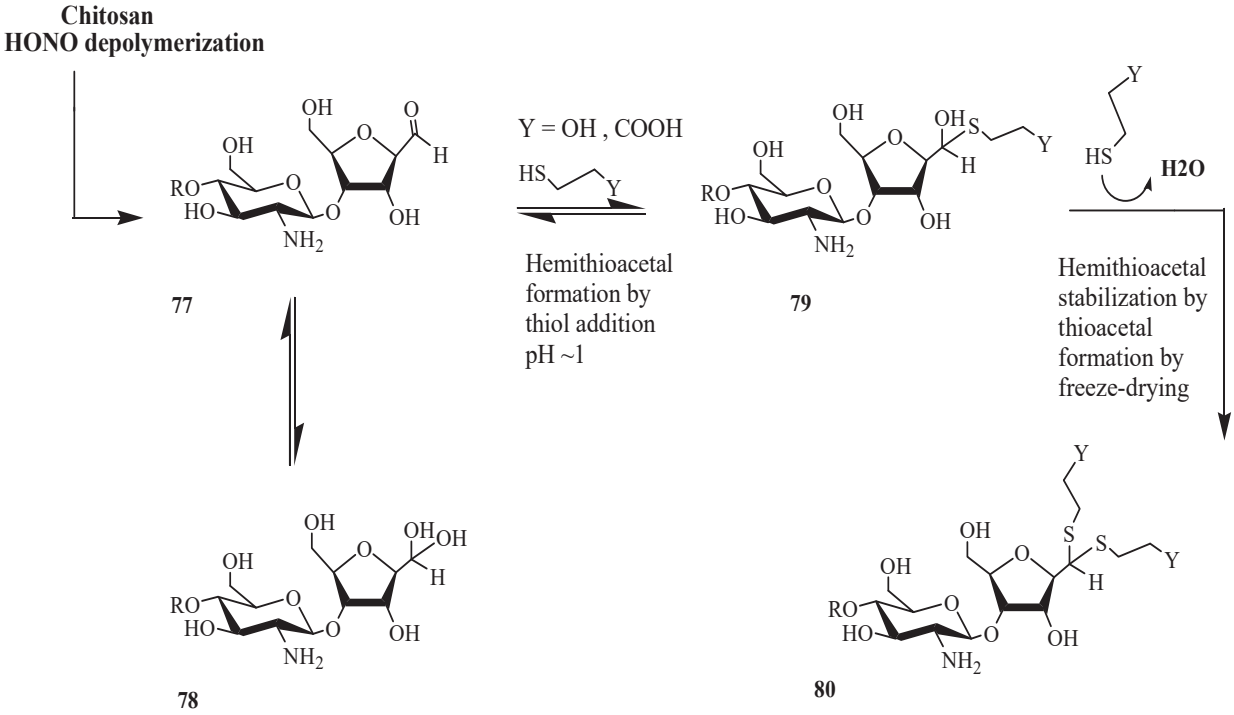

Figure 37: Schematic representation of the COS end-group thioacetylation.

In a second study 2017, Pickenhahn *et al.*[155] developed a novel COS end-group thioacetylation approach relying on a new regioselective linker that bears three thiol moieties. This trivalent linker is referred to as triskelion. This was performed in several steps. First the depolymerization of chitosan (COS; 8% DA, Mw = 200 kg/mol) with nitrous acid (HONO), to obtain a COS mix with Mw 2–4 kg/mol. Second, the trivalent linker **81**, leads to the formation of **82** by promoting the thiol-hook attack on the COS aldehyde. Finally, The terminally-activated COS (*i.e.* the COS-*b*-triskelion adduct) can freely react with any thiol-reactive species or structure through its remaining thiol-tail, as represented in **83** (Figure 38).

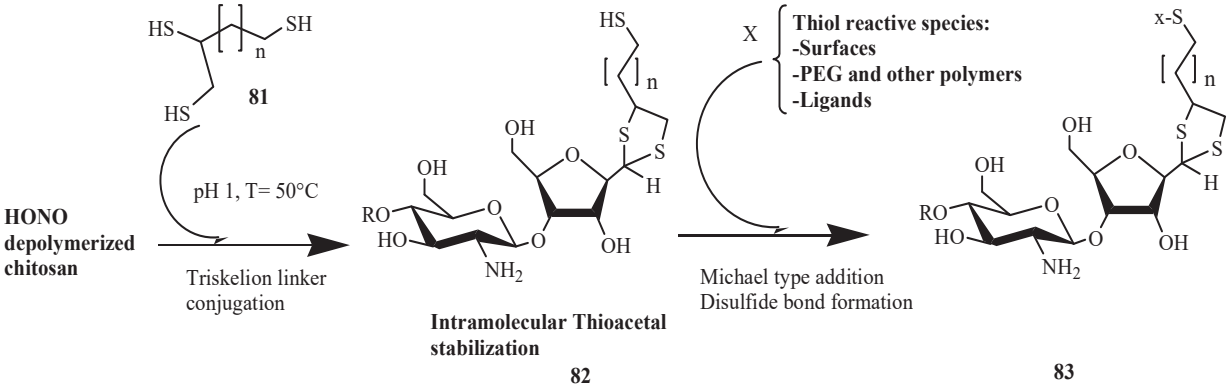

Figure 38: Schematic representation of the COS end-group thioacetylation.

In addition, Carballal *et al*. [157] showed that the oxime click reaction is a straightforward methodology for the synthesis of polyethylene glycol (PEG)-polysaccharide diblock copolymers. This method was applied to un-modified polysaccharides with a reductive end such dextran, hyaluronic acid and chitosan. Specifically for chitosan, the team first described the nitrous acid depolymerization of chitosan with intial Mw = 53 600g/mol and DA 1% to obtain COS of 4 to 10 kg/mol with 2,5-anhydro-D-mannofuranose end group free aldehyde at the reducing end. Then, COS was dissolved in AcOH 0.5% w/v and MeO-PEG-ONH2 (2 or 5 kg/mol, 5 Eq.) was dissolved in DMSO (50 mg/mL). Both solutions were mixed and stirred at 45ºC. The solution was dialyzed against ethanol until the excess MeO-PEG-ONH2 was eliminated. A molar mass cut off of 50 kg/mol was used to remove PEG 2 kg/mol and 100 kg/mol to remove PEG 5kg/mol (see Figure 39).

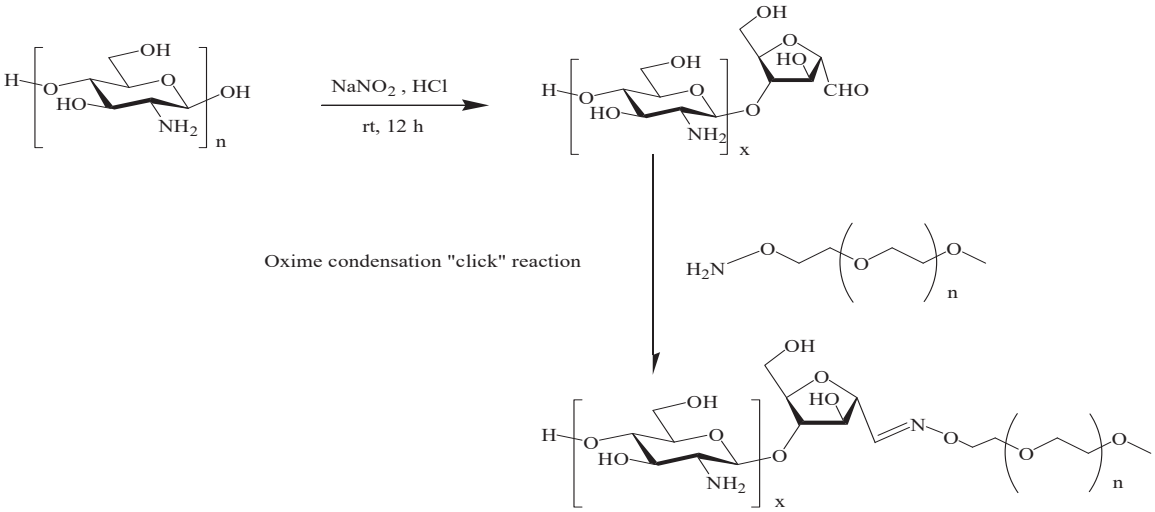

Figure 39: Approach proposed for the COS-b-PEG synthesis [157].

5.4.Conclusion for the modifications of chitooligosaccharides

Several methods are reported in the literature to modify chitooligosaccharides. These studies mainly focus of mixes of oligosaccharides with different DPs and DAs. They can be grouped in two parts: firstly, modifications of the backbone of COS, this was either via *N*-substitution or *O*-substitution, and secondly, modifications via the reducing end, this included masked or unmasked aldehyde. All types of modifications have advantages in improving the scope of chitooligosaccharide properties. *N*-substitution modifications were the most widely used method. Phenolic, gallic, sulfated and carboxylated acid were used widely in improving the properties of chitooligosaccharides in medical and pharmaceutical fields. However, these types of modifications will decrease the number of amine moieties over the COS backbone. *O*-substitution modifications of COS have not been described extensively, however, some studies have shown that these types of modifications can add new properties with sustaining COS properties as a cationic polymer electrolyte. Finally, reducing end modifications for both masked and unmasked aldehyde is gaining much interest since this type of modifications can be used to attach various functional groups and obtain amphiphilic and zwitterionic structures. Progresses in this area are quite rapid and the developed derivatives of chitooligosaccharides seem to exhibit an unlimited application range, although the commercial applications require a robust preparation scheme and absence of toxic residues.

6. Conclusions

In this chapter, we have detailed the diverse biological properties of chitooligosaccharides, highlighting the strong potential of this family of saccharides. They could find many applications in the fields of medicine, pharmacy, agriculture, food industry or even cosmetics. In addition, we have detailed several methods used to depolymerize chitosan to obtain chitooligosaccharides. These methods include both the depolymerization of chitosan and the syntheses including chemical, physical and enzymatic methods have their own drawbacks and advantages. Finally, we finished by showing the possible methods used to modify chitooligosaccharides including *O*-substitution, *N*-substitution and reducing end modification. Studies are still rare in this field but are showing a promising future in terms of the biological applications of the obtained conjugates. Based on this bibliographic search, we have seen that varying both the size and structure of oligomers would affect the biological interest. We have

also seen that optimizing the modifications conditions could lead to chitooligosaccharides with a better control in structure, a key aspect in this field.

In this context, we decided first to synthetize chitooligosaccharides with a good (ideally: 'perfect') control of DP and DA parameters, this will be described in chapter 2. Second, we want to study the effect of these two parameters and their influence on different biological applications: this will be discussed in chapter 3. Finally, we will focus on developing a strategy allowing the synthesis of modified chitooligosaccharides with a 'perfect' (as perfect as possible) control of chemical structure.

Chapter II

Synthesis and characterization of well-defined chitooligosaccharides structures

Introduction

Chitooligosaccharides have received much attention for their properties exploitable for diverse applications such as pharmaceutics and medicine [60], agriculture [61], food industry [62] (as antimicrobial agents, preservatives) and in cosmetic fields [63, 64]. Previous studies showed that by changing the degree of polymerization (DP) or degree of *N*-acetylation (DA), this will have a direct effect on the targeted application.

Our goal in this chapter is to present the synthesis of chitooligosaccharides with a perfectly defined chemical structure that is to say in practice with defined degrees of polymerization and *N*-acetylation. The synthesized chitooligosaccharides will be tested for the synthesis of supermagnatic particles and to be tested as a potential candidates in neurobiology to impact the perineuronal net formation around neuronal-like cells. For that, we will describe the synthetic strategy to obtain chitooligosaccharides with different degrees of polymerization, from 4 to 45 and with different degrees of *N*-acetylation from 0 to 85%.

In details, the first part of this work is dedicated to the elaboration of partially *N*-acetylated chitooligosaccharides with DP 4 and DA ranging from 0 till 85%. For this task, we focused on the *N*-acetylation of the commercially chitotetraose hydrochloride as starting material. In the second part of this work, the aim is to synthesize chitooligosaccharides with different degrees of polymerization from 10 to 45, by means of the nitrous acid depolymerization of a fully *N*-deacetylated chitosan, then to prepare various partially *N*-acetylated reduced chitooligosaccharides from DA 0 till 45%.

1. Synthesis and characterization of partially *N*-acetylated chitotetraose oligomers

In this part, we will describe the synthesis of partially *N*-acetylated chitotetraose oligomers from DA 0 till 90% by *N*-acetylation of commercially chitotetraose hydrochloride (GlcN, HCl)$_4$. In more details, herein we will report four main parts: (i) the objective and the strategy of the synthesis; (ii) the characterization of the (GlcN, HCl)$_4$ starting material; (iii) the method to synthesize partially *N*-acetylated chitotetraose oligomers; and (iv) their structural characterization.

1.1. Objective and strategy of the synthesis

The synthesis strategy under mild conditions involved the *N*-acetylation of a commercially starting material chitotetraose (GlcN, HCl)$_4$ by using an acetylating agent (Figure 40). The acetylation reaction was performed in a manner where the number of acetylated amine groups varies with the amount of the acetylating agent used. Herein we report the specific reaction parameters used to obtain chitotetraose oligomers with different degrees of *N*-acetylation along with different characterization techniques used to analyze chemical structures of the final reaction products.

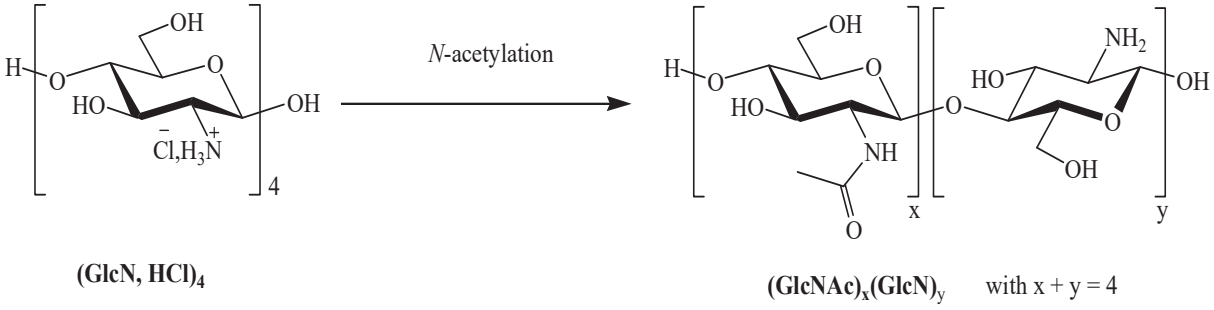

Figure 40: Synthesis strategy for the preparation of partially *N*-acetylated chitotetraose oligomers by controlled *N*-acetylation of commercial chitotetraose hydrochloride (GlcN, HCl)$_4$.

1.2. Characterization of the starting material chitotetraose hydrochloride $(GlcN, HCl)_4$

Chitotetraose used as starting material in this part was commercialized by TCI company ((Reference C2641 (XPM7D-RP)) in the hydrochloride form which is its stable form. In order to confirm its chemical structure and to determine its quality, a series of analyses has been performed.

1.2.1. Characterization by ^{1}H NMR spectroscopy

Firstly, ^{1}H NMR spectroscopy analysis was performed by solubilizing the commercial chitotetraose hydrochloride in D_2O in the presence of 0.5% (v/v) of concentrated HCl (12N). The data analysis and the attribution of different signals of the ^{1}H NMR spectrum of the commercial chitotetraose hydrochloride was deduced from ^{1}H NMR data of GlcN and GlcNAc oligomers, as reported by Sugiyama *et al*. [161]. Figure 41 represents the ^{1}H NMR spectrum of the commercial chitotetraose hydrochloride and shows clearly the presence of signals corresponding to the $(GlcN,HCl)_4$ oligomer: (i) H_1 protons of GlcN units at 4.85 ppm, in addition to the presence of the H_1 proton of the GlcN unit at the reducing end with a doublet signal at 5.45 ppm having a coupling constant J = 3.7 Hz that represents the alpha anomer and a doublet signal at 4.95 ppm having a coupling constant J = 8.7 Hz which represents the beta anomer (note that the alpha/beta anomer ratio which was calculated from the integration value, found to be around 60:40); (ii) H_3 to H_6 protons of GlcN units from 3.50 to 4.10 ppm and (iii) H_2 protons of GlcN units at 3.15 ppm, in addition to the presence of the H_2 proton of the GlcN unit at the reducing end at 3.05 ppm for the beta anomer and at 3.35 ppm for the alpha anomer. Moreover, the integration sum for H_1 protons and H_2 protons were both found to be equal to 4, when calbritating the integration sum of H_3 to H_6 protons around 20.

We can conclude that the proton NMR analysis confirmed the chemical structure of the chitotetraose hydrochloride sample, due to the presence of characteristic signals that were in complete agreement with literature data published by Sugiyama *et al*. [160] for the $(GlcN,HCl)_4$ oligomer. In addition, the integration sum for H_1, H_2 and H_3 to H_6 confirmed the presence of four GlcN repetitive units that correspond to the expected tetramer structure.

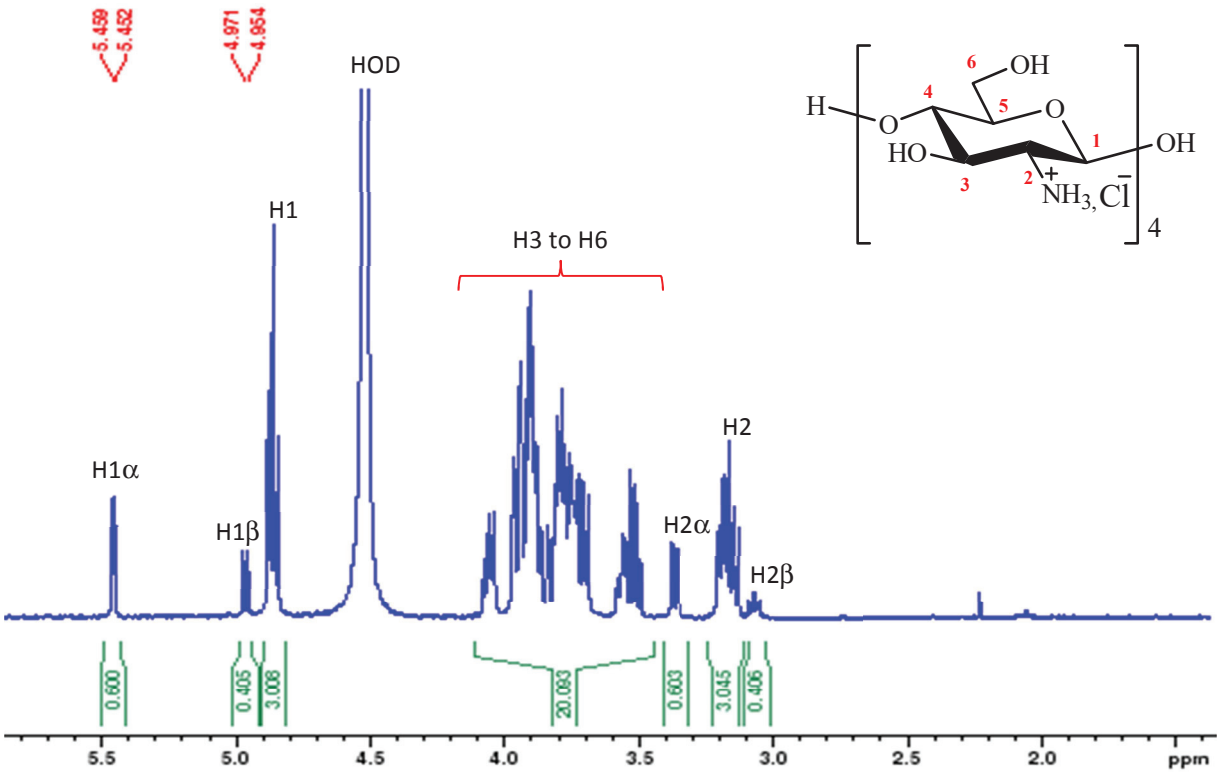

Figure 41: ^{1}H NMR spectrum (500 MHz, 321 K) of commercial chitotetraose hydrochloride $(GlcN,HCl)_4$ in D_2O with 0.5% (v/v) of HCl (12N).

1.2.2. Characterization by MALDI-TOF mass spectrometry

MALDI-TOF mass spectrometry was also performed to confirm the chemical structure of the commercial chitotetraose hydrochloride and to identify if other oligomer species present eventually in the starting material. Figure 42 represents the MALDI-TOF mass spectrum of commercial chitotetraose hydrochloride and Table 1 summarizes Figure 42 by showing all the possible peaks along with their expected molecular formula, assignments and adducts. In Figure 42 and Table 1, a high intensity peak (3) at *m/z* 685.3 along with a low intensity peak (2) at 663.3 *m/z* were attributed to the oligomer $(GlcN)_4$ with both adduct Na and H, respectively. In addition, low intensity peaks (1) at *m/z* 524.2, (4) at *m/z* 846.4 and (5) at *m/z* 888.4 were also detected and identified as oligomers with Na adducts, namely $(GlcN)_3$, $(GlcN)_5$ and $(GlcN)_4(GlcNAc)_1$, respectively.

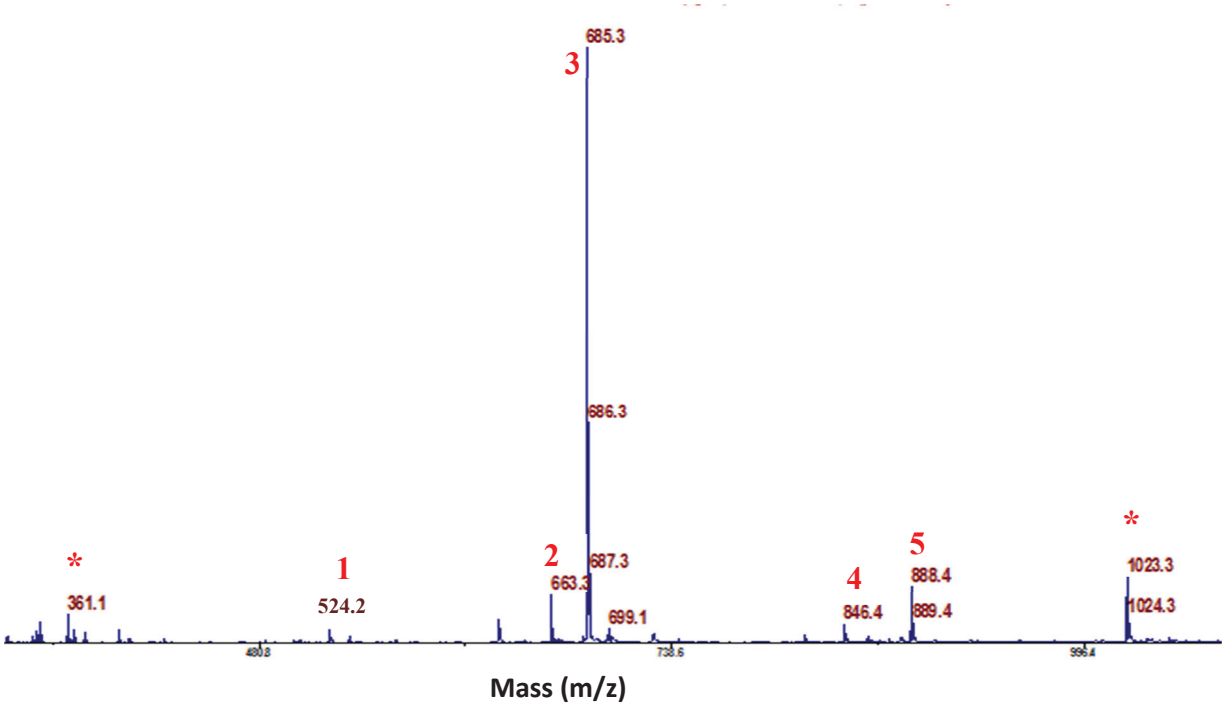

Figure 42: MALDI-TOF mass spectrum (reflectron, positive mode) of commercial chitotetraose hydrochloride (GlcN, HCl)$_4$ (peak numbers 1 to 5 are assigned in Table 1; peaks denoted by an asterisk (*) are due to the DHB (2,5 Dihydroxybenzoic Acid) matrix used for the analysis).

Table 1: Analysis of the MALDI-TOF mass spectrum of commercial chitotetraose hydrochloride (GlcN, HCl)$_4$.

Peak Nb	Mass/charge ratio *(m/z)*	Molecular formula	Assignment	Adduct
1	524.2	$[C_{18}H_{34}O_{13}N_3+Na]^+$	$(GlcN)_3$	Na
2	663.3	$[C_{24}H_{45}O_{17}N_4+H]^+$	$(GlcN)_4$	H
3	685.3	$[C_{24}H_{45}O_{17}N_4+Na]^+$	$(GlcN)_4$	Na
4	846.4	$[C_{30}H_{56}O_{21}N_5+Na]^+$	$(GlcN)_5$	Na
5	888.4	$[C_{32}H_{58}O_{22}N_5+Na]^+$	$(GlcN)_4(GlcNAc)_1$	Na

As a conclusion, this MALDI-TOF MS analysis confirmed that the oligomer $(GlcN)_4$ is the major component of the commercial chitotetraose hydrochloride sample, as previously shown by the ^{1}H NMR analysis. In addition, the MALDI-TOF MS analysis highlighted the presence of 3 other oligomers, $(GlcN)_3$, $(GlcN)_5$ and $(GlcN)_4(GlcNAc)_1$, in very small proportions compared to the oligomer $(GlcN)_4$.

1.2.3. Characterization by HPLC

HPLC analyses were also performed in order to determine the quality of the commercial chitotetraose hydrochloride. According to the literature, several methods were developed to detect the glucosamine monomer $(GlcN,HCl)_1$ using HPLC method [162-165]. For example, Yu Shao *et al*. [165] used an amino functionalized column, Phenomenex Luna (150 mm x 4.6 mm, 5 µm particle size) and acetonitrile/phosphate buffer (2 mM, pH 7.5) as a mobile phase for the detection of $(GlcN,HCl)_1$ at a wavelength 195 nm and a flow rate 1.5 mL/min. However attempts at using this method did not achieve a good separation for GlcN oligomers with higher DP such as $(GlcN,HCl)_4$. For that, our aim was to develop a simple and validated method to detect glucosamine oligomers with high DP, specifically for DP 4. During the method development, several chromatographic conditions were tested in order to optimize the mobile phase, the flow rate and the column type. Various mobile phases were tested: water:methanol (9:1, 8:2, and 7:3, v/v), water:acetonitrile (9:1, 7:3, and 5:5, v/v), buffer:acetonitrile (9:1, 7:3, and 5:5, v/v) including different buffer types (acetate buffer (pH 4.5), carbonate buffer (pH 7 and pH 10) and phosphate buffer (pH 7 and pH 10)). Several flow rates were also tested 0.8, 1.0, 1.5, and 2 mL/min. Also several column types were tested: amide functionalized column such as TSKgel Amide-80, amino functionalized column such as shodex Asahipak and ionic type such as SP-STAT ion exchange. Better results were obtained when using an amino functionalized column, shodex Asahipak (NH2P-50G-4A, 250 mm x 4.6 mm, 5 µm particle size) pretreated over one night with (i) phosphate buffer (0,02M, pH 10) then with (ii) CH_3CN/H_2O (70:30, v/v) for 30 min before the injections. After the pretreatment, the mobile phase used during the analysis was CH_3CN/H_2O (70:30, v/v) with a flow rate of 1 mL/min. Based on the MALDI-TOF MS analysis that revealed the presence of oligomers $(GlcN)_3$, $(GlcN)_5$ and $(GlcN)_4(GlcNAc)_1$ next to $(GlcN)_4$, our first attempts was to determine the exact retention time for commercial glucosamine oligomers from DP 1 till DP 6. For that, 10 mg/mL of commercial glucosamine oligomers $(GlcN, HCl)_x$ from DP 1 till DP 6 (References and company informations are found in the Experimental details part, 4.1) solubilized in CH_3CN/H_2O (70:30, v/v) were analyzed using the chromatographic conditions previously described. Figure 43 shows a superposition of chromatograms for commercial glucosamine oligomers from DP 1 till DP 6. The superposed chromatogram shows major peaks at retention times around 5.7, 7.4, 9.2, 11.3 and 14.1 min that correspond to $(GlcN, HCl)_1$ $(GlcN, HCl)_3$ $(GlcN, HCl)_4$ $(GlcN, HCl)_5$ and $(GlcN, HCl)_6$, respectively. These results

will be used as a reference for the analysis of the commercial chitotetraose hydrochloride sample.

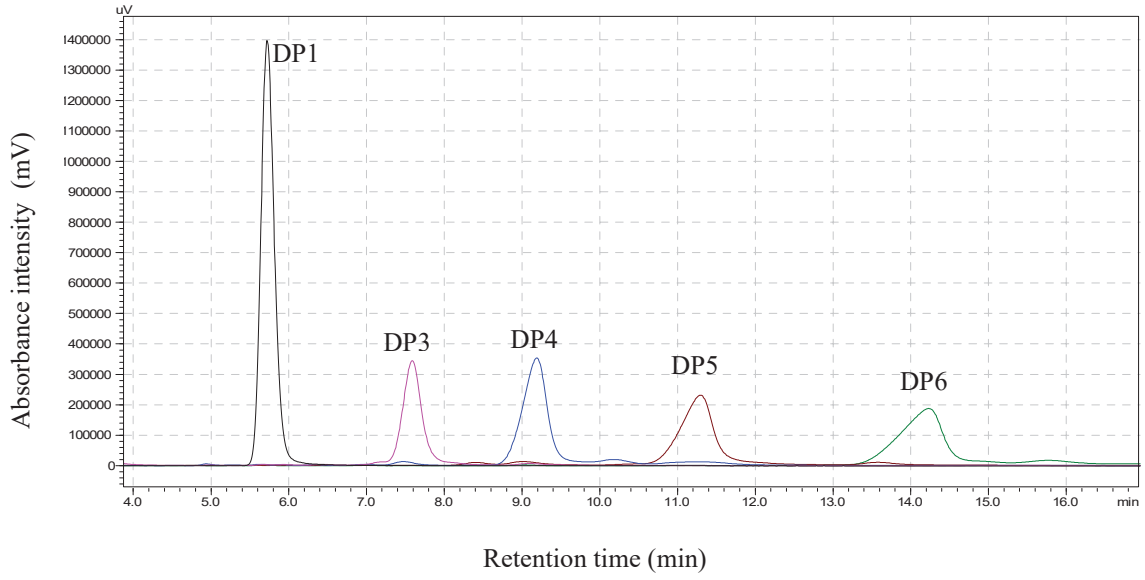

Figure 43: HPLC chromatograms of 10 mg/mL of glucosamine oligomers (GlcN, HCl)$_x$ from DP 1 till DP 6 solubilized in Acetonitrile/H_2O (70:30, v/v), using amino functionalized shodex Asahipak NH2P-50G-4A column, UV detection (λ = 195 nm), and eluted with CH_3CN/H_2O (70:30, v/v) for 20 min with a flow rate of 1 mL/min at RT.

Specifically for the commercial chitotetraose hydrochloride sample, the corresponding chromatogram is given in Figure 44 and its analysis is detailed in Table 2. The chromatogram in Figure 44 shows a major peak (2) at 9.2 min that correspond to the oligomer (GlcN, HCl)$_4$ along with two other minor peaks (1) at 7.4 min and (3) at 11.3 min that correspond to oligomers (GlcN, HCl)$_3$ and (GlcN, HCl)$_5$, respectively. Table 2 gives the percentage of area of each peak calculated in considering the total area of the three present peaks. Such as, the percentage of the peak area of the oligomer (GlcN, HCl)$_4$ is about 92.9% and for the oligomers (GlcN, HCl)$_3$ and (GlcN, HCl)$_5$, the percentage of the peak area is about 2.7 and 4.4%, respectively.

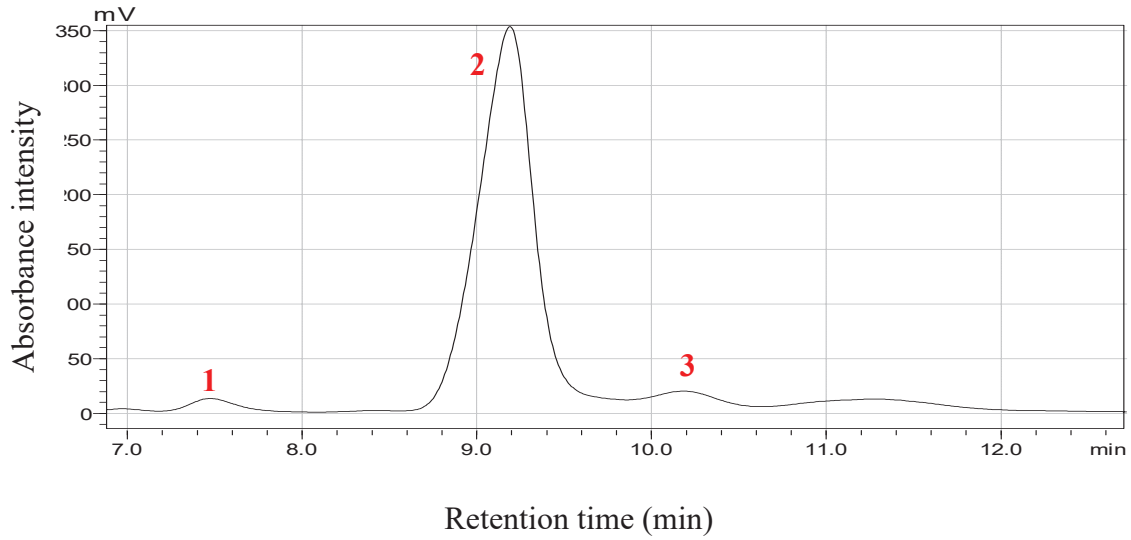

Figure 44: HPLC chromatogram of 10 mg/mL of the commercial chitotetraose hydrochloride sample, solubilized in Acetonitrile/H_2O (70:30, v/v), using amino functionalized shodex Asahipak NH2P-50G-4A column, UV detection (λ = 195 nm), and eluted with CH_3CN/H_2O (70:30, v/v) for 20 min with a flow rate of 1 mL/min at RT (peak numbers 1 to 3 are attributed in Table 2).

Table 2: Analysis of the HPLC chromatogram of the commercial chitotetraose hydrochloride shown in Figure 44.

Peak number	Assignment	Retention time (min)	Peak area (%)
1	$(GlcN, HCl)_3$	7.4	2.7
2	$(GlcN, HCl)_4$	9.2	92.9
3	$(GlcN, HCl)_5$	11.3	4.4

Herein, we confirmed from the HPLC analysis the quality of the commercial chitotetraose hydrochloride sample. It showed that the oligomer $(GlcN, HCl)_4$ is present in high percentage, in agreement with the MALD-TOF MS analysis that was previously described. Thus, the MALD-TOF MS analysis showed the presence of minor peaks of oligomers $(GlcN)_3$, $(GlcN)_5$ and $(GlcN)_4(GlcNAc)_1$ next to $(GlcN)_4$. This was also quantitatively confirmed by HPLC analysis by the presence of oligomers $(GlcN)_3$ and $(GlcN)_5$ next to $(GlcN)_4$. However, the oligomer $(GlcN)_4(GlcNAc)_1$ is not commercially available as a control

sample to be injected. Hence, it was not possible to highlight the presence of this acetylated compound in the HPLC chromatogram of the commercial chitotetraose hydrochloride.

In conclusion, we have characterized the commercial chitotetraose hydrochloride sample that will be used in this part as starting material for the synthesis of partially *N*-acetylated chitotetraose oligomers. ^{1}H NMR and MALDI-TOF MS analyses allowed us to confirm the chemical structure of oligomer (GlcN, HCl)$_4$ as the main oligomer present in the commercial sample. In addition, HPLC analyses also confirmed the satisfactory quality of the commercial (GlcN, HCl)$_4$ sample that will be used directly without purification in the rest of the study.

1.3. Chemical synthesis of partially *N*-acetylated chitotetraoses

The chemical synthesis of partially *N*-acetylated chitotetraoses by *N*-acetylation of the commercially chitotetraose hydrochloride (GlcN, HCl)$_4$ is described herein. In this part, the *N*-acetylation reaction of the commercial oligomer (GlcN, HCl)$_4$ was performed in mild conditions according to a previous published work in the IMP lab [138]. Indeed, Abla *et al*.[138] have studied the reaction conditions for the partially *N*-acetylation of chitopentaose hydrochloride (GlcN, HCl)$_5$. Different parameters were studied including: (i) the solvent composition which has an impact on the medium homogeneity, (ii) the base which has a direct influence on the reactivity of the chitopentaose amino groups, and finally (iii) the acetylating agent which has to be sufficiently stable in the reaction medium towards hydrolysis. According to this study, the *N*-acetylation conditions were set by using methanol/water (90:10, v/v) as the solvent, trimethylamine (TMA, pKa ~9.8) as the base and acetic anhydride as the acetylating agent, as shown in Figure 45.

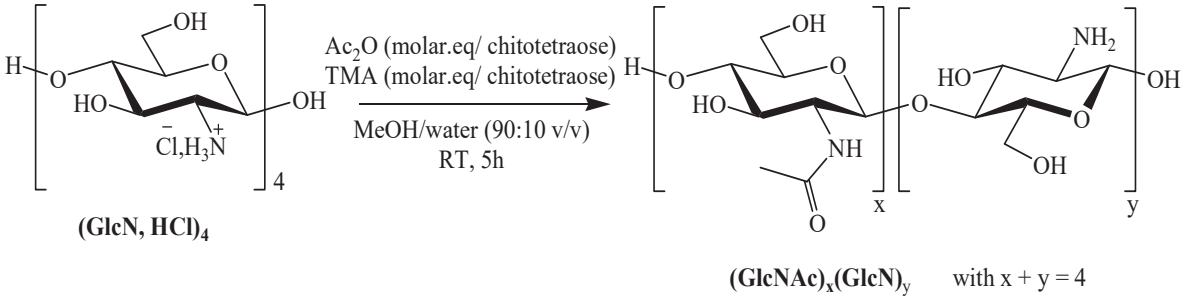

Figure 45: Chemical synthesis of partially *N*-acetylated-chitotetraoses from the commercial chitotetraose hydrochloride.

1.3.1. Amount of acetic anhydride and trimethylamine used

The partially *N*-acetylation reaction of the commercial chitotetraose hydrochloride was performed *via* a one-pot deprotonation/*N*-acetylation reaction. In this reaction, the base trimethylamine (TMA) was used to deprotonate the ammonium groups of the chitotetraose hydrochloride, followed by the *N*-acetylation of the resulting free amino groups using acetic anhydride (Ac_2O) as acetylating agent at room temperature. Thus, six different reactions were performed by using well defined molar equivalence of both the base and the acetylating reactant, with respect to the chitotetraose, as shown in Table 3.

Table 3: Different quantities of acetic anhydride and trimethylamine used with respect to molar equivalences of chitotetraose.

Reaction number	S1	S2	S3	S4	S5	S6
TMA (molar equiv. /chitotetraose)	1	1.5	2	3	3	3.3
Ac_2O (molar equiv. /chitotetraose)	1.2	1.8	2.4	3.3	4	5.2

After the solubilization of the starting material $(GlcN, HCl)_4$ in methanol/water (90:10, v/v), different molar equivalences of trimethylamine followed by different molar equivalences of acetic anhydride were added to the solubilized solutions. Both molar ratios were varied together to ensure the success of the *N*-acetylation. After 5 h of stirring at room temperature, the reactions were stopped by quenching with water and the pH of the solutions was found to be around ~5.7. Finally, solutions were concentrated by evaporation, and then lyophilized to obtain a white powder form. According to the quantities of Ac_2O and TMA used, lyophilized samples may consist of a mixture of totally *N*-acetylated oligomers which results from the total *N*-acetylation and partially *N*-acetylated oligomers, and these oligomers are obtained in their ammonium form (free amine in its protonated form).

1.3.2. Purification by ion-exchange chromatography

The ion-exchange chromatography was used as purification method to separate totally *N*-acetylated oligomers from partially *N*-acetylated oligomers. This was done for reactions S1

till S4 displayed in Table 3. However, this was not applied for reactions S5 and S6 in order to achieve satisfactory yields at high DA values. The resin Dowex 50WX8 hydrogen form composed of styrene-divinylbenzene matrix with sulfonic acid functional active group served as a stationary phase (Figure 46). In more details, this was done by solubilizing the lyophilized samples in water with a minimum volume < ~0.5 mL, then adsorbed on the Dowex50WX8 ion exchange resin. The separation between totally *N*-acetylated oligomers and partially *N*-acetylated oligomers can be explained by the pH effect of the eluent. Such as, partially *N*-acetylated oligomers which are in their ammonium form under the pH conditions used will be attached to the ionic stationary phase as shown in Figure 46-a. Hence, in a first elution step, the totally *N*-acetylated oligomers that do not carry cationic charges will be eluted upon the elution with water (Figure 46-a). Then, in a second elution step, the partially *N*-acetylated oligomers that carry a cationic charge will be neutralized when eluted with dilute ammonia solution (7% v/v in water). The neutralization of the ammonium groups will lead to the loss of cationic charges along the oligomer chains. Thus, partially *N*-acetylated oligomers will be recovered as shown in Figure 46-b.

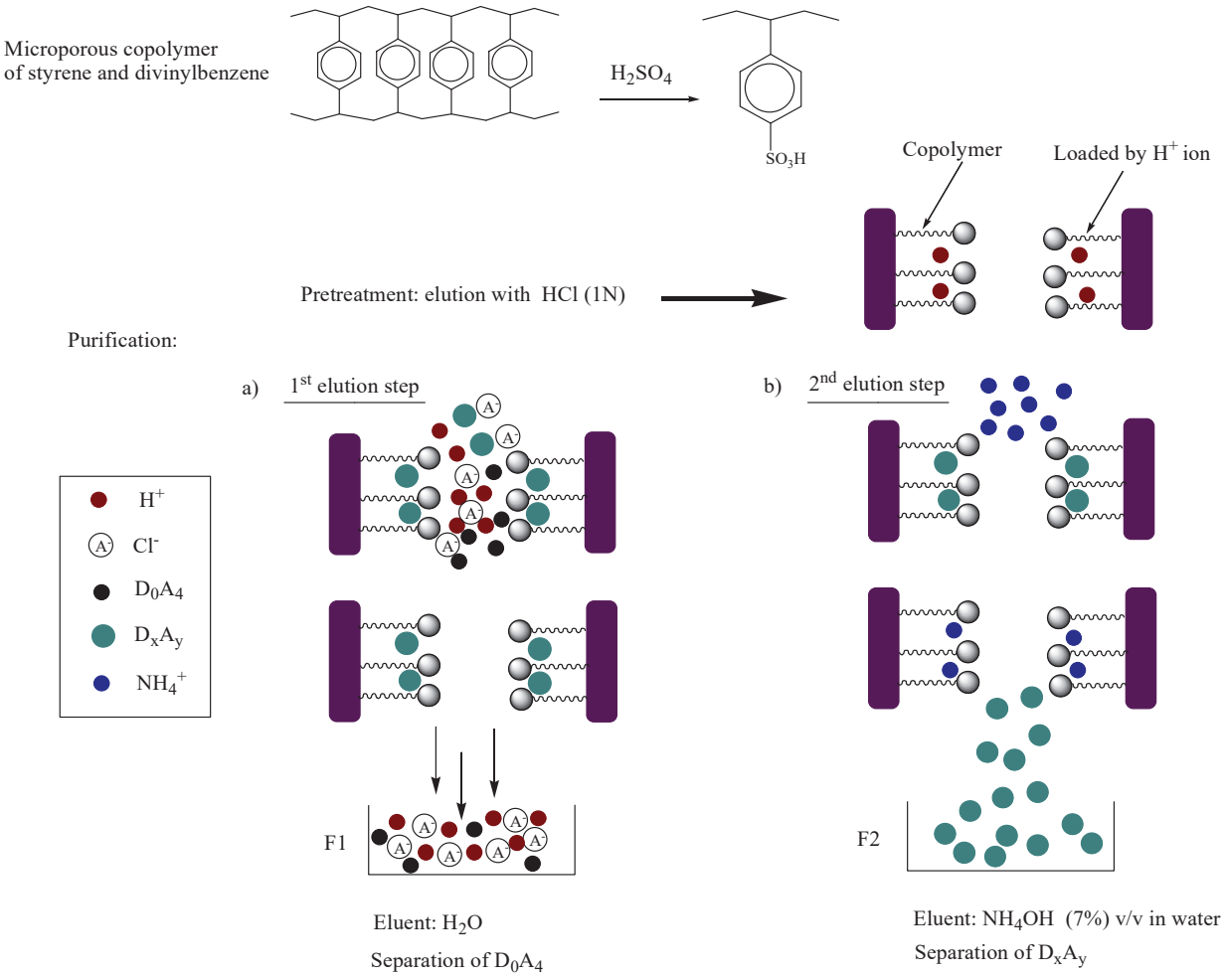

Figure 46: Ion-exchange chromatography schema representing the separation between totally *N*-acetylated chitotetraose (a) and partially *N*-acetylated chitotetraoses (b) for reactions S1 till S4.

At the end, solutions from the second elution that represent the partially *N*-acetylated oligomers were lyophilized to obtain a white powder samples with mass yields summarized in Table 4. The mass yields obtained for reactions S5 and S6, 70 and 85 % respectively were considered high compared to the mass yields obtained for reactions S2 till S4 that were around 35 and 47 %, respectively. This can be explained by the fact that reactions S5 and S6 were not purified by ion-exchange chromatography. As for reaction S1, the mass yield (fraction of partly acetylated oligomers) obtained was 67 % which is higher in comparison with reactions S2 to S4. Indeed, reaction S1 yields a low mean DA value, hence low probability to have a high percentage of totally *N*-acetylated oligomers to be separated.

Table 4: Mass yields obtained for the synthesis of partially *N*-acetylated chitotetraoses in reactions S1 to S6.

Reaction number	S1	S2	S3	S4	S5	S6
Mass yields (%)	67	47	47	35	70	85

1.4. Structural characterization of partially *N*-acetylated chitotetraose oligomers

In this part, we will discuss the techniques used to characterize the chemical structure of the partially *N*-acetylated chitotetraoses synthesized in reactions S1 to S6. The structural characterization of samples S1 to S6 was systematically performed by both ^{1}H NMR spectroscopy and MALDI-TOF mass spectrometry.

1.4.1. Characterization by ^{1}H NMR spectroscopy

The different partially *N*-acetylated chitotetraose samples S1 to S6 were analyzed thanks to ^{1}H NMR spectroscopy, by solubilizing each sample in D_2O in the presence of 0.5% (v/v) of HCl (12N). The analysis of ^{1}H NMR spectra and the data attribution of different signals in spectra of samples S1 till S6 were deduced from ^{1}H NMR data of GlcN and GlcNAc oligomers (from DP 2 to 6) reported by Sugiyama *et al*. [161]. Table 5 and Table 6 gives ^{1}H NMR assignments specifically for oligomers $(GlcNAc)_4$ and $(GlcN, HCl)_4$, respectively [161]. These tables were used as a reference to analyze spectra of partially *N*-acetylated chitotetraose samples S1 till S6.

Table 5: Proton NMR assignments of $(GlcNAc)_4$ in D_2O, ppm from TSP ($J_{n,n+1}$ and $J_{6,6'}$ in Hz); α or β, reducing end α or β anomer residue; m, middle residue; n, non-reducing end residue [161].

Proton		1	2	3	4	5	6	6′	CH_3
$(GlcNAc)_4$	α	5.20 (2.6)	3.86 (10.4)	3.88 (8.2)	3.63 (8.2)	3.89 (5.0, 2.2)	3.72 (−12.0)	3.80	2.05
	β	4.71 (8.4)	3.69 (10.4)	3.66 (8.4)	3.62 (10.2)	3.53 (5.0, 2.2)	3.67 (−12.0)	3.84	2.05
	m	4.60 (8.8)	3.77 (10.6)	3.73 (8.4)	3.65 (10.0)	3.56 (5.0, 2.2)	3.66 (−12.0)	3.85	2.07
	n	4.59 (8.8)	3.75 (10.4)	3.58 (8.4)	3.47 (10.0)	3.48 (5.0, 2.2)	3.73 (−12.0)	3.93	2.07

Table 6: Proton NMR assignments of $(GlcN, HCl)_4$ in D_2O, ppm from TSP ($J_{n,n+1}$ and $J_{6,6'}$ in Hz); α or β, reducing end α or β anomer residue; m, middle residue; n, non-reducing end residue [161].

Proton		1	2	3	4	5	6	6′
$(GlcN,HCl)_4$	α	5.45 (3.7)	3.35 (10.6)	4.04 (8.8)	3.88 (10.0)	4.04 (5.0, 2.0)	3.77 (12.5)	3.84
	β	4.95 (8.4)	3.05 (10.6)	3.88 (8.4)	3.71 (10.0)	3.88 (5.0, 2.0)	3.75(12.5)	3.94
	m	4.88 (8.4)	3.16 (10.6)	3.89 (8.4)	3.74 (10.0)	3.93 (5.5, 2.0)	3.77 (12.5)	3.94
	n	4.85 (8.4)	3.14 (10.6)	3.70 (8.4)	3.50 (10.0)	3.55 (5.0, 2.0)	3.77 (12.5)	3.94

Figure 47 corresponds to the ^1H NMR spectrum of the sample S1. This spectrum shows clearly the presence of specific signals that correspond to protons that belong to GlcNAc units such as: (i) a singlet at 2.06./2.08 ppm assigned to the *N*-acetyl protons, (ii) a signal at 5.20 ppm corresponding to H_1 protons of the reducing end α anomer unit and (iii) a signal at δ 4.70 ppm for H_1 protons of the reducing end β anomer unit, in addition to (iv) H_2 to H_6

protons of GlcNAc units from 3.50 to 4.10 ppm. Moreover, characteristic signals of the GlcN units were also found such as: (i) a large signal around 4.85 ppm for H_1 protons of non-reducing end units, (ii) a signal at 5.45 ppm corresponding to H_1 protons at the reducing end (anomer α), (iii) a signal at 4.95 ppm that represents the anomer β of the reducing end and (iv) H_3 to H_6 protons of GlcN units from 3.50 to 4.10 ppm, in addition to (v) a large signal around 3.20 ppm for H_2 protons of non-reducing end units and two signals at 3.35 and 3.05 ppm for H_2 protons corresponding to reducing end α and β anomer units, respectively. The prersence of H_1 and H_2 alpha and beta is due to the position of the substituent at the anomeric carbon.

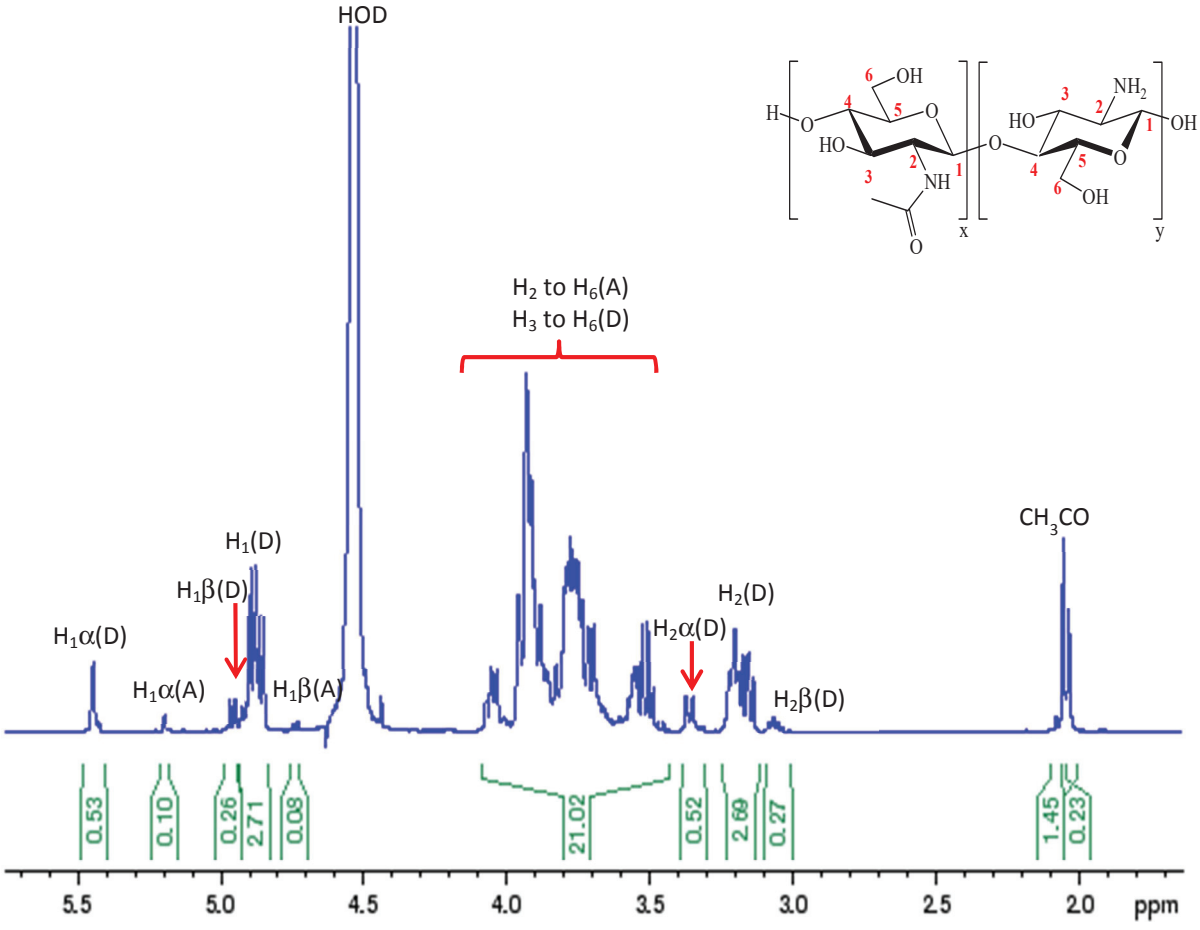

Figure 47: ^{1}H NMR spectrum of partially *N*-acetylated chitotetraose (sample S1) in D_2O with 0.5% (v/v) HCl (12N) (500MHz, 48°C, A for GlcNAc unit and D for GlcN unit).

As for the other samples S2 till S6, they were also structurally characterized by ^{1}H NMR. Figure 48 represents ^{1}H NMR spectra of the partially *N*-acetylated chitotetraose samples S1 to S6 along with the commercial oligomer $(GlcN, HCl)_4$. The attribution of the different

signals for samples S2 till S6 was similar to that of sample S1 described in Figure 47. Such as, characteristic signals were identified to protons that belong to both GlcNAc and GlcN units as described before. However, significant differences were observed between these different spectra as we move from S1 to S6 (Figure 48). It was noticed: (i) a decrease in the intensity of the signal of H_2 protons of GlcN units, (ii) a decrease in the intensity of the signals of H_1 alpha and beta protons of the GlcN reducing unit, (iii) an increase in intensities of the signals of H_1 alpha and beta protons of the GlcNAc reducing unit and (iv) an increase in the intensity of CH_3CO signal. Despite this variation in the intensities, the integration sum for H_1, H_2 and H_3 to H_6 in which the integrals appear in Annex A, from Figure 78 till 82 confirmed the presence of four GlcN/GlcNAc repetitive units that correspond to the expected tetramer structure with the different DA values

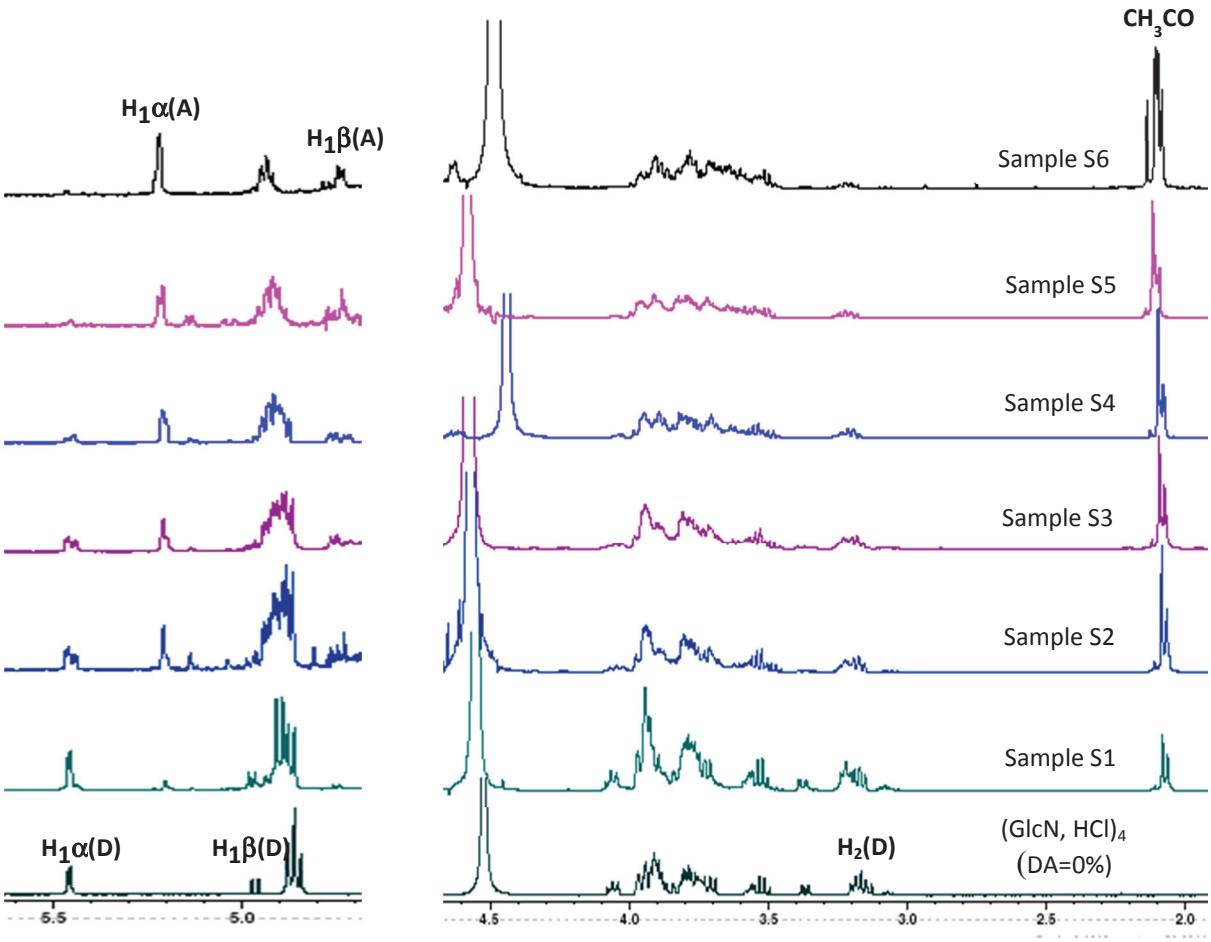

Figure 48: Comparison of ^{1}H NMR spectra of the oligomer (GlcN, HCl)$_4$ and partially *N*-acetylated chitotetraoses (samples S1 to S6) in D_2O with 0.5% (v/v) HCl (12N) (500MHz at 48°C for samples S1 to S3 and S5 at 50°C for samples S4 and S6; A = GlcNAc, D = GlcN, integration values numbers are assigned in Table 9). Spectra show an enlargement zone between 4.7 and 5.6 pm.

In addition, the determination of the average degree of *N*-acetylation (DA (%)) for the partially *N*-acetylated chitotetraose samples S1 to S6, was carried out by ^{1}H NMR spectroscopy according to the method proposed by Hirai *et al*. [166]. Thus, the average DA of samples S1 to S6 was determined according to both signal areas of H_2 to H_6 protons of GlcN and GlcNAc units and acetyl protons of GlcNAc units according to Equation 4.

$$\text{DA}\ (\%) = \frac{\left(\frac{1}{3}\right) \times \text{I}_{\text{CH}_3}}{\left(\frac{1}{6}\right) \times \sum_{i=2}^{6} \text{I}_{\text{Hi}}} \times 100 \qquad \text{Eq. 4}$$

The results of the average DA values for all the performed experiments S1 to S6 are summarized in Table 7. The DA values range from 12 till 85%. The variation in the DA (%) values obtained means that the number of the acetylated amine groups varied as expected with the amount of the acetylating agent and base used, which confirms the success of the *N*-acetylation reaction.

Table 7: Final average DA (%) values for partially *N*-acetylated chitotetraoses S1 till S6 calculated according to Eq. 4

Sample	**S1**	**S2**	**S3**	**S4**	**S5**	**S6**
DA (%) values determined by ^{1}H NMR	12 ±0.6%	32 ±1.6%	37 ±1.9%	54 ±2.7%	64 ±3.2%	85 ±4.25%

Moreover, additional information could be deduced from Figure 48 concerning the evolutions of the H_1 protons from GlcN and GlcNAc units at the reducing end. For that, Table 8 summarizes the % of *N*-acetylated units on the reducing end that was calculated by the following Equation 5.

$$\%\ \text{of GlcNAc unit at the reducing end} = \frac{I_{H1\alpha(A)} + I_{H1\beta(A)}}{I_{H1\alpha(A)} + I_{H1\beta(A)} + I_{H1\alpha(D)} + I_{H1\beta(D)}} \times 100 \qquad \text{Eq. 5}$$

It was remarkable that as the DA increases from 12 till 85%, the % of GlcNAc unit at the reducing end increases from 19 till 90 %, that means the % of GlcN unit at the reducing end decreased from 81 to 10 %.

Table 8: % of GlcNAc and GlcN unit at the reducing end of partially *N*-acetylated chitotetraose samples S1 till S6.

Samples	DA (%)	% of GlcNAc unit at the reducing end	% of GlcN unit at the reducing end
S1	12	19	81
S2	32	43	57
S3	37	55	45
S4	54	74	26
S5	64	84	16
S6	85	90	10

Results given in Table 8 show the evolution of the H_1 protons from GlcN to GlcNAc units at the reducing end. If we compare the DA values with the % of GlcNAc unit at the reducing end, in the vast majority of cases, the % of GlcNAc unit at the reducing end is higher than the DA values. This phenomenon could be explained that the GlcN reducing unit is significantly more reactive than the other GlcN units (central and non-reducing end) with respect to *N*-acetylation.

To summarize this study, proton NMR analysis was useful in many aspects. First ^{1}H NMR confirmed the chemical structure of the partially *N*-acetylated chitotetraoses (samples from S1 till S6), due to the presence of characteristic signals. Also, the determination of the average degree of *N*-acetylation (DA (%)) for the samples S1 to S6, was carried out by ^{1}H NMR spectroscopy according to the method proposed by Hirai *et al*. [166] and the determination of degree of polymerization (DP) from the integral sum. Moreover, we deduced that the reducing end seems to show better reactivity toward *N*-acetylation compared to other units.

1.4.2. Characterization by MALDI-TOF mass spectrometry

MALDI-TOF mass spectrometry was performed to further characterize the chemical structure of synthesized partially *N*-acetylated chitotetraoses from sample S1 to S6, by means of the identification of the main oligomer species present in each sample. For instance, Figure 49 shows the MALDI-TOF mass spectrum of sample S1 (DA 12%) and Table 9 gives in more

details the assignment of main peaks of the spectrum corresponding to fully *N*-deacetylated and partially *N*-acetylated chitooligosaccharides. Thus, for the sample S1, three different categories of oligomer species with different degrees of polymerization from DP 3 to DP 5 were detected, with higher peak intensities for DP 4 species compared to DP 3 and DP 5 species. Thus, in more details, starting with DP 3 oligomer species, two minor peaks were detected: the peak (1) at *m/z* 524.3 was identified as the oligomer $(GlcN)_3$ and the peak (2) at m/z 566.3 was identified as the oligomer $(GlcN)_2(GlcNAc)_1$. As for DP 4 oligomer species, three major peaks were detected such as the peak (3) at *m/z* 685.3 identified as the oligomer $(GlcN)_4$, the peak (4) at *m/z* 727.4 attributed to the oligomer $(GlcN)_3(GlcNAc)_1$ and the peak (5) at *m/z* 769.4 assigned to the oligomer $(GlcN)_2(GlcNAc)_2$. Finally, for DP 5 oligomer species, three minor peaks were detected such as the peak (6) at *m/z* 846.4 identified as the oligomer $(GlcN)_5$, the peak (7) at m/z 888.4 identified as the oligomer $(GlcN)_4(GlcNAc)_1$ and the peak (8) at m/z 930.5 identified as the oligomer $(GlcN)_3(GlcNAc)_2$.

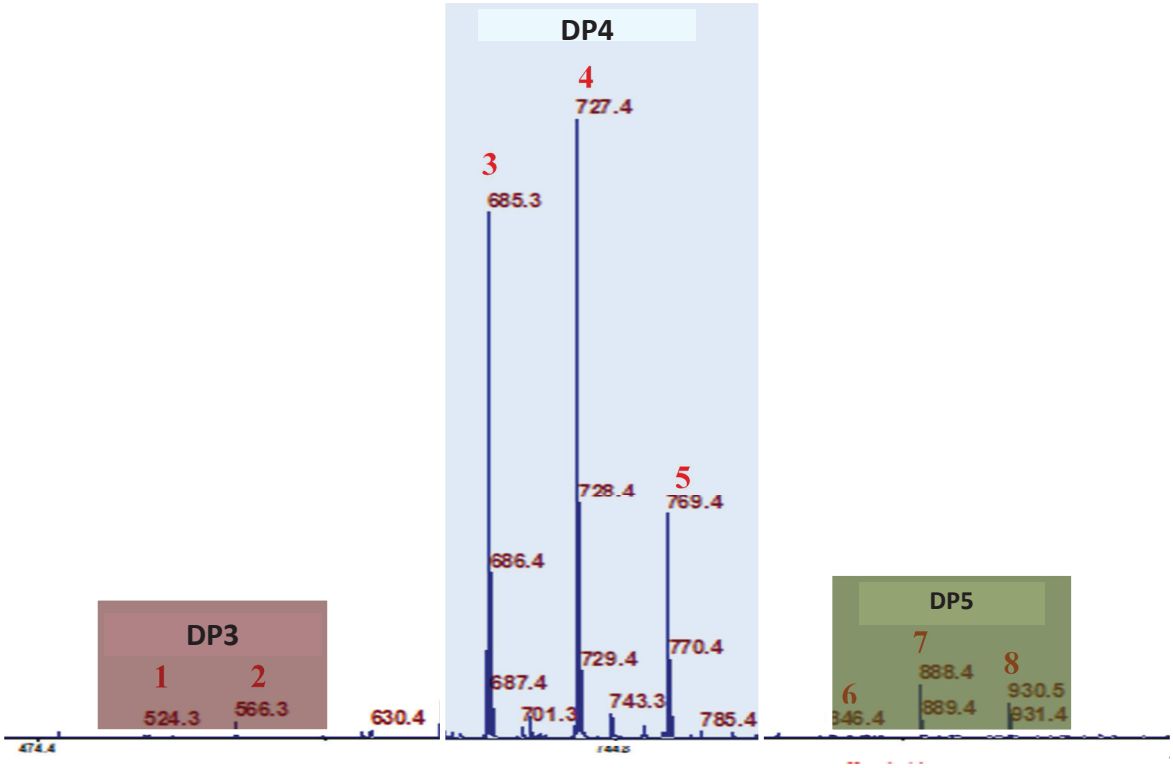

Figure 49: MALDI-TOF mass spectrum of partially *N*-acetylated chitotetraose (sample S1, DA 12%, peak numbers 1 to 8 are assigned in Table 9).

Table 9: Main oligomer species identified by MALDI-TOF mass spectrometry in the sample S1 (DA 12%, see also Figure 49 for the corresponding mass spectrum).

Peak Nb	Mass (m/z)	Molecular formula	Assignment	Adduct
1	524.3	$[C_{18}H_{34}O_{13}N_3+Na]^+$	$(GlcN)_3$	Na
2	566.3	$[C_{20}H_{36}O_{14}N_3+Na]^+$	$(GlcN)_2(GlcNAc)_1$	Na
3	685.3	$[C_{24}H_{45}O_{17}N_4+Na]^+$	$(GlcN)_4$	Na
4	727.4	$[C_{26}H_{45}O_{17}N_4+Na]^+$	$(GlcN)_3(GlcNAc)_1$	Na
5	769.4	$[C_{28}H_{49}O_{19}N_4+Na]^+$	$(GlcN)_2(GlcNAc)_2$	Na
6	846.4	$[C_{30}H_{56}O_{21}N_5+Na]^+$	$(GlcN)_5$	Na
7	888.4	$[C_{32}H_{58}O_{22}N_5+H]^+$	$(GlcN)_4(GlcNAc)_1$	H
8	930.5	$[C_{34}H_{58}O_{22}N_5+Na]^+$	$(GlcN)_3(GlcNAc)_2$	Na

The MALDI-TOF MS analysis of the sample S1 highlighted the presence of oligomers that result from the *N*-acetylation reaction such as, $(GlcN)_2(GlcNAc)_1$, $(GlcN)_3(GlcNAc)_1$, $(GlcN)_2(GlcNAc)_2$ and $(GlcN)_3(GlcNAc)_2$. In addition, the analysis confirmed that the DP 4 oligomer family including both partially *N*-acetylated and *N*-deacetylated oligomers is the major component of the sample S1. These present information demonstrates the reliability of this technique to confirm the success of *N*-acetylation for the rest of the samples S2 till S6.

As for the other samples S2 till S6, MALDI-TOF mass spectrometry was performed in order to determine the presence of all the species in them. Table 10 summarizes all the identified structures present in samples S1 till S6 that were detected by MALDI-TOF mass spectroscopy. However, to simplify the nomenclature in Table 10, the letters A and D were used instead of GlcNAc and GlcN. Thus, MALDI-TOF mass spectra of samples S2 and S3 with DA 32 and 37% respectively, revealed the presence of minor peaks of oligomers D_2A_1 and D_1A_2 for the DP 3 oligomer family, major peaks for oligomers D_3A_1, D_2A_2, D_1A_3 and minor peak of oligomers D_4A_0 for the DP 4 family, in addition to minor peaks of oligomers D_3A_2, D_2A_3 for the DP 5 family. As the DA increases to 54% (Table 10: S4) and comparing with the samples S2 and S3, MALDI-TOF mass spectrum showed the presence of an additional one minor peak at m/z 608.4 that correspond to D_1A_4 for the DP 5 family and the absence of the peak D_4A_0 for the DP 4 family. As the DA continues to increase to 64% (Table 10: S5) MALDI-TOF mass spectrum showed the presence of the oligomers described for the sample S4, but also the presence of one major peak at m/z 869.4 that correspond to D_0A_4 for

the DP 4 family and the absence of the peak D_3A_2 for the DP 5 family. Exclusively for DA 85% (Table 10: S6), in addition to the presence of the peaks that correspond to D_1A_2, D_2A_2, D_1A_3 and D_1A_4 its MALDI-TOF mass spectrum showed the presence of totally *N*-acetylated oligomers that belong to the DP 3, DP 4 and DP 5 families. Indeed, two minor peaks at m/z 650.4 and 1056.7 and one major peak at m/z 853.6 were detected. These peaks have respectively been assigned to oligomers D_0A_3, D_0A_5 and D_0A_4. To summarize, MALDI-TOF mass spectrum confirms that as the DA increase from 12 till 85%, the spectrums showed majority for the oligomers that correspond to partially and totally *N*-acetylated species and minority or absent for the oligomers that correspond to *N*-deacetylated species. Further interesting information was obtained especially in examining the degree of polymerization for each sample. More precisely, it was remarkable for all the samples that DP 4 family represent major peaks (compared to DP 3 and DP 5 family) which makes it as the major product for all the reactions.

Table 10: Main oligomer species identified by MALDI-TOF mass spectroscopy in samples S1 till S6.

Samples	Reaction products[(a)]															DA(%)[(b)]
	DP3				DP4					DP5						
	D_3A_0	D_2A_1	D_1A_2	D_0A_3	D_4A_0	D_3A_1	D_2A_2	D_1A_3	D_0A_4	D_5A_0	D_4A_1	D_3A_2	D_2A_3	D_1A_4	D_0A_5	
S1	+	+			+++	+++	+++			+	+	+				12
S2		+	+		+	+++	+++	+++				+	+			32
S3		+	+		+	+++	+++	+++				+	+			37
S4		+	+			+	+++	+++				+	+	+		54
S5		+	+			+	+++	+++	+++				+	+		64
S6			+	+			+	+++	+++					+	+	85

(a) The identification of the different oligomer species was carried out by MALDI–TOF mass spectrometry; black bars for detected species and empty boxes for not detected species; the sign (+) corresponds to minor peaks and the sign (+++) correspond to major peaks.
(b) The average degree of *N*-acetylation (DA) was detected by ^{1}H NMR spectroscopy.

Herein we identified, from the MALDI-TOF mass analysis, all the possible oligomer species present in each sample that result from the *N*-acetylation reaction. As expected, despite the fact that the MALDI-TOF mass spectrometry is not a quantitative technique, it was remarkable for all the samples that the DP 4 oligomer family is always present as a majority for all the reactions.

In this part, a one pot chemical synthesis of the *N*-partially acetylated chitotetraose by the *N*-acetylation of the chitotetraose hydrochloride under mild conditions compared to other published studies [125, 134, 144] was reported. The *N*-acetylation reaction was performed for six different reactions by using specific molar equivalence of both the base TMA and the acetylating reactant Ac_2O, with respect to the chitotetraose. The different oligomers were separated by ionic chromatography in a moderate mass yield %. Their characterization by ^1H NMR analysis has permitted us to confirm the chemical structure and to calculate the average degree of *N*-acetylation of the *N*-partially acetylated chitotetraose. In addition the chemical structure along with all the present species was confirmed by MALD-TOF mass spectrometry. However, to achieve our goal, the synthesis of higher DP values from 10 to 45 with different DA from 0 to 55% will be discussed below. The synthesis along with the method of purification will be different from the ones discussed above. This is because working with higher DP value demands different strategies and different techniques to deal with. In more details, the work below will be divided in to two main parts. The first part will be dedicated to the synthesis of chitooligosaccharides with different degree of polymerization and the second part will deal with the *N*-acetylation of the synthesized chitooligosaccharides.

2. Synthesis and characterization of partially *N*-acetylated reduced chitooligosaccharides with different average degrees of polymerization

In the following part, we will describe the synthesis and the characterization of different samples of chitosan oligomers ranging by their DP from 10 to 45 and varying by their DA from 0 to 55%. This was performed first by nitrous acid depolymerization and reduction reactions of a commercial *N*-deacetylated chitosan followed by *N*-acetylation of the depolymerized chitooligosaccharides. Herein we will highlight the work in three main parts: (i) the objective and the strategy of the synthesis; (ii) the method to synthesize partially *N*-acetylated reduced chitooligosaccharides with different degrees of polymerization; and (iii) their structural characterization.

2.1. Objective and strategy of the synthesis

The main objective in this part is to synthesize partially *N*-acetylated reduced chitooligosaccharides with different average degrees of polymerization under mild

conditions. The synthesis strategy involved three chemical reaction steps as shown in Figure 50: (i) the first step involved the nitrous acid depolymerization of a fully *N*-deacetylated commercial chitosan to produce chitooligosaccharides samples with 2,5-anhydro-D-mannofuranose at their reducing end (COSamf) with different degrees of polymerization; (ii) the second step involved the reduction of the aldehyde group of the COSamf obtained leading to the stable form of the reduced COSamf with different degrees of polymerization; (iii) the third step include the partial *N*-acetylation of GlcN units of the reduced COSamf to obtain the targeted chitooligosaccharides with different DP and DA. The depolymerization reaction was performed in a control manner such as the number of glycosidic bonds broken is roughly stoichiometric to the amount of nitrous acid used [83]. In addition, the *N*-acetylation reaction was performed in a controlled manner where the number of acetylated amine groups increases with the amount of the acetylating agent used. Below we will detail specific reaction parameters followed to obtain partially *N*-acetylated reduced chitooligosaccharides with different average degrees of polymerization, along with different characterization techniques used to characterize the final reaction products.

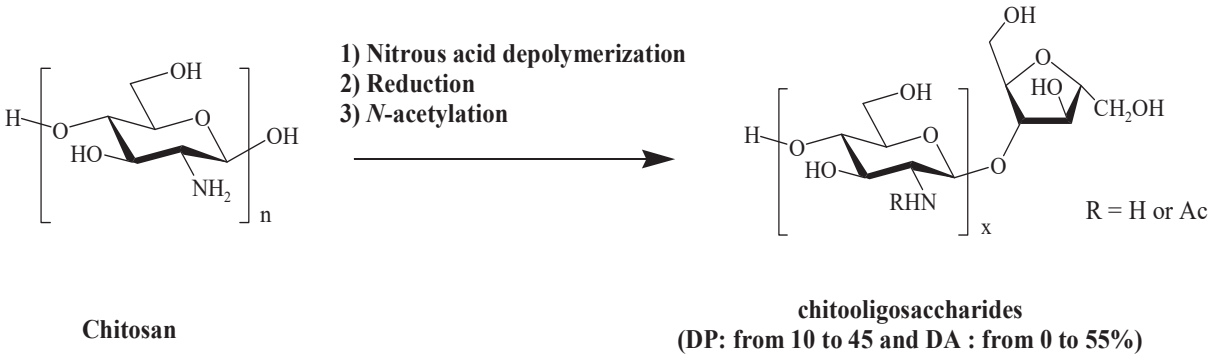

Figure 50: Synthesis strategy for the preparation of partially *N*-acetylated reduced chitooligosaccharides by nitrous acid depolymerization and reduction reaction (1) followed by *N*-acetylation reaction (2).

2.2. Chemical synthesis of partially *N*-acetylated reduced chitooligosaccharides with different degrees of polymerization

The chemical synthesis of partially *N*-acetylated reduced chitooligosaccharides with different average degrees of polymerization is described herein in two parts. The first part, describes the synthesis of the reduced form of chitooligosaccharides with different degrees of

polymerization. After, the second part will deals with the *N*-acetylation of the reduced chitooligosaccharides leading to the targeted chitooligosaccharides with different DP and DA.

2.2.1. Chemical synthesis of reduced chitooligosaccharides with different degrees of polymerization

The chemical synthesis of reduced chitooligosaccharides with different average degrees of polymerization was performed by means of nitrous acid depolymerization then reduction reaction. The nitrous acid depolymerization reaction of the commercially fully *N*-deacetylated chitosan polymer was performed according to previous published work by the IMP team [158-160]. In these studies, the nitrous acid depolymerization of commercially *N*-deacetylated chitosan was performed in an aqueous solution under mild conditions of temperature and acidity and is schematized in Figure 51 to produce chitooligosaccharides composed of 2,5-anhydro-D-mannofuranose unit at their reducing end (COSamf). This reaction is homogeneous, in acidic aqueous solvent and performed at room temperature.

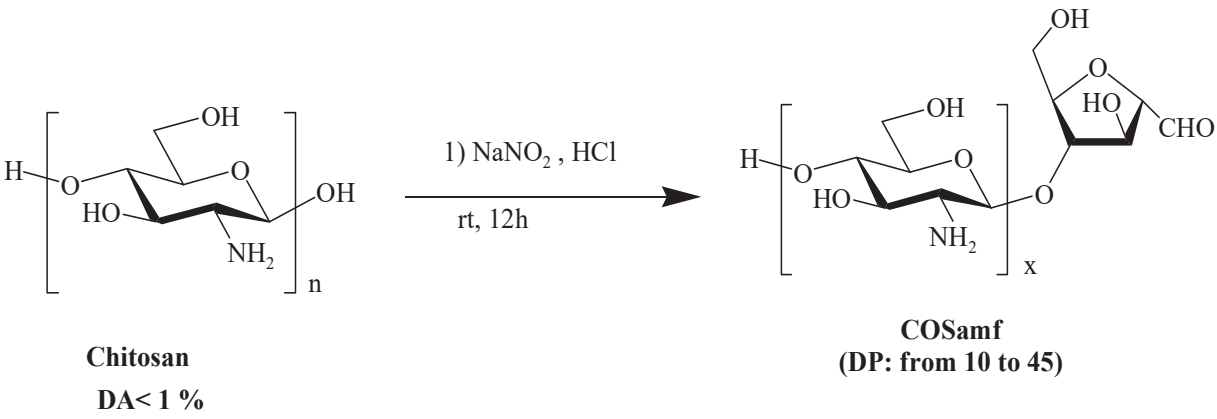

Figure 51: Chemical synthesis of COSamf (DA 0%) with DP 10 to 45 by nitrous acid depolymerisation of fully *N*-deacetylated commercial chitosan.

In further details, the nitrous acid depolymerization of fully *N*-deacetylated commercial chitosan was performed to produce three COSamf samples with an average number of GlcN repeating units DP ~10, 24 and 45 respectively. To this aim, commercial chitosan (batch type 244/020208) supplied by Mahtani Chitosan Ldt (Veraval, India) with DA < 1% calculated by ^{1}H NMR and $\overline{Mw}$ = 270 kg/mol; $\overline{Mn}$ = 115 kg/mol; Đ = 2.3 calculated by SEC-MALLS was used in this study. The nitrous acid depolymerization reaction was typically performed as described in our previous studies [158-160]. It was performed by mixing a dilute aqueous

acid solution of chitosan 2.9 % (w/w) with a specific molar quantity of $NaNO_2$ such as GlcN/$NaNO_2$ molar ratio = 4:1, 10:1 and 30:1 at room temperature for 12 h as shown in Table 11. As expected these ratios will lead to three chitooligosaccharides with different DP ~10, 24 and 45 respectively, composed of 2,5-anhydro-D-mannofuranose (amf) unit at their reducing end. However, these synthesized chitooligosaccharides molecules are rather unstable in acidic conditions and can decompose with time due to the reaction of aldehyde group and amine function leading to the formation of 5-hydroxymethylfurfural (HMF) [83]. Consequently, standard procedure generally includes additional post-treatment of the reaction mixture containing sodium borohydride ($NaBH_4$) [1, 83]. For that, after 12 h of stirring, sodium borohydride ($NaBH_4$) was added for 12h at room temperature. $NaBH_4$ was added in excess to reduce the aldehyde (-CHO) group of the terminal 2,5-anhydro-D-mannofuranose, this will lead to reduced chitooligosaccharides S7, S8 and S9 as shown in Figure 52.

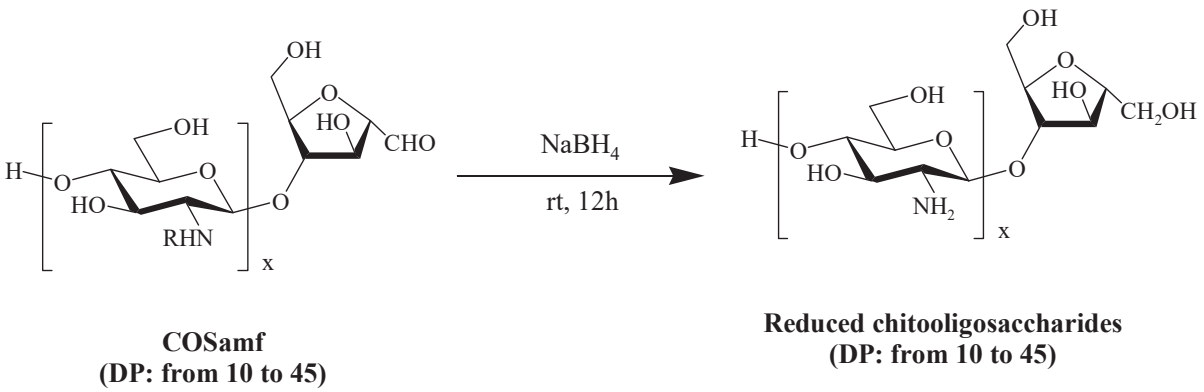

COSamf
(DP: from 10 to 45)

Reduced chitooligosaccharides
(DP: from 10 to 45)

Figure 52: Chemical synthesis of reduced chitooligosaccharides (DA 0%) by reduction of COSamf with $NaBH_4$.

At the end of the reduction reactions, samples S7, S8 and S9 were neutralized by the addition of concentrated ammonia until pH ~8-9 to insure the presence of the neutralized form of the amines group in the GlcN repeating units. It was noticed the products of S8 and S9 were easily precipitated when increasing the pH of the solution. However sample S7 showed good water solubility whatever the pH, instead it was precipitated in acetone. Finally, samples were all lyophilized and were produced in powder form with mass yields from 70 to 85% (Table 11). The mass yields obtained for reactions S8 and S9, were found to be 81 and 85%, respectively. These mass yields were considered high when comparing with reaction S7 which was found to be 70%. This was due to the loss of low molar mass oligosaccharides for the reaction S7 during precipitation.

Table 11: GlcN/NaNO2 molar ratios used and mass yields obtained for the synthesis of reduced chitooligosaccharides in reactions S7 to S9.

Reaction number	GlcN/$NaNO_2$ molar ratio	Mass yield (%)
S7	4	70
S8	10	81
S9	30	85

2.2.1.1 Structural characterization of synthesized reduced chitooligosaccharides

In this part, we will discuss the techniques used to characterize the chemical structure of the reduced chitooligosaccharides synthesized in reactions S7 to S9. The structural characterization of samples S7 to S9 was performed by NMR spectroscopy. The mass- and number-average molar masses of the samples were performed by SEC chromatography.

2.2.1.1.1. Characterization by ^{1}H and ^{13}C NMR spectroscopies

The reduced chitooligosaccharides, *i.e.* samples S7 to S9 were analyzed thanks to NMR spectroscopy, by solubilizing each sample in D_2O in the presence of 0.5% (v/v) of HCl (12N). The analysis of NMR spectra and the attribution of the different signals in spectra of the reduced chitooligosaccharides were based on the NMR data published for COSamf structures [83, 156]. Tommeraas *et al.* [83] reported the synthesis of (GlcN, HCl)$_2$-amf produced by nitrous depolymerization of chitosan. More specifically, when describing the NMR attribution for the synthesized COSamf, Tommeraas *et al*. explained that neither the ^{1}H nor the ^{13}C spectrums showed the expected resonances for the free aldehyde group of the amf unit (^{1}H: 9–10 ppm and ^{13}C: 180 ppm). Instead, the H_1 and C_1 resonances of the amf unit at 5.01 and 89.5 ppm, respectively, indicated the presence of a hydrated aldehyde called gem diol. Also, Tommeraas *el al.* have shown ^{1}H NMR and ^{13}C NMR assignments specifically for the reducing end of the oligomer (GlcN, HCl)$_2$-amf summarized in Table 12 and Table 13, respectively. These tables along with the 2D NMR (COSY and HSQC) performed were sufficient and useful for the analysis of the spectra of reduced chitooligosaccharides S7 till S9.

Table 12: ^{1}H NMR (400.13 MHz) chemical shifts (ppm) and vicinal coupling constants (in Hz, given in parenthesis) for the reducing end (amf unit) of the oligomer (GlcN, HCl)$_2$-amf in D_2O at 43 °C and pH = 5.7 according to Tommeraas *et al.*[83].

H_1, gem diol	H_2	H_3	H_4	H_5	H_{6a}	H_{6b}
5.09	3.84	4.44	4.22	4.13	3.7-3.9	3.7-3.9
(5.3)	(5.3, 5.3)	(4.4, 5.3)	(4.7, 5.3)	(5.3, 9.9)	(9.9)	(9.9)

Table 13: ^{13}C NMR (100.64 MHz) chemical shifts (ppm) for the reducing end (amf unit) of the oligomer (GlcN, HCl)$_2$-amf in D_2O at 25 °C and pH = 5.7 according to Tommeraas *et al.*[83].

C_1, gem diol	C_2	C_3	C_4	C_5	C_6
89.8	86.5	77.0	85.6	82.6	63.1

Figure 53 represents the ^{1}H NMR spectrum for the reaction product S9. This spectrum shows clearly the presence of specific signals that correspond to protons that belong to GlcN units (D unit in Figure 53) as: (i) a signal at 4.85 ppm attributed to the H_1 proton, (ii) a high intensity signal between 4.00 and 3.40 ppm corresponding to H_3 till H_6 protons and (iii) a signal at 3.15 ppm for the H_2 proton. In addition characteristic signals were assigned to the reduced amf unit at the reducing end (r unit in Figure 53): (i) three typical low intensity signals at 4.35, 4.23 and 4.13 ppm attributed to H_3, H_4 and H_5, respectively and (ii) overlapped signals between 4.00 and 3.40 ppm attributed to H_1, H_2 and H_6. Moreover, characteristic signals of the GlcN units neighboring of the amf unit (D' unit in Figure 53) were observed such as: (i) a signal at 4.90 ppm attributed to the H_1 proton, (ii) overlapped signals were assigned between 4.00 and 3.40 ppm corresponding to H_3 and H_6 protons and between 3.25 and 3.1 ppm corresponding to H_2, moreover (iii) two low intensity signals assigned to H_4 and H_5 at 3.50 and 3.55 ppm, respectively. Most importantly, the success of the reduction reaction was confirmed by the absence of a signal assigned to H_1 amf unit at 5.10 ppm.

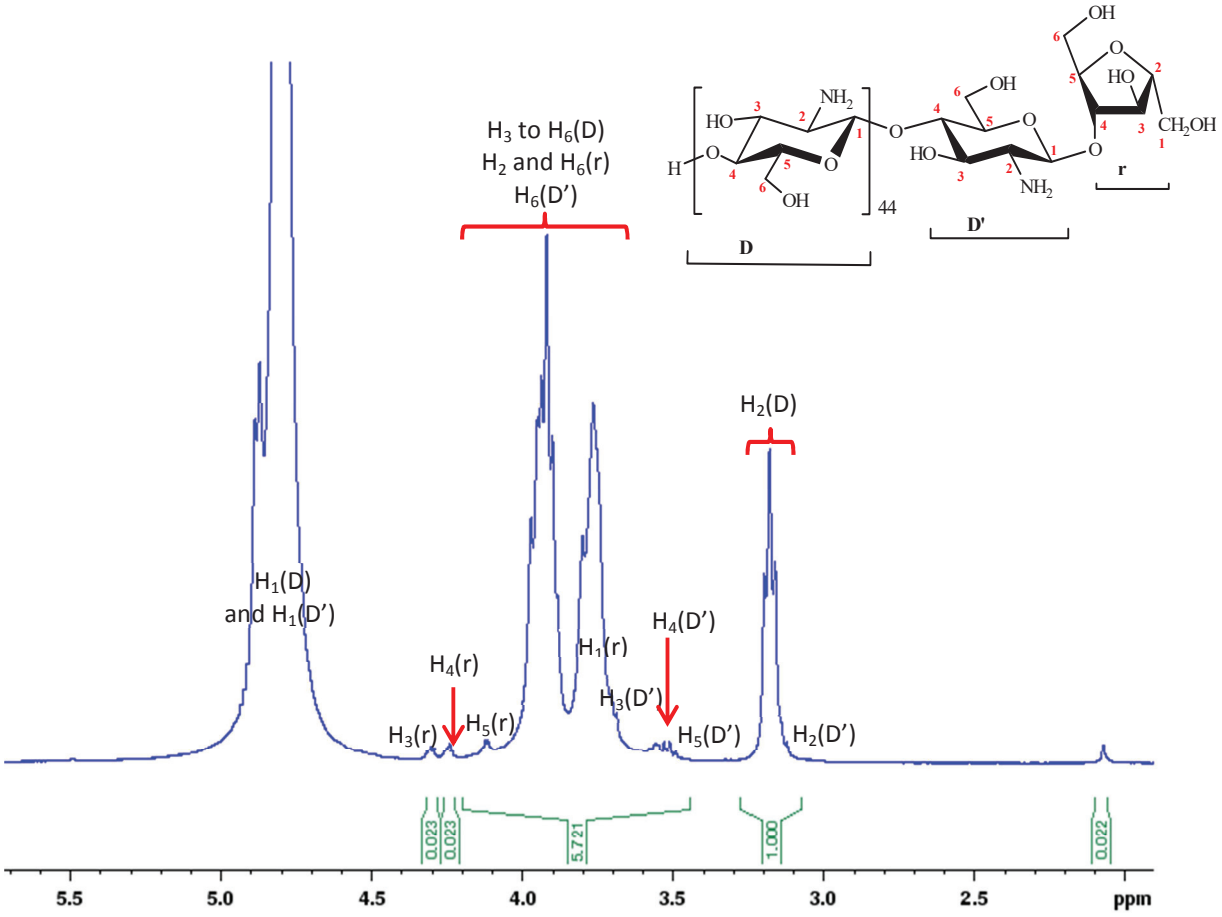

Figure 53: ^{1}H NMR spectrum of the reduced chitooligosaccharide (sample S9) in D_2O with 0.5% (v/v) HCl (12N) (500 MHz, 25 °C, (D) for proton atoms of the GlcN unit, (D') for proton atoms of the GlcN unit linked to the amf unit and (r) for the proton atoms of the reduced amf unit.

In addition, the ^{13}C NMR (allows the identification of carbons) and DEPT 135 spectra (allows the differentiation of signals between CH_2, negative, while CH and CH_3 will be positive) in Figure 54 shows clearly the high intensity peaks assigned to GlcN units carbon atoms (D unit in Figure 54), such as: (i) signals for C_1 at 98.6 ppm, C_4 at 77.0 ppm, C_5 at 75.3 ppm, C_3 at 71.0 ppm, C_6 at 60.6 ppm and C_2 at 56.5 ppm. In addition low intensity peaks corresponding to reducing-end for amf unit (r unit in Figure 54), such as: (i) signals for C_4 at 86.5 ppm, C_2 at 85.6 ppm, C_5 at 82.6 ppm C_3 at 77.2 ppm, C_6 at 61.4 ppm and C_1 at 61.0 ppm. In addition to that, low intensity peaks were detected and assigned to carbon atoms of the GlcN unit linked to the amf (D' unit in Figure 54), such as (i) signals for C_1 at 99.2 ppm, C_5 at 76.9 ppm, C_3 at 72.5 ppm, C_4 at 70.2 ppm, C_6 at 60.9 ppm and C_2 at 56.2 ppm.

Moreover, the success of the reduction reaction was confirmed by the absence of signal C_1 of the amf unit at 89.5 ppm.

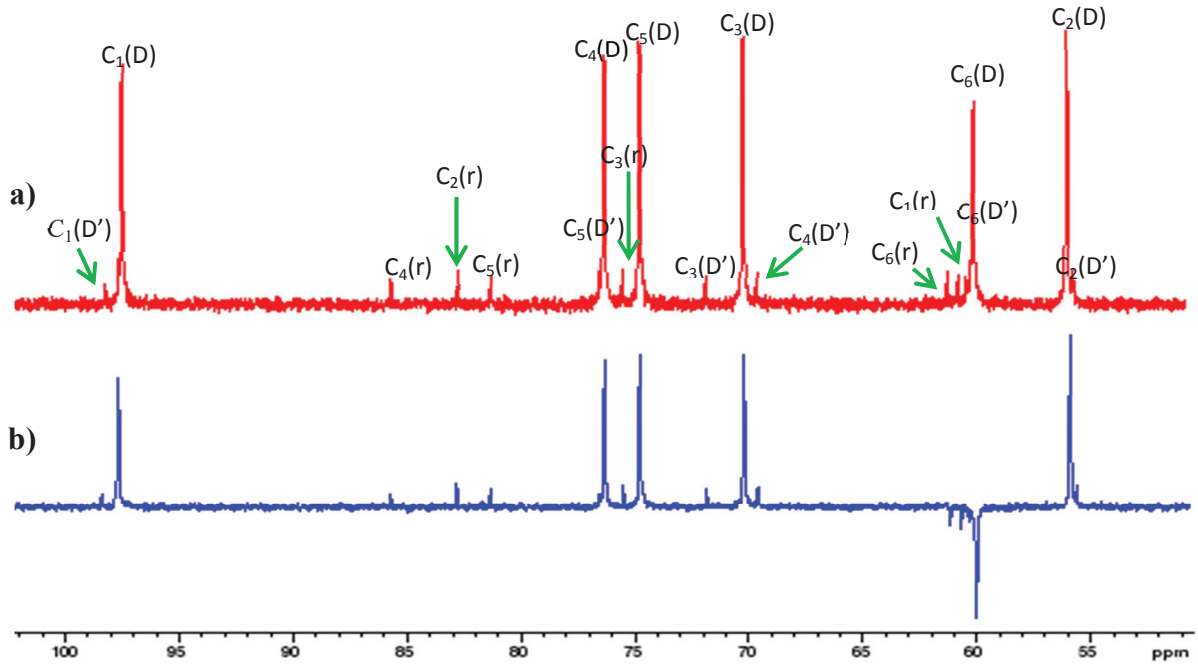

Figure 54: ^{13}C NMR (a) and DEPT135 (b) spectra of the reduced chitooligosaccharides (sample S9) in D_2O with 0.5% (v/v) HCl (12N) (125 MHz, 25 °C, (D) for carbon atoms of the GlcN unit, (D') for carbon atoms of the GlcN unit linked to the amf unit and (r) for the carbon atoms of the reduced amf unit.

The different signals attributions especially for the overlapped peaks were possible and complete for the ^1H and ^{13}C / DEPT135 NMR, thanks to the 2D COSY (proton-proton correlations) and HSQC NMR (proton-carbon correlations) that were demonstrated in Figure 55 and Figure 56.

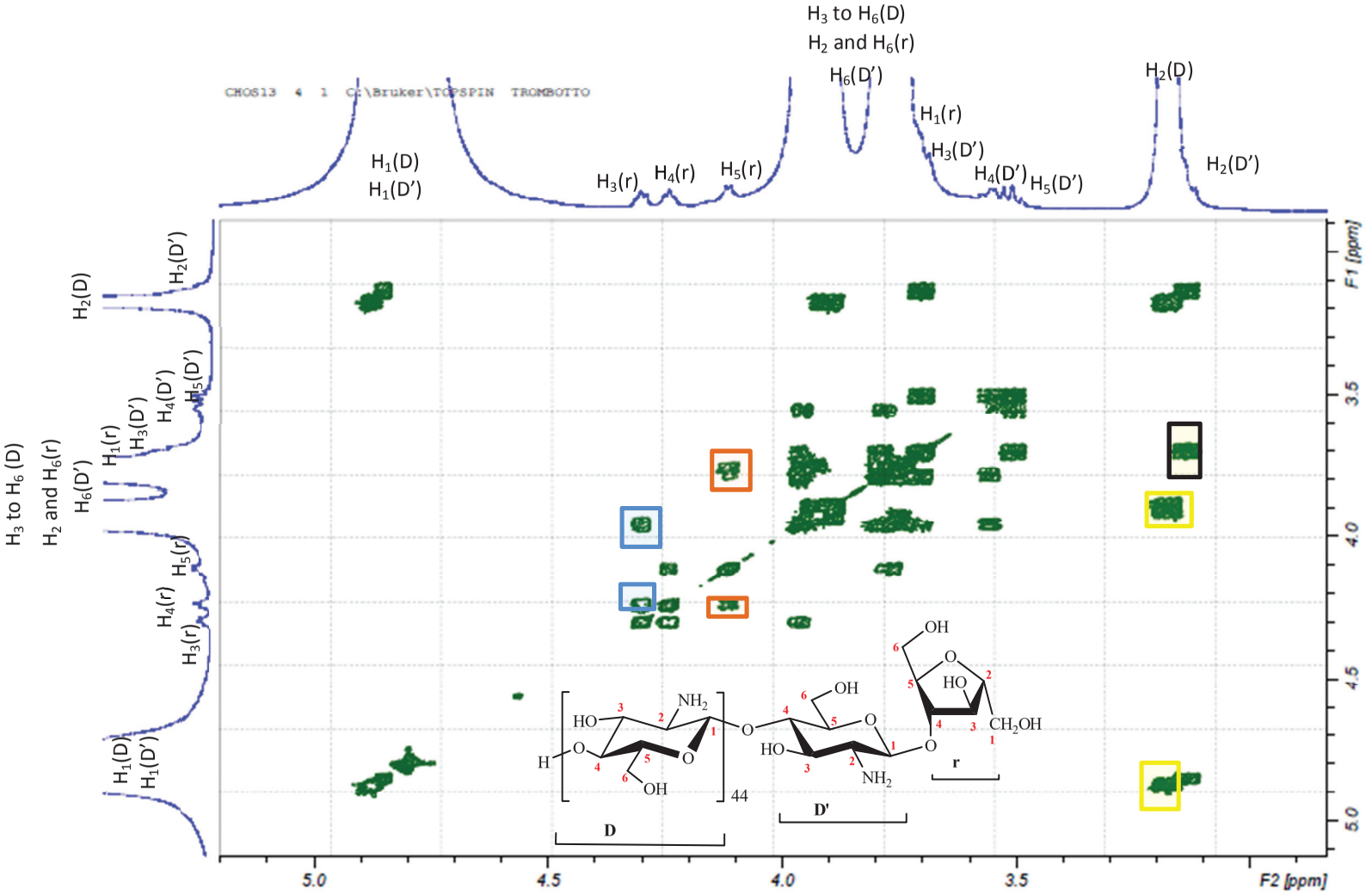

Figure 55: 2D COSY NMR spectrum of sample S9 in D_2O with 0.5% (v/v) HCl (12N) (125 MHz, 25°C).

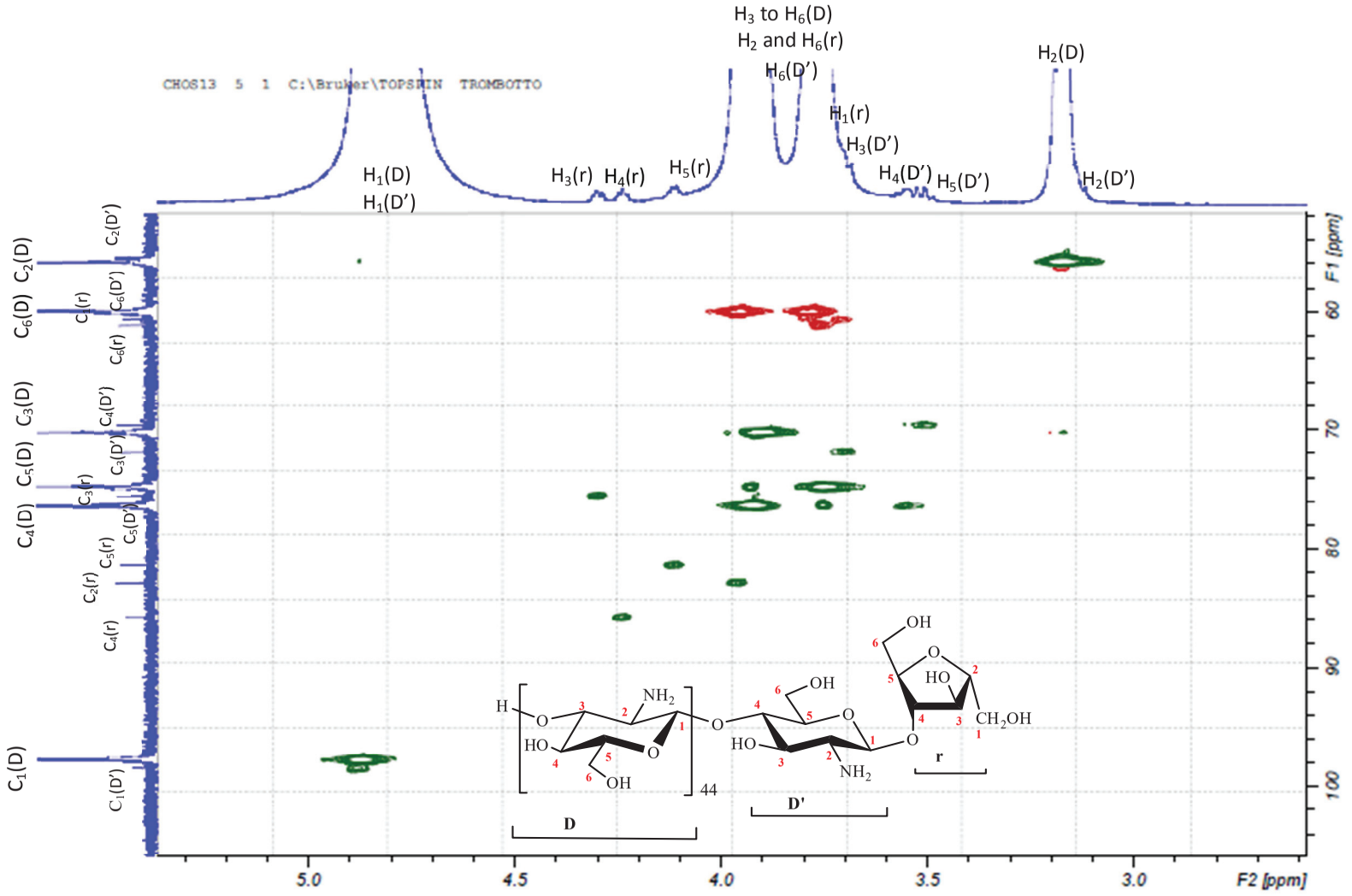

Figure 56: 2D HSQC NMR spectrum of the sample S9 in D2O with 0.5% (v/v) HCl (12N) (125 MHz, 25°C).

Thanks to NMR analyses, all ^{1}H and ^{13}C resonances corresponding to GlcN and reduced amf units of COS were attributed. Thus the expected chemical structure of sample S9 was determined. As for samples S7 and S8 the ^{1}H NMR spectra was comparable to that of sample S9 (see Annex A, Figure 83 and 84), which makes it possible to prove their expected structure. In addition, the determination of the average degree of polymerization (DP) of the reduced COSamf samples S7, S8 and S9 was determined by ^{1}H NMR spectroscopy and demonstrated in Table 14. The average DP was calculated according to the relative peak intensities of H_4 (reduced amf) and H_2 (GlcN) signals at 4.23 and 3.15 ppm respectively, according to Equation 6.

$$\overline{DP} = \frac{I_{H-2\ (GlcN)}}{I_{H-4\ (reduced\ amf)}} \qquad \text{Eq. 6}$$

Table 14: Average degree of polymerization (DP) of the reduced chitooligosaccharides samples determined by ^{1}H NMR spectra.

Sample	$\overline{DP}$ +/- 2
S7	9
S8	24
S9	43

Results given in Table 14 show clearly that the average DP values determined by ^{1}H NMR are in close agreement with the expected used ratios of GlcN/$NaNO_2$ molar ratio = 4:1, 10:1 and 30:1 shown in Table 11. To confirm these results, we attempted to determine the average DP of each reduced COSamf sample also by SEC chromatography.

2.2.1.1.2. Characterization by SEC

The conditions used during the SEC-MALLS analysis were similar to previous published work by the IMP team [159, 160]. 2-5 mg/mL of the reduced chitooligosaccharides samples were solubilized in ammonium acetate buffer pH 4.5 and injected in to two TSK gel G2500 and G6000 columns (Tosoh Bioscience). The samples were detected by a multi-angle laser light scattering (MALLS) detector HELEOS II (Wyatt Technology) operating at 664 nm was coupled on line to a Wyatt Optilab T-Rex differential refractometer. Figure 57 shows a series

of chromatograms for the reduced chitooligosaccharides samples S7, S8 and S9 detected by differential refractometer. Sample S9 was eluted at a retention time 31.5 min, then sample S8 was eluted at a retention time 33 min and finally sample S7 was eluted at a retention time 35min. This confirms the presence of three different molecular sizes of chitooligosaccharides.

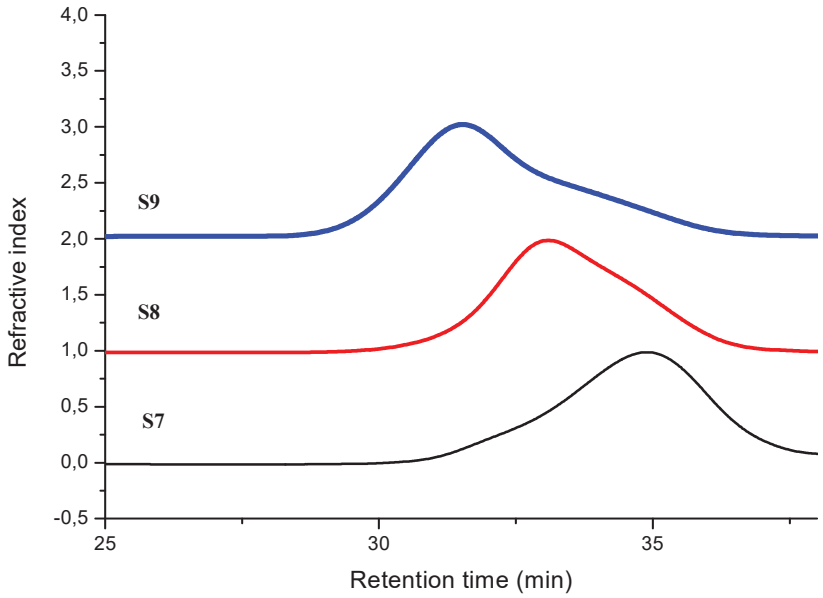

Figure 57: Size exclusion elution diagrams of reduced chitooligosaccharides samples S7, S8 and S9 (2-5 mg/mL) in ammonium acetate buffer (pH 4.5).

The mass- and number-average molar masses and the dispersity, $\overline{Mw}$ $\overline{Mn}$ and Đ, respectively are summarized in Table 15. The number-average molar masses ($\overline{Mn}$) of all the polymer chains in the samples of S7, S8 and S9 were found to be 1.9×10^3, 4.42×10^3 and 7.76×10^3 g/mol, respectively. In addition, the mass average molar masses ($\overline{Mw}$,) of S7, S8 and S9 were found to be 2.10×10^3, 6.77×10^3 and 11.90×10^3 g/mol, respectively. It was remarkable that the dispersity index Mw/Mn, (Đ) values of S7, S8 and S9 samples seems to decrease from 1.5 to 1.1 when the DP decreases from 45 to 24.

Table 15: Determination of the mass- and number-average molar masses ($\overline{Mw}$ and $\overline{Mn}$, respectively) and the dispersity (Đ) of reduced chitooligosaccharides samples S7, S8 and S9 by SEC-MALLS in ammonium acetate buffer (pH 4.5), using dn/dc = 0.198 mL/g.

Sample	$\overline{Mw}$ (g/mol)	$\overline{Mn}$ (g/mol)	Đ

S7	2.13×10^3	1.94×10^3	1.1
S8	5.74×10^3	4.42×10^3	1.3
S9	11.64×10^3	7.76×10^3	1.5

It was thus possible to compare and to confirm the obtained DP value by SEC-MALLS chromatography and NMR, as shown in Table 16. Such results were obtained according to the number-average molar mass ($\overline{Mn}$) of reduced COSamf SEC analysis, the molar mass of the GlcN repeating unit (M_0 = 161g/mol) and molar mass of the reduced amf unit ($M_{(reduced\ amf)}$ = 164 g/mol) according to Equation 7.

$$\overline{DP} = \frac{\overline{Mn} - M(\text{reduced amf})}{M_0} \qquad \text{Eq. 7}$$

Table 16: Average degree of polymerization (DP) of the reduced chitooligosaccharides samples determined by a) ^{1}H NMR spectra and by b) SEC-MALLS chromatography.

Sample	$\overline{DP}^a$ +/- 2	$\overline{DP}^b$ +/- 2
S7	9	11
S8	24	26
S9	43	47

Compared to DP values determined by ^{1}H NMR, the average DPs calculated by SEC chromatography were found to be very similar. Even if a slight difference was observed, the good correlation obtained with these two techniques was sufficient to calculate the average degree of polymerization for the synthesized oligomers and to confirm the success of the nitrous acid depolymerization.

As a conclusion, the synthesis of reduced COSamf samples with different degree of polymerization around 10 till 45 was performed by means of nitrous acid depolymerization and reduction reaction of commercially fully *N*-deacetylated chitosan polymer. The nitrous acid depolymerization reaction was performed in a control manner such as the number of glycosidic bonds broken is roughly stoichiometric to the amount of nitrous acid used. As for

the reduction reactions, it was performed by the use of excess amount of $NaBH_4$ to obtain a stable form of chitooligosaccharides. The chemical structures of the different reduced COSamf samples were analyzed by NMR analyses. In addition, SEC chromatography allowed the calculations of mass- and number-average molar masses. These two techniques were sufficient to calculate the average degree of polymerization for the synthesized oligomers. The synthesized reduced COSamf samples will be used in the coming part as a starting material for the synthesis of partially *N*-acetylated reduced chitooligosaccharides.

2.2.2. Chemical synthesis of partially *N*-acetylated reduced chitooligosaccharides with different average degrees of polymerization and *N*-acetylation

The chemical synthesis of partially *N*-acetylated reduced chitooligosaccharides by *N*-acetylation of the previously synthesized oligomers S7, S8 and S9 is described below. The *N*-acetylation reaction of the synthesized oligomers was performed in mild conditions according to previous published work by the IMP team [138] that was described in part 1.3 (Synthesis and characterization of partially *N*-acetylated chitotetraose). As mentioned before, one of the important parameters in the *N*-acetylation reaction of GlcN oligomers is the solvent. According to Abla *et al*. study, the team used the solvent mixture methanol/water 90/10 (v/v) when acetylating chitopentaose hydrochloride. We followed the same ratio when acetylating chitotetraose in part 1.3. However, in this section, the chitooligosaccharides to be *N*-acetylated are samples S7, S8 and S9 that correspond to higher DP ~10, ~24 and ~45 respectively. COS with high DP requires the presence of water in the solvent due to its poor solubility in pure methanol [167]. For the oligomer S7, we succeeded in solubilizing it using the methanol/water ratio 90/10 v/v. However, it was impossible to obtain a homogenous medium by using 10% v/v of water for oligomers S8 and S9. Hence, several tests were performed to find the appropriate solvent composition ratios, keeping in mind that the quantity of water has to remain as small as possible to insure the success of the *N*-acetylation reaction. Although different ratios were tested for oligomers S8 and S9, it was impossible to solubilize them even in pure water. For that, several drops of acetic acid 1.5 % (w/v) were added to acidify water pH~6, then the solvent mixtures methanol/water 70/30 (v/v) and 50/50(v/v) were tested for oligomers S8 and S9. After choosing the appropriate ratios for the

methanol/aqueous AcOH 1.5% (w/v) solvent, the *N*-acetylation reactions were performed at room temperature for 12h as shown in Figure 58.

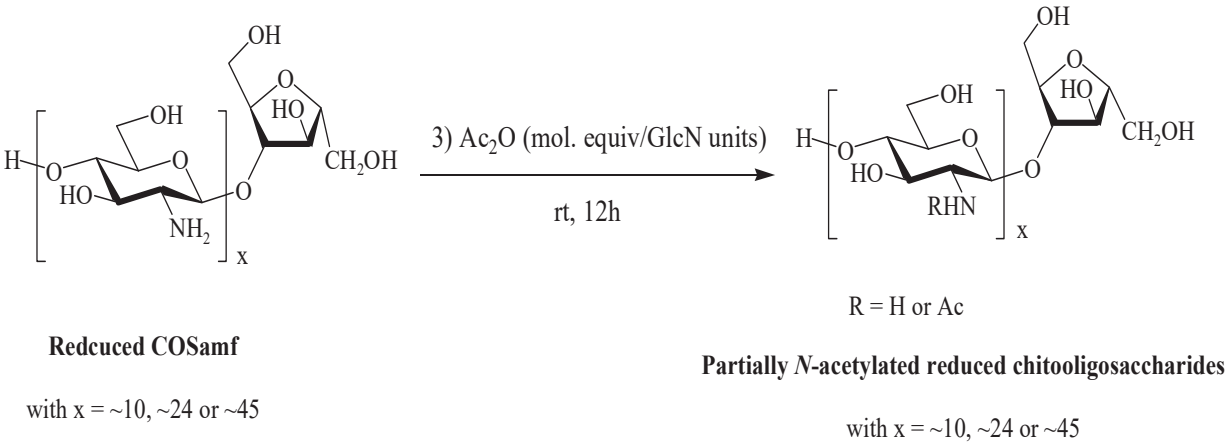

Figure 58: Syntheses of partially *N*-acetylated reduced chitooligosaccharides by *N*-acetylation of reduced chitooligosaccharides S7 (DP ~10), S8 (DP ~24) and S9 (DP ~45).

The partially *N*-acetylation reactions were carried out so as to control the number of GlcNAc units along the oligomer chain. The *N*-acetylation reaction of the free amino groups was performed by using acetic anhydride (Ac_2O) as acetylating agent at room temperature. If we want to compare with the *N*-acetylation reaction done in part 1.3, the base (trimethylamine) was not used in order to preserve the solutions homeginety and to avoid the precipitation of oligomers especially for the reduced COSamf S8 and S9. Thus, several different reactions were performed by using controlled molar equivalences of the acetylating reactant, with respect to glucosamine units for each reaction as shown in Table 17.

Table 17: Different molar equivalences of acetic anhydride used with respect to glucosamine units in reduced chitooligosaccharides samples.

Reduced COSamf samples	DP of reduced COSamf samples	*N*-acetylated chitooligosaccharide samples	Quantity of Ac_2O (Molar equiv. /GlcN units)
S7	10 ±2	S7-1	0.1
		S7-2	0.25
		S7-3	0.5
S8	24 ±2	S8-1	0.1
		S8-2	0.25
		S8-3	0.3
		S8-4	0.5

S9	45 ±2	S9-1	0.25
		S9-2	0.5

After the solubilization of the reduced chitooligosaccharides in methanol/water 90:10 (v/v) for S7 and in methanol/acidic aqueous solution (AcOH 1.5% (w/v)) 70:30 (v/v) for S8 and 50:50 (v/v) for S9 reactions, different molar equivalences of acetic anhydride were added to the solubilized solutions. After 12 h of reaction with magnetic stirring at room temperature, solutions were neutralized by the addition of ammonia till pH~8. Sample S8-1 was precipitated at pH~8, centrifuged, washed abundantly with water then freeze-dried. As for the other samples, S7-1, S7-2 and S7-3, S8-2, S2-3 and S8-4 and S9-1, S9-2, they did not precipitate at basic pH 8-9, instead the reaction solutions were concentrated by vacuum evaporation and then *N*-acetylated chitooligosaccharides were precipitated, abundantly washed with acetone and finally dried under vacuum to obtain *N*-acetylated chitooligosaccharides in their free amine form as white powder with mass yields summarized in Table 18.

Table 18: Mass yields of the synthesis partially *N*-acetylated reduced chitooligosaccharides from reduced chitooligosaccharides S7 to S9

Reduced COSamf samples	DP of reduced COSamf samples	*N*-acetylated reduced chitooligosaccharides samples	Mass yields (%)
S7	10 ±2	S7-1	55
		S7-2	58
		S7-3	57
S8	24 ±2	S8-1	65
		S8-2	62
		S8-3	60
		S8-4	57
S9	45 ±2	S9-1	65
		S9-2	63

The % mass yields obtained in Table 18 for the different partially *N*-acetylated reduced chitooligosaccharides were slightly increased from 55 to 65% as the DP increase from 10 till 45. Despite this increase, the moderate obtained values may be explained due to the loss of soluble or low molar mass oligomers. It is important to mention that all the acetylated oligomers except of S8-1 (not soluble) and S8-2 (partially soluble) were soluble at neutral pH.

It was reported that the water solubility of oligomers under alkaline conditions was related to the molar mass and the distribution of acetylated and non-acetylated residues along the polymer backbone. Specifically the solubility of the oligomers as the DA increase till 50% was explained by the regularly dispersed acetyl groups along the chain that promotes polarity and water/chitosan interactions resulting in soluble oligomers at neutral pH [2, 6, 168] (as for polymers).

2.2.2.1. Structural characterization of synthesized partially *N*-acetylated reduced chitooligosaccharides

Below, we will discuss the characterizations of the partially *N*-acetylated reduced chitooligosaccharides samples. The structural characterization of partially *N*-acetylated reduced chitooligosaccharides was carried out by ^{1}H NMR and RAMAN spectroscopies. The determination of the mass- and number-average molar masses of the partially *N*-acetylated reduced chitooligosaccharides was performed by SEC chromatography.

2.2.2.1.1. Characterization by ^{1}HNMR spectroscopy

The different partially *N*-acetylated reduced chitooligosaccharides samples were analyzed thanks to ^{1}H NMR spectroscopy, by solubilizing each of the samples in D_2O in the presence of 0.5% (v/v) of HCL (12N). The analysis of ^{1}H NMR spectra and the data attribution of different signals in spectra of different partially *N*-acetylated reduced chitooligosaccharides were deduced from ^{1}H NMR data of GlcN and GlcNAc oligomers, from DP 2 to 12 and DA 0 to 90 % reported by Trombotto *et al*. [76] and from ^{1}H NMR data of GlcN and GlcNAc oligomers, from DP 2 to 6, reported by Sugiyama *et al*.[161]. In addition to the parent reduced chitooligosaccharides, discussed in part 2.2.1.1.1. Figure 59, Figure 60 and Figure 61 correspond to the partially *N*-acetylated reduced chitooligosaccharides series of the reduced COSamf S7, S8 and S9, respectively. These spectra shows the presence of specific signals that correspond to the protons that belong to GlcN and GlcNAc units such as: (i) a signal at 4.85 ppm and 4.60 ppm assigned to H_1 protons for GlcN units and H_1 protons for GlcNAc units respectively, (ii) a high intensity signals assigned to GlcN and GlcNAc protons between 4.00 and 3.40 ppm that correspond to protons of H_3 to H_6 (GlcN) and protons of H_2 to H_6 (GlcNAc), (iii) the presence of H_2 (GlcN) at 3.15 ppm and (iv) a peak related to *N*-acetyl protons which correspond to a signal at 2.06/2.08 ppm. In addition, the reduced amf unit at

the reducing end was confirmed by: (i) three typical low intensity signals at 4.45, 4.23 and 4.13 ppm assigned to H_3 (reduced amf), H_4 (reduced amf) and H_5 (reduced amf), respectively and (ii) overlapped signals assigned to H_1, H_2 and H_6 (reduced amf) between 4.00 and 3.40 ppm, respectively. It was remarkable that the signals of H_2 GlcN protons were sufficiently well separated and do not overlap with signals of other repeating unit protons. Hence, the average DA of the different acetylated samples was determined by considering both signal areas of H_2 protons of GlcN units ($I_{GlcN\text{-}H2}$) and acetyl protons of GlcNAc units (I_{CH3}) according to Equation 8 [76]. The results are indicated on the ^{1}H NMR spectra in Figure 59, Figure 60 and Figure 61. In addition, it was remarkable that the presence of acetic acid peaks was close to the signal of the acetyl groups. Of course this was taken into consideration when calculating the DA.

$$DA\ (\%) = \frac{\left(\frac{1}{3}\right) \times I_{CH_3}}{\left(\frac{1}{3}\right) I_{CH_3} + I_{GlcN-H2}} \times 100 \qquad \text{Eq. 8}$$

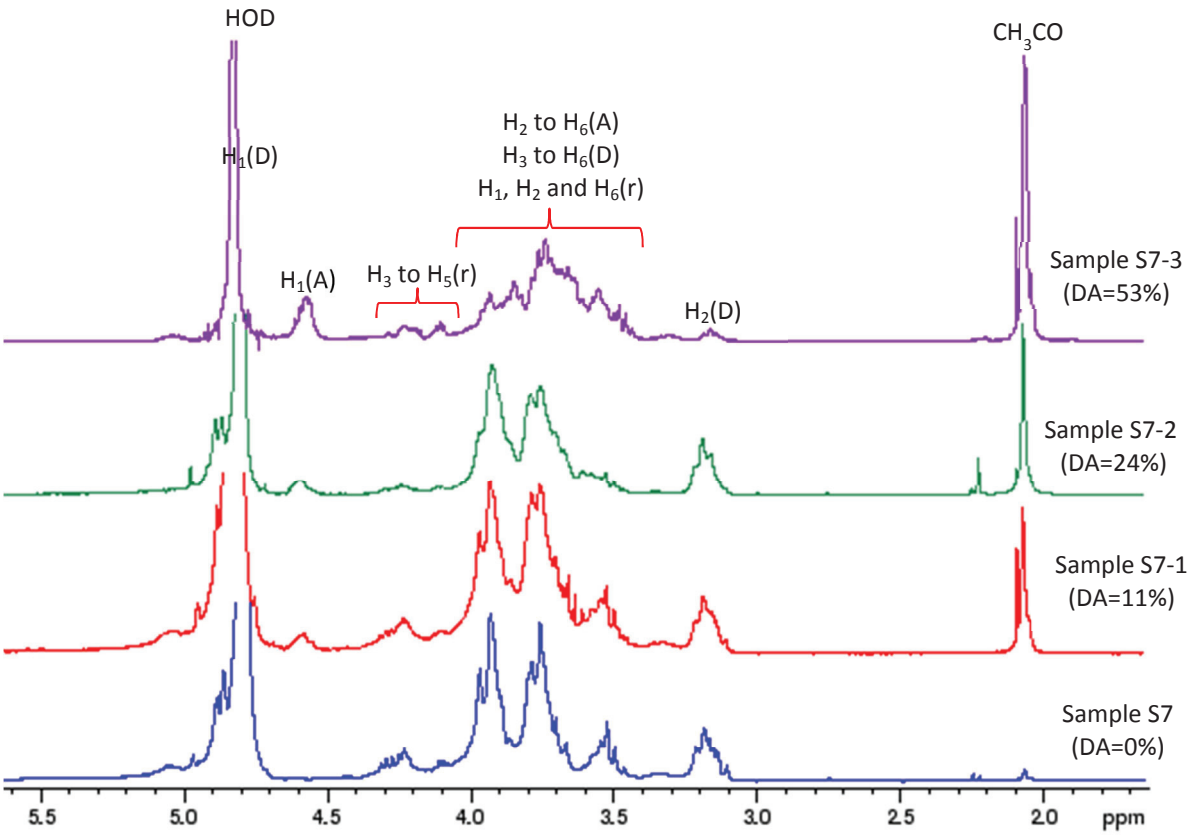

Figure 59: ^{1}H NMR spectra of partially *N*-acetylated reduced chitooligosaccharides of S7 series with different DA in D_2O with 0.5% (v/v) HCl (12N) (500 MHz, 25°C).

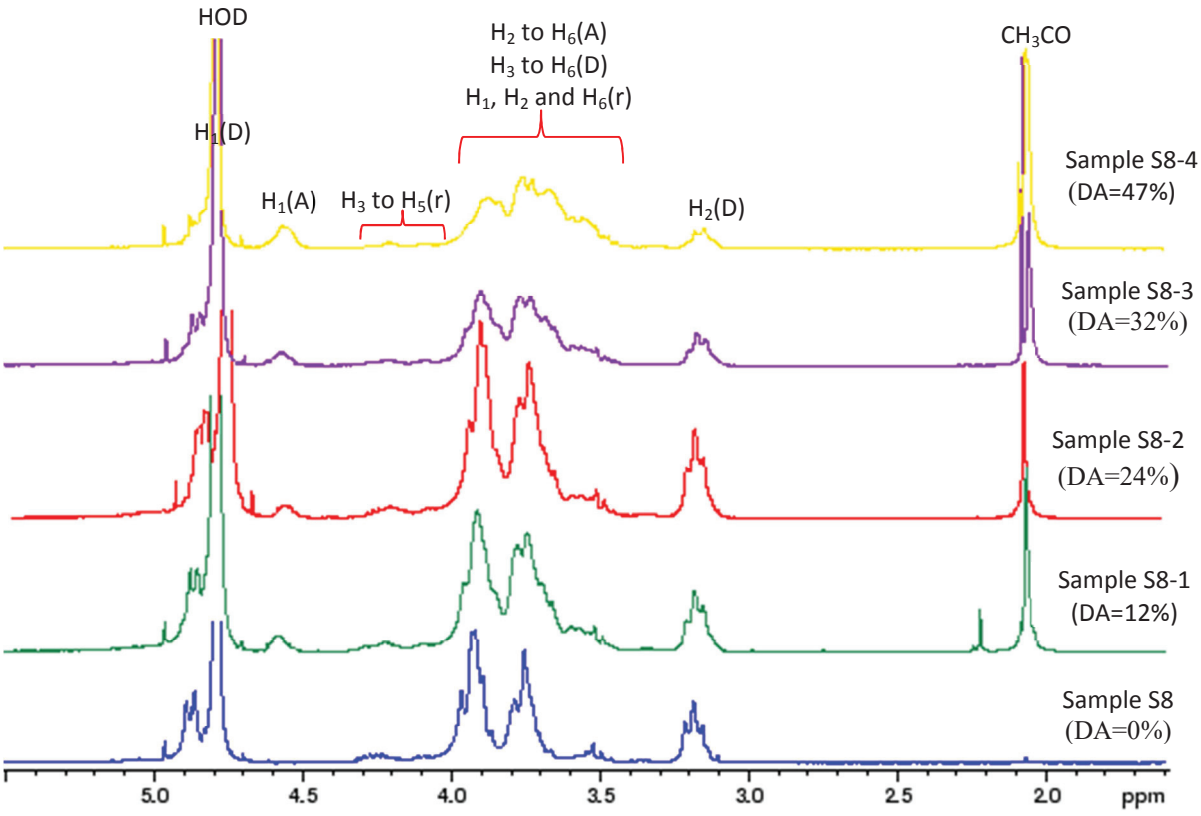

Figure 60: ^{1}H NMR spectrum of partially *N*-acetylated reduced chitooligosaccharides of S8 series with different DA in D_2O with 0.5% (v/v) HCl (12N) (500 MHz, 25°C).

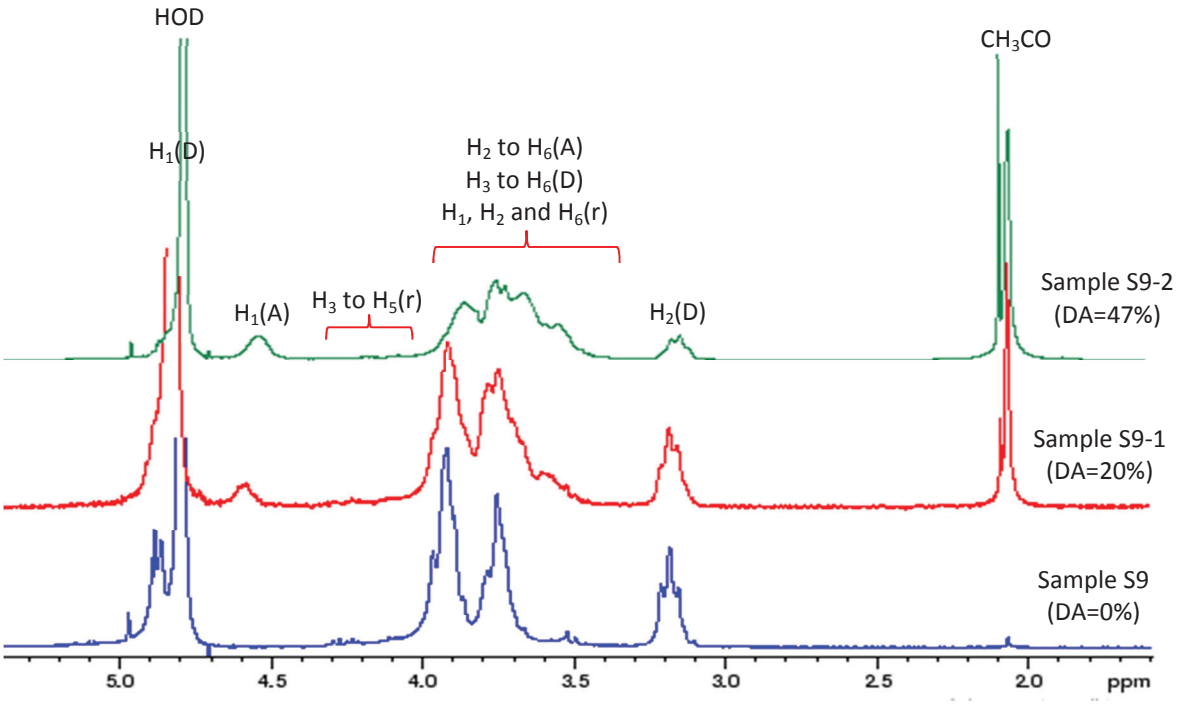

Figure 61: ^{1}H NMR spectrum of partially *N*-acetylated reduced chitooligosaccharides of S9 series with different DA in D2O with 0.5% (v/v) HCl (12N) (500MHz, 25°C).

2.2.2.1.2. Characterization by SEC

SEC-MALLS was performed to determine the mass- and number-average molar masses in order to calculate the DP values for the partially *N*-acetylated reduced chitooligosaccharides. Samples were solubilized in ammonium acetate pH 4.5 solution and injected in to two TSK gel G2500 and G6000 columns (Tosoh Bioscience) in series. The samples were detected by multi-angle light scattering (MALLS) detector HELEOS II (Wyatt Technology) operating at 664 nm was coupled on line to a Wyatt Optilab T-Rex differential refractometer and the results are summarized in Table 19 along with the values of the refractive index increment dn/dc used for the molar mass calculations. The number-average molar masses ($\overline{\mathrm{Mn}}$) increased from 2.20×10^3 till 8.76×10^3 g/mol and the mass average molar masses ($\overline{\mathrm{Mw}}$,) increased from 2.66×10^3 to 12.43×10^3 g/mol with an increase of dispersity from 1.2 to 1.4 from S7-1 to S9-2. This increase in the molar masses for the oligomers is expected since theirs an increase in both the DA and DP as we move from S7-1 to S9-2. These obtained number-average molar masses will be used in order to calculate the average degree of polymerization for each oligomer.

Even if the average DP values were calculated for the reduced COSamf S7, S8 and S9 in Table 14 and Table 16, however the average DP values for the acetylated oligomers were calculated to check if there is an effect of the *N*-acetylation on the calculated average DP values of the reduced COSamf. Therefore, the average DP for the acetylated oligomers was calculated according to the number-average molar mass ($\overline{\mathrm{Mn}}$) of the partially *N*-acetylated reduced chitooligosaccharides, the molar mass of the reduced amf unit ($M_{(\text{reduced amf})}$ = 164 g/mol) and the molar mass of the repeating unit (M_0). However in this case M_0 depends on the DA, hence in Equation 9, M_0 includes the molar mass of the GlcN/GlcNAc unit ($M_{(\text{GlcN})}$ = 164 g/mol and $M_{(\text{GlcNAc})}$ =203 g/mol). The results are shown in Table 19.

$$\overline{\mathrm{DP}} = \frac{\overline{\mathrm{Mn}} - \mathrm{M}_{(\text{reduced amf})}}{\mathrm{M}_{(\mathrm{GlcN})} \times \frac{(100 - \mathrm{DA})}{100} + \mathrm{M}_{(\mathrm{GlcNAc})} \times \frac{\mathrm{DA}}{100}} \qquad \text{Eq 9}$$

Table 19: Characterization data of synthesized partially *N*-acetylated reduced chitooligosaccharides by: a) ^{1}H NMR spectra and by b) SEC-MALLS chromatography.

N-acetylated reduced chitooligosaccharides samples	$\overline{DA}$(%)[a]	dn/dc (mL/g)	$\overline{Mw}$[b] (kg/mol)	$\overline{Mn}$[b] (kg/mol)	Đ [b]	$\overline{DP}$ [b]
S7-1	11	0.188	2.66	2.20	1.21	12 ±2
S7-2	24	0.182	2.89	2.41	1.20	13 ±2
S7-3	53	0.176	3.12	2.52	1.24	13 ±2
S8-1	12	0.187	5.63	4.44	1.27	26 ±2
S8-2	24	0.182	5.97	4.63	1.29	26 ±2
S8-3	32	0.182	6.10	4.72	1.31	26 ±2
S8-4	47	0.179	6.49	4.81	1.35	26 ±2
S9-1	20	0.183	11.78	8.42	1.40	49 ±2
S9-2	47	0.179	12.43	8.76	1.42	48 ±2

Compared to the DP values for the starting oligomers S7, S8 and S9, the average DP calculated by SEC chromatography for the *N*-acetylated reduced chitooligosaccharides were found to be very similar and close to the DP of the starting oligomers. The *N*-acetylation conditions were sufficiently soft to preserve the degree of polymerization. Even if a slight increase of DP was observed, this can be explained by the loss of low DP oligomers due to the purification method that was subjected to the oligomers after *N*-acetylation.

2.2.2.1.3. Characterization by Raman spectroscopy

Raman spectroscopy analysis was performed for the different partially *N*-acetylated chitooligosaccharides samples at room temperature. This technique, in general, is fast, not destructive (when used during a short time for the analyses) and does not require any especial sample preparation step (*e.g.* dissolution). Instead samples in a form of powder were pressed and the pellets were analysed. At the end of the analyses all the samples were recovered. Raman spectroscopy is an effective analysis tool that provides some structural information of the chitooligosaccharides, showing their chemical fingerprints. Raman spectra of the oligomer samples with different degree of polymerization (DP) and degree of *N*-acetylation (DA) are shown in Figure 62 (a), (b) and (c). The main vibrational bands of these samples are

summarized in Table 20 as well as the vibrational assignment based on the literature [169-172].

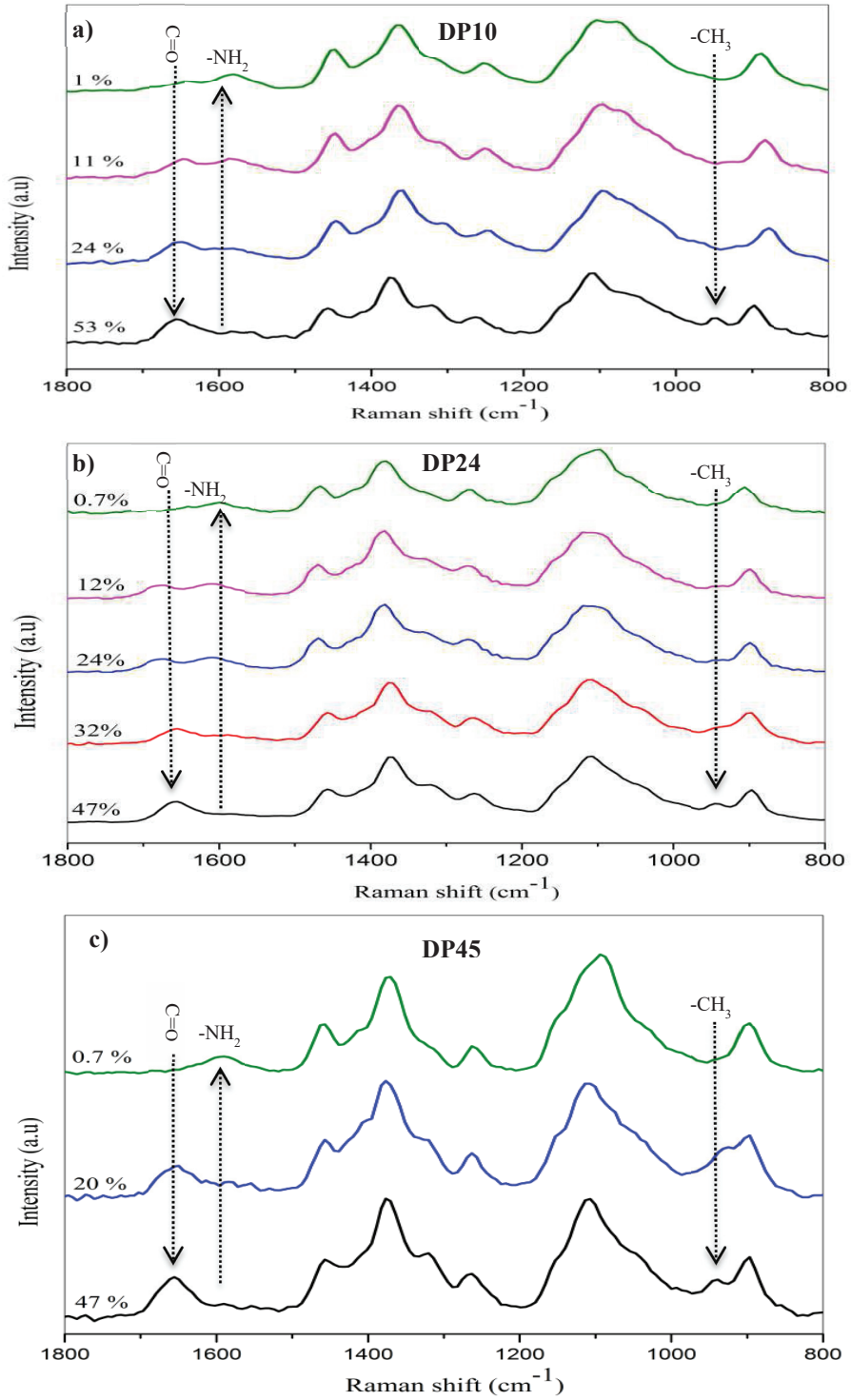

Figure 62 : Evolution of the Raman spectra of partially *N*-acetylated reduced chitooligosaccharides with DP ~10 (a), 24 (b) and 45 (c), respectively in function with their DA varying from ~0 to 53%.

Table 20: Main Raman shift of the vibrational bands observed for the chitooligosaccharides samples and respective vibrational assignments.

Raman shift (cm^{-1})	Vibration assignment
1654	ν(C=O)
1591	$\delta(NH_2)$
1458	$\delta(CH) + \omega(CH_2) + \delta(OH)$ $\delta(CH) + \delta(OH)$
1415-1377	$\delta(CH_3) + \delta(CH)$ $\delta(CH_2) + \delta(CH) + \delta(OH) + \nu(\Phi)$
1325	ν(CN) + δ(CH)
1263	δ(OH…O) + ν(C-C) + ν(C-O) + δ(CH)
1146-1093	ν(C-O-C) + ν(Φ) + ν(C-OH) + $\nu(C\text{-}CH_2)$ + δ(CH)
945	$\delta(CH_3)$
896	ν(Φ) + $\rho(CH_2)$

Φ, pyranoid ring; ν, stretching; δ, in-plane bending vibrations; ρ, rocking; γ,ω, out-of plane bending.

Specifically some band intensities are dependent on the degree of *N*-acetylation ratio of chitooligosaccharides, since the concentration of specific groups is varying. Consequently, remarkable differences on the Raman spectra at 1654, 1591 and 945 cm^{-1} were observed in the series of samples that were analysed, as assigned in Figure 62. The band at 1654 cm^{-1} is attributed to amide I vibration of the amide group in the *N*-acetyl-D-glucosamine unit. The band at 1591 cm^{-1} is assigned to the vibration of the $-NH_2$ group in the D-glucosamine unit. Finally the band located at 945 cm^{-1} is attributed to the methyl group of the *N*-acetyl-D-glucosamine unit of chitosan [169, 170]. Hence, the intensity of these three bands directly correlated with the DA, the intensity at 1654 cm^{-1} and 945 cm^{-1} increases when that at 1591 cm^{-1} decreases as a result of an increase in the DA.

As already known, using the ^{1}HNMR it is possible to determine precisely the DA of oligosaccharides samples. This analysis was used to determine the DA of our samples, as already shown in this manuscript. Thus, these data were used amongst the relation between some specific vibrational bands of Raman spectra to propose calibration curves to estimate rapidly the DA of other samples with unknown DA. First, some graphics were built using the reference DA values, determined by ^{1}HNMR, and the band intensity ratios of 1654/896,

1591/896 for all series of samples analysed with DP 10, 24 and 45. As already mentioned, the bands at 1654 and 1591 cm^{-1} are originated from the amide and amine groups of chitosan, respectively. The band at 896 cm^{-1} is related to the vibration of the saccharide ring and its intensity is constant in each series of COS analysed. The calibration curves resulting from these relations can be observed in Figure 63. Similar calibration curves for DA (or DD, degree of deacetylation) determination were already proposed by Zajac *et al*. [169]. They used the DD specified by their provider and the Raman spectra measured in their study to prepare their calibration curves. In this case, they used the intensities of the bands extracted after the deconvolution of determined region of the Raman spectra. To simplify this analytical process, we used the intensities of the bands extracted directly from the normalised Raman spectra at given wavenumber values, to prepare our calibration curves. Additionally, we propose the use of the ratio of two bands directly linked with the concentration of amide and amine groups on chitosan, *i.e*. the bands at 1654 and 1591 cm^{-1}, to prepare calibration curves to determine the DA. The intensity ratios of 1654/1951 bands values, for the series of samples at DP 10, 24 and 45, were calculated and used to design the graphs showed in Figure 63.

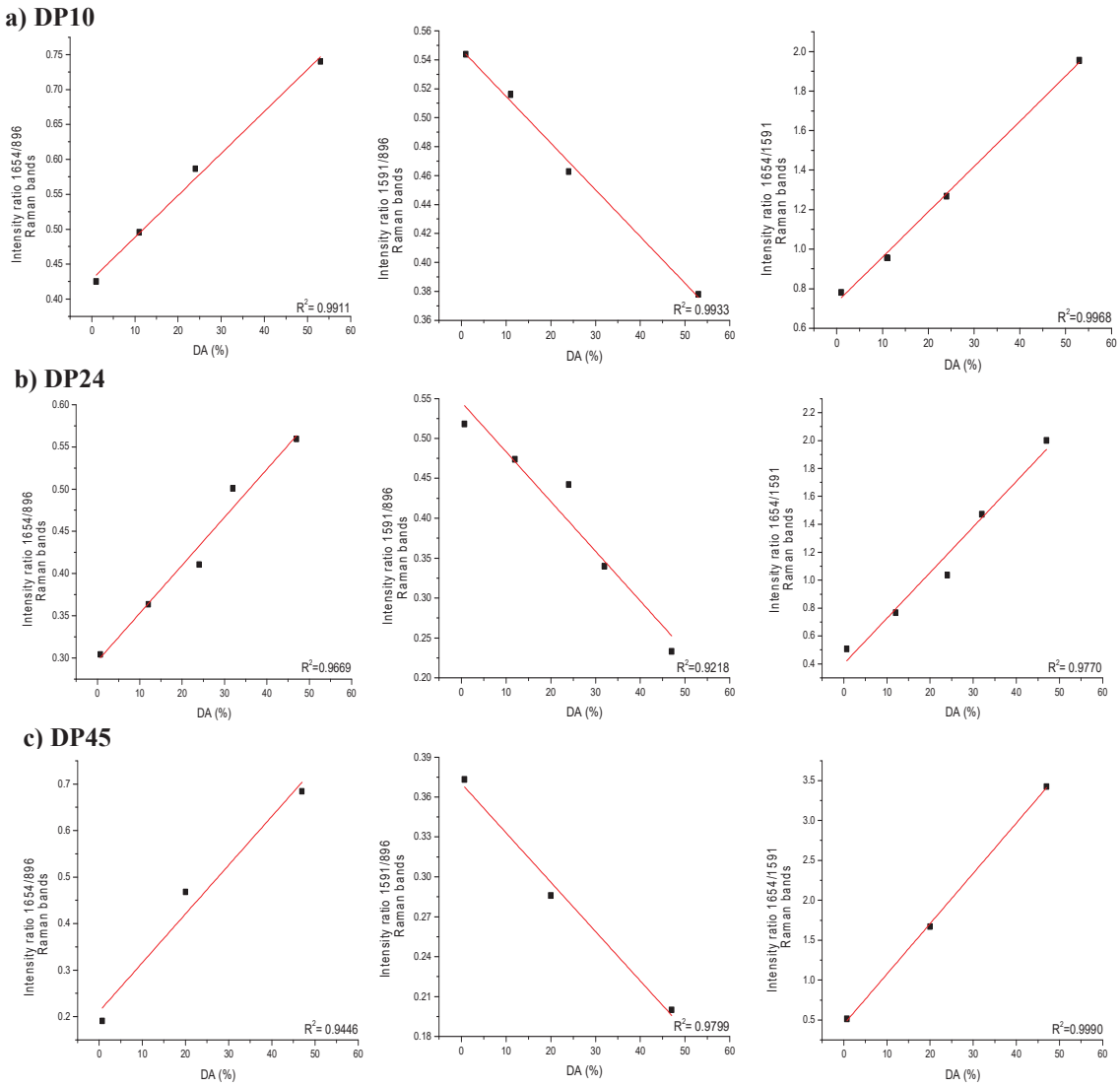

Figure 63: Relation between the DA calculated from NMR analysis and intensities of the Raman bands for partially *N*-acetylated reduced chitooligosaccharides a) DP10 b) DP24 c) DP45 at 1654/896, 1591/896 and 1654/1591 cm^{-1}, respectively.

The curves traced from the DA versus the intensity ratios of the bands 1654/896, 1591/896 and 1654/1591, for all series of samples analysed, presented a linear response and were fitted using a linear equation as shown in Equation 10. The equations resulting from linear regressions are shown in Table 21.

$$y = ax + b \qquad \text{Eq. 10}$$

Table 21: Equations obtained by the fitting of the curves traced from the DA versus the intensity ratios of the bands 1654/896, 1591/896 and 1654/1591 and their coefficient of determination (R^2), for the indicated DP.

Sample DP*x*	Linear equation for each proposed graphic	Coefficient of determination (R^2)
DP10	1654/896 = 0.00601 DA + 0.42807	0.99113
	1591/896 = -0.00323 DA + 0.54699	0.9933
	1654/1591 = 0.02292 DA + 0.73048	0.9968
DP24	1654/896 = 0.00569 DA + 0.29618	0.96697
	1591/896 = -0.00623 DA + 0.54557	0.92183
	1654/1591 = 0.03268 DA + 0.40055	0.96701
DP45	1654/896 = 0.01048 DA + 0.21113	0.94462
	1591/896 = -0.00371 DA + 0.37014	0.97999
	1654/1591 = 0.06308 DA + 0.4458	0.99903

It should be noted that there is an excellent linearity of the derived relations. However, the fittings that present a slightly better coefficient of determination (R^2) were those one performed in the curves with the DA versus the intensity ratios of 1654/1591 bands, as can be observed in the Table 21. Thus, we can suggest that the best way to estimate the DA of a chitooligosaccharide sample is using the calibration curve with the DA versus the ratio between the intensity bands at 1654 and 1591 cm^{-1}. The estimation of DA values is valid, since the curve for the same DP of the analysed sample is used. Since, the relative intensities of the bands for the same DA change concerning the DP.

As a variation in the relative intensities of the bands for the same DA at different DP could be observed, it was attempted to establish a relation among the intensity ratios of the bands at a specific DA to estimate the DP of a chitooligosaccharide sample. Therefore, we plotted the intensity ratio at 1654/896, 1591/896 and 1654/1591 versus the DA, as shown in Figure 64. The graphs displays the 3 DP analysed, DP 10, 24 and 45. However, it was not possible to

visualize a direct relation in these graphics to estimate both the DP and the DA of a chitooligosaccharide.

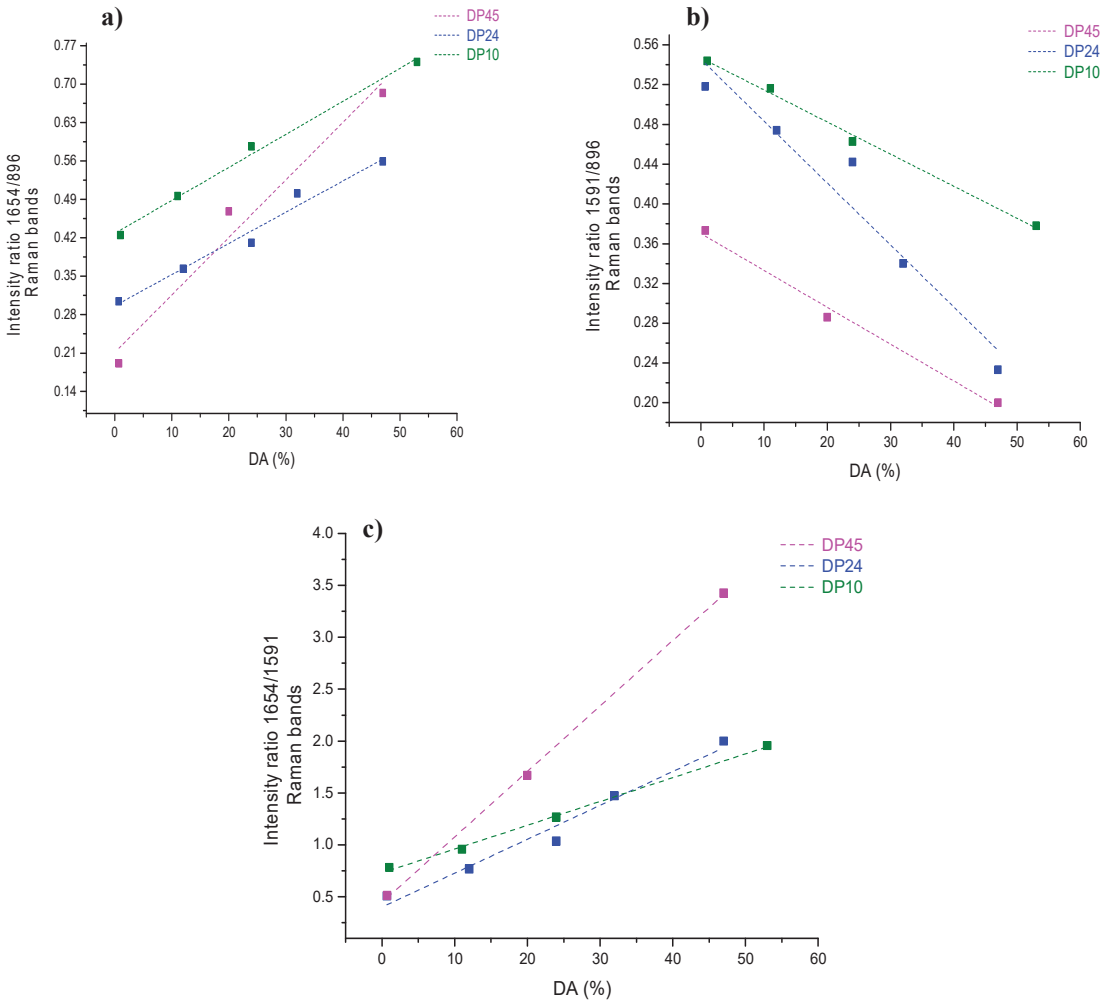

Figure 64: Relation between the DA calculated from NMR analysis and intensities of the Raman bands for partially *N*-acetylated reduced chitooligosaccharides DP10, 24 and 45 at a) 1654/896, b) 1591/896 and c) 1654/1591 cm^{-1}.

The final group of the chitooligosaccharides prepared using the synthesis method that was previously described in our work result in an 2,5-anhydro-D-mannofuranose (amf) ring with 4 carbons and 1 oxygen, as can be observed in Figure 65. The similarity of this structure with the saccharide structure and consequently the superposition of bands, make it difficult to find a specific vibrational band that could be used to estimate the DP of samples. Maybe a more accurate analysis will be able to find a relation among the Raman spectra to determine the DP of chitooligosaccharides. In this way, we can propose the use of chemometrics analyses.

These analyses are still in process in collaboration with the LMOPS (http://lmops.univ-lorraine.fr/equipe-spectrometrie) in Collaboration with P. Bourson and D. Chapron.

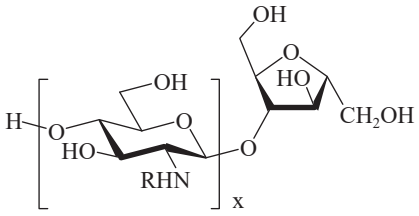

R = H or Ac

Partially *N*-acetylated reduced chitooligosaccharides

with x = ~10, ~24 or ~45

Figure 65: General structure of the chitooligosaccharides prepared using the synthesis method described in this work.

Summarizing, Raman spectroscopy analysis showed the characteristics bands that identify the chemical groups of partially *N*-acetylated reduced chitooligosaccharides (chemical fingerprints) were in complete agreement with literature [169, 170]. Consequently, these results corroborate with the previous characterizations performed in this work. In addition a relationship between the degree of *N*-acetylation and the intensity ratios of bands was proposed to be used in the estimation of unknown DA values. Estimation that is valid, but taking in to account the DP of the samples.

In this part, the partially *N*-acetylated reduced chitooligosaccharides with different average degree of polymerization were synthesized in three chemical reaction steps (i) the first step involved the nitrous acid depolymerization of a fully *N*-deacetylated commercial chitosan to produce chitooligosaccharides samples with 2,5-anhydro-D-mannofuranose (amf) at their reducing end (COSamf) with different degrees of polymerization; (ii) the second step involve the reduction of the COSamf obtained leading to the reduced COSamf with different degrees of polymerization; (iii) the third step involved the partially *N*-acetylation of reduced COSamf to obtain the targeted chitooligosaccharides with different DP and DA. The determination of the average DP value of the GlcN units was carried out by SEC-MALLS spectroscopy. For each sample of the series, the average DA was determined by ^{1}H NMR. ^{1}H NMR was also helpful to proof the structural characterization of the oligomers that was also confirmed by Raman spectroscopy.

3. Conclusions

In the first part of this work, we discussed the elaboration of partially *N*-acetylated chitooligosaccharides with DP 4 and DA from 0 till 90%. For this task, we focused on the *N*-acetylation of the commercially chitotetraose hydrochloride as starting material. The second part of this work was dedicated to synthesize partially *N*-acetylated reduced chitooligosaccharides from around DP 10 to 45 and DA 0 till 50%. This was performed by means of the nitrous acid depolymerization of a fully *N*-deacetylated chitosan and reduction reaction, followed by *N*-acetylation to prepare various partially *N*-acetylated reduced chitooligosaccharides from DA 0 till 45%. As a deliverable of this work, a total of 19 samples of chitooligosaccharides with different DA and DP along with commercial oligomers labeled in red, DP3 to DP 6 with DA 0 and 100 were structurally characterized by different techniques and are located in the DP-DA plane as summarized in
Figure **66**.

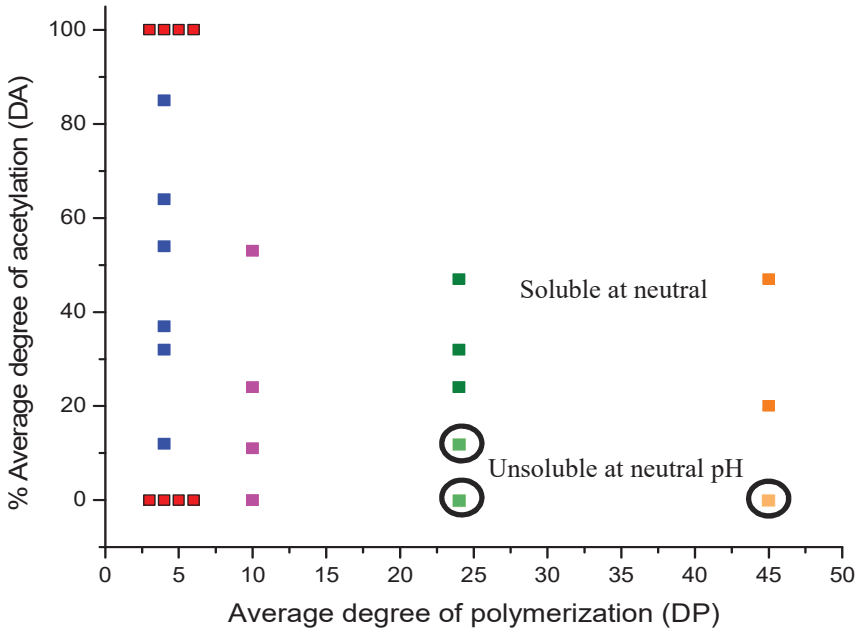

Figure 66: Summary of all the synthesized chitooligosaccharides with different degrees of polymerization and *N*-acetylation.

The synthesized partially *N*-acetylated chitooligosaccharides except of DP 24 DA 12, DP 45 DA 0 (not soluble) and DP 24 DA 24 (partially soluble) were generally soluble at neutral pH.

These solubilized partially *N*-acetylated reduced oligomers will be tested in chapter 3 in contact with neuronal–like cell lines and for the synthesis of supermagnatic particles.

4. Experimental Details

4.1. Materials

Commercial chitotetraose (Reference C2641 (XPM7D-RP); degree of *N*-acetylation (DA) ~ 0%) was supplied by TCI. Commercial chitotriose and chitopentaose (Reference 01032016; degree of *N*-acetylation (DA) ~ 0%) was supplied by Qingdao. Commercial chitohexose (Reference 400436 (081100); degree of *N*-acetylation (DA) ~0%) was supplied by Seikagaku. Commercial chitosan (batch 244/020208; degree of *N*-acetylation (DA) ~ 0%; M_w = 270,000 g/mol; M_n = 115,000 g/mol; Đ = 2.3) was supplied by Mahtani Chitosan Ltd (Veraval, India). Fresh acetic anhydride (purity ≥ 99%), sodium nitrite (purity > 99%), deuterium oxide (D_2O, assay > 99.96% atom D), aqueous ammonia 28% (purity ≥ 99%) and all others solvents were provided by Sigma-Aldrich (Saint-Quentin Fallavier, France).

4.2. Procedures used for the synthesis of chitooligosaccharides

4.2.1. Syntheses of partially *N*-acetylated chitotetraose oligomers

150 mg (185 µmol, M=808 g/mol) of chitotetraose hydrochloride $(GlcN, HCl)_4$ were dissolved in 7.5 mL of methanol/water 90/10 (v/v). Trimethylamine (30, 45, 60, 121, 121, and 132 µmol M=59.1 g/mol) and pure fresh acetic anhydride (32, 35, 46, 84, 102, and 127 µL) were added in a molar equivalence with respect to chitotetraose to reach the expected average percentage DA (~12, 32, 37, 54, 64, and 85 %) respectively. The mixture was stirred at room temperature. After 5 h of stirring, the reaction was stopped by addition of water (7.5 mL). The solutions were then concentrated by roto-evaporation to remove methanol. Then the solution was lyophilized after addition of water (5 mL). At the end, for samples S1 till S4 (DA ~ 12 till 54 %) the powder was solubilized with 2 mL of water and separated by adsorption on a Dowex 50WX8 ion exchange resin followed by successive desorptions: (i) with pure water for the recovery of totally *N*-acetylated chitotetraose, and then (ii) with dilute ammonia solution (7% v/v in water) for the recovery of partially *N*-acetyl-chitotetraoses. As for samples S5 and S6 (DA ~ 64 and 85 %) the powders were solubilized with 2 mL of water and then co-evaporated several times with 10 mL of water. Finally all the partially *N*-acetylated chitotetraose oligomers were isolated as a white powder after lyophilization.

4.2.2. Syntheses of reduced chitooligosaccharides with different degree of polymerization from 10 to 45

Chitosan (30 g, 187 mmole of GlcN unit) was solubilized in 1L of water by addition of 15.5 mL of HCl (37% w/w). A freshly prepared 25 mL aqueous solution of $NaNO_2$ (GlcN/$NaNO_2$ molar ratio = 4, 10 and 30 for S7, S8 and S9 respectively) was added and the reaction was stirred for 12 h at room temperature. After, the solutions were filtered on 1.2 µm nitrocellulose membrane. $NaBH_4$ (37.8 g/mol, 4, 1.8 and 0.65g, 125, 48 and 16 mmol for S7, S8 and S9 respectively) were added at ~ 0°C and the solution was stirred for 12 h. For sample S7 (DP ~10) the solution was neutralized by the addition of ammonium hydroxide solution (28% w/w) until pH ~8 and concentrated by evaporation. Sample S7 (x ~10) was obtained as a white powder after precipitation in ethanol and drying under vacuum. For samples S8 (x ~24) and S9(x ~45), oligomers were precipitated by addition of ammonium hydroxide solution (28% w/w) to pH ~9, washed several times with deionized water until neutral pH, then freeze-dried leading to samples S8 and S9 as a white powder.

4.2.3. Synthesis of partially *N*-acetylated reduced chitooligosaccharides

The partial *N*-acetylation reaction was performed in dissolving 0.5 g of the reduced samples S7, S8 and S9 in 20 mL of methanol/water 90:10 (v/v) for sample S7 (DP 10) and in 20 mL of methanol/acidify water (AcOH 1.5%(w/v)) 70:30 (v/v) and 50:50 (v/v) for samples S8 (DP 24) and S9 (DP 45) to ensure solution homogeneity. Various amounts (34, 76, 101, 149 µL) of pure and fresh acetic anhydride were added in a stoichiometric manner to reach the expected DA (10, 20, 30, and 50 % respectively). After 12 h of stirring at room temperature, solutions were neutralized by the addition of ammonia till pH~8. For sample S8-1 (DP 24, DA ~12) was precipitated at pH~8, washed abundantly with water then freeze dried. As for the other samples, S7-1, S7-2 and S7-3, S8-2, S2-3 and S8-4 and S9-1, S9-2, the reactions solutions were concentrated by evaporation under vacuum and then *N*-acetylated chitooligosaccharides were precipitated, abundantly washed with acetone and finally dried under vacuum to obtain *N*-acetylated chitooligosaccharides as white powder.

4.3. Techniques used for the characterization of chitooligosaccharides

4.3.1. ^{1}H NMR Spectroscopy

Average DAs of the chitooligosaccharides were determined by ^{1}H NMR spectroscopy. Spectra were recorded on a Bruker 500 MHz spectrometer for partially *N*-acetylated chitotetraose and partially *N*-acetylated reduced chitooligosaccharides samples at 321 and 300K respectively. 10mg/mL of oligomers were dissolved in D_2O and 5 µL of concentrated HCl 12 N. The signal of HOD (δ 4.80 ppm) was used as reference.

4.3.2. MALDI-TOF Mass Spectrometry

All mass spectra were acquired with a Voyager-DE STR (ABSciex, Framingham, MA) equipped with a nitrogen laser emitting at 337nm with a 3ns pulse, operated in reflectron mode. Ions were accelerated to a final potential of 20kV. The positive ions were detected in all cases. Mass spectra were the sum of 300 shots and an external mass calibration of mass analyzer was used (mixture of peptides from Sequazyme TM standards kit, AB Sciex). The matrix used for all experiments was 2,5-dihydroxybenzoic acid (DHB) purchased from Sigma–Aldrich and used directly without further purification. The solid matrix and oligomer samples were dissolved at 10 mg/mL in water. A volume of 9uL of matrix solution was then mixed with 1uL of oligomer solutions. An aliquot of 1uL of each resulting solution was spotted onto the MALDI sample plate and air-dried at room temperature.

4.3.3. High performance liquid chromatography (HPLC)

Chromatography analysis was performed using a system Shimadzu HPLC Model CBM-20A. Samples were dissolved in eluent (Acetonitrile/H_2O 7/3, v/v) at 10 mg/mL and injected (20 µL) into a Shodex Asahipak NH2P-50G-4A column (5 µm granulometry, 250 mm × 4.6 mm) at room temperature, with a flow rate of 0.8 mL/min and a UV detection at λ = 195 nm. Pre-conditions of the column with with (1) Phosphate buffer/0,02M pH 10, flow rate 0,2 mL/min, 15h ; (2) CH_3CN/H_2O, flow rate 0,5 mL/min, 5h.

4.3.4. Size-exclusion chromatography (SEC)

SEC was performed on a chromatographic equipment composed of a 1260 Infinity Agilent Technologies pump connected to two TSK gel G2500 and G6000 columns (Tosoh Bioscience) in series. A multi-angle laser light scattering (MALLS) detector Dawn EOS

(Wyatt Technology) operating at 664 nm was coupled on line to a Wyatt Optilab T-Rex differential refractometer. Sample solutions at 2-5 mg/mL were prepared and eluted in AcOH (0.2 M)/AcONH4 (0.15 M) buffer (pH 4.5). Solutions were previously filtered through 0.22 µm pore size membranes (Millipore) before injection. The eluent flow rate was 0.5 mL/min. The refractive index increment dn/dc used for molar mass calculations was equal to 0.198, 0.187, 0.182, 0.182, 0.178 $cm^3.g^{-1}$ respectively for DA ~ 0, 10, 25, 30, 50 %.

4.3.5. Raman spectroscopy

Raman spectra were recorded by BaySpec RamSpec^{TM} instrument, using a laser excitation at 1064nm. The measurements are performed at room temperature in the spectral range of 3000–300 cm^{-1}, with the spectral resolution of 4 cm^{-1}. Samples in a powder form were pressed as pellets, analysed and material could be recovered at the end of the analysis. The spectroscopic measurements of all samples were independently repeated two times with the use of 16 accumulation scans, using an exposition time of 20s. All the experimental data were processed using Origin software version 8.5, OriginLab Corporation.

Chapter III

Applications of well-defined and characterized chitooligosaccharides in biology and material science

Introduction

Our goal in this chapter is to show that chitooligosaccharides with a partial control of degrees of polymerization and *N*-acetylation synthesized in chapter 2, exhibit several biological activities. As a reminder, the chitooligosaccharides synthesized in chapter 2 have a specific chemical structure in terms of degrees of polymerization, from 4 to 45 and with different degrees of *N*-acetylation from 0 to 85%.

In this chapter we will start by evaluating the toxicity of some chosen synthesized chitooligosaccharides. This was performed in the Cell-Environment Interaction team (ICE) at VetAgro-Sup (Campus vétérinaire de Lyon at the University of Lyon), with the help of Pr. Didier PIN, Nadège Milhaud and Dr. Caroline Prouillac. After, we will describe the screening of different COS with different DP and DA to test their impact on neuron-like cell lines. This study was performed at the School of Biomedical Sciences at the University of Leeds, under the supervision of Dr. Jessica Kwok. Finally we will describe the synthesis of supermagnatic particle from iron ions complexes with chitooligosaccharides, and how COS impact the toxicity of Fe_3O_4 nanoparticles. This work was performed in collaboration with ICE group see above) and Dr. Paula Oliveria at Laboratory of Polymer Materials Engineering (IMP@Lyon1 UMR 5223) at the University Claude Bernard Lyon 1, France.

1. Toxicity of synthesized chitooligosaccharides with different degree of polymerization and *N*-acetylation

The chitooligosaccharides synthesized in chapter 2, fully characterized with specific degree of polymerization and *N*-acetylation were screened in order to evaluate their toxicity on canine dermal fibroblasts. This was be performed i) by isolating the canine fibroblast from beagle dog then ii) culturing the canine dermal fibroblasts with chitooligosaccharides (COS), iii) assessing the cytotoxicity of COS by following the international standard operation procedures or cytotoicity evaluations.

1.1. Review of the literature concerning chitooligosaccharides toxicity

Chitosan is widely considered as a non-toxic polymer [173]. It is approved for dietary applications in Japan, Italy and Finland [174] and it has been approved by the FDA for use in wound dressings [175]. However, toxicity of COS has not been widely studied and contradictory conclusions are reported. Fernandes *et al*. [176] studied the toxicity of COS on human lymphocytes. They demonstrated that COS have higher cytotoxic effect on these cells at 24h at high molar mass (in the range $1.763x10^3$g/mol to $4.134x10^3$g/mol; DP 10 to 23) despite an approximately of same DA (~30%). These authors suggest that the chain length plays a crucial role upon induction of cytotoxicity. Absence of toxic effects by COS (DA 30% and molar mass $6.0\text{-}7.0x10^3$g/mol; DP 34-40) at concentrations ranging from 0.050–1.0 mg/mL at 24h was also reported on human and mouse leukocyte cell lines [13]. Beside another study report that at 0.80 mg/mL COS (DA 5% and DP 3-9) induces apoptosis upon human hepatocellular carcinoma cells [177]. In addition, De Assis *et al*. [14] studied the cytotoxicity of COS (DA 15% DP 2-6) on human tumor cell lines (HepG2 and HeLa) and mouse embryonic 3T3 cells. Their results showed a high proliferative activity on normal 3T3 cells when they used COS (0.5 and 1.0 mg/ml). They showed that COS exert a pronounced proliferative effect on HeLa cells but not on HepG2.

Because of the lack of clear data on COS cytotoxicity in partly due to the diversity of COS studied and the various cell lines that have been used, we decided to investigate the cytotoxicity of our well controled COS in different conditions. The aim of our work was to clearly establish a relation between cytotoxicity and structural parameters, namely molar masses and degree of *N*-acetylation. In this part, we described the protocol that we have used

to evaluate the cytotoxicity of the synthesized COS. In a first step we have chosen soluble COS at neutral pH with different DA and DP, $COS_{DP/DA}$ such as, $COS_{10/53}$, $COS_{24/47}$, $COS_{45/47}$, $COS_{10/0}$ and $COS_{24/24}$. The chosen COS are labeled in Figure 67 as blue spots in the solubility domain.

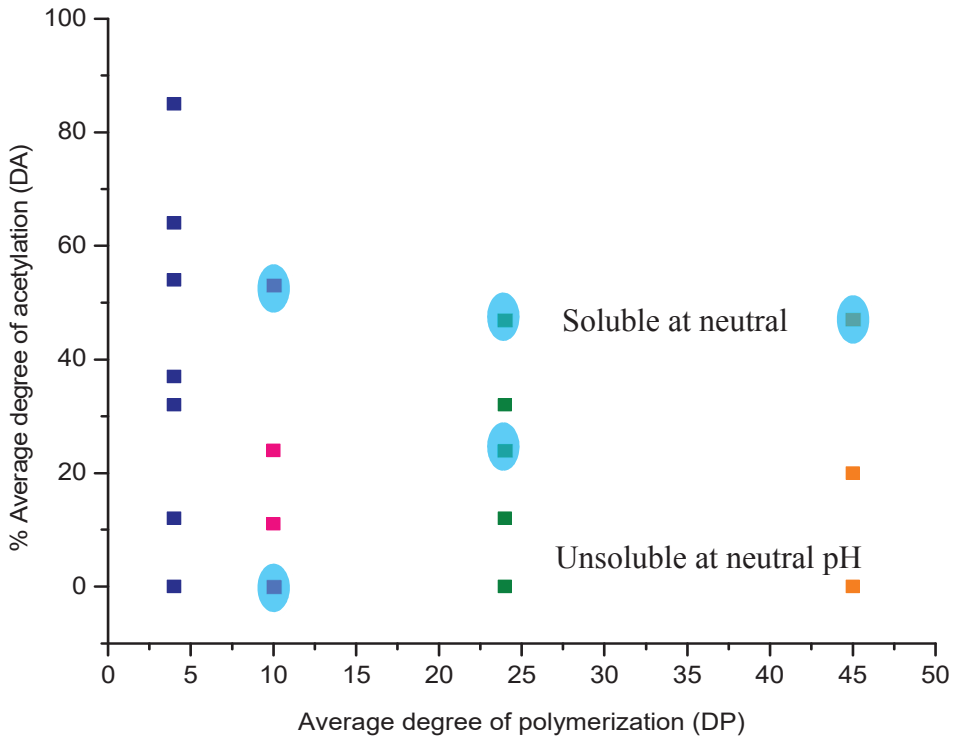

Figure 67: Summary of oligomers with different degree of polymerization and *N*-acetylation tested forcytotoxicity (canine dermal fibroblasts model).

1.2. Canine dermal fibroblasts culture conditions

1.2.1. Biopsies of beagle dogs

The fibroblasts are derived from skin biopsies (6 mm in diameter) made at the dorsal surface of beagle dogs of the Institut Claude Bourgelat (VetAgro Sup -Campus Vétérinaire de Lyon, Marcy l'Etoile, France). The procedure consists first on cleaning and disinfecting the area to be sampled. This was done by passing a mower on the area to be sampled and then disinfect the chosen area with betadine soap using a compress (Figure 68-a). This step was repeated three times by changing the compress every time. After disinfecting, an anesthesic (xylocaine)

injection was done on the site of the sampling site to limit pain and after few minutes biopsies were obtained by using a 6 mm punch. Using this punch we took a piece of skin by turning it always in the same direction with light pressure. The punch was gently removed the biopsy was taken from below and cut at the level of the hypodermis with a pair of scissors as shown in details in Figure 68-b. Finally, we transferred the biopsy to a transport medium supplemented with antibiotics. The open area (Figure 68-c) was sewed and the wound was cleaned. During all the process, dogs were softly restrained.

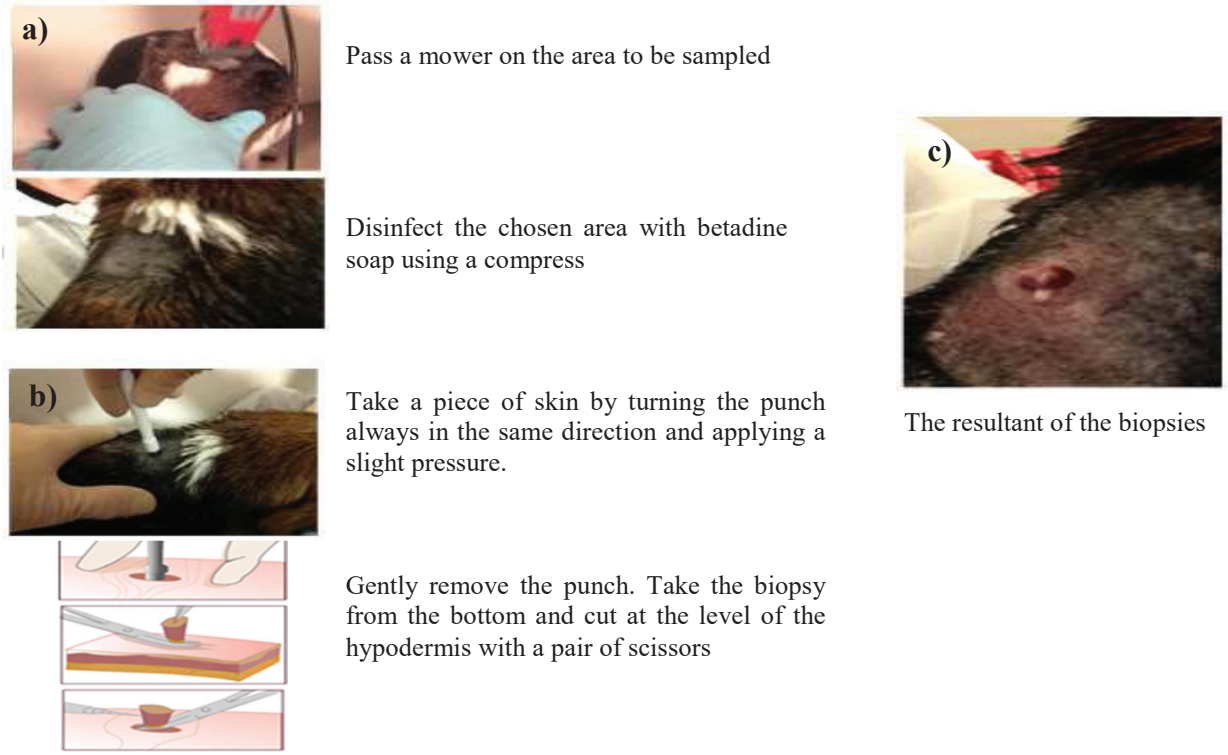

Figure 68: Steps performed to biopsies a beagle dog, a) cleaning and disinfecting the sampled area b) biopsies by using a 6 mm punch, c) resulting skin after the biopsies before sewing.

1.2.2. Culture of fibroblasts

The fibroblasts were removed and isolated in a sterile condition. They were obtained after dilacerations of biopsies with scissors (Figure 69-a), the obtained pieces were treated for 10 minutes with trypsin at 37°C (Figure 69-b). The cells were obtained after centrifuging for 1 min at 8000 rpm and placed in culture DMEM medium containing 20% Fetal Calf Serum (FCS) and 2% penicillin/streptomycin/amphotericin B as shown in Figure 69-c. The fibroblasts were incubated at 37°C / 5% CO_2.

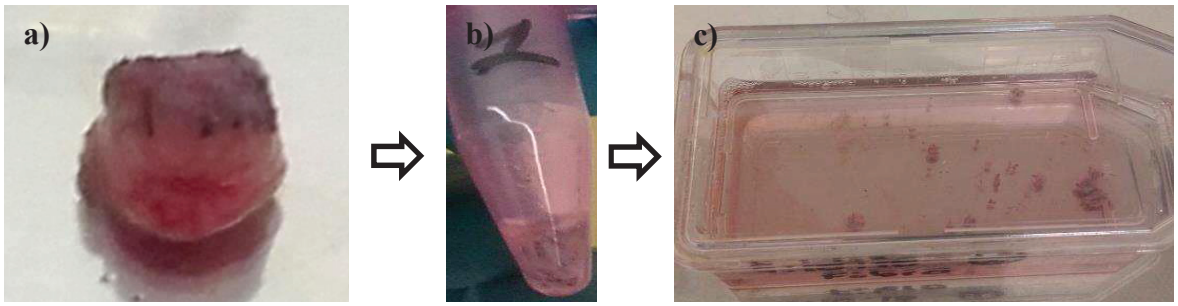

Figure 69: Steps performed to culture fibroblast a) Piece of the biopsy from beagle dog, b) treatment of the biopsy with trypsin in an eppendorf then centrifuged, c) culture of fibroblast medium cells with DMEM.

1.2.3. Evolution of the fibroblast culture

Fibroblasts are adherent cells. Colonization of the support by fibroblasts takes approximately ten days at 37°C / 5% CO_2. During this time, the culture medium is periodically (two times a week) changed to remove tissue debris and dead cells. Once the cells reached confluence, it is necessary to place them in a new larger culture flask to allow them multiplying. Cells are detached from the support using 0.25% trypsin/EDTA medium. Cells were used between passages 3 and 10.

1.3. Cytotoxicity testing

The canine fibroblasts were seeded at a density of 1×10^4 cells/ well in 96-well plate at 37°C with 5% CO_2. After 2 days of culture, the medium was replaced with fresh medium containing COS over a range of concentration (0 [control], 0.1, 0.5, 1, 5 and 10 mg/ml for COS). Two exposure times (24h and 48h) were tested.

1.3.1. Test of viable cells

After 24h and 48h, the cell viability was investigated in accordance with the international standard operation procedure “Tests for in vitro cytotoxicity” ISO 10993-5. It consists on adding a reagent that will be metabolized into a product by the living cells, capable on absorbing UV. In more details, cell cytotoxicity was assessed by the CCK-8 assay (Sigma Aldrich, Saint Quentin Fallavier, France) according to the manufacturer’s instructions. This kit contains highly water-soluble tetrazolium salt [WST-8, 2-(2-methoxy-4-nitrophenyl)-3-(4-nitrophenyl)-5-(2,4-disulfophenyl)-2H-tetrazolium, monosodium salt] which is reduced by

dehydrogenases in living cells to give formazan a yellow in color as shown in Figure 70. The amount of formazan generated is directly proportional to the number of living cells.

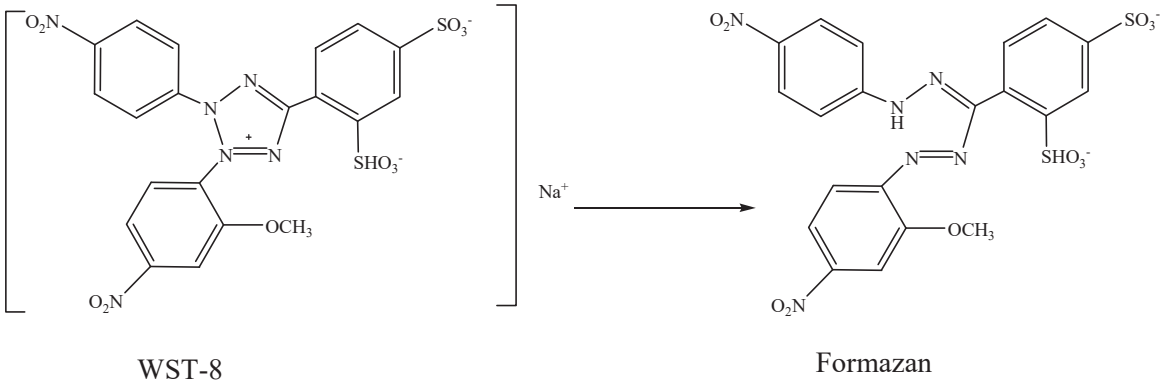

WST-8 Formazan

Figure 70: reduction reaction of WST-8 in living cells to give formazan.

The in vitro cytotoxicity results with different COS such as, $COS_{10/0}$, $COS_{10/53}$ and $COS_{24/24}$, $COS_{24/47}$ and $COS_{45/47}$ with various concentrations (ranging from 60 µg/mL to 10000 µg/mL=10mg/ml) are illustrated in Figure 71 after 24 h and 48 h. As shown in Figure 71 , the different COS generally had a low impact on the cell viability after 48 h and 24 h at low concentrations of incubation. Significant differences could be observed for $COS_{10/0}$, $COS_{10/53}$ and $COS_{45/47}$ after 24 h of exposure and for $COS_{24/24}$ and $COS_{45/47}$ after 48 h of exposure at the highest concentrations (5000 and 10000 µg/mL). The slight increase in the cell viability at 48 h when comparing to 24 h could be explained due to a proliferation effect of the COS [178]. In addition, it was noticed that the cell viability stayed between 80 % and 90 % in comparison with control cells (cultured fibroblast cells in the absences of COS) after 24 h and 48 h of exposure time. Relying to the international standard operation procedure “Tests for in vitro cytotoxicity” ISO 10993-5, which sets a threshold of 70% of cell viability to evidence a toxic effect, we can conclude that all the tested COS were not cytotoxic at 24 and 48h in the observed conditions.

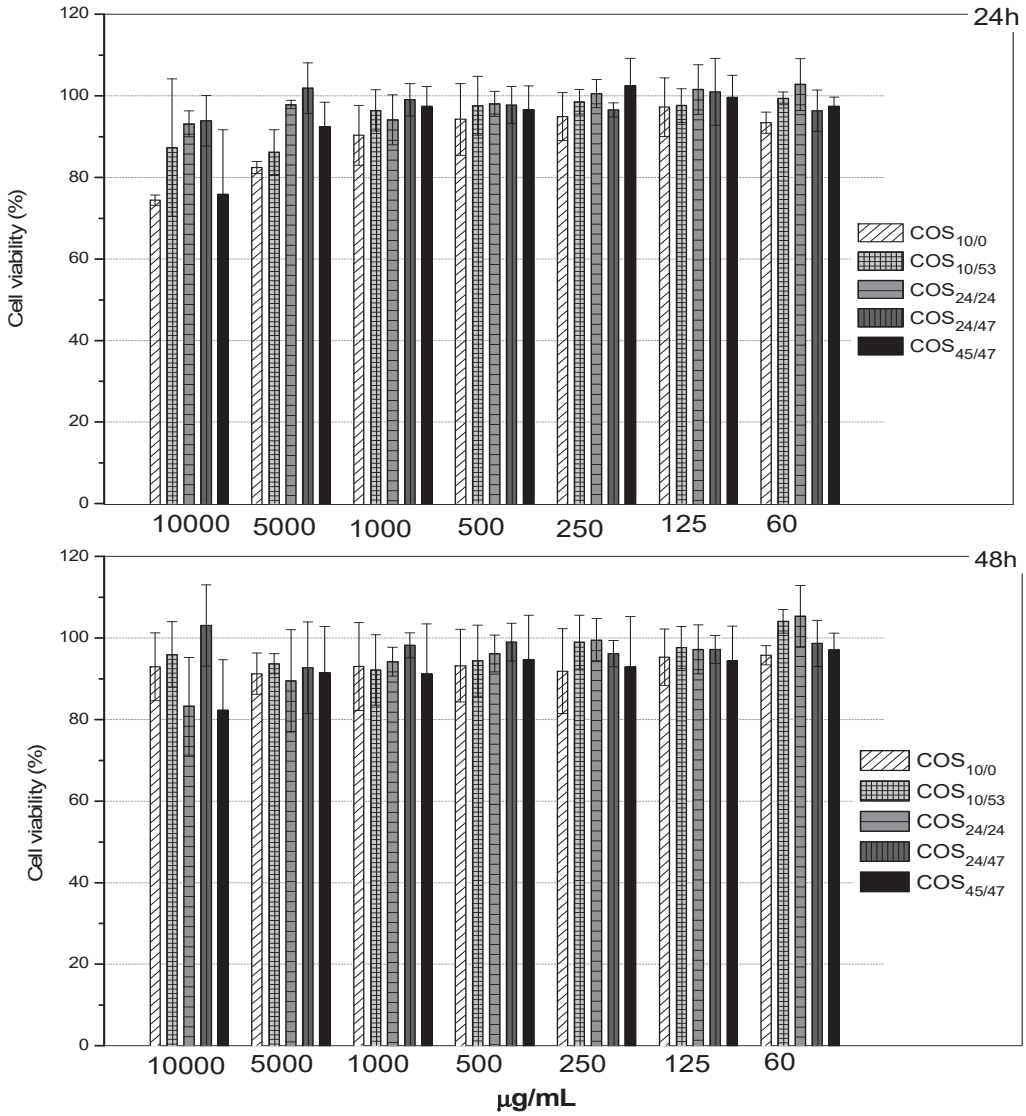

Figure 71: Cell viability assay of chitooligosaccharides, $COS_{10/0}$, $COS_{10/53}$ and $COS_{24/24}$, $COS_{24/47}$ and $COS_{45/47}$ against canine fibroblasts cells, at different COS concentrations (60 to 104 µg/mL) at 24 h and 48 h. Data are mean ± S.D. expressed as % of control response.

Briefly, cell viability was determined as the ratio of the optical density (OD) of exposed cells to the OD of the untreated cells. For each concentration of COS, mean values of the mean absorbance rates from eight wells were calculated; all experiments were performed in triplicate on fibroblasts obtained from three different dogs. Results were expressed as mean ±

standard deviation. Thus in light of such experiments, all the synthesized oligomers were considered nontoxic. In his context, below, the synthesized oligomer will be screened to test their capability to favor tissue regeneration with the establishment of synaptic connection between neurons, acting on the Perineuronal nets.

2. Screening for the use of well controlled chitooligosaccharides for an application in nervous tissue regeneration: cytotoxicity analyses.

In this part, we will describe the screening of the synthesized chitooligosaccharides for an application in nervous tissue engineering. This will be performed (i) by culturing specific cell lines with chitooligosaccharides (COS), ii) fixing and staining of the cultured cells and finally iii) screening the cell cultures by fluorescent microscopy.

2.1. Review of the literature concerning perineuronal net plasticity

Perineuronal nets (PNNs) are condensed extracellular matrix that ensheath the cell bodies and dendrites of neurons in the central nervous system (CNS) which were first described by Camillo Golgi in 1882 [179]. PNNs play a direct role in the control of neuronal plasticity. Thus, their removal is one way in which plasticity can be re-activated in the adult CNS. To develop methods for controlling the plasticity, it is important to understand how the PNNs are formed and how to manipulate them. PNN are mainly composed of hyaluronan (HA), chondroitin sulfate proteoglycans (CSPGs), link proteins, chondroitin sulfate glycosaminoglycan (CS-GAGs) and tensascin R (Tn-R) (Figure 72). Lecticans are a family of chondroitin sulfate proteoglycans (CSPG), composed of aggrecan, versican, neurocan and bervican which have a HA-binding domain, that bind to the pericellular hyaluronan synthesized by the transmembrane HAS. This binding is stabilized by link protein. Each CSPGs binds to CS-GAGs via tetrasaccharide linkage (Xylose-Galctose-Galctose-Glucuronic acid-GAGS). On the other hand, the carboxyl-terminals of these CSPGs then binds to tensascins which in turn bind to another CS-GAGs chain, all forming a massive macromolecule as shown in Figure 72 [180, 181]. To summarize, the lectican family of CSPGs form a major functional part of the brain extracellular matrix, where the CSPGs function is to stabilize normal brain synapses as part of perineuronal nets [180].

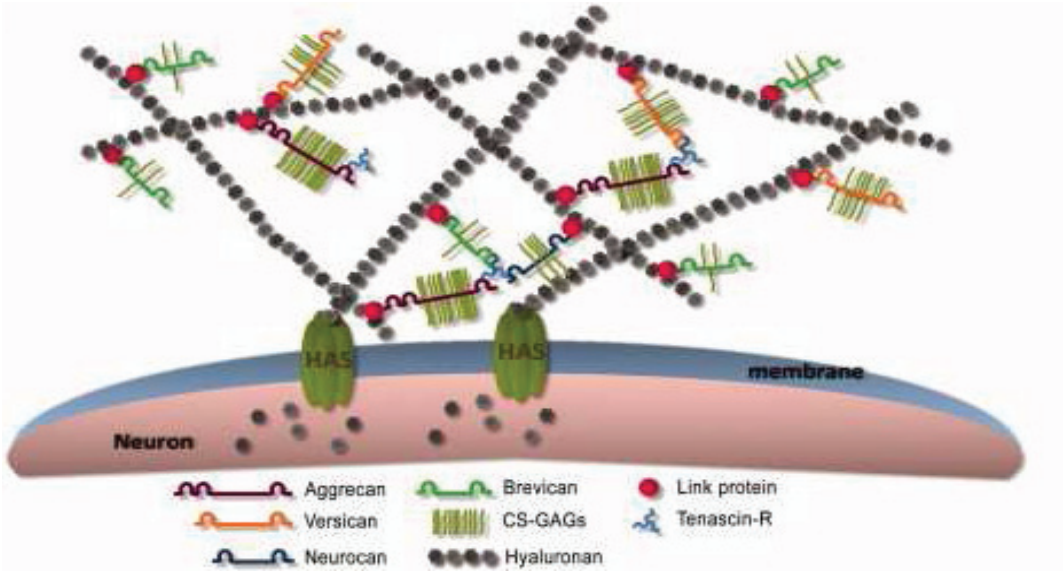

Figure 72: The structure of the PNN present on the neuronal surface. HAS synthesized HA and secrete it to the perineuronal area. Members of the lectican family, including aggrecan, neurocan, versican and bervican bind to the HA back bone through a link protein then each CSPGs binds to CS-GAGs via tetrasaccharide linkage via tetrasaccharide linkage (Xylose-Galctose-Galctose-Glucuronic acid-GAGS), the carboxyl-terminals of these CSPGs then binds to tensascins which in turn bind to another CS-GAGs chain [181].

The central nervous system (CNS: brain and spinal cord) of mammals has a low capacity to self-repair in response to a lesion [182]. Usually, recovery after a lesion fails due to endogenous axon regeneration inhibitors such as chondroitin sulfate proteoglycans (CSPGs) that accumulate at the injury site [183]. Therapeutic targeting of these inhibitors and their receptors may facilitate axon outgrowth and enhance recovery. Some therapeutic interventions neutralize inhibitors associated with residual myelin [184, 185] or chondroitin-sulfate proteoglycan. [186] [187, 188]. Although the enzymatic digestion by using chondroitinase ABC (ChABC) degrades CSPGs, restore plasticity and recover spinal cord injury in adult animals [189], side effects are encountered due to the long enzymatic activity ChABC that leads to a complete digestion of CSPGs [190]. Hence, the invasive activity of the enzyme prohibits their uses in therapeutic applications. Other investigators in biomaterials engineering have provided a potential synthetic platform for neural regeneration. This includes the synthesis of scaffold material based with synthetic polymer such as poly-L-lactic acid (PLA) [191] or PEG [192] or from naturally polymer such as chitosan [193, 194]. In a recent study, Chedly *et al*. [195], developed a chitosan-based implantable formulation [196]

in the form of a suspension of physical chitosan hydrogel fragments for spinal cord injury restoration. In this study, a high molar mass chitosan (Mw ~550 kg/mol) with defined degree of *N*-acetylation (DA~ 4%) was used. Chitosan implantation can repair spinal cord tissue inducing massive axonal regrowth through the lesion site (rat hemisection model). Since the material is resorbed *in vivo*, the degradation products are chitosan oligosaccharides. The understanding of the interaction mechanism of COS with the cells of the nervous tissue could explain the interest of fragmented chitosan hydrogels in this application. Hence, herein we describe the impact of different COS with different DP and DA in an objective to favor tissue regeneration with the establishment of synaptic connection between neurons, possibly acting on the PNN. To this aim, we selected the COS that were soluble at neutral pH. This series comprises commercial oligomers (source details are described in the *experimental details* section at the end of this chapter) with different DPs (3, 4, 5 and 6) at 2 DAs (0 and 100%) and our series of reacetylated soluble COS. All the tested samples are presented in Figure 73.

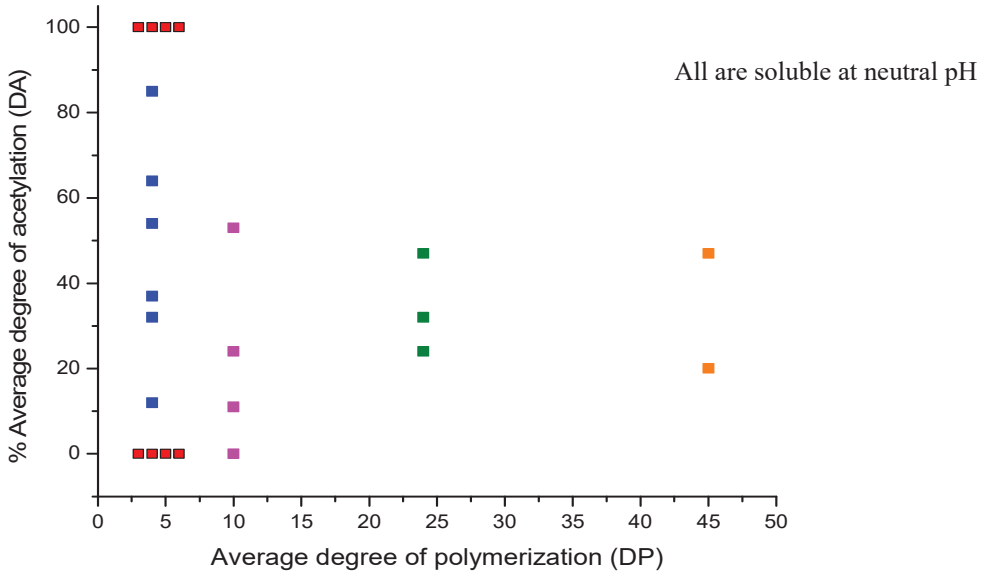

Figure 73: Summary of the commercial oligomers represented in yellow color and synthesized chitooligosaccharides $COS_{DP/DA}$ represented in blue ($COS_{4/DA}$), pink ($COS_{10/DA}$), green ($COS_{24/DA}$) and orange ($COS_{45/DA}$) colors in DP-DA plane to be used in the neural cell toxistudy.

2.2. Perineuronal nets cell lines culture conditions

2.2.1. Culture of cells exhibiting perineuronal nets

The impact of chitooligosaccharides was studied on well-established and mastered neuron-like cell lines ('PNN cells') developed by Kwok *et al*. [189]. The PNN cells were seeded at a density of 4×10^4 cells/ well in 24-well plate at 37°C with 5% CO_2. After 1 night of culture, the medium was washed twice with DMEM and replaced with fresh medium containing COS with concentration of 2mM (Table 22). Three exposure times (1, 3 and 5 days) were tested. The culture medium was changed every morning to ensure the presence of nutrients.

Table 22: Characterization data of chitooligosaccharides to be tested including a) average degree of polymerization (DP) and average degree of *N*-acetylation (DA), b) M_0 is the molar mass of the GlcN/GlcNAc unit ($M_{(GlcN)}$ = 164 g/mol and $M_{(GlcNAc)}$ =203 g/mol) and c) mass concentrations in mg/ml for each oligosaccharide.

$\overline{DP}$ [a]	$\overline{DA}$(%)[a]	$\overline{Mo}$[b] (g/mol)	Concentration[c] (mg/mL)
10	0	1,774	3.57
10	11	1,820	3.64
10	24	1,875	3.75
10	53	1,997	4.00
24	32	4,351	8.77
24	47	4,502	9.00
45	20	7,787	15.57
45	47	8,298	16.59
3	0	504	1.01
3	100	627	1.26
4	0	666	1.33
4	12	682	1.36
4	32	716	1.44
4	37	724	1.45
4	54	753	1.50

4	64	770	1.54
4	85	805	1.61
4	100	830	1.66
5	0	828	1.65
5	100	1,033	2.08
6	0	990	1.98
6	100	1,236	2.5

2.2.2. Fixation and staining of the cell cultures

After cultures, fixation of the cells was performed by using 4% Paraformaldehyde (4% PFA) in PBS. PFA will cause covalent cross-links between proteins that will keep cell structure intact after freezing. After 15min, the cells were washed with PBS then with 1% ammonium chloride in PBS, to permit the washing of any remnants of PFA. After fixation, the cells are ready to be stained for immunohistochemistry analysis. This was performed with 1% normal donkey serum (NDS) treatment. Then the PNN antigen was attacked by the first antibody WFA-bio, lectine source for 30min. Enlargement of the cell surface area was performed by washing twice the cells with PBST (0.1 % Tx-100 in 1xPBS). After comes the attack of the (second) florescent antibody (Strep-488, 1:500) + Hoechot (1:30,000) for 2 hr. At the end, the removal of all the salts from the medium was performed by washing once with 1xPBS then twice with 1xTNS.

2.3. Screening the cultured PNN medium by fluorescent microscopy

Fluorescent microscopy was then used to study the impact of COS oligomers on the PNN cells. The fluorescent images were performed at day 1 and day 5 of culture by using two different wavelengths. Hoechot (blue color) was detected at a wave length of 405nm to observe the labeled DNA of the cells and Strep (green color) was detected at a wave length of 488nm to observe the labeled antibody-antigen interaction on the surface of the cells. Different optical micrographs were taken at different areas with a scale of 25 µm. Starting with control, Figure 74 corresponds to PNN cells after 5 days of culture at 37°C with 5% CO_2 in DMEM solution. Figure 74 shows clearly clusters of PNN cells in green, as a reference to show their behavior without the presence of chitooligosaccharides.

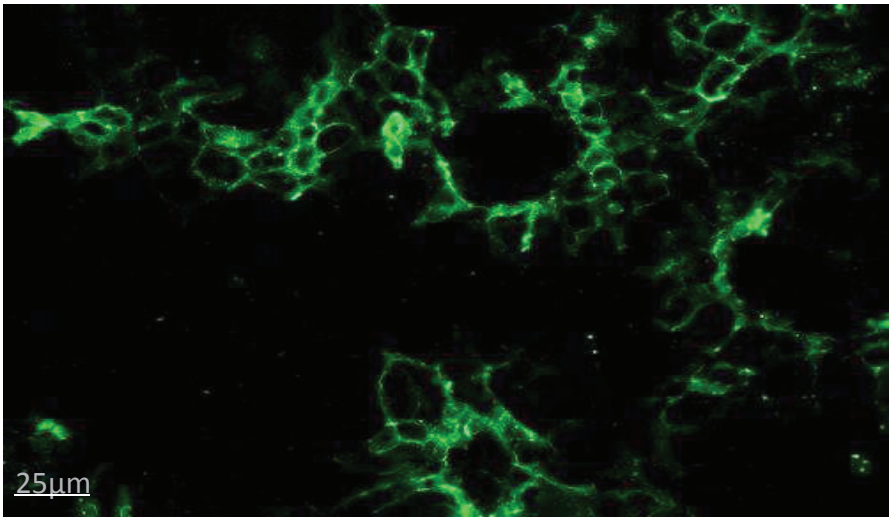

Figure 74: Florescent microscopy of PNNs cells represented in green color after 5 days of culture at 37°C with 5% CO_2 in DMEM solution at a wave length of 488nm. Culture image at day 5.

Impact of DA for chitotetraose:

Figure 75 shows fluorescent images of the PNN cells cultured with chitooligosaccharides with DP 4 and different DAs, namely $COS_{DP/DA}$ such as, $COS_{4/0}$ (A,B), $COS_{4/64}$ (C,D), $COS_{4/85}$ (E,F) and $COS_{4/100}$ (G,H) at day 1 and day 5 respectively. Comparing to the control in Figure 73, the PNN cells after 1 day of culture show no cluster of cells nor PNN net formation. Instead, cells were well evidenced in nearly spherical form. In addition, the presence of alive cell was confirmed first by the DNA labeling demonstrated in blue thanks to Hoechot, second by the antibody-antigen interaction on the surface of the same cells evidenced in green (Strep labeling). This demonstration also confirms the success of the cell culture conditions (ex: staing). After 5 days of culture, major differences were observed in terms of cell viability. Such as, for low DA value 0%, $COS_{4/0}$ (B), we can notice that the number of cells decreased with less staining, and shrinking indicating the death of the cells. This cell death was also present for $COS_{4/12,}$ $COS_{4/32}$ $COS_{4/37}$ and $COS_{4/54,}$ hence the fluorescent images of these COS were not shown here, but dead or even no cells were observed after 5 days of culture. For $COS_{4/64}$ (D), a significant amount of dead cells were observed after 5 days of culture. However for $COS_{4/85}$ (F), major differences were observed by the presence of viable cells. This difference was even more evident in the case of DA 100%, $COS_{4/100}$ (H).

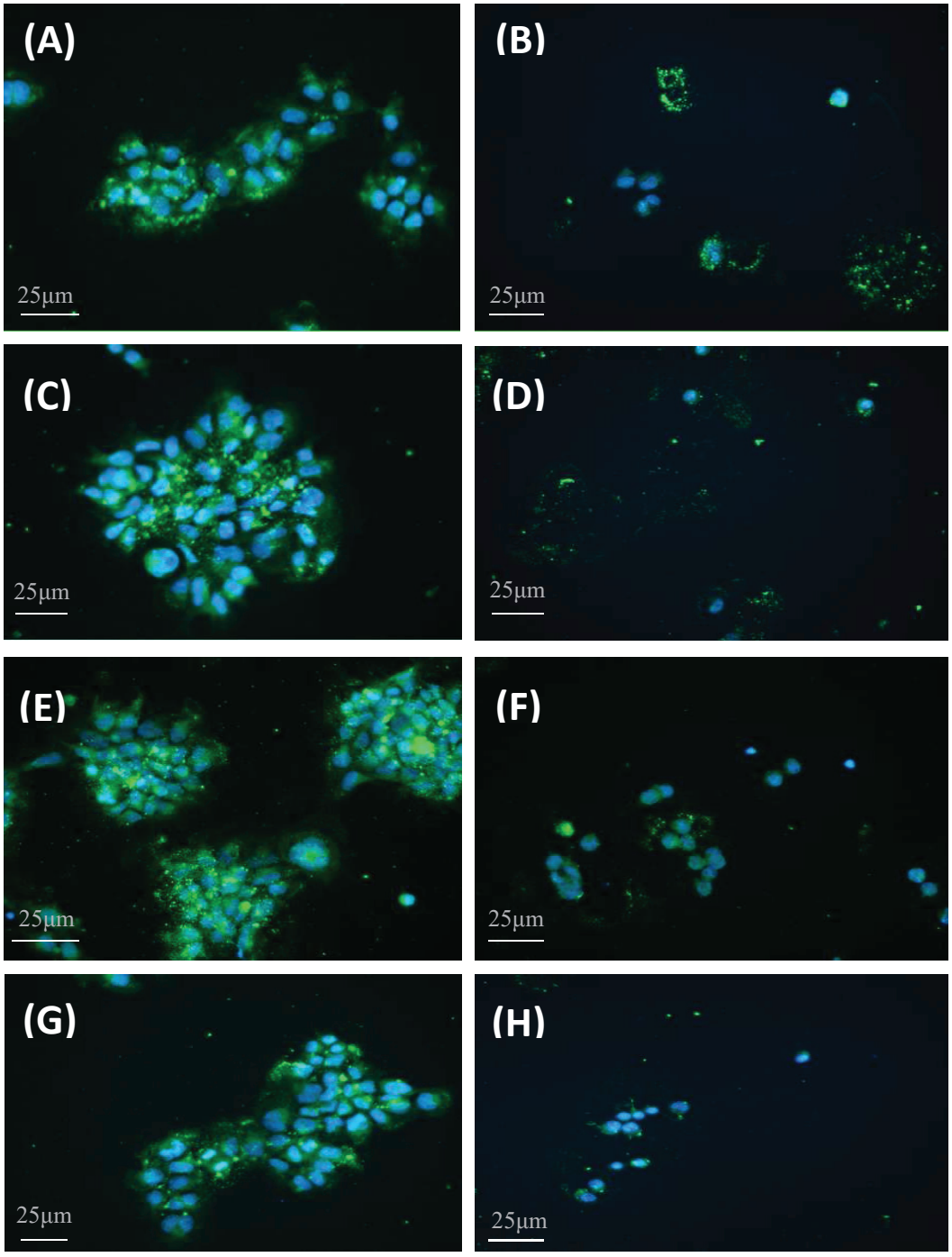

Figure 75: This florescent microscopy illustrates PNN cell lines cultured with chitooligosaccharides with DP 4 and with different DA $COS_{DP/DA}$: $COS_{4/0}$ (A,B), $COS_{4/64}$ (C,D), $COS_{4/85}$ (E,F) and $COS_{4/100}$ (G,H) at day 1 and day 5 of culture respectively. Each image corresponds to a superposition of two images obtained at different wavelengths. 405nm to observe the labeled DNA of the cells and 488nm to observe the labeled antibody-antigen interaction on the surface of the cells. We observe that high DA COS induces less the death of the cells.

Impact of DP at high DA:

It has been shown that cells survive better as the DA value is high. Thus, high DA values of COS with different DP were screened. Figure 76 shows PNN cell cultures for different $COS_{DP/DA}$: $COS_{3/100}$ (A,B), $COS_{5/100}$ (C,D) and $COS_{6/100}$ (E,F) at day 1 and day 5 respectively of culture, in the aim to see if there's evidence effect of DP. The images processed at day 1 (A, C, E) also show cells that could be well identified, stained and alive. However after 5 days of culture, an increase in the viability of the cells was observed with decrease in the DP from DP 6 to DP 3 (F to B). In parallel, low DA value (0%) with different DP (3, 4, 5and 6) were also screened to double check the effect of DA, as a result no cells were detected on the coverslip, this shows that cells were dead and shows again that cells could survive only in presence of COS with high DA values.

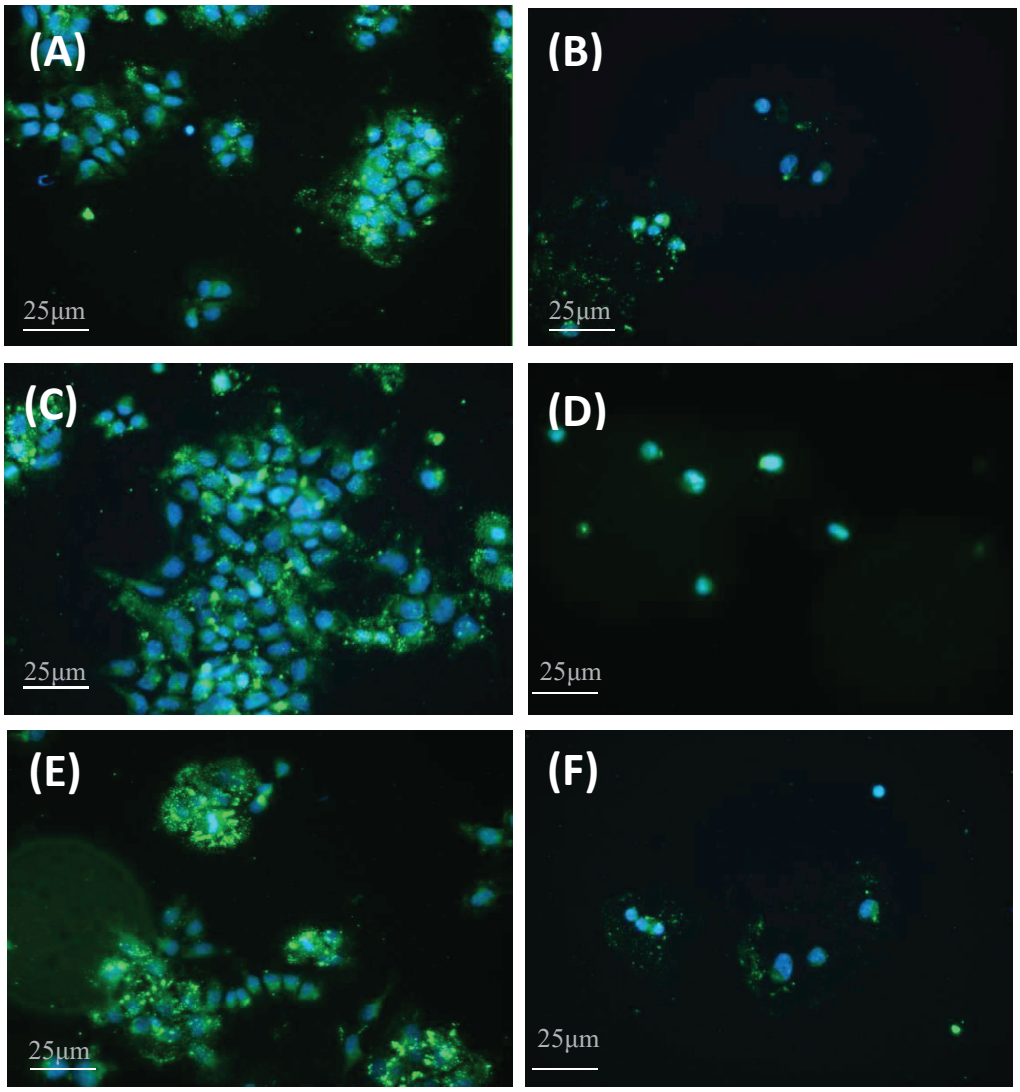

Figure 76: This florescent microscopy illustrates PNN cell lines cultured with commercial oligomers with different DP and with DA 100 $COS_{DP/DA}$: $COS_{3/100}$ (A,B), $COS_{5/100}$ (C,D) and $COS_{6/100}$ (E,F) at day 1 and day 5 of culture respectively. Each image corresponds to a superposition of two images obtained at different wavelengths. 405nm to observe the labeled DNA of the cells and 488nm to observe the labeled antibody-antigen interaction on the surface of the cells. We observe that high DA COS induces less the death of the cells.

Study of the impact of larger DPs:

As a final screening, other series of different DP and DA were also tested. This includes DP 10 with DA (11, 24 and 53), DP 24 with DA (32 and 47) and DP 45 with DA (20 and 47).

Figure **77** shows fluorescent images of PNN cells cultured with chitooligosaccharides with DA ~50% and different DP, $COS_{DP/DA}$ such as, $COS_{10/53}$ (A,B), $COS_{24/47}$ (C,D) and $COS_{45/47}$ (E,F) at day 1 and day 5 of culture respectively. As for the other mentioned oligomers, their fluorescent images were not shown here, since only dead cells (or absence of cells) were observed. As described before, images at day 1 (A, C, E) also show cells that are well identified, stained and alive. Interestingly, after 5 days of culture, an increase in the viability of the cells was observed with an increase in the DP from DP 10 to DP 45 (B to F). Indeed, for $COS_{45/47}$ (F) numerous numbers of alive and stained cells were observed, showing that high DP value is more suitable for this tested DA ~50.

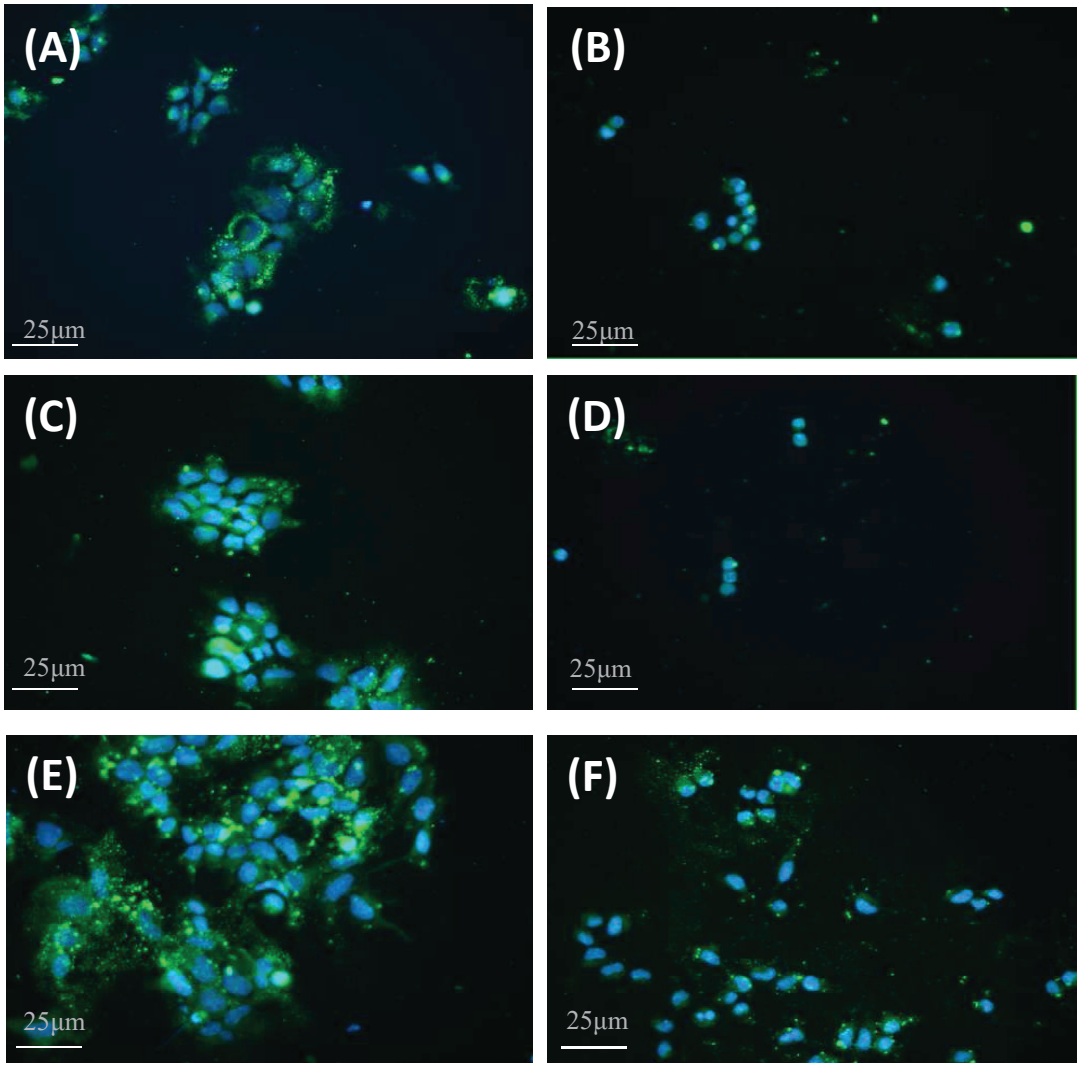

Figure 77: This florescent microscopy illustrates PNN cell lines cultured with COS with different DP and with DA 50 $COS_{DP/DA}$: $COS_{10/53}$ (A,B), $COS_{24/47}$ (C,D) and $COS_{45/47}$ (E,F) at day 1 and day 5 of culture respectively. Each image correspond to a superposition of two wavelengths such as Hoechot (blue color) was detected at a wave length of 405 to observe the labeled DNA of the cells and Strep (green color) was detected at a wave length of 488nm to observe the labeled antibody-antigen interaction on the surface of the cells. We hypothesis that high DP values were better for the cells for DA ~ 50%, as a result the higher the DP, the lower the death of the cells at DA ~ 50%.

The cell viability at day 5 was affected by both the degree of polymerization and degree of *N*-acetylation. However, these obtained results are primary, should be repeated by taking into consideration the effect of concentration. Indeed, we have used 2mM concentration for all the tested chitooligosaccharides. Meanwhile, the tested oligomers exhibit different DP values, implying that the mass concentration is not constant. Hence their concentration in mg/ml is different and higher at higher DP. Usually inliterature, concentrations in mmol/l unit for

simple molecules are used. However, for chitosan oligomers, authors seem to use mass concentrations for the comparison oligosaccharides of different structure. De Assi *et al*. [14] calculated the 'anti-proliferative activity' of COS using (1mg/ml). In addition, according to the cytotoxicity tests performed in the first part, we have shown that that COS are non-toxic, but the cell viability increased continually with the decreasing in the COS concentration.
Despite this methodology debate, the results show that all chitooligosaccharides are inhibiting PNN formation. Strong cell death after 3 or 5 days of incubation occurred we suspect this is due to the concentration used. These preliminary results suggest that decreasing polymerization degree and increasing *N*-acetylation degree qualitatively induce higher survival of cells in case of low DP values (DP3 and DP4). In parallel increasing polymerization degree for DA ~50 induce higher survival of cells. The toxicity of COS depend on their structure, but apparently, the type of cells and/or the time for toxicity evaluation is also of major importance (fibroblasts at 24 or 48h do not show the same behavior as PNN cells cultured at day 5). Thus, the question of a “universal behavior” [197] of COS vs all type of cells is still to be questioned.

As a future perspective, experiments on fibrobasts could be designed to follow the cell cultures over longer times (5 days), and PNN cell culture could be repeated using the more favorable oligomers (DP3-DA100, DP4-DA100, DP10-DA53, DP24-DA47 and DP45-DA53), at different constant mass concentrations. Then the safer oligosaccharides from the above experiments will then be tested in primary neuronal culture. Cortical neurons will be cultured from E18 rat brains and in vitro mature for 28 days. By 28 days, these neurons will form PNNs. The oligosaccharide with chosen polymerization and concentration will be added to the culture at day 20 and the neurons will continue to be cultured until 28 days. The neurons will then be fixed and processed for immunocytochemistry as mentioned above. In case of success, we shall then further evaluate COS in *in vivo* experiments.

3. In situ synthesis of Fe_3O_4 nanoparticles coated by chitooligosaccharide, characterization and toxicity evaluation for biomedical application

Overview

In this part, we will describe the synthesis of Fe_3O_4 nanoparticles coated with COS by a simple co-precipitation method. The impact of COS with different DPs (DP 10 and 24) and DA~50 % (exhibiting high solubility) ($COS_{DP/DA}$) was evaluated on the synthesis and behaviours of coated magnetic nanoparticles (MNPs). The resulting coated nanoparticles were characterized convergently with respect to their physical and magnetic properties, as well as their colloidal stability by: Fourier transform infrared (FT-IR), X-ray diffraction patterns (XRD), thermogravimetry analysis (TGA), transmission electron microscopy (TEM), zeta potential determination and vibrating sample magnetometer (VSM). In addition, the *in vitro* cytotoxicity of COS and COS coated Fe_3O_4 MNPs was evaluated in a canine fibroblasts model to validate their biomedical application. This work was written as a technical journal article and will be submitted to "Journal of Nanoparticle Research".

Paper I

In situ synthesis of Fe_3O_4 nanoparticles coated by chito-oligosaccharide, characterization and cytotoxicity evaluation for biomedical applications

P.N. Oliveira[1], A. Moussa[1], N. Milhau[2], R.D. Bini[3], C. Prouillac[2], L.F. Cótica[3], S. Trombotto[1], T. Delair[1], D. Pin[2], L. David[1]

[1]IMP, CNRS UMR 5223, Univ Claude Bernard Lyon 1, Univ Lyon, 15 bd Latarjet, 69622 Villeurbanne, FR

[2]Université de Lyon, VetAgro Sup, Unité ICE, 1 av. Bourgelat, 69280 Marcy L'Etoile, FR

[3]Department of Physics, Maringá State University, Av. Colombo, 5790, Maringá, Paraná, Brazil, 87020-900

Abstract

Fe_3O_4 nanoparticles coated by COS were prepared *in-situ* by a simple co-precipitation method through a mixing of iron ions (Fe^{3+} and Fe^{2+}) and COS aqueous solutions followed by precipitation with ammonia, at 60 °C. The impact of COS with different DPs (DP 10 and 24) and DA~50 % (exhibiting high solubility) ($COS_{DP/DA}$) was evaluated on the synthesis and behaviours of coated magnetic nanoparticles (MNPs). Several advantages were found when the magnetic nanoparticles were prepared in the presence of both COS, $COS_{10/53}$ and $COS_{24/47}$, such as: preparation of functionalised ultra-small MNPs with narrower size distributions (with smaller aggregates) and consequently a higher saturated magnetisation (M_s) values (~60 emu/g); and an increase of cell viability for COS coated MNPs in comparison with pure Fe_3O_4 MNPs (with concentration dependence). However, to determine the real impact of COS structure it is necessary to perform other tests, such as the internalisation of the MNPs by the cells. These promising results could be useful in different biomedical applications such as, magnetic-field assisted drug delivery, enzyme or cell immobilization, or as a marker in cell tracking and in addition to others.

Keywords: chito-oligosaccharides; magnetic nanoparticles; biomedical applications; co-precipitation

1. Introduction

Nanoparticles (NPs) characteristic dimensions are of the same order of magnitude and not more than 100 nm, resulting in a high surface area to volume ratio[198]. Generally, they show different behaviours when compared to the bulk state and can be used in several applications [199, 200]. Thanks to recent evolution and demands in nanobiotechnologies, magnetic nanoparticles (MNPs) in particular are attracting increasing attention [201, 202]. This is owing to the fact that they have a great potential to improve conventional therapeutic procedures and traditional clinical diagnostic, introducing novel approaches in biomedicine and tissue engineering. [203-207]. The most frequently used magnetic nanomaterial is the iron oxide nanoparticles, comprising magnetite (Fe_3O_4) and maghemite (γ-Fe_2O_3) due to their lower toxicity [208, 209]. They possess different physicochemical properties originating from the difference in their iron oxidation states. Fe_3O_4 differs from most other iron oxides in that it contains both divalent and trivalent iron. Fe_3O_4 has a cubic inverse spinel structure that consists of a cubic close packed array of oxide ions [210]. The octahedral sites within the oxygen lattice are randomly occupied by approximately equal numbers of Fe^{3+} and Fe^{2+} ions, while the tetrahedral sites are occupied exclusively by the smaller Fe^{3+} ions [210, 211]. In stoichiometric magnetite $Fe^{2+}/ Fe^{3+} = 1/2$, and the divalent iron ions may be partly or fully replaced by other divalent ions (Co, Mn, Zn, etc). Thus, magnetite displays both *n*-type and *p*-type semiconductor behaviour with a Fermi level in a low-mobility spin-polarised *3d* band. Fe_3O_4 possesses low band gap energy (0.1 eV) and consequently exhibits the lowest resistivity of any metal oxide *(ca.* 5.10^{-5} **Ω**m [212]), a property attributable to the rapid exchange of electrons between Fe^{2+} and Fe^{3+} in octahedral sites [210, 213].

Some of physico-chemical properties of the magnetic nanoparticles originate from their size and form, as well as their magnetic properties [209]. Consequently, many of their applications rely on the use of magnetic fields to manipulate their properties. A desired property for these nanoparticles is superparamagnetism, *i.e.* magnetization can be saturated under an external magnetic field, but in the absence of this field, their net magnetic moments are randomized to zero [209, 211]. In general, magnetite (Fe_3O_4) NPs show this property when their sizes are smaller than 20 nm in diameter and this is exploited for their dispersion in physiological solutions, facilitating NPs coupling with biological agents [209, 214]. Once exposed to an external magnetic field, these MNPs can align along the field direction, achieving magnetic saturation at a magnitude that far exceeds that from any of the known

biological entities. This unique property of MNPs allows not only the detection of the MNP containing biological samples, but also the easy manipulation of these biological samples with an external magnetic field [214, 215].

Although very small particles are ideal for biological applications, they have high surface energy resulting from their large surface-volume ratio. This effect can induce to nanoparticles aggregation, even for MNPs that are superparamagnetic, resulting in the formation of large clusters which limits their bio-applications [211]. To avoid this aggregation, the MNPs are typically coated and it can promote their colloidal stability, water dispersibility and also provide biochemical functionality with the addition of bioactive molecules [202, 208, 216]. The use of suitable coating can also minimize precipitation and the formation of agglomerates and prolong the circulation time [217-219]. Many researchers have used silica, carbon, and biopolymers to modify the Fe_3O_4 nanoparticles surfaces [220-222]. In this work, we propose the use of chito-oligosaccharides with controlled structure, derived from chitosan polymer, in order to improve the chemical stability and biocompatibility of the MNPs. Additionally, we intend to take advantage of the presence of amino and hydroxyl groups that can interact with iron ions to assist the synthesis of MNPs.

Chitosan is a well know natural amino-polysaccharide that has drawn interest due to its properties, *e.g.* non-toxic, hydrophilic, biocompatible, biodegradable, and anti-bacterial [223]. In addition, another advantage of chitosan is the reactive amino and hydroxyl groups offering many active sites to conjugate or complex different ligands [2]. Chitosan and its derivatives have been widely envisioned in many biomedical applications, including gene and drug delivery, tissue repair, water purification and cosmetics [8]. Unfortunately, some of chitosan applications are affected by its high molecular weight, its solubility limited in diluted acid medium or its poor solubility at neutral pH. In order to address these limitations chito-oligosacharides (COS) have been used are defined as oligomer forms of chitosan or chitin prepared either chemically or enzymatically [91]. COS not only maintain some of original properties of chitosan, nonetheless also provides water-solubility at neutral pH, non-toxicity, biocompatibility and unique physiological activities [224, 225]. They also exhibit antibacterial, antifungal and antitumor activities, as well as immuno-enhancing effects on animals [9, 91]. A few studies showed the preparation and application of COS:Fe_3O_4 nanoparticles [226, 227], in which, in general, first, Fe_3O_4 MNPs suspension was prepared and after, COS solution was added to the media promoting the COS adsorption on the NPs surface [228-230].

In our work we propose the use of chito-oligosacharides as complexing agents to assist the synthesis of magnetite nanoparticles. We aim to take advantage of the interactions between the amino groups from COS, and the iron ions and, *in situ*, prepare functionalized coated magnetite nanoparticles with narrow size distributions. To this purpose, COSs with different degree of polymerization (DP, with narrow distribution) and mean degree of *N*-acetylation (DA) were synthesized by nitrous deamination and reacetylation. COS structures were precisely characterized by proton nuclear magnetic resonance spectroscopy (^{1}H NMR) and size exclusion chromatography (SEC). After, COS coated Fe_3O_4 NPs were synthesized, *in situ*, by co-precipitation from an aqueous solution with mixed iron ions (Fe^{3+} and Fe^{2+}) and COS. Thus, COSs with DP, 10 and 24, and DA ~50 % were tested to evaluated the impact of their mean molar mass and mean degree of *N*-acetylation on the magnetic nanoparticle properties. The resulting coated nanoparticles were characterized convergently with respect to their physical and magnetic properties, as well as their colloidal stability by: Fourier transform infrared (FT-IR), X-ray diffraction patterns (XRD), thermogravimetry analysis (TGA), transmission electron microscopy (TEM), zeta potential determination and vibrating sample magnetometer (VSM). In addition, the *in vitro* cytotoxicity of COS and COS coated Fe_3O_4 MNPs was evaluated in a canine fibroblasts model to validate their biomedical application.

2. Material and methods

2.1. Materials

Commercial chitosan (batch 244/020208; degree of *N*-acetylation (DA) < 1%; $\overline{Mw}$ = 270 kg/mol; $\overline{Mn}$ = 115 kg/mol; Đ = 2.3) was supplied by Mahtani Chitosan Ldt (Veraval, India) and characterized by 1H NMR [166] and SEC [231]. Iron(III) chloride hexahydrate ($FeCl_3.6H_2O$), iron(II) chloride tetrahydrate ($FeCl_2.4H_2O$), and aqueous ammonia (28%) were purchased from Sigma-Aldrich.

2.2. Synthesis procedures

2.2.1 Preparation of reduced low DA chito-oligosaccharides

Chitosan 244 (30 g, 187 mmole of GlcN unit) was solubilized in 1 L of water by addition of 15.5 mL of HCl (37% w/w). A freshly prepared 25 mL of $NaNO_2$ aqueous solution (GlcN/$NaNO_2$ molar ratio = 4 and 10 for COS_{10} (~DP10) and COS_{24} (~DP 24), respectively) were added and the reactions were stirred for 12 h at room temperature. $NaBH_4$ (4 and 1.8g (125 and 48 mmol) for COS_{10}, and COS_{24}, respectively) were added at ~0°C and

the solutions were stirred for 12h. For COS_{10}, the solution was neutralized by the addition of ammonium hydroxide solution (28% w/w) until pH ~8 then concentrated using a rotavapor. COS_{10} was obtained as a white powder after precipitation in acetone, followed by several washings and finally dried under vacuum. Whereas, COS_{24} was precipitated by addition of ammonium hydroxide solution (28% w/w) to pH ~9, washed several times with deionized water until neutral pH and then freeze-dried. At the end, two different samples were isolated $COS_{10/1}$ and $COS_{24/0.69}$ ($COS_{DP/DA}$), as a white powder with 70 and 81 % mass yield, respectively.

2.2.2. *N*-acetylation of reduced chito-oligosaccharides

In order to increase the solubility of COS in the physico-chemical conditions of the precipitation of Fe_3O_4 nanoparticles, *i.e.* at basic pH, reactetylated COS with DA close to 50% were prepared in homogeneous conditions [232]. The partial *N*-acetylation of low DA COS was performed in dissolving 0.5 g of each of the reduced chito-oligosaccharides in 20 mL of methanol/water 90:10 (v/v) for COS_{10} and in 20 mL of methanol/acidify water (AcOH 1.5%(w/v)) 70:30 (v/v) for COS_{24} to ensure solution homogeneity. Fresh acetic anhydride (149µL; 0.5 eq/GlcN unit) was added in a stoichiometric amount to reach the expected DA ~50 %. After 14 h of stirring at room temperature, solutions were neutralized by the addition of ammonia till pH~8. The reaction solutions of the different *N*-acetylated chitooligosaccharides $COS_{10/53}$ and $COS_{24/47}$ were precipitated, abundantly washed with acetone and finally dried under vacuum. This will permit the removal of acetone, methanol along with other reaction impurities. At the end, the *N*-acetylated chitooligosaccharides were produced in their amine form as white powder with mass yields 57 and 61 % for $COS_{10/53}$, and $COS_{24/47}$ respectively. Their characterization shows that their molar mass distribution Đ is rather narrow. The details for the calculations of $\overline{DP}$ and $\overline{DA}$ are given in Table 1, SM-Figure 1 and SM-Figure 2 in the Supporting Material in Annex B section.

Table 1 – Chito-oligosaccharides characterisation, such as: weight average molar mass ($\overline{Mw}$), number average molar mass ($\overline{Mn}$), dispersity (Đ) and average number of GlcN repeating unit $\overline{DP}_n$ and average degree of *N*-acetylation $\overline{DA}$:

Samples $COS_{DP/DA}$	$\overline{Mw}$ [a] (kg/mol)	$\overline{Mn}$ [a] (kg/mol)	Đ [a]	$\overline{DP}_n$ [b]	$\overline{DA}$ [b]
Chitosan244	270	115	2.3	714 ±2	1
$COS_{10/1}$	2.13	1.94	1.1	10 ±2	1

$COS_{24/0.69}$	5.74	4.42	1.3	24 ±2	0.69
$COS_{10/53}$	3.12	2.52	1.24	10±2	53
$COS_{24/47}$	6.49	4.81	1.35	24±2	47

(a) $\overline{Mw}$, $\overline{Mn}$ and Đ were determined by SEC-MALLS in ammonium acetate;
(b) the $\overline{DP_n}$ and the $\overline{DA}$ were determined by ^1H NMR in D_2O at 300 K.
- The details about $\overline{DP_n}$ and $\overline{DA}$ calculus are given in the Support Material.

2.2.3. Synthesis of Fe_3O_4 magnetic nanoparticles

The Fe_3O_4 magnetic nanoparticles (MNPs) were prepared by the chemical co-precipitation route. Stoichiometric ratio 2:1 of ferric chloride hexahydrate ($FeCl_3 \cdot 6H_2O$) and ferrous chloride tetrahydrate ($FeCl_2 \cdot 4H_2O$) were dissolved in deionized water under argon atmosphere and vigorous stirring at 60 °C. HCl (1M) aqueous solution was added in to this salt solution to reach at the final concentration of 0.1 M to avoid the oxidation of iron ions. Chemical precipitation was achieved by dropwise adding NH_4OH solution (28%) to reach pH 10 under vigorous stirring. The precipitation of magnetite is visible from the immediate change of the colour of solution from dark orange to black. After continuously stirring for 1 h, the black precipitates of Fe_3O_4 were magnetically decanted and washed several times with distilled water. The nanoparticles were then dried in an oven under vacuum for 12 h at 50 °C.

2.2.4. Synthesis of COS coated Fe_3O_4 magnetic nanoparticles

Chito-oligosaccharides coated magnetic iron oxide nanoparticles (COSMNPs) were synthesized *in situ* by the co-precipitation of Fe (II) and Fe (III) salts in the presence of reacetylated chito-oligosaccharides (COS). The reacetylated chito-oligosaccharides used in this study are listed in the Table 1. First, 0.25 g of COS ($COS_{10/53}$ or $COS_{24/47}$) was dissolved in 100 mL of deionized water. Iron salts (0.333 g of $FeCl_2 \cdot 4H_2O$ and 0.905 g of $FeCl_3 \cdot 6H_2O$) were dissolved in 20 ml of deionized water at 60 °C, under the argon gas flow and vigorous stirring. 50 µL of HCl (37 %) was added in this salt solution. Then, COS solution was slowly added in to the flask, still under argon atmosphere and mechanical stirred. After 1 h at 60 °C, 15 mL of ammonium hydroxide was added in dropwise manner to the flask with continuous and vigorous stirring over the next 1 h (pH ≅ 10). The colloidal COS coated magnetic Fe_3O_4 nanoparticles were extensively washed with deionized water and separated by magnetic decantation. Finally, the COS-coated MNPs were dried in an oven (12 h, undervacuum at 50 °C) and stored at room temperature.

2.2.5. Primary cultures of canine dermal fibroblasts

Canine dermal fibroblasts were isolated from three healthy Beagle dogs owned by Institut Claude Bourgelat (VetAgro Sup - Campus Vétérinaire de Lyon, Marcy l'Etoile, France) in accordance with the VetAgro Sup animal ethics committee. Skin biopsy specimens were collected on dorsal surface of dogs after local anaesthesia (lidocaine, Xylovet, Ceva, Libourne, France) and using a 6 skin biopsy punch under sterile conditions. Skin biopsies were cut into small fragments and digested with 0.25% trypsin/EDTA (Eurobio, Courtaboeuf, France) 15 min at 37°C. After digestion, the skin fragments were washed with PBS. Dermal fibroblast cultures were established by explant culture in 25 cm^2 flasks (Falcon, VWR international, Strasbourg, France) containing Dulbecco's Modified Eagle's Medium (DMEM, Eurobio, Courtaboeuf, France) supplemented with 20% fetal calf serum, 2 mM L-glutamine and 2% penicillin/streptomycin/amphotericin B (Eurobio, Courtaboeuf, France) at 37°C in humidified atmosphere with 5% CO_2. After 4 days, fibroblasts started to grow out and fragments were removed. After 10 days, cells reached confluence and were sub-cultured after 0.25% trypsin/EDTA treatment in 75 cm^2 flasks (Falcon, VWR international, Strasbourg, France). Culture medium was changed twice a week. Cells are used between 3 and 10 amplification passages.

2.3. Characterization

2.3.1 ^{1}H NMR spectroscopy:

Proton nuclear magnetic resonance spectroscopy (^{1}H NMR) was recorded on a Bruker 500 MHz spectrometer at 300 K. All samples were dissolved at 10 mg/mL in D_2O with 5 µL HCl 12 N, and transferred to 5 mm NMR tubes. Trimethylsilyl-3-propionic-2,2,3,3-D_4 acid sodium salt (99% atom D, TMSPA from Sigma-Aldrich, Saint-Quentin Fallavier, France) was used as internal reference (δ 0.00 for ^{1}H).

2.3.2. Size-exclusion chromatography (SEC)

SEC was performed on a chromatographic equipment composed of a 1260 Infinity Agilent Technologies pump connected to two TSK gel G2500 and G6000 columns (Tosoh Bioscience) in series. A multi-angle laser light scattering (MALLS) detector Dawn EOS (Wyatt Technology) operating at 664 nm was coupled on line to a Wyatt Optilab T-Rex differential refractometer. Sample solutions at 2-5 mg/mL were prepared and eluted in AcOH (0.2 M)/$AcONH_4$ (0.15 M) buffer (pH 4.5). Solutions were previously filtered through 0.22 µm pore size membranes (Millipore) before injection. The eluent flow rate was 0.5 mL/min.

2.3.3. FT-IR spectroscopy

Infrared spectra were recorded with a Thermo Scientific Nicolet iSO10 FTIR spectrophotometer. The powder samples were ground with KBr and compressed into pellets. FT-IR spectra in the range 4000– 400 cm^{-1} were recorded by accumulation of 200 scans, with a resolution of 4 cm^{-1}.

2.3.4. Thermal characterization

The thermal stability of Fe_3O_4 sample and COS:Fe_3O_4 were determined by thermogravimetric analysis (TA Instruments TGA-Q500). The TGA thermograms were recorded at a heating rate of 10 °C/min^{-1} in the temperature range from 30 to 700 °C under air. The residual mass, in each case, was used to estimate the COS mass (organic material) on the nanoparticles.

2.3.5. X-ray diffraction

The structure and composition of the magnetite nanoparticles (MNP) were examined by X-ray diffraction (XRD), using a Shimadzu XRD 7000 with Cu-K_α radiation equipped with counter monochromator, in the scattering angle 2θ from 15° to 70°. The crystallite size was estimated from line broadening of the most intense diffraction peak ((311) reflexion at 2θ ~35.5°) by Scherrer's equation (equation 1).

$$D_{XRD} = \frac{k \,.\, \lambda}{\beta \cos\theta} \qquad \textbf{Eq. 1}$$

where k is a constant (k = 0.9 for spheres), λ is the wavelength of Cu-$K_{\alpha 1}$ radiation (λ = 1.5406 Å), β is the full width at half-maximum and θ is the Bragg angle.

2.3.6. Transmission Electron Microscopy (TEM)

The morphology, particle size and microstructure characterizations were performed using a Transmission Electron Microscopes Philips CM120 and JEOL 2100F. A nanoparticles suspension in deionized water was prepared and submitted to ultrasonic bath for 10 min, then dropped in the grid and the solvent was dried at room temperature. It was used the software ImageJ (https://imagej.nih.gov/ij/) to measure the size of particles from the treatment of two images.

2.3.7. Zeta potential determination

The electrophoretic zeta potential (ζ) of the processed nanoparticles were evaluated by using Zetasizer Nano Series – Nano ZS, Malvern Instruments. The instrument determines the electrophoretic mobility of particles and converts it to zeta potential using Smoluchowski's equation [233]. The measurements were conducted dispersing dilute sonicated magnetite nanoparticle samples, at room temperature in ultrapure water.

2.3.8. Vibrating Sample Magnetometer (VSM)

The magnetic curves (hysteresis loops) were determined, at room temperature, with a custom-made vibrating sample magnetometer by varying the magnetic field up to 15 kOe.

2.3.9. In vitro cytotoxicity analysis of COS, Fe_3O_4 and Fe_3O_4:COSs

Cell viability was investigated in accordance with the international standard operation procedure "Tests for in vitro cytotoxicity" ISO 10993-5. Cell cytotoxicity was assessed by the CCK-8 assay (Sigma Aldrich, Saint Quentin Fallavier, France) according to the manufacturer's instructions. Canine fibroblasts were seeded at a density of 1.10^4 cells/ well ($2.6.10^4$ celss/cm^2) in 96-well plate at 37°C in humidified atmosphere with 5% CO_2. After 2 days of culture, the medium was replaced with fresh medium containing COS ($COS_{10/53}$ and $COS_{24/47}$) or nanoparticles (Fe3O4, Fe_3O_4:$COS_{10/53}$ and Fe_3O_4:$COS_{24/47}$). Two ranges of concentration, (0 [control], 0.060, 0.125, 0.250, 0.500 and 1 mg/ml and 0 [control], 0.1, 0.5, 1.0, 5.0 and 10.0 mg/ml) were used for COS and nanoparticles, respectively. Two exposure times (24h and 48h) were tested in all cases. After 24h or 48h of incubation, 10 µl CCK8 were added into each well and incubated at 37 °C for 2h. The absorbance was measured at 450 nm using a microplate reader (MultiSkan, Thermofisher).

Cell viability was determined as the ratio of the optical density (OD) of exposed cells to the OD of the untreated cells. For each concentration of COS or nanoparticles, mean values of the mean absorbance rates from eight wells were calculated. All experiments were performed in triplicate using fibroblasts obtained from three different dogs. Results were expressed as mean ± standard deviation. Differences between $COS_{10/53}$ and $COS_{24/47}$ or among Fe_3O_4, Fe_3O_4:$COS_{10/53}$ and Fe_3O_4:$COS_{24/47}$ were analyzed at each concentration using an unpaired Student's t test. Graphs and statistical analyses were performed using GraphPad Prism version 7 software. p-values ≤ 0.05 were considered significant.

3. Results and discussion

In order to characterize the initial of reacetylated COS, infrared spectra were recorded and are shown in Figure 1 (A). The most characteristic absorption bands from COS are [169, 234-236]: a) axial stretching of O-H and N-H bonds in the range from 3750 to 3000 cm^{-1}; b) axial stretching of C-H bond in $–CH_2$ (2930 cm^{-1}) and $-CH_3$ (2875 cm^{-1}); c) the amide I presents absorption band at 1655 cm^{-1} and it is attributed to axial stretching of C=O bonds of acetamide groups; d) angular deformation of N-H from amine groups ($-NH_2$) at 1558 cm^{-1}; e) the absorption bands at 1417 cm^{-1} and 1377 cm^{-1} which result from the coupling of C-H angular deformation and C-N axial stretching; (f) the absorption bands corresponding to the polysaccharide skeleton, including the vibrations of the glycosidic bonds, C-O and C-O-C stretching, in the range 1153 to 897 cm^{-1}.

Figure 1 (B) shows the FT-IR spectra of Fe_3O_4, Fe_3O_4:$COS_{10/53}$ and Fe_3O_4:$COS_{24/47}$. The characteristic absorption bands of the Fe-O bond of bulk magnetite it was reported to be at 570 and 375 cm^{-1} [237]. However, in Figure 1(B) these two absorption bands shift to high wavenumbers of about 600 and 440 cm^{-1} respectively, and the band near 600 cm^{-1} is divided into two absorption bands at 622 and 590 cm^{-1}. The principal effect of the small size of nanoparticles is the breaking/distorcion of a large number of bonds in the vicinity of the surface, resulting in the rearrangement of delocalized electrons on the particle surface. As a result, the apparent surface bond force constant increases as Fe_3O_4 is reduced to nanoscale dimension, so that the absorption bands of infrared spectra shift to higher wavenumbers. In addition, the split of the bands is attributed to the split of the energy levels of the quantized Fe_3O_4 nanoparticles [238]. In comparison with the Fe_3O_4 FTIR spectrum, the spectra of Fe_3O_4:$COS_{10/53}$ and Fe_3O_4:$COS_{24/47}$ also exhibited the typical absorption bands of magnetite at 622, 590 and 440 cm^{-1}, besides the absorption bands that characterize the presence of COS on their surface. As an example, the absorption band at 1070 cm^{-1} attributed to stretching of C-O-C, at 2930 cm^{-1} C-H and 2875 cm^{-1} (axial stretching of $-CH_2$ and $-CH_3$, respectively) and the coupling of absorption bands at 1417 cm^{-1} (angular deformation of -C-H) and at 1377 cm^{-1} (axial stretching of -C-N) can be observed. It can be noticed that for the sample Fe_3O_4:$COS_{24/47}$, these absorption bands are a lightly more intense (see Figure 1 (B)), suggesting a higher quantity of COS on their surface. As can be seen in the spectra of Fe_3O_4:$COS_{24/47}$ and Fe_3O_4:$COS_{10/53}$ the presence of the characteristic absorption bands of COS indicates that the magnetite nanoparticles were successfully coated by COS.

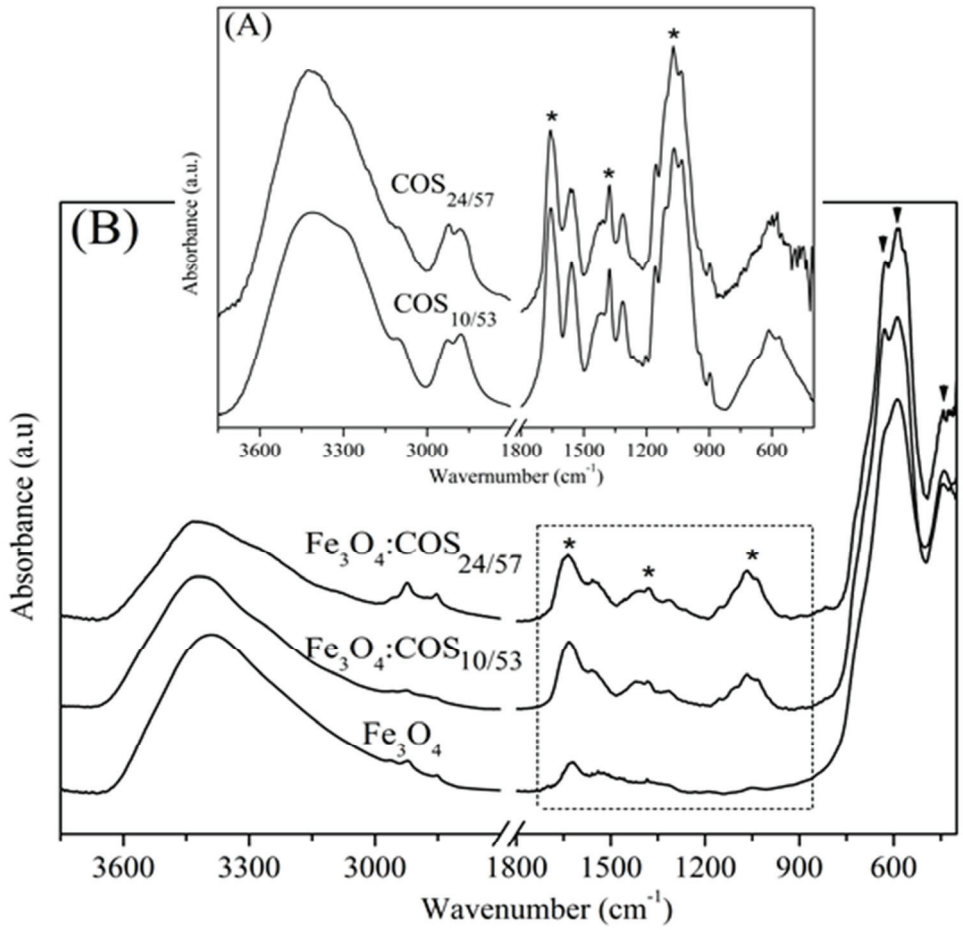

Figure 1 – Normalized infrared spectra of the chito-oligosaccharides: $COS_{10/53}$ and $COS_{24/47}$ (A). And normalized infrared spectra for Fe_3O_4, Fe_3O_4:$COS_{10/53}$ and Fe_3O_4:$COS_{24/47}$ (B);

TGA was performed in the temperature range of 30 to 700 °C to emphasize the existence of COS on the surface of Fe_3O_4 NPs and estimate the proportion of organic and inorganic phases. Pure COSs ($COS_{10/53}$ and $COS_{24/47}$) started to be degraded at 200 °C and were completely degraded at 600 °C, as shown in Figure 2. The degradation of COSs, which stayed on the coated Fe_3O_4 nanoparticles, starts at lower temperature in comparison with pure COS, *i.e.* at 160 °C for both $COS_{10/53}$ and $COS_{24/47}$. It can also be observed that the degradation of COS, on the coated Fe_3O_4 NPs, finish around 400 °C (see Figure 2). The low temperature part of thermograms are due to water loss and could be deduced that the pure COSs had more adsorbed water (~3.90 %) than the other analysed samples (Fe_3O_4 NPs and coated NPs ~1.57 %)). As expected, the subsequent degradation events correspond to decomposition of COS (organic part), that could be observed for the COS samples and COS coated NPS (starting at 200 and 160 °C, respectively). In the case of Fe_3O_4 NPs and coated

NPs, it can be suggested that the formation of Fe_2O_3 occurred at high temperature, since the TGA analyses were performed under air [239, 240]. Moreover, air atmosphere was used in the TGA analyses to induce the complete degradation of COS which, when performed under inert atmosphere, always leaves residual mass. Then, for the calculation of the COS mass on the coated nanoparticles, Fe_2O_3 was hypothesised as final inorganic product [239]. This was grounded by the fact that the initial products show a black colour (characteristic for magnetite) whereas at the end of TGA experiment, the final powder showed a red colour (characteristic for hematite), which is an evidence of Fe_2O_3 formation (see SM Fig. 3). Thus, the mass percentage of organic material, COS, on the coated NPs was calculated and reported in Table 2. For the nanoparticles coated with $COS_{10/53}$ the percentage of organic material on the nanoparticles was close to 13 % and for Fe_3O_4:$COS_{24/47}$ system, the organic content was close to 17 %. These estimations are in good agreement with the results of FTIR analysis, which showed more intense absorption bands characteristics of COS for the sample Fe_3O_4:$COS_{24/47}$.

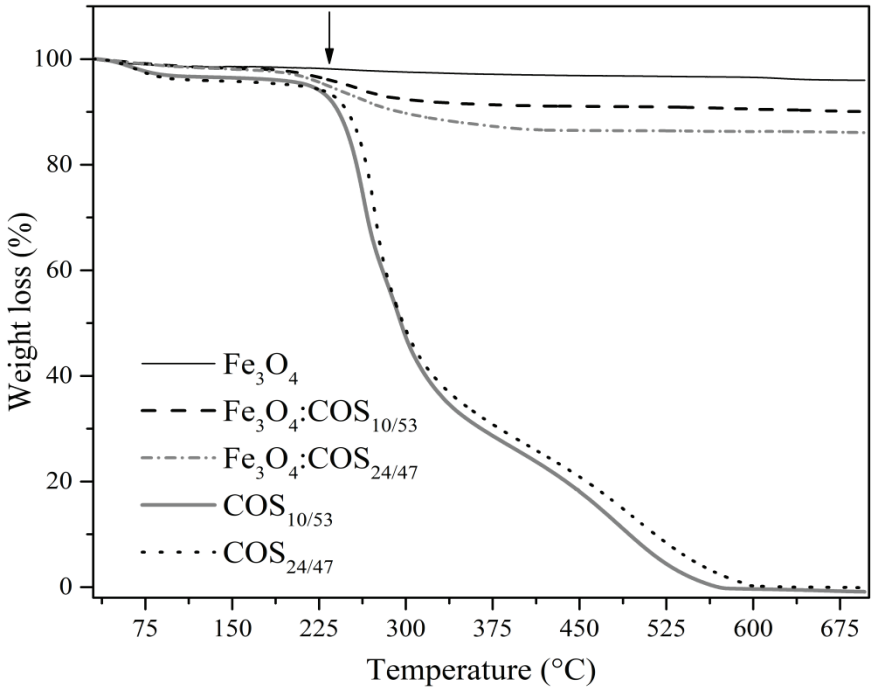

Figure 2 - Thermogravimetric curves to Fe_3O_4, Fe_3O_4:$COS_{10/53}$, Fe_3O_4:$COS_{24/47}$, $COS_{10/53}$ and $COS_{24/47}$.

The XRD analysis was further performed to evidence the formation of magnetite crystalline structure during the synthesis by the precipitation process used in this work. The XRD patterns for Fe_3O_4, Fe_3O_4:$COS_{10/53}$ and Fe_3O_4:$COS_{24/47}$ nanoparticles are shown in

Figure 3. The X-ray diffraction pattern of all synthesized nanoparticles were similar and exhibited the characteristic diffraction peaks of Fe_3O_4 at 2θ values of 18.15° (111), 30.11° (220), 35.54° (311), 43.28° (400), 53.77° (422), 57.27° (511) and 62.95°(440). The diffraction peaks were indexed with a cubic spinel structure (*Fd*$\bar{3}$*m* space group), which is consistent with the standard data for magnetite (JCPDS card n° 88-0315, see Figure 3). However, the formation of nanoparticles in the presence of COS impacts the X-ray diffraction: the (311) plane reflection intensities were increased in presence of COS (see Fig. 3 (A) and (B), inset), indicating a more ordered crystalline structure in the sample Fe_3O_4:$COS_{24/47}$. The peak width decreased when the Fe_3O_4 was synthesized in the presence of COS and this effect was slightly more pronounced using the COS with smaller DP ($COS_{10/53}$), as shown in Figure 3 (B), reflecting an increase of the crystal size and/or perfection. The crystallite sizes of the synthesized Fe_3O_4, Fe_3O_4:$COS_{10/53}$ and Fe_3O_4:$COS_{24/47}$, nanoparticles were calculated from the XRD patterns using the Scherrer equation (Equation 1) for the (311) peak. The estimated crystallite sizes for the three analysed samples are shown in the Table 2.

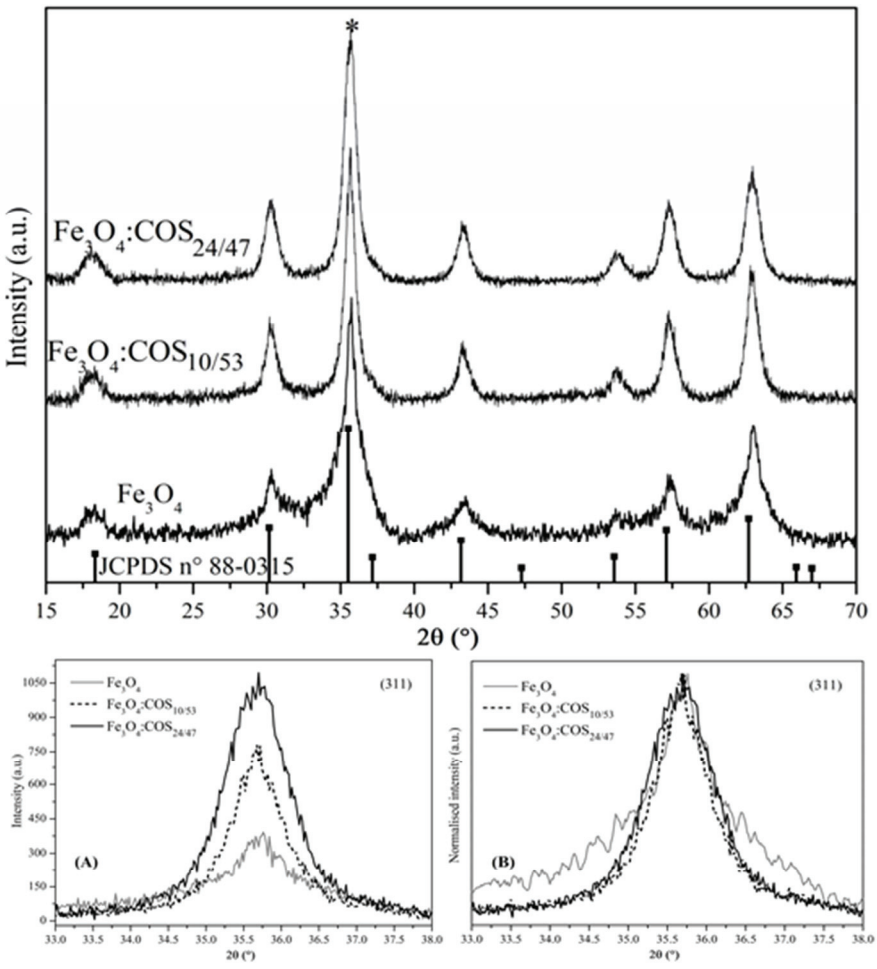

Figure 3 – X-ray diffraction patterns of nanoparticles: Fe_3O_4, Fe_3O_4:$COS_{10/53}$, Fe_3O_4:$COS_{24/47}$ and comparison with JCPDS n° 88-0315. Inserts display the relative intensities (A) and the normalized intensities (B) of the (311) reflexion peak.

TEM was further used to deduce the size of the nanoparticles. Figure 4 shows TEM images of Fe_3O_4 (A, B and C), Fe_3O_4:$COS_{10/53}$ (D, E and F), Fe3O4:$COS_{24/47}$ (G, H and I) NPs and their nanoparticles size histograms fitted by log-normal distribution functions. The Fe_3O_4 nanoparticles were nearly spherical in shape with an average diameter of 6.1±1.7 nm. Aggregates were presents, with smaller particles which the diameter could be not measured. The obtained Fe_3O_4:$COS_{10/53}$ NPs exhibit a mean particle size of 6.0±1.3 nm, a spherical morphology with lower size dispersity in comparison with Fe_3O_4 NPs. Fe_3O_4:$COS_{24/47}$ NPs also presented a spherical morphology with improved dispersity. However, two distinct populations could be observed with average diameter of 5.8±1.5 and 2.3±0.4 nm (see Figure 4 (H) and (I)). Such TEM results are a strong indication that COS might act as steric stabilization agent and prevent aggregation of Fe_3O_4 NPs, acting in the nucleation process and helping to narrow the size distribution of nanoparticles.

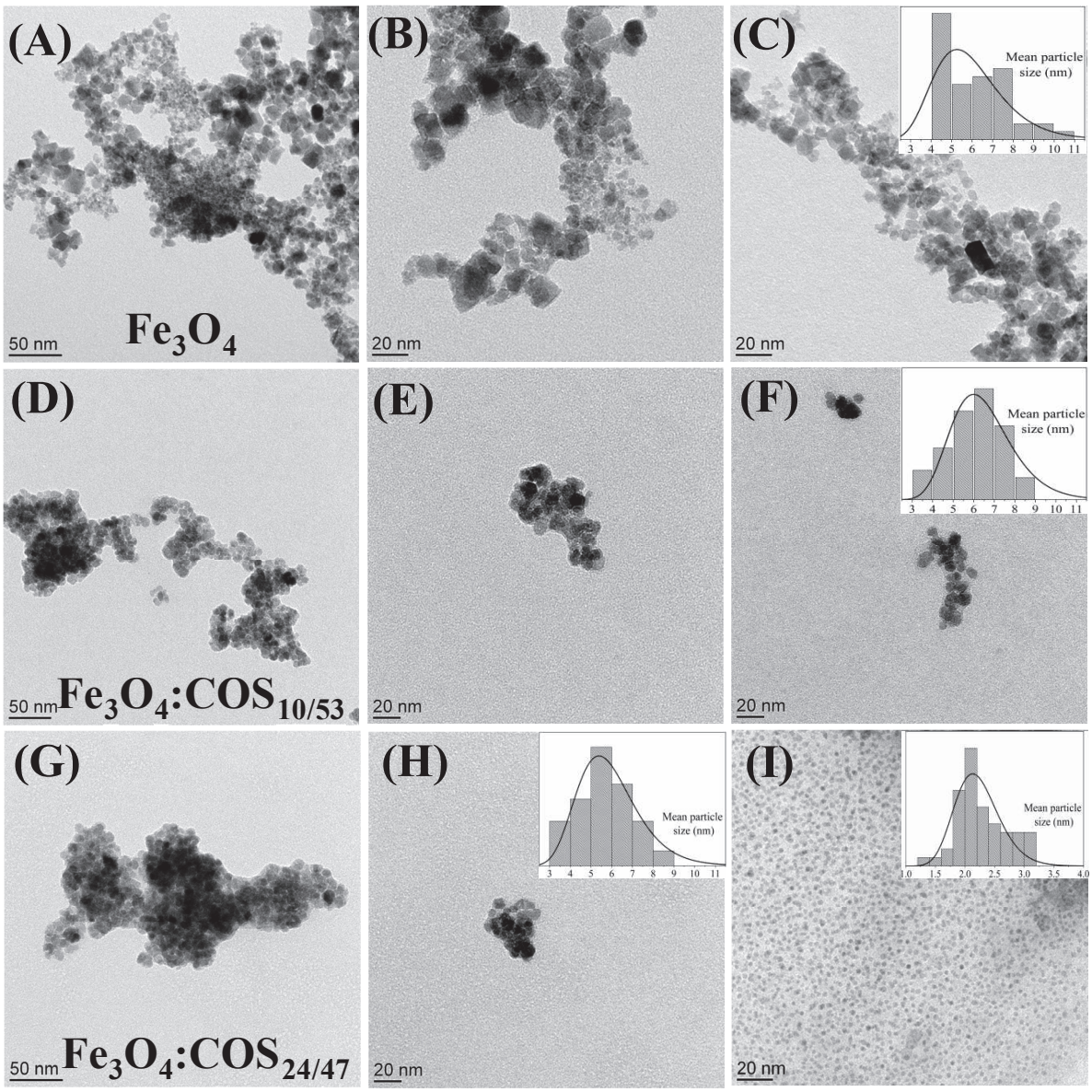

Figure 4 – TEM images of nanoparticles: Fe_3O_4 (A, B and C), Fe_3O_4:$COS_{10/53}$ (D, E and F) and Fe_3O_4:$COS_{24/47}$ (G, H and I); Inserts: Histograms showing particle size distribution profiles (the straight lines are lognormal fittings).

The zeta potential is an important parameter in the examination of the stability of nanoparticle dispersions in aqueous media [241]. The ξ-potentials of the polymer-coated NPs were measured in solution of ultrapure water with 5.0 mM of NaCl. The ξ-potential values for Fe_3O_4, Fe_3O_4:$COS_{10/53}$, Fe_3O_4:$COS_{24/47}$ were +8.9 mV, +13.7 mV and +16.6 mV, respectively (see Table 2). This is ascribed to protonated hydroxyl groups present on the magnetite surface, and chitosan protonated amino groups, on the coated magnetite, in the weakly acidic

environment (pH ≅ 6.0). This resulted in the dispersion of the nanoparticles in aqueous solution and suggests the efficient coating of the Fe_3O_4 NPs by the chito-oligosaccharides [242].

Table 2 – Mass percentage of COS present on the coated Fe_3O_4, zeta potential (ζ), saturation magnetization (M_s), mean particle diameters determined from the magnetization curves (M X H) at room temperature and crystallite sizes determined from XRD results applying Scherrer equation and physical size from TEM analysis, for Fe_3O_4:

Samples	COS mass	ζ-potential*	M_s	D_m	Scherrer Crystallite size	Apparent diameter
	TGA (%)	(mV)	(emu/g)	*M X H* (nm)	XRD (nm)	TEM (nm)
Fe_3O_4	-	+ 8.9	28.3	5.33	6.5	6.1±1.7
$COS_{10/53}$: Fe_3O_4	12.8	+ 13.7	60.6	4.49	10.0	6.0±1.3
$COS_{24/47}$: Fe_3O_4	16.6	+ 16.6	59.8	4.50	8.8	5.8±1.5/2.3±0.4

*Samples analysed in aqueous solution with 5 mM of NaCl.

In order to study the magnetic behaviour of Fe_3O_4, Fe_3O_4:$COS_{10/53}$ and Fe_3O_4:$COS_{24/47}$, magnetization measurements were performed. According to Figure 5, the saturation magnetization (M_s) values obtained for synthesized magnetite nanoparticles are lower than that reported for multi-domain bulk magnetite (≅90 emu/g) [243] and are listed in Table 2. It is reported in the literature that saturation magnetization of ferrite nanoparticles sharply decreases with decreasing of particle size, being correlated to surface spin contributions, stoichiometric deviation and surface defects [244, 245]. In fact, defects on the surface decrease the coercivity of the nanoparticles system and increase the magnetic anisotropy [246]. An organic layer on the particle can also contributed to an apparent decrease in the M_s values, since it is proportional to the mass used in the tests [247]. In our case, this reduction was more pronounced for the Fe_3O_4 NPs (28.3 $emu.g^{-1}$) than for COS coated Fe_3O_4 NPs (Fe_3O_4:$COS_{10/53}$ = 60.6 $emu.g^{-1}$ and Fe_3O_4:$COS_{24/47}$ = 59.8 $emu.g^{-1}$). As the mass of COS on the NPs was determined by TGA analysis, the M_s values can be normalised and theoretically it is possible to determine the M_s value only for the magnetic core of the particle. The normalised M_s values are 69.5 and 71.7 $emu.g^{-1}$, for Fe_3O_4:$COS_{10/53}$ and for Fe_3O_4:$COS_{24/47}$, respectively. Discrepancies in the saturation values of magnetization reported by different groups may be explained by variations in the methods employed to synthesize magnetite, which can generate different particle sizes, magnetite surfaces, crystalline defects

and chemical compositions [228, 229, 248]. Another explanation is that Fe_3O_4 NPs can undergo as oxidative process and thus their external part can lose their magnetic properties. As the Fe_3O_4:COS NPs have COS on their surface, it can act as a protective layer avoiding the oxidation of internal part of the particles (Fe_3O_4). In this work, the presence of COS may help to favour the synthesis process of magnetite, possibly through the complexation between the iron ions and amino groups of COS. This resulted in a more ordered crystalline structure, as could be evidenced by X-ray diffraction analysis, also leading to a high saturation magnetization values in comparison with the pure Fe_3O_4 NPs.

As can be observed in Figure 5, the magnetization curves measured for uncoated magnetite and coated magnetite nanoparticles showed hysteresis curves completely reversible. In which were observed almost zero coercivity (H_c) and zero remanence magnetization (M_r). This phenomenon proved that the synthesized magnetic nanoparticles exhibit superparamagnetic-like behaviour, a feature that is expected for nanometer-scaled particle size [198, 249].

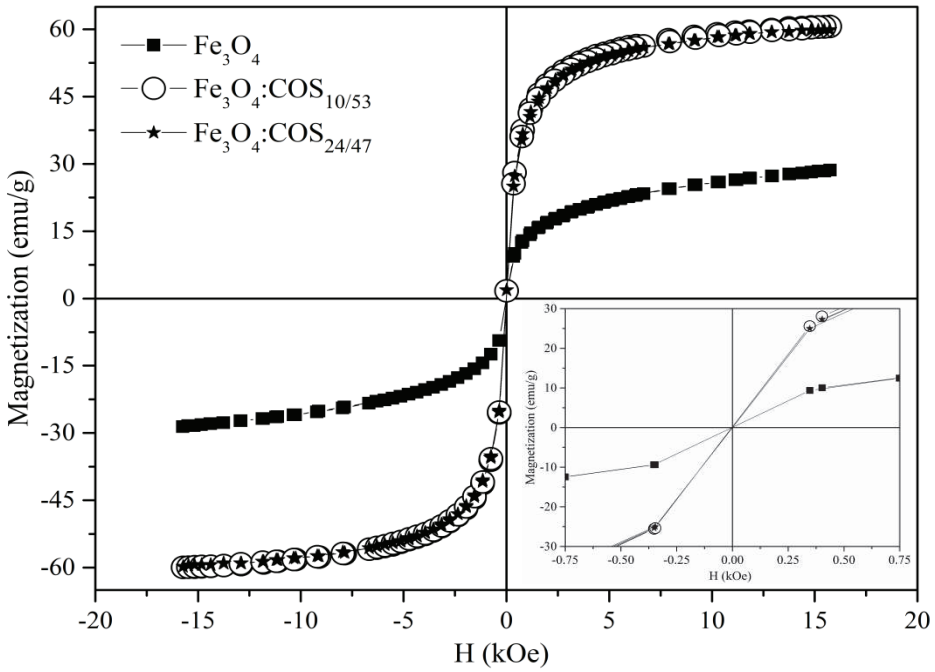

Figure 5 - *M X H* curves, at room temperature, for magnetite nanoparticles: Fe_3O_4, Fe_3O_4:$COS_{10/53}$ and Fe_3O_4:$COS_{24/47}$.

In case of almost zero H_c and zero M_r, an approximation of the average magnetic size of the magnetite nanoparticles can be estimated from the initial susceptibility ($\chi_i =$

$(dM/dH)_{H\to 0}$), which is determined by the largest particles. Therefore an upper limit for magnetic size, D_m, can be roughly estimated according to **Equation 2** [250, 251]:

$$D_m = \left(\frac{18kT\chi_i}{\pi\rho M_S^2}\right)^{\frac{1}{3}} \qquad \textbf{Eq. 2}$$

where D_m is the maximum diameter, k is the Boltzmann constant, T is the absolute temperature (300 K), χ_i is susceptibility at low magnetic field, ρ the density of magnetite (5.24 g/cm^3) and M_s the saturation magnetization. Accounting the M_s and χ_i values obtained for Fe_3O_4 NPs, Fe_3O_4:$COS_{10/53}$ and Fe_3O_4:$COS_{24/47}$ the resulting diameter of 5.33 nm, 4.49 nm and 4.50 nm, respectively. These values are comparable, but smaller than the measurements obtained by TEM or X-ray diffraction analysis. This difference could result from the underestimation of the susceptibility values as shown in the insert of Figure 5. Moreover, the density of the magnetite, used for calculation, does not necessarily correspond to that of the true phase composition and this may have also contributed to the discrepancy.

In order to validate the use of nanoparticles synthesised by the COS-assisted precipitation process, the cytotoxicity of COSs ($COS_{10/53}$ and $COS_{24/47}$) and magnetic nanoparticles (Fe_3O_4, Fe_3O_4:$COS_{10/53}$ and Fe_3O_4:$COS_{24/47}$) have been assessed through CCK8 assay. This assay is based on reduction of soluble tetrazolium salt to an orange-coloured formazan (WST-8) through a cellular deshydrogenase. Therefore, the amount of WST-8 formazan is directly proportional to total cellular deshydrogenase expression and hence number of viable cells [252]. The outcomes of in vitro cytotoxicity studies that have been achieved after 24 h and 48 h of incubation with various concentrations of COS or nanoparticles are illustrated in Figure 6 and 7, respectively.

As shown in Figure 6, $COS_{10/53}$ and $COS_{24/47}$ generally had a low impact on the cell viability even after 48 h of incubation. Significant differences could be observed especially using $COS_{10/53}$ at higher concentrations after 24 h of exposure. However, it was noticed that the cell viability was between 85 % and 90 % (in comparison with control cells) after 24 h and 48 h of exposure time. Relying to the international standard operation procedure “Tests for in vitro cytotoxicity” ISO 10993-5, which sets a threshold of 70% of cell viability to evidence a toxic effect, we can conclude that $COS_{10/53}$ and $COS_{24/47}$ were not cytotoxic in the observed conditions.

Previous studies also laid emphasis on the low cytotoxicity of COS on human and mouse fibroblast at 1 mg/mL [253]. For mouse fibroblasts L929 cell line, COS cytotoxicity was observed for concentrations higher than 5 mg/mL [254]. Lv *et all.* that studied the introduction of COS in hydrogels based on carboxymethyl chitosan and alginate (COS with M_n ~1000 g/mol, DA < 10%, prepared by enzymolysis method). The presence of COS promoted the proliferation of human umbilical cord mesenchymal stem cells. In addition, the injectable hydrogels with COS remarkably accelerated the wound healing process in mouse skin defect model, induced anti-inflammatory effect and absence of cytotoxicity [178]. Comparing literature data about COS cytotoxicity, it still difficult due the diversity of COS molecular structures (chain size, DA and sequence of repeat units).

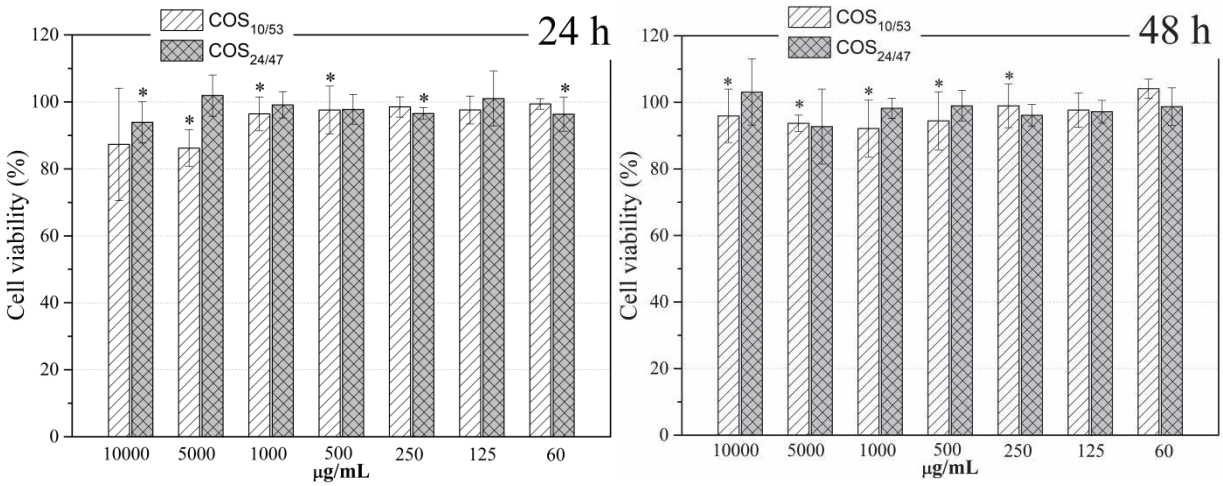

Figure 6 – Cell viability assay of chito-oligosaccharides, $COS_{10/53}$ and $COS_{24/47}$, against canine fibroblasts cells, at different COS concentrations (60 to 10^4 µg/mL) at 24 h and 48 h. Data are mean ± S.D. expressed as % of control response. *Statistically different from control cell monolayers, using $p < 0.05$.

Previous studies have shown that the cytotoxicity of magnetic particle suspensions depend on the NPs concentration, as well as the surface coating material [255-257]. The variation of cell viabilities with respect to Fe_3O_4, Fe_3O_4:$COS_{10/53}$ and Fe_3O_4:$COS_{24/47}$, at the incubation time of 24 and 48 h, are shown in Figure 7. Each nanoparticles display a dose effect. In the case of Fe_3O_4 nanoparticles in particular, a significant impact on primary canine fibroblasts viability was observed, with cell viability at 24 h increasing from 20% to 85% with concentrations varying from 1000 to 60 µg/mL. Similar results were obtained at 48 h and agree with previous works, showing Fe_3O_4 MNPs cytotoxicity on cell lines, as well as primary cells, above the concentration of 100 µg/mL [258, 259].

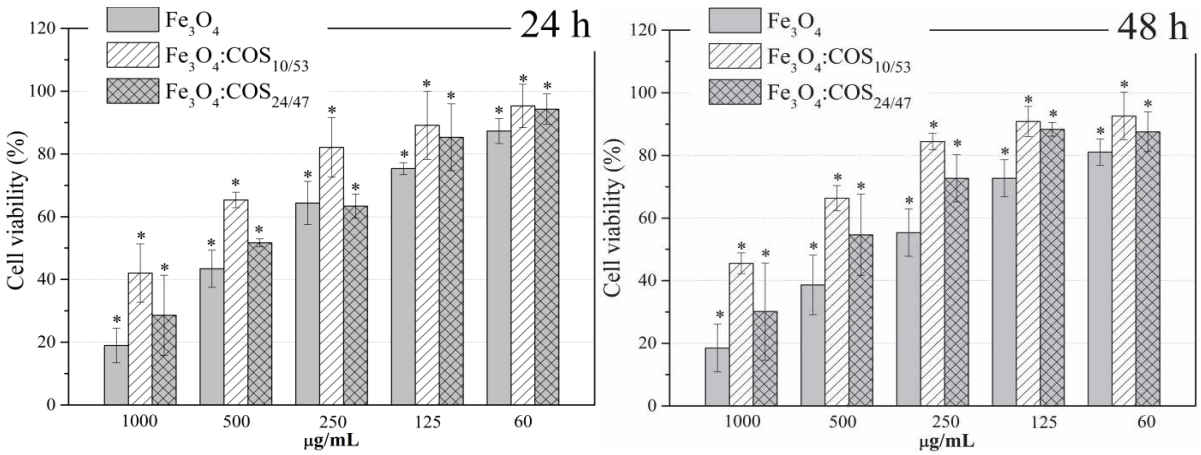

Figure 7 - Cell viability assay of magnetic nanoparticles, Fe_3O_4, Fe_3O_4:$COS_{10/53}$ and Fe_3O_4:$COS_{24/47}$, against canine fibroblasts cells, at different concentrations (60 to 1000 µg/mL) at 24 h and 48 h. Data are mean ± S.D. expressed as % of control response. *Statistically different from control cell monolayers, $p < 0.05$.

Figure 7 shows that the COS coating of Fe_3O_4 MNPs, $COS_{10/53}$ and $COS_{24/47}$, strongly increases the cell viability, although concentration dependence also was observed. The cell viability of the MNPs coated by the $COS_{10/53}$ stayed above 40 % at the concentration of 1000 µg/mL. Differently, the protective effect was less pronounced when the iron oxide NPs was coated by $COS_{24/47}$, in which the cell viability at the concentration of 1000 µg/mL was close to 30 %. Cell viability results were over 80% at the concentration of 125 and 250 µg/mL, for Fe_3O_4:$COS_{10/53}$ and Fe_3O_4:$COS_{24/47}$, respectively. Similar results were observed at 24 and 48 h. Coating Fe_3O_4 NPs with polymers is known to decrease their toxicity and our results agreed with it. Mahmoudi *et al*. showed that uncoated particles induced greater toxicity than the biocompatible polyvinyl alcohol (PVA)-coated particles on a mouse fibroblast cell line [260]. Shukla *et al*. demonstrated that chitosan oligosaccharide coating on iron oxide nanoparticles decrease cellular damage, ROS production, and the cytotoxic impact of the iron nanoparticles [227]. In addition, it could be observed that the Fe_3O_4:$COS_{10/53}$ MNPs demonstrated to be a little less cytotoxic in all concentrations and in both incubation times tested. However, it is necessary to perform other tests to be more systematic about the impact of the COS structure (chain size and DA and sequence of residues) on the cytotoxicity results. For further application of COS coated Fe_3O_4 nanoparticles, it is also necessary to analyse the cell uptake and determine the intracellular behaviour of this type of nanoparticles. Fe_3O_4 MNPs coated by COS may be suitable as magnetic nanocarriers in biomedical applications such as targeted

drug delivery, magnetic resonance imaging (MRI), marker cell tracking and magnetic hyperthermia.

4. Conclusions

A simple co-precipitation method has been developed for *in-situ* preparation of COS coated magnetic Fe_3O_4 nanoparticles through a mixing of iron ions (Fe^{3+} and Fe^{2+}) and COS aqueous solutions followed by precipitation with ammonia, at 60 °C. The impact of COS with DA ~50 % (exhibiting high solubility) and different DPs (DP 10 and 24) was evaluated on the synthesis and behaviours of coated nanoparticles. The results showed that Fe_3O_4 NPs were well encapsulated by COSs, $COS_{10/53}$ and $COS_{24/47}$, without change the spinal structure of Fe_3O_4 NPs. Fe_3O_4 NPs coated by COS presented a more ordered crystalline structure than pure Fe_3O_4, especially in the case of the sample Fe_3O_4:$COS_{24/47}$. TGA analysis permitted to estimate a lower organic content in the Fe_3O_4:$COS_{10/53}$ (12.8 %) than in the Fe_3O_4:$COS_{24/47}$ (16.6 %). TEM analysis revealed that COS layer did not change significantly the size of the nanoparticles and all of synthesized nanoparticles have a mean size close to 6 nm. The COS coated nanoparticles showed a nearly spherical morphology with a narrower size distribution than pure Fe_3O_4 MNPs. VSM results indicated superparamagnetic nature with negligible coercivity (H_c) and remanence (M_r). The COS coated Fe_3O_4 MNPs showed higher saturation magnetization (Fe_3O_4:$COS_{10/53}$ = 60.6 emu.g^{-1} and Fe_3O_4:$COS_{24/47}$ = 59.8 emu.g^{-1}) than the control sample, Fe_3O_4 NPs (28.3 emu.g^{-1}). The calculated magnetic diameters (D_m) were in agreement with the apparent diameter. A cytotoxicity study on canine fibroblasts showed an increase of cell viability for COS coated nanoparticles in comparison with pure Fe_3O_4 MNPs, with concentration dependence.

Although of good results of Fe_3O_4:COS MNPs, such as nanoparticles with narrower size distributions (with smaller aggregates) and consequently a higher M_s value than pure magnetite, it is hard to indicate the impact of COS structure in the nanoparticle behaviours. To better explain the effect of the COS structure on the magnetic core other analyses are necessary, such as the internalization of NPs by the cells. Summarising, we were able to prepare functionalised ultra-small superparamagnetic nanoparticles exhibiting high saturation magnetization. In which, the free amino and hydroxyl groups on their surface allow to design a double functionalisation of the nanoparticles, to be used in magnetic-field assisted drug

delivery, enzyme or cell immobilization, as a marker in cell tracking and other biomedical applications.

4. Conclusions

In this chapter we have started by describing the toxicity of the synthesized chitooligosaccharides. This was performed by culturing the different oligomers on canine dermal fibroblasts. According to the international standard operation procedure we concluded that COS exerts no toxic effect after 24 and 48h. However it was notice that the cell viability increased continually with the decreasing in the chitooligosaccharides concentration. In the second part we described the screening of different COS with different DP and DA to test their capability to favor tissue regeneration with the establishment of synaptic connection between neurons, possibly acting on the PNN. Based on the obtained preliminary results, we concluded, that all chitooligosaccharides are inhibiting PNN formation. Moreover promising results were obtained for specific oligomers, these results should be taken into consideration for future development. Finally, we described the synthesis of supermagnatic nanoparticles from iron ions complexes with chitooligosaccharides. Our results showed that, we were able to prepare functionalised ultra-small superparamagnetic nanoparticles exhibiting high saturation magnetization. In which, the free amino and hydroxyl groups on their surface allow to design a double functionalisation of the nanoparticles, to be used in magnetic-field assisted drug delivery, enzyme or cell immobilization, as a marker in cell tracking and other biomedical applications.

5. Experimental details

5.1. Protocols used to test the toxicity of the synthesized COS

5.1.1. Primary cultures of canine dermal fibroblasts

Canine dermal fibroblasts were isolated from three healthy Beagle dogs owned by Institut Claude Bourgelat (VetAgro Sup -Campus Vétérinaire de Lyon, Marcy l'Etoile, France) in accordance with the VetAgro Sup animal ethics committee. Skin biopsy specimens were collected on dorsal surface of dogs after local anesthesia (lidocaine, Xylovet, Ceva, Libourne, France) and using a 6 skin biopsy punch under sterile conditions. Skin biospsies were then cut

into small fragments and digested with 0.25% trypsin/EDTA (Eurobio, Courtaboeuf, France) 15 min at 37°C. After digestion, skin fragments were washed with PBS. Dermal fibroblast cultures were established by explant culture in 25 cm^2 flasks (Falcon, VWR international, Strasbourg, France) containing Dulbecco's Modified Eagle's Medium (DMEM, Eurobio, Courtaboeuf, France) supplemented with 20% fetal calf serum, 2 mM L-glutamine and 2% penicillin/streptomycin/amphotericin B (Eurobio, Courtaboeuf, France) at 37°C in humidified atmosphere with 5% CO_2. After 4 days, fibroblasts started to grow out and fragments were removed. After 10 days, cells reached confluence and were sub-cultured after 0.25% trypsin/EDTA treatment in 75 cm2 flasks (Falcon, VWR international, Strasbourg, France). Culture medium was changed two times a week. Cells are used between passages 3 and 10.

5.1.2. Cytotoxicity analysis

Cell viability was investigated in accordance with the international standard operation procedure "Tests for in vitro cytotoxicity" ISO 10993-5. Cell cytotoxicity was assessed by the CCK-8 assay (Sigma Aldrich, Saint Quentin Fallavier, France) according to the manufacturer's instructions. This kit contains highly water-soluble tetrazolium salt [WST-8, 2-(2-methoxy-4-nitrophenyl)-3-(4-nitrophenyl)-5-(2,4-disulfophenyl)-2*H*-tetrazolium, monosodium salt] which is reduced by dehydrogenases in cells to give formazan, a yellow colored product. The amount of formazan generated is directly proportional to the number of living cells.

Canine fibroblasts were seeded at a density of 1×10^4 cells/ well in 96-well plate at 37°C in humidified atmosphere with 5% CO_2. After 2 days of culture, the medium was replaced with fresh medium containing nanoparticles or COS over a range of concentration (0 [control], 0.1, 0.5, 1, 5 and 10mg/ml for COS respectively). Two exposure times (24h and 48h) were tested. After 24h or 48h of incubation, 10 µl CCK8 was added into each well and incubated at 37°C for 2h. The absorbance of the formazan product was measured at 450 nm using a microplate reader (MultiSkan, Thermofisher).

Cell viability was determined as the ratio of the optical density (OD) of exposed cells to the OD of the untreated cells. For each concentration of COS or nanoparticles, mean values of the mean absorbance rates from eight wells were calculated; all experiments were performed in triplicate on fibroblasts obtained from three different dogs. Results were expressed as mean ± standard deviation.

5.2. Protocols used for the screening for the use of well controlled chitooligosaccharides for an application in nervous tissue regeneration: cytotoxicity analyses

5.2.1. Materials

Commercial chitotetraose (Reference C2641 (XPM7D-RP); degree of *N*-acetylation (DA) ~ 0%) was supplied by TCI. Commercial chitotriose and chitopentaose (Reference 01032016; degree of *N*-acetylation (DA) ~0%) was supplied by Qingdao. Commercial chitohexose (Reference 400436 (081100); degree of *N*-acetylation (DA) ~0%) was supplied by Seikagaku. Commercial chitotriose (degree of *N*-acetylation (DA) ~100%) was synthesized by IMP team. Commercial chitotetraose, chitopentaose and chitohexose (Reference GLU434, GLU435 and GLU436 respectivly; degree of *N*-acetylation (DA) ~100%) were supplied by Elicityl.

5.2.2. Cells culture with chitooligosaccharides

500ul of PNN cell line in DMEM with 10% fetal bovine serum and 1% penicillin–streptomycin–fungizone (PSF; Sigma) was cultured on cover slips coated with Poly-lysine t (Sigma, St Louis, MO, USA; 20µg/mL). The PNN cells were cultured in a tissue-culture incubator for one night. After on night, the cells were washed twice with DMEM followed by the addition of 500ul of 2mM oligosaccharides of glucosamine (reacetylated oligosaccharides with different DP and DA) in DMEM with 10% of Insulin-Transferrin-Selenium (ITS). The medium was cultured in a tissue-culture incubator supplemented with 5% CO2. Cells were fixed at 1, 3 and 5 days after plating with 4% paraformaldehyde and washed once with phosphate-buffered saline (PBS), with 1% ammonium chloride.

5.2.3. Cells staining for immunocytochemistry

Immunocytochemistry will be performed using antibodies against PNN molecules. First block the cell surface with 1% normal donkey serum (NDS) in 1xPBS for 30min. After, attack with first antibody biotinylated WFA (WFA-bio, 1:300) in PBS for 30 min. Then wash once with 1xPBS and twice with PBST (0.1 % Tx-100 in 1xPBS). After that, attack with second florescent antibody (Strep-488, 1:500) + Hoechot (1:30,000) for 2 hr. Finally, wash twice with 1xPBS and once with 1xTNS for 5 mins each, at the end coverslips are ready to be analyzed after drying well for one night at room temperature.

Chapter IV

Reducing end modification of chitooligosaccharides

Overview

We here described the reducing end modifications of Chito-oligo-saccharides (COS) via the unmasked aldehyde group. This type of modification is gaining much interest since it could preserve both the chemical nature of COS backbones and inherent bioactivities of COS. Briefly, this type of modification will take place in two steps. In a first step, including the preparation and the structural characterization of chitooligosaccharides obtained by nitrous acid depolymerization of chitosan, we then obtained COS terminated at the reducing end by of 2,5-anhydro-D-mannofuranose (amf) bearing a "non-masked" aldehyde group. In a second step, we performed the reaction between the amf unit and various functionalized anilines, hydrazides and *O*-hydroxylamines by both reductive amination and oximation. Thus, we will describe in details the synthesis of new COS-based building blocks functionalized at their reducing end by different "clickable" chemical groups (*i.e.* alkyne, alkene, azide, thiol, and hydrazide). This chapter is written in a pulication form and published in "Carbohydrate Polymers" journal.

Paper II

Reducing-end "clickable" functionalizations of chitosan oligomers for the synthesis of chitosan-based diblock copolymers

Amani Moussa, Agnès Crépet, Catherine Ladavière, Stéphane Trombotto

Ingénierie des Matériaux Polymères (IMP, UMR 5223 - CNRS), Université Claude Bernard Lyon 1, Univ Lyon, F-69622 Villeurbanne, France

Received 14 February 2019; Received in revised form 8 April 2019; Accepted 25 April 2019
Available online 11 May 2019

Abstract: Chitooligosaccharides (COS) produced by nitrous acid depolymerization of chitosan are unique chitosan oligomers due to the presence of the 2,5-anhydro-D-mannofuranose (amf) unit at their reducing end. In this work, we focused on the reductive amination and the oximation of the amf aldehyde group towards various functionalized anilines, hydrazides and *O*-hydroxylamines. The aim of this work was to synthesize new COS-based building blocks functionalized at their reducing end by different "clickable" chemical groups such as alkene, alkyne, azide, hydrazide and thiol. Targeted functionalized COS were synthesized in excellent mass yields and fully characterized by NMR spectroscopy and MALDI-TOF mass spectrometry. Our results showed these functionalizations are quantitative, versatile and can be easily performed in mild reaction conditions. Finally, these COS-based building blocks could be useful intermediates for the development of advanced functional COS-based conjugates, as illustrated in this work by the synthesis of new COS-poly(ethylene glycol) (PEG) diblock copolymers.

Keywords: nitrous deamination; reducing-end functionalization; chitosan oligomer-based building block; click chemistry; diblock copolymer;

Introduction

Chitosan is a linear polysaccharide, copolymer of (1→4)-linked units of 2-amino-2-deoxy-β-D-glucopyranose (GlcN) and 2-acetamido-2-deoxy-β-D-glucopyranose (GlcNAc) (Yeul, & Rayalu, 2013). Although naturally present in *Mucoraceae* fungi, chitosan is obtained

industrially by thermochemical *N*-deacetylation of chitin, a structural polysaccharide widely present in arthropod exoskeletons and cephalopod endoskeletons (Younes, & Rinaudo, 2015). Over the past decades, chitosan has received more attention as a functional biopolymer due to its biocompatibility, biodegradability and numerous biological activities (Hamed, Ozogul, & Regenstein, 2016). Chitosan and their derivatives have been proposed for applications including agriculture, biomedicals, cosmetics and food (Dash, Chiellini, Ottenbrite, & Chiellini, 2011; Hamed *et al.*, 2016). However many applications of chitosan are often hampered by its high viscosity in dilute aqueous acid solutions or its poor solubility in neutral and basic pH solutions. Consequently, a growing interest has been shown to chitooligosaccharides (COS) defined as oligomer forms of chitosan or chitin. Compared to chitosan, COS show a better water solubility and a lower viscosity in aqueous solutions, in addition to several specific biological properties, such as antibacterial, antifungal and antitumour activities, as well as immuno-enhancing effects on animals (Li, Xing, Liu, & Li, 2016; Liaqata, & Eltemb, 2018; Mourya, Inamdar, & Choudhari, 2011; Xia, Liu, Zhang, & Chen, 2011). COS have also been shown to elicit increasing protective responses in various plants and possess antimicrobial activities against a wide spectrum of phytopathogens (Das *et al.*, 2015). Conventional methods for preparing COS are either chemical or enzymatic. Chemical methods consist of the depolymerization of chitin or chitosan including mainly hydrochloric acid hydrolysis, nitrous acid deamination, fluorolysis in anhydrous hydrogen fluoride, and oxidative-reductive reaction by hydrogen peroxide for instance (Mourya *et al.*, 2011). Additionally, total chemical syntheses of COS, involving multiple protection and deprotection steps, have also been reported (Yang, & Yu, 2014). Enzymatic methods include the hydrolysis of chitin and chitosan with hydrolytic enzymes and the synthesis of COS by means of enzymes having transglycosylation activities (Aam *et al.*, 2010).

Besides, chemical functionalizations of COS are currently being explored intensively in order to design new properties and to develop advanced functional COS-based conjugates (Liaqata *et al.*, 2018; Lodhi *et al.*, 2014). In particular, the functionalization of COS with “clickable” chemical groups is of primary interest, based on the robustness, high efficiency, compatibility with sensitive functional groups and versatility of “click” reactions, such as Cu(I)-mediated azide/alkyne cycloadditions (CuAAC) (Guerry *et al.*, 2013; Huang *et al.*, 2009; Marzaioli *et al.*, 2012) or thiol/ene additions (Illy *et al.*, 2014). A convenient route for the incorporation of “clickable” groups into COS is based on the reactivity of amine groups along the oligosaccharide backbone (Huang *et al.*, 2009; Illy *et al.*, 2014; Marzaioli *et al.*, 2012).

However, as inherent physico-chemical and biological properties of COS are closely related to the presence of free amine groups, this simple strategy is often unfavorable for many applications. In order to circumvent the use of amine groups and to preserve the chemical nature of COS backbones, an alternative approach consists of exploiting the presence of the aldehyde group at the reducing end of COS. Thus, Guerry *et al.* (2013) have shown that alkyne-bearing aniline constituted a powerful tool for the easy derivatization of COS and the preparation of novel chitosan oligosaccharide-based advanced materials.

Surprisingly, this reducing-end approach has rarely been investigated for the introduction of "clickable" chemical groups in COS produced by nitrous acid depolymerization of chitosan (Pickenhahn, Grange, De Crescenzo, Lavertu, & Buschmann, 2017). These COS are indeed particularly advantageous since their reducing-end unit is composed of a 2,5-anhydro-D-mannofuranose (amf) moiety (Liu, Tokura, Nishi, akairi, 2003; Strand, Issa, Christensen, Vårum, & Artursson, 2008; Tømmeraas, Vårum, Christensen, & Smidsrød, 2001; Pickenhahn *et al.*, 2015). Compared to GlcNAc or GlcN, amf does not mutarotate in aqueous solution and the aldehyde group is more available for reactions since it does not participate in intramolecular hemiacetals. Furthermore, the nitrous acid depolymerization can be performed in aqueous medium under mild conditions and the extent of depolymerization can be controlled through the stoichiometry of reaction. Finally, thanks to this depolymerization method, chitosan oligomers can be easily prepared in gram scale quantity (Hussain, Singh, & Chittenden, 2012; Mourya, Inamdar, & Choudhari, 2011).

As part of our investigations about the preparation of functionalized chitosan oligomer derivatives (Abla *et al.*,2013; Moussa, & Trombotto, 2016; Salim, Ailincai, & Trombotto, 2014; Salim, Galais, & Trombotto, 2014), herein we report the synthesis of new COS-based building blocks functionalized at their reducing ends with various "clickable" chemical groups, such as alkene, alkyne, azide, hydrazide and thiol. Reducing-end derivatizations were performed by reaction of the COSamf aldehyde group with the amine group of anilines, hydrazides and O-hydroxylamines bearing different "clickable" groups. The aim of the present study is to demonstrate that numerous "clickable" COS-based building blocks can be easily obtained from COS produced by nitrous acid depolymerization of chitosan and can be used for the preparation of high potential COS-based conjugates, as illustrated in this work by the synthesis of new COS-*b*-PEG copolymers.

Materials and methods

2.1. Materials

Commercial chitosan (batch 244/020208; degree of *N*-acetylation (DA) ~ 0%; M_w = 270,000 g/mol; M_n = 115,000 g/mol; Đ = 2.3) was supplied by Mahtani Chitosan Ltd (Veraval, India). Methoxypolyethylene glycol succinimidyl carboxymethyl ester (mPEG-NHS ester, M_n = 2,000 g/mol, Đ = 1.01, purity > 95%) was provided by Jenkem Technology (Plano, USA). Sodium nitrite (purity > 99%), 4-(propargyloxy)aniline (purity > 95%), 4-(mercapto)aniline (purity > 97%), 4-(azido)aniline (purity > 97%), *O*-Allylhydroxylamine hydrochloride (purity > 98%), *O*-2-Propynylhydroxylamine hydrochloride (purity > 98%), adipic dihydrazide (purity > 98%), succinic dihydrazide (purity > 96%), sodium cyanoborohydride (purity > 95%), deuterium oxide (D_2O, purity > 99.96% atom D), methoxypolyethylene glycol azide (mPEG-azide, M_n = 2,000 g/mol, Đ = 1.02, purity > 95%) and all others chemicals and solvents were provided by Sigma-Aldrich (Saint-Quentin Fallavier, France).

2.2. Characterization methods

2.2.1 NMR spectroscopy

^1H and ^{13}C NMR spectra were recorded on a Bruker 500 MHz spectrometer at 300 K. All samples were dissolved at 10 mg/mL in D_2O with 5 µL HCl 12 N, and transferred to 5 mm NMR tubes. Trimethylsilyl-3-propionic-2,2,3,3-D_4 acid sodium salt (99% atom D, TMSPA from Sigma-Aldrich, Saint-Quentin Fallavier, France) was used as internal reference (δ 0.00 and -2.25 ppm for ^1H and ^{13}C NMR, respectively). ^1H NMR spectral data are presented as follows: chemical shifts (δ ppm downfield from TMSPA), multiplicity (s = singlet, d = doublet, t = triplet, m = multiplet), coupling constants (Hz), integration, proton assignment. ^{13}C NMR spectral data are presented as follows: chemical shifts (δ ppm), carbon assignment. Proton and carbon signals were assigned thanks to 2D NMR techniques (*i.e.* COSY, HSQC and HMBC).

2.2.2. MALDI-TOF mass spectrometry

MALDI-TOF mass spectra were acquired with a Voyager-DE STR (AB Sciex, Framingham, MA) equipped with a nitrogen laser emitting at 337 nm with a 3 ns pulse. The instrument was operated in the linear or reflectron mode. Ions were accelerated to a final potential of 20 kV. The positive ions were detected in all cases. Mass spectra were the sum of 300 shots and an external mass calibration of mass analyzer was used (mixture of peptides from Sequazyme™ standards kit, AB Sciex). The matrix used for all experiments was 2,5-dihydroxybenzoic acid (DHB) purchased from Sigma-Aldrich and used directly without further purification. The

solid matrix and samples were dissolved at 10 mg/mL in water. A volume of 45 µL matrix solution was then mixed with 5 µL of sample solutions. An aliquot of 0.5 µL of each resulting solution was spotted onto the MALDI sample plate and air-dried at room temperature.

2.2.3. Size-exclusion chromatography (SEC)

SEC was performed on a chromatographic equipment composed of a 1260 Infinity Agilent Technologies pump connected to two TSK gel G2500 and G6000 columns (Tosoh Bioscience) in series. A multi-angle light scattering (MALS) detector HELEOS II (Wyatt Technology) operating at 664 nm was coupled on line to a Wyatt Optilab T-Rex differential refractometer. Sample solutions at 2-5 mg/mL were prepared and eluted in AcOH (0.2 M)/$AcONH_4$ (0.15 M) buffer (pH 4.5). Solutions were previously filtered through 0.45 µm pore size membranes (Millipore) before injection. The eluent flow rate was 0.5 mL/min. The values of the refractive index increment dn/dc used for molar mass calculations were equal to: (*i*) 0.198 mL/g for commercial chitosan and COSamf samples, (*ii*) 0.169 and 0.164 mL/g for the copolymers **18** and **19**, respectively.

3. Results and discussion

3.1. Preparation of COSamf by nitrous acid depolymerization of chitosan

The nitrous acid depolymerization is a well-known chemical method for the preparation of low molar mass chitosans (Allan, & Peyron, 1989). This reaction can be performed in aqueous solution under mild conditions of temperature and acidity and is specific to GlcN units. Thus, this is a homogeneous reaction where the number of glycosidic bonds broken is roughly stoichiometric to the amount of nitrous acid used (Hussain *et al.*, 2012). Briefly, the depolymerization mechanism involves the reaction of nitrous acid with the amine group of the GlcN unit, leading to *(i)* the release of N_2, *(ii)* the breaking of the GlcN unit glycosidic linkage and *(iii)* the transformation of the GlcN unit into 2,5-anhydro-D-mannofuranose at the new reducing end (Scheme 1).

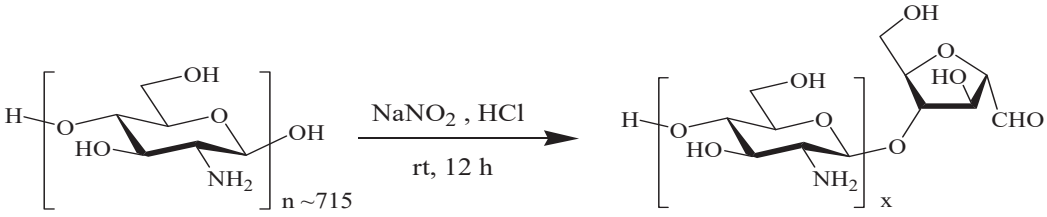

Chitosan (DA ~ 0%)

COSamf: **1** (x ~10) **2** (x ~22) **3** (x ~45)

Scheme 1. Synthesis of COSamf **1-3** by nitrous acid depolymerization of fully *N*-deacetylated chitosan

In this study, the nitrous acid depolymerization of fully *N*-deacetylated chitosan was used to produce three COSamf samples **1-3** with an average number of GlcN repeating units (x) ranging from 10 to 45 (Scheme 1). The nitrous acid depolymerization was typically performed by mixing a dilute aqueous acid solution of chitosan and a specific molar quantity of $NaNO_2$ at room temperature for 12 h, as described in our previous studies (Salim *et al.*, 2014; Salim *et al.*, 2014; Moussa *et al.*, 2016). At the end of the reaction, COSamf samples were isolated and purified by precipitation using appropriate conditions according to x values. Thus, COSamf **2** (x ~22) and **3** (x ~45) were easily precipitated by increasing the pH of the solution by addition of ammonia until pH ~8-9. Since COSamf **1** (x ~10) showed good water solubility whatever the pH, it was advantageously precipitated in acetone. Finally, COSamf **1-3** were produced in gram-scale quantities with mass yields ranging from 80 to 85% after purification (Table 1).

Table 1. Characterization data of synthesized COSamf **1-3**

Sample	GlcN unit/$NaNO_2$ molar ratio	Mass yield (%)	x [a]	M_w [b] (g/mol)	M_n [b] (g/mol)	Đ [b]
COSamf **1**	4	80	10 ±1	2.33×10^3	2.08×10^3	1.12
COSamf **2**	10	82	22 ±2	3.89×10^3	3.38×10^3	1.15
COSamf **3**	30	85	45 ±2	9.98×10^3	7.74×10^3	1.29

(a) The average number of GlcN repeating unit (x) in COSamf was determined by ^{1}H NMR in D_2O at 300 K; (b) weight- and number-average molar masses (M_w and M_n, respectively) and dispersity value (Đ) were determined by SEC-MALS. Molar masses results were expressed as means of ± 10%.

The expected chemical structure of COSamf **1-3** was fully confirmed by ^{1}H and ^{13}C NMR spectroscopy and MALDI-TOF mass spectrometry (MS) analyses. Thanks to two-dimensional NMR analyses, all ^{1}H and ^{13}C resonances corresponding to GlcN and amf units of COSamf were assigned (Figure S4, Supplementary data). As shown in Figure 1a, the ^{1}H NMR spectrum of COSamf **2** presents high intensity signals assigned to GlcN protons at 4.87 ppm for H-1 (GlcN), between 4.07 and 3.62 ppm for H-3 to H-6 (GlcN) and at 3.15 ppm for H-2 (GlcN). The presence of the amf unit at the reducing end is confirmed by four typical low

intensity signals at 5.10, 4.45, 4.23 and 4.13 ppm assigned to H-1 (amf), H-3 (amf), H-4 (amf) and H-5 (amf), respectively. These assignments corroborate previous NMR data published for analogous COSamf structures (Tømmeraas *et al.*, 2001; Pickenhahn *et al.*, 2015). Moreover, the ^{1}H NMR spectrum shows clearly two other low intensity signals assigned to H-4 and H-5 of the GlcN unit neighboring of the amf unit at 3.50 and 3.55 ppm, respectively. In addition, the ^{13}C NMR spectrum of COSamf **2** presents high intensity peaks assigned to GlcN units and low intensity peaks corresponding to both the reducing-end amf unit and the GlcN unit linked to the amf unit (Figure 1b). It is worth mentioning that neither the ^{1}H spectrum nor the ^{13}C spectrum showed the resonances expected for the free aldehyde group of the amf residue (*i.e.* ^{1}H: ca. 9.49 ppm and ^{13}C: ca. ~180 ppm) (Tømmeraas *et al.*, 2001). Thus, the H-1 (amf) and C-1 (amf) resonances at 5.10 and 89.5 ppm, respectively, pointed out that the aldehyde moiety appears to be present only in its hydrated form -$CH(OH)_2$ in the NMR conditions used in this study (RT, pH < 3), as already observed by Pickenhahn *et al.* (2015). Finally, COSamf **1, 2** and **3** led to similar ^{1}H and ^{13}C spectra with comparable assignments.

For each COSamf, the average GlcN repeating unit number (x) given in Table 1 was determined by ^{1}H NMR spectroscopy from the relative peak intensities of H-3 (amf) and H-2 (GlcN) signals at 4.45 and 3.15 ppm (Figure 1a), respectively, according to the formula (1):

$$x = \frac{I_{H-2\ (GlcN)}}{I_{H-3\ (amf)}} \qquad (1)$$

Additionally, COSamf **1-3** were also characterized by SEC-MALS according to their weight- and number-average molar masses (M_w and M_n, respectively) and dispersity values (Đ) in Table 1. The average GlcN repeating unit number (x) estimated by the ^{1}H NMR spectroscopy and SEC-MALS measurements linearly increased by increasing the GlcN unit/$NaNO_2$ molar ratio in the nitrous acid depolymerization reactions (Fig. 2).

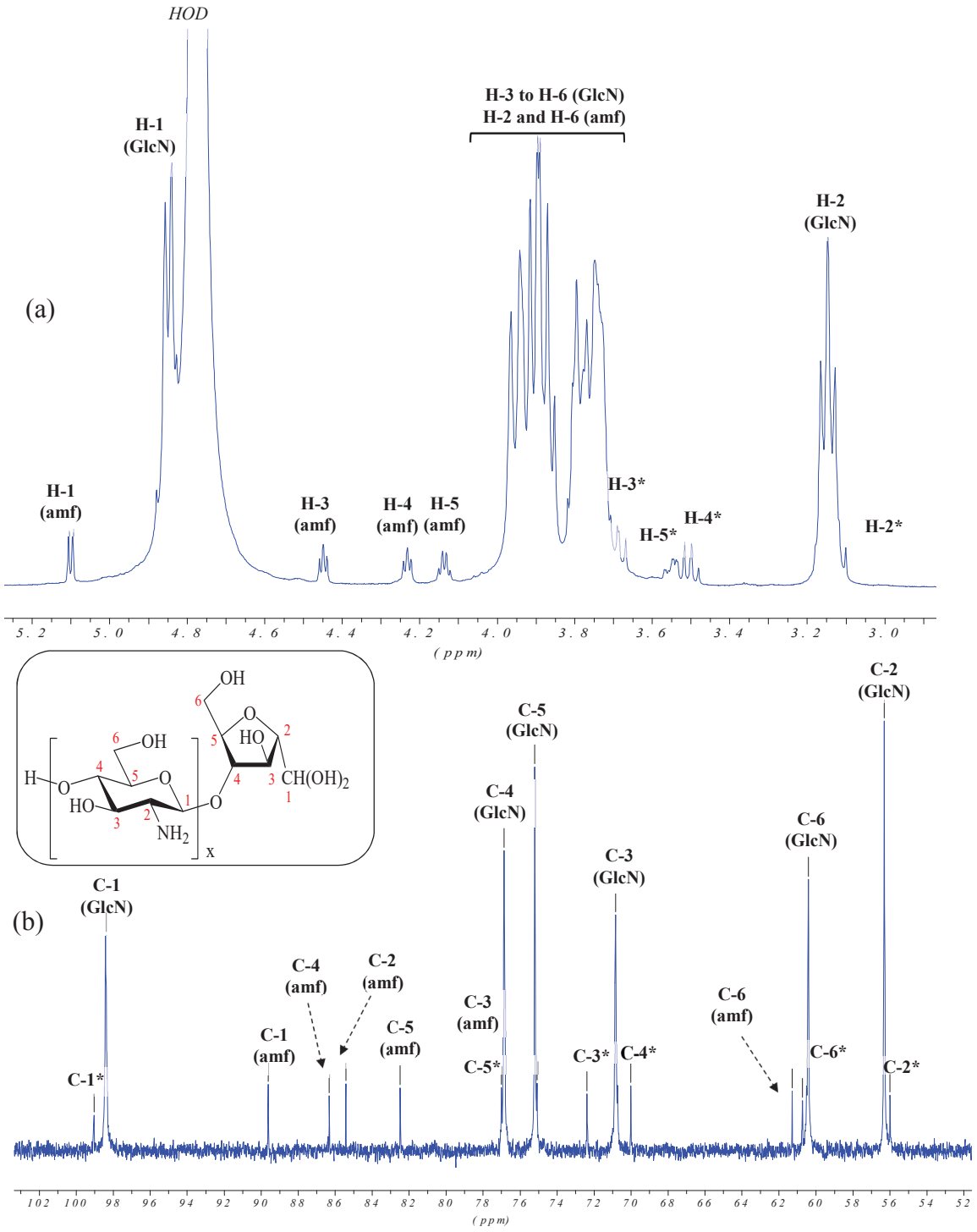

Figure 1. (a) ^{1}H NMR spectrum (500 MHz) and (b) ^{13}C NMR spectrum (125 MHz) of COSamf **2** (x ~22) in D_2O at 300 K. H and C atoms of the GlcN unit linked to the amf unit are indicated by an asterisk.

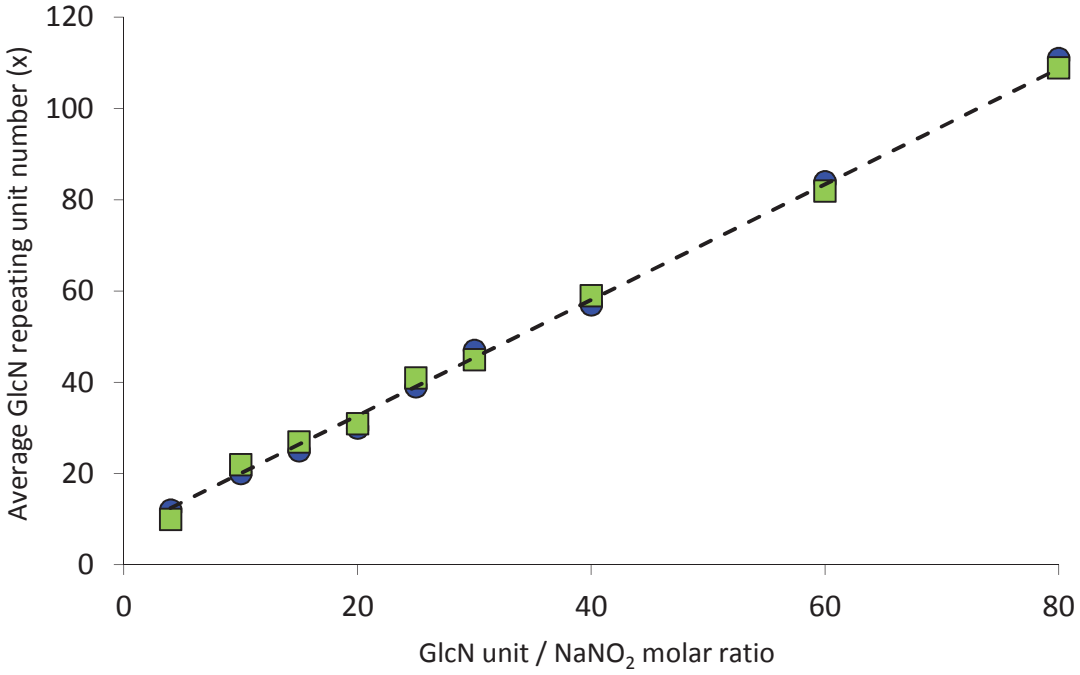

Figure 2. Relationship between the GlcN unit/$NaNO_2$ molar ratio and the average GlcN repeating unit number (x) of COSamf. Fully *N*-deacetylated chitosan (2 % w/w) was depolymerized by sodium nitrite in 0.15M hydrochloric acid solution for 12 h at room temperature. x values were estimated by: (■) ^{1}H NMR from relative peak intensities of H-3 (amf) and H-2 (GlcN) signals at 4.45 and 3.15 ppm, respectively (see Figure 1) according to the formula $x = (I_{H\text{-}2(GlcN)} / (I_{H\text{-}3(amf)})$; (●) SEC-MALS from the measured number-average molar mass (M_n) of COSamf and the molar mass of the GlcN repeating unit (M_0 = 161 g/mol) according to the formula $x = (M_n\text{-}162) / M_0$. Results are expressed as means ± 5%.

3.2. Functionalizations of COSamf reducing ends

The aim of this study is to show the potential reactivity of the aldehyde group of COSamf towards several functionalized amine derivatives, so as to generate original COS-based building blocks with "clickable" groups at their reducing ends. Amine derivatives were selected from aniline, *O*-hydroxylamine and hydrazide derivatives due to their lower pKa values (*ca* 3-6) compared to chitosan oligomers (pKa ~6.5-7). Hence, we expected that amine groups of these derivatives are more nucleophilic than amine groups of COSamf towards aldehyde groups in slightly acid conditions (pH ~5.5) required for the complete solubilization of COSamf in aqueous solutions. Thus, chemical functionalizations of COSamf reducing ends were carried out by means of reductive amination and oximation using above-mentioned

amine derivatives bearing different "clickable" chemical groups, such as alkene, alkyne, azide, hydrazide and thiol, as illustrated in Scheme 2.

3.2.1. Reductive amination of COSamf with functionalized anilines

The reactivity of COSamf towards aniline derivatives has been studied through the reductive amination of COSamf with three different functionalized anilines, *i.e.* 4-(propargyloxy)aniline, 4-(mercapto)aniline and 4-(azido)aniline (pathways a, b, c in Scheme 2, respectively). Thus, the reductive amination of COSamf **2** (x ~22) by an excess of 4-(propargyloxy)aniline (2 eq./amf unit) was carried out in the presence of $NaBH_3CN$ in ammonium acetate buffer (0.15 M, pH 5.5) at 40°C for 2 days, based on reaction conditions described by Guerry *et al.* (2013) (pathway a in Scheme 2). The functionalized COSamf **5** was isolated in 90% mass yield by precipitation in basic conditions by addition of concentrated ammonia. The NMR spectroscopy and MALDI-TOF MS analyses were in complete agreement with the expected chemical structure of the compound **5**, indicating that the functionalization reaction is quantitative. Indeed, thanks to 2D NMR analyses, all resonances of ^{1}H and ^{13}C NMR spectra were assigned (Figure S13, Supplementary data). Thus, the ^{1}H NMR spectrum showed clearly the occurrence of CH_2N protons at 3.40-3.25 ppm, in addition to the presence of the alkyne proton (C≡CH) at 2.95 ppm. Additionally, the ^{13}C NMR spectrum of the compound **5** showed a signal at 46.9 ppm corresponding to the CH_2N carbon and two signals at 79.5 and 77.2 ppm for C≡CH carbons. Thus, both ^{1}H and ^{13}C NMR analyses confirmed the coupling reaction between the COSamf aldehyde group and the amine group of the aniline derivative. Besides, the ^{1}H NMR analysis allowed us to determine the x value of COSamf **5** (*i.e.* x ~23) taking into account signal intensities of both H-2 (GlcN) and aromatic protons. This result confirmed that the reductive amination condition used in this study did not hydrolyze the oligomer chain of the starting COSamf **2** (x ~22). In similar reaction conditions, the reductive amination of COSamf **1** (x ~10) and **3** (x ~45) with 4-(propargyloxy)aniline led also to expected functionalized COSamf **4** (x ~12) and **6** (x ~46) in 87 and 89% mass yields, respectively. However, when applying these reaction conditions with propargylamine as starting amine, the expected functionalized COSamf was not obtained. This result can be explained by the protonation of the amine group of propargylamine (pKa ~10.6) in the reaction conditions (pH ~5.5), which makes the amine group not reactive enough towards the COSamf aldehyde.

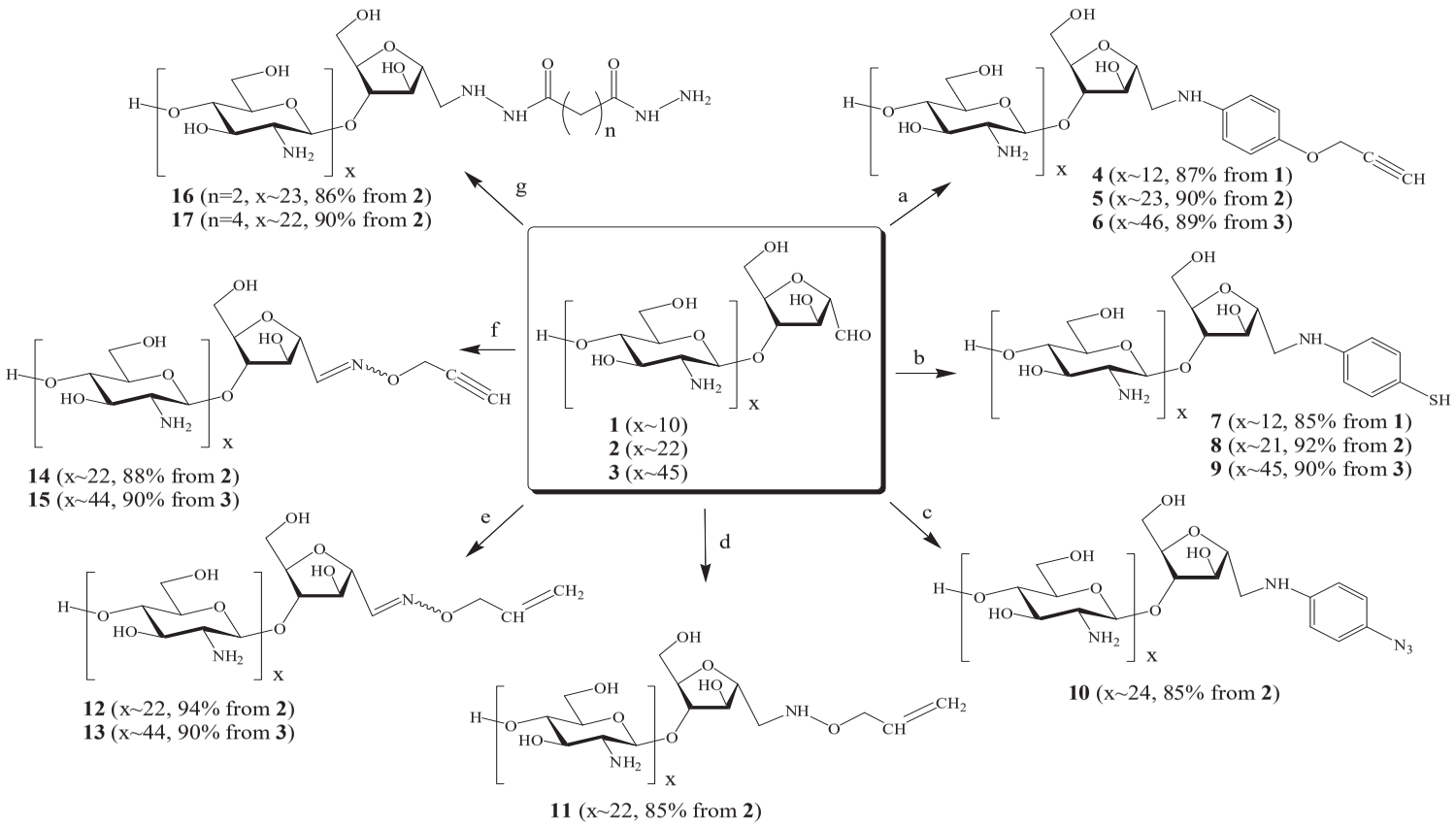

Scheme 2. Pathways of the reducing-end functionalization of COSamf with various functionalized amine derivatives: (a) 4-(propargyloxy)aniline, $NaBH_3CN$, ammonium acetate buffer (pH 5.5)/ethanol, 2 days, 40°C; (b) 4-(mercapto)aniline, $NaBH_3CN$, ammonium acetate buffer (pH 5.5)/ethanol, 2 days, 40°C; (c) 4-(azido)aniline, $NaBH_3CN$, ammonium acetate buffer (pH 5.5), 2 days, 40°C; (d) *O*-allylhydroxylamine, $NaBH_3CN$, acetic acid (pH 4.5)/DMSO, 3 days, 40°C; (e) *O*-allylhydroxylamine, acetic acid (pH 4.5)/DMSO, 2 days, 40°C; (f) *O*-propynylhydroxylamine, acetic acid (pH 4.5)/DMSO, 2 days, 40°C; (g) succinic dihydrazide, $NaBH_3CN$, ammonium acetate buffer (pH 5.5), 2 days, RT; adipic dihydrazide, $NaBH_3CN$, ammonium acetate buffer (pH 5.5), 2 days, 40°C. Note that % values given in brackets correspond to mass yields.

In the same way, the reductive amination of COSamf **1-3** with 4-(mercapto)aniline led to expected 4-(mercapto)aniline-linked COSamf **7-9** in 85-92% mass yields (Scheme 2). Moreover, the reducing end of COSamf **2** (x ~22) could also be functionalized by an azido group in 85% mass yield using 4-(azido)aniline (Scheme 2, compound **10** (x ~24)).

3.2.2. Reductive amination and oximation of COSamf with O-functionalized hydroxlyamines

The reactivity of COSamf towards *O*-functionalized hydroxylamine derivatives has been investigated through the coupling reactions of COSamf with *O*-allylhydroxylamine (pathways d and e in Scheme 2) and *O*-propynylhydroxylamine (pathway f in Scheme 2) by reductive amination or oximation.

a) Reductive amination with O-allylhydroxylamine. The reductive amination of COSamf **2** (x ~22) was carried out with an excess of *O*-allylhydroxylamine (10 eq./amf unit) in the presence of $NaBH_3CN$ in a mixture of aqueous acetic acid (1.5% w/v, pH 4.5)/DMSO (3:1 v/v) at 40°C for 2 days. *O*-allylhydroxylamine-linked COSamf **11** (x ~22) was isolated in 85% mass yield by precipitation in basic conditions (pH ~8-9) by addition of concentrated ammonia (Scheme 2). Thanks to 2D NMR analyses, all ^{1}H and ^{13}C resonances of the compound **11** were assigned confirming the reductive amination of the amf aldehyde group with *O*-allylhydroxylamine (Figure S31, Supplementary data). The ^{1}H NMR spectrum showed clearly the occurrence of CH_2N protons at 3.10 ppm in addition to the presence of alkene protons ($CH=CH_2$) at 5.95 and 5.40-5.25 ppm. Moreover, the ^{13}C NMR spectrum of the compound **11** showed a signal at 52.7 ppm corresponding to the CH_2N carbon and two signals at 133.9 and 119.7 ppm for CH= and $=CH_2$ carbons, respectively. Furthermore, MALDI-TOF MS analyses confirmed the chemical structure of the compound **11** (Figure S32, Supplementary data).

b) Oximation with O-allylhydroxylamine. The possibility to link directly COSamf **2** with *O*-allylhydroxylamine without the need of the $NaBH_3CN$ reduction step was also studied. Typically, the oximation of COSamf **2** (x ~22) was carried out in aqueous acetic acid (1.5% w/v, pH 4.5) with an excess of *O*-propynylhydroxylamine (10 eq./amf unit) solubilized in DMSO at 40°C for 2 days, leading to the compound **12** (x ~22) in 96% mass yield (Scheme 2). The expected chemical structure of the compound **12** was fully determined by ^{1}H and ^{13}C NMR analyses and confirmed by MALDI-TOF MS analyses (Figure S36, Supplementary data). Compared to the compound **11**, the ^{1}H and ^{13}C NMR spectra showed the presence of the imine group ($CH_2=N$, in *E* and *Z* isomers) at 7.65/7.05 ppm and 152.4/150.6 ppm, respectively. As for the reductive amination, it seems that the oximation reaction did not

affect the COS backbone, since the x value of compound **12** and COSamf **2** (x ~22) did not change. Additionally, successful coupling was also observed for the oximation between *O*-allylhydroxylamine and COSamf with higher x values (COSamf **3**, x ~45) leading to the targeted compound **13** (x ~44) in 95% mass yield (Scheme 2).

c) Oximation with O-propynylhydroxylamine. The grafting of an alkyne group into the reducing-end unit of COSamf was also studied by using *O*-propynylhydroxylamine according to similar oximation conditions described for the compound **12**. In these conditions, the targeted compound **14** (x ~22) was obtained in 88% mass yield from COSamf **2** (x ~22) (Scheme 2). The NMR and MALDI-TOF MS analyses of the compound **14** were found to be in complete agreement with the expected chemical structure (Figures S38 to S41, Supplementary data). The ^{1}H NMR spectrum of the compound **14** showed the occurrence of CH_2=N protons as a mixture of *E* and *Z* isomers at 7.65 and 7.10 ppm, in addition to the presence of the alkyne proton (C≡CH) at 2.90 ppm. Moreover, the ^{13}C NMR spectrum showed two signals at 153.8 and 151.8 ppm corresponding to the CH_2=N carbon (*E* and *Z* isomers) and two signals at 79.9 and 76.7 ppm for both C≡CH carbons. In the same manner, the oximation between *O*-propynylhydroxylamine and COSamf with higher x values (COSamf **3**, x ~45) was successfully performed, leading to the targeted compound **15** (x ~44) in 90 % mass yield (Scheme 2).

3.2.3. Reductive amination of COSamf with hydrazides

The reactivity of COSamf towards hydrazide derivatives has been investigated through the reductive amination of COSamf **2** by two commercial hydrazides, *i.e.* succinic and adipic dihydrazides (pathway g, Scheme 2). Thus, the reductive amination of COSamf **2** by succinic dihydrazide was carried out with a large excess of dihydrazide in order to promote the coupling reaction with one hydrazide group only. Typically, COSamf **2** (x ~22) and succinic dihydrazide (10 eq./amf unit) were fully solubilized in ammonium acetate buffer (pH 5.5). The mixture was stirred at room temperature for 1 day, and then $NaBH_3CN$ was added in excess to the solution. After stirring during 1 day at room temperature, the addition of concentrated ammonia (28% w/w) resulted in the precipitation of the expected compound **16** (x ~23) in 86% mass yield (Scheme 2). The chemical structure of the compound **16** was confirmed by NMR spectroscopy and MALDI-TOF MS analyses. Thus, ^{1}H and ^{13}C NMR spectra were fully characterized thanks to 2D NMR analyses, showing the coupling reaction between the COSamf aldehyde group and the hydrazide amine (Figures S43 to S45,

Supplementary data). Thus, NMR analyses showed signals at 3.05 and 52.4 ppm in ^{1}H and ^{13}C NMR spectra, respectively assigned to the presence of the CH_2N group. This result is in good agreement with a single coupling between COSamf and succinic dihydrazide, as confirmed also by MALDI-TOF MS analyses (Figure S46, Supplementary data). In the same way, the reductive amination of COSamf **2** was studied with adipic dihydrazide. In this case, best coupling conditions were obtained at 40°C compared to room temperature for succinic dihydrazide, leading to the expected compound **17** (x ~22) in 90% mass yield (Scheme 2).

3.3. Preparation of COS-b-PEG copolymers

To illustrate the potential of these COS-based building blocks for the development of functional COS-based conjugates, we further investigated the synthesis of COS-PEG diblock copolymers. Despite the huge interest around PEGylated chitosans as cationic nanocarriers for applications in delivery of drugs, genes and siRNA, the synthesis of chitosan-PEG block copolymers has rarely been studied in the literature compared to chitosan-PEG graft copolymers (Casettari *et al.*, 2012). However, as mentioned by Novoa-Carballal and Müller (2012), block copolymers present several advantages compared to graft copolymers such as: (*i*) they preserve the structure of the polysaccharide (none of their lateral groups are modified) and therefore will better preserve its chemical and biological properties, and (*ii*) they allow a much greater control over nanostructure assembly than graft copolymers do. Concerning the synthesis of chitosan-PEG block copolymers, only few chemical methods were currently reported in the literature. Thus, Ganji and Abdekhodaie (2008) described the first preparation of chitosan-PEG diblock copolymers by introducing an acrylate PEG macromer onto the chitosan chain by means of a radical depolymerization process using potassium persulfate as initiator. Then, Novoa-Carballal and Müller (2012) proposed the synthesis of chitosan-PEG diblock copolymers by oxime condensation of aminooxy PEG and the reducing end of chitosan. More recently, Pickenhahn *et al.* (2017) developed a novel regioselective thioacetylation of chitosan end-groups for the synthesis of chitosan-*b*-PEG_2 block copolymers.

In this study, COS-PEG diblock copolymers **18** and **19** were synthesized according to two different end-to-end click reactions (Scheme 3). The first way was based on the CuAAC click reaction using the terminal alkyne-functionalized COS building block **5** and a commercial mPEG-azide (M_n = 2,000 g/mol). The coupling reaction was performed under similar CuAAC conditions ($CuSO_4$/sodium ascorbate) described by Guerry *et al.* (2013) leading to the diblock

copolymer **18** (M_n = 6,520 g/mol, Đ = 1.26, see Table 2) with an overall mass yield of 72% after purification. However, it worth noting that the use of copper catalyst in the synthesis of COS-PEG diblocks could be a drawback, considering that (*i*) chitosan can present a strong affinity with copper ions (Rhazi *et al.*, 2001) and (*ii*) the copper contamination in COS-based conjugates can limit their biomedical applications (Kalia and Raines, 2010). Consequently, in order to overcome this limitation, we have investigated an alternative strategy for the synthesis of COS-PEG diblock copolymers free of copper ions. Thus, the synthesis of COS-*b*-PEG **19** (M_n = 6,330 g/mol, Đ = 1.15, see Table 2) was carried out by hydrazide condensation of the COS building block **17** with a commercial mPEG-NHS ester (M_n = 2,000 g/mol) in 70% mass yield after purification (Scheme 3). In both syntheses, COS-*b*-PEG copolymers were advantageously isolated after several washings in ethanol and dialyses to remove the excess of PEG starting material. The absence of free PEG in diblock copolymer samples was observed by SEC (Figures S52 and S54, Supplementary data). Chemical structures of copolymers were confirmed by ^{1}H NMR spectroscopy which indicated the expected resonances that are distinctive for each block (Figures S51 and S53, Supplementary data). In particular, for the diblock copolymers **18**, a characteristic peak of the triazole ring proton around 8.2 ppm demonstrated the coupling reaction (Guerry *et al.*, 2013).

Table 2. Characterization data of COS-*b*-PEG copolymers **18** and **19** and their corresponding COS-based building blocks **5** and **17** (see Scheme 3).

Sample	M_w **(g/mol)** [a]	M_n **(g/mol)** [a]	**Đ** [a]
Building block **5**	4.86×10^3	4.23×10^3	1.15
COS-*b*-mPEG **18**	8.21×10^3	6.52×10^3	1.26
Building block **17**	4.41×10^3	3.94×10^3	1.12
COS-*b*-mPEG **19**	7.28×10^3	6.33×10^3	1.15

(a) weight- and number-average molar masses (M_w and M_n, respectively) and dispersity value (Đ) were determined by SEC-MALS. Molar masses results were expressed as means of ± 10%.

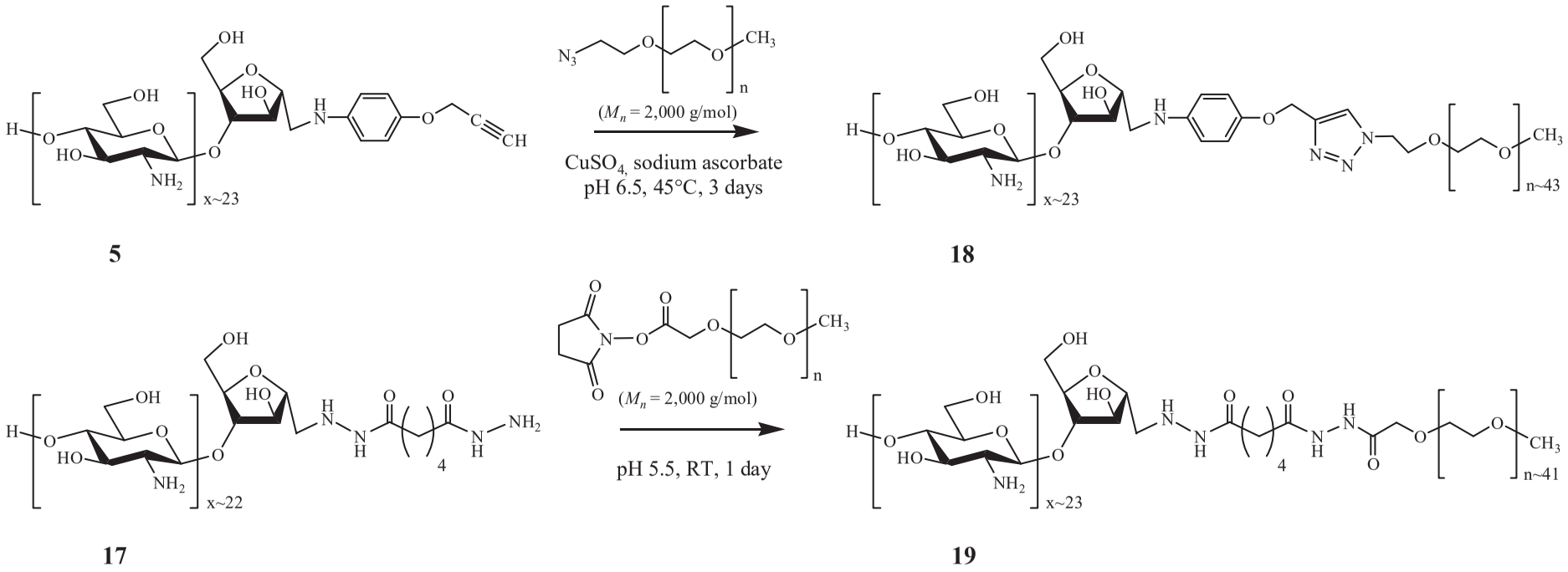

Scheme 3. Chemical syntheses of COS-*b*-PEG copolymers **18** and **19**

4. Conclusion

COSamf compounds with a well-defined average number of GlcN repeating units (x) ranging from 10 to 45 were easily synthesized by nitrous acid depolymerization of fully *N*-deacetylated chitosan. Then, the reducing-end functionalization of these COSamf was performed based on the reactivity of the aldehyde group of the amf unit. Thus, reductive amination and oximation with various "clickable" functionalized aniline, *O*-hydroxylamine and hydrazide derivatives led to expected COS-based building blocks in excellent mass yields. Building blocks were fully characterized by NMR spectroscopy and MALDI-TOF mass spectrometry. In this study, we showed that our strategy for the chemical reducing-end functionalization of chitosan oligomers is powerful and versatile. Thus, the introduction of various "clickable" chemical groups (*e.g.* alkene, alkyne, azide, hydrazide and thiol) can be quantitatively carried out from COSamf in one reaction step only. These promising results open the way for the preparation of high potential COS-based conjugates, as illustrated in this work by the synthesis of new COS-*b*-PEG diblock copolymers.

Acknowledgments

This work has benefited from the facilities and expertise of the Liquid Chromatography for Polymers and NMR platforms of the Institut de Chimie de Lyon for the structural characterization of synthesized compounds.

Appendix A. Supplementary data

Supplementary data (synthesis methods and structural characterizations by NMR spectroscopy, MALDI-TOF mass spectrometry and size-exclusion chromatography) associated with this article can be found, in the online version, at doi:https://doi.org/10.1016/j.carbpol.2019.04.078.

References

Aam, B.B., Heggset, E.B., Norberg, A.L., Sørlie, M., Vårum, K.M., & Eijsink, V.G.H. (2010). Production of chitooligosaccharides and their potential applications in medicine. *Marine Drugs*, *8*, 1482-1517.

Abla, M., Marmuse, L., Delolme, F., Vors, J.-P., Ladavière, C., & Trombotto, S. (2013). Access to tetra-N-acetyl-chitopentaose by chemical N-acetylation of glucosamine pentamer. *Carbohydrate Polymers*, *98*, 770-777.

Allan, G. G., & Peyron, M. (1989). The kinetics of the depolymerization of chitosan by nitrous acid. In G. Skjak-Bræk, T. Anthonsen, & P. Sandford (Eds), *Chitin and chitosan: sources, chemistry, biochemistry, physical-properties and applications* (pp. 443–466). Springer Netherlands.

Casettari, L., Vllasaliu, D., Castagnino, E., Stolnik, S., Howdle, S., & Illum, L. (2012). PEGylated chitosan derivatives: Synthesis, characterizations and pharmaceutical applications. *Progress in Polymer Science*, *37*, 659-685.

Das, S.N., Madhuprakasha, J., Sarma, P.V.S.R.N., Purushotham, P., Suma, K., Manjeet, K., Rambabu, S., El Gueddari, N.E., Moerschbacher, B.M., & Podile, A.R. (2015). Biotechnological approaches for field applications of chitooligosaccharides (COS) to induce innate immunity in plants. *Critical Reviews in Biotechnologies*, *35*, 29-43.

Dash, M., Chiellini, F., Ottenbrite, R.M., & Chiellini, E. (2011).Chitosan, a versatile semi-synthetic polymer in biomedical applications. *Progress in Polymer Science*, *36*, 981–1014.

Ganji, F., & Abdekhodaie, M.J. (2008). Synthesis and characterization of a new thermosensitive chitosan–PEG diblock copolymer. *Carbohydrate Polymers*, *74*, 435-441.

Guerry, A., Bernard, J., Samain, E., Fleury, E., Cottaz, S., & Halila, S. (2013). Aniline-catalyzed reductive amination as a powerful method for the preparation of reducing end-"clickable" chitooligosaccharides. *Bioconjugate Chemistry*, *24*, 544-549.

Hamed, I., Ozogul, F., & Regenstein, J.M. (2016). Industrial applications of crustacean by-products (chitin, chitosan, and chitooligosaccharides): a review. *Trends in Food Science & Technology, 48*, 40-50.

Huang, H., Jin, Y., Xue, M., Yu, L., Fu, Q., Ke, Y., Chu, C., & Liang, X. (2009). A novel click chitooligosaccharide for hydrophilic interaction liquid chromatography. *Chemical Communications*, 6973-6975.

Hussain, I., Singh, T., & Chittenden, C. (2012). Preparation of chitosan oligomers and characterization: their antifungal activities and decay resistance. *Holzforschung*, *66*, 119–125.

Illy, N., Robitzer, M., Auvergne, R., Caillol, S., David, G., & Boutevin, B. (2014). Synthesis of water-soluble allyl-functionalized oligochitosan and its modification by thiol–ene addition in water. *Journal of Polymer Science, Part A: Polymer Chemistry*, *52*, 39-48.

Kalia, J., & Raines, R. T. (2010). Advances in Bioconjugation. *Current Organic Chemistry*, *14*, 138–147.

Li, K., Xing, R., Liu, S., & Li, P. (2016). Advances in preparation, analysis and biological activities of single chitooligosaccharides. *Carbohydrate Polymers*, *139*, 178-190.

Liu, X.D., Tokura, S., Nishi, N., & Sakairi, N. (2003). A novel method for immobilization of chitosan onto nonporous glass beads through a 1,3-thiazolidine linker. *Polymer*, *44*, 1021-1026.

Liaqata, F., & Eltemb, R. (2018). Chitooligosaccharides and their biological activities: a comprehensive review. *Carbohydrate Polymers*, *184,* 243–259.

Lodhi, G., Kim, Y.S., Hwang, J.W., Kim, S.K., Jeon, Y.J., Je, J.Y., Ahn, C.B., Moon, S.H., Jeon, B.T., & Park, P.J. (2014). Chitooligosaccharide and its derivatives: preparation and biological applications. *BioMed Research International*, Article ID 654913, 13p.

Marzaioli, A.M., Bedini, E., Lanzetta, R., Perino, V., Parrilli, M., & De Castro, C. (2012). Preparation and NMR characterization of glucosamine oligomers bearing an azide function using chitosan. *Carbohydrate Polymers*, *90*, 847- 852.

Mourya, V.K., Inamdar, N.N., & Choudhari, Y.M. (2011). Chitooligosaccharides: synthesis, characterization and applications. *Polymer Science Series A*, *53*, 583-612.

Moussa, A., & Trombotto, S. (2016). Octanoic Hydrazide-Linked Chitooligosaccharides-2,5-anhydro-D-mannofuranose. *Molbank*, M904.

Novoa-Carballal, R., & Müller, A.H.E. (2012). Synthesis of polysaccharide-*b*-PEG block copolymers by oxime click, *Chemical Communications*, *48*, 3781-3783.

Pickenhahn, V.D., Darras, V., Dziopa, F., Biniecki, K., De Crescenzo, G., Lavertu, M., & Buschmann, M.D. (2015). Regioselective thioacetylation of chitosan end groups for nanoparticle gene delivery systems. *Chemical Science*, *6*, 4650-4664.

Pickenhahn, V.D., Grange, M., De Crescenzo, G., Lavertu M., & Buschmann M.D. (2017). Regioselective chitosan end-group activation: the triskelion approach. *RSC Advances*, *7*, 18628-18638.

Rhazi, M., Tolaimate, A., Desbrieres, J., Rinaudo, M., Alagui, A., & Vottero, P. (2001). Contribution to the study of the complexation of copper by chitosan and oligomers. *Polymer*, *43*, 1267-1276.

Salim, E., Ailincai, D., & Trombotto, S. (2014). Chitooligosaccharide-2,5-anhydro-D-mannonic Acid. *Molbank*, M832.

Salim, E., Galais, A., & Trombotto, S. (2014). 4-(Hexyloxy) aniline-linked chitooligosaccharide-2,5–anhydro-D- mannofuranose. *Molbank*, M815.

Strand, S.P., Issa, M.M., Christensen, B.E., Vårum, K.M., & Artursson, P. (2008). Tailoring of chitosans for gene delivery: novel self-branched glycosylated chitosan oligomers with improved functional properties. *Biomacromolecules*, 9, 3268-3276.

Tømmeraas, K., Vårum, K.M., Christensen, B.M., & Smidsrød, O. (2001). Preparation and characterisation of oligosaccharides produced by nitrous acid depolymerization of chitosans. *Carbohydrate Research*, *333*, 137-144.

Tømmeraas, K., Strand, S.P., Christensen, B.E., Smidsrød, O., & Vårum, K.M. (2011). Preparation and characterization of branched chitosans. *Carbohydrate Polymers*, *83*, 1558-1564.

Xia, W., Liu, P., Zhang, J., & Chen, J. (2011). Biological activities of chitosan and chitooligosaccharides. *Food Hydrocolloids*, *25*, 170-179.

Yang, Y., & Yu, B. (2014). Recent advances in the synthesis of chitooligosaccharides and congeners. *Tetrahedron*, *70*, 1023-1046.

Yeul, V.S., & Rayalu, S.S. (2013). Unprecedented chitin and chitosan: a chemical overview. *Journal of Polymers and the Environment, 21*, 606–614.

Younes, I., & Rinaudo, M. (2015). Chitin and chitosan preparation from marine sources. Structure, properties and applications. *Marine Drugs*, *13*, 1133-1174.

General conclusions

This multidisciplinary study was guided in an aim to synthesis well controlled/modified structure of chitooligosaccharides in order to decipher their physico-chemical or biological properties. Several key concepts could be validated and show that chitooligosaccharides form a good candidate for widely different applications, such as:

- ***First:*** The tissue engeneering of neuronal cells: Screening for the use of well controlled chitooligosaccharides for an application in nervous tissue regeneration: cytotoxicity analyses.
- ***Second:*** The preparation of functionalised ultra-small superparamagnetic nanoparticles exhibiting high saturation magnetization.
- ***Third:*** The development of advanced functional COS-based conjugates.

In order to better explain the effect of chitooligosaccharides on each application, the synthesis of chitooligosaccharides structure was performed in control maner. Such as, our strategy was based on the synthesis of chitooligosaccharides with a well-defined average number of GlcN repeating units (DP) by means of nitrous acid depolymerization of fully *N*-deacetylated chitosan. Different techniques were demonstrated in bibliographic research to synthesis chitooligosaccharides. However, the nitrous acid depolymerization has advantages over others since it is considered fast, not highly costed and could be performed in aqueous medium under mild conditions and most importantly allow the extent of depolymerization to be controlled through the stoichiometry of reaction. A gram scale quantity of chitooligosaccharides with different degree of polymerization from 10, 24 and 45 were obtained and modified in two ways.

The first type of modification was vi*a* amine *N*-substitution. Such as, the *N*-acetylation reaction of the free amino groups was performed by using acetic anhydride (Ac_2O) as an acetylating agent at room temperature. This reaction was carried out in a manner to control the number of GlcNAc units along the oligomer chain. In addition, it offers advantage due to facilty and low cost. The *N*-acetylation reaction had a direct impact on the solubility of chitosan which highly depends on the DA. These synthesized oligomers used below in two fields are quit stable, since the base shift reaction was prohibite as the reducing-end was reduced.

- ***First:*** Usually, recovery after a lesion in perineuronal nets (PNNs) in the central nervous system fails due to endogenous axon regeneration inhibitors such as chondroitin sulfate proteoglycans (CSPGs) that accumulate at the injury sites. Although some therapeutic interventions including the enzymatic digestion by using chondroitinase ABC (ChABC) that degrades CSPGs, restore plasticity and recover spinal cord injury in adult animals [189], problems are encountered due to the prolongs enzymatic activity that leads to a complete digestion of CSPGs [190]. Recently it was published that chitosan implantation can repair spinal tissue without being combined with other therapeutic agents. At the same time, it provides major advantages, as it is safe, does not provoke immune reactions in the host tissue, and does not pose any ethical concerns for its use in humans [195]. Hence the screening of different COS with different DP and DA was performed to test their capability in modulating the perineuronal net of neurons and synaptic effect. The obtained results are primary however promising. The obtained results should be repeated by taking into consideration the concentration effect. Such as, when performing the experiments, we have used a millimolar concentration for all the tested chitooligosaccharides. But, the oligomers are different in DP, implies that the mass concentration is not constant. Despite the concentration debate and based on the obtained preliminary results, we concluded, that all chitooligosaccharides are inhibiting PNN formation. Moreover promising results were obtained for specific oligomers, these results should be taken into consideration for future development.
- ***Second:*** Very small particles are ideal for biological applications however; they have high surface energy resulting from their large surface-volume ratio. This effect can induce to nanoparticles aggregation [211]. In order to avoid this effect, the MNPs are typically coated to promote their colloidal stability, water dispersibility and also provide biochemical functionality with the addition of bioactive molecules [202, 208, 216]. To this end, we proposed the use of chitooligosaccharides as complexing agents to assist the synthesis of magnetite nanoparticles. Hence a simple co-precipitation method has been developed for *in-situ* preparation of COS coated magnetic Fe_3O_4 nanoparticles through a mixing of iron ions (Fe^{3+} and Fe^{2+}) and COS aqueous solutions followed by precipitation with ammonia, at 60 °C. The impact of COS with DA~50 % (exhibiting high solubility) and different DPs (DP 10 and 24) was evaluated on the synthesis and behaviours of coated nanoparticles. The results showed that Fe_3O_4 NPs were well encapsulated by COSs, $COS_{10/53}$ and $COS_{24/47}$, without changing

the spinal structure of Fe_3O_4 NPs. Fe_3O_4 NPs coated by COS presented a more ordered crystalline structure than pure Fe_3O_4, especially in the case of the sample Fe_3O_4:$COS_{24/47}$. TGA analysis permitted to estimate a lower organic content in the Fe_3O_4:$COS_{10/53}$ (12.8 %) than in the Fe_3O_4:$COS_{24/47}$ (16.6 %). TEM analysis revealed that COS layer did not change significantly the size of the nanoparticles and all of synthesized nanoparticles have a mean size close to 6 nm. The COS coated nanoparticles showed a nearly spherical morphology with a narrower size distribution than pure Fe_3O_4 MNPs. VSM results indicated superparamagnetic nature with negligible coercivity (H_c) and remanence (M_r). The COS coated Fe_3O_4 MNPs showed higher saturation magnetization (Fe_3O_4:$COS_{10/53}$ = 60.6 emu.g^{-1} and Fe_3O_4:$COS_{24/47}$ = 59.8 emu.g^{-1}) than the control sample, Fe_3O_4 NPs (28.3 emu.g^{-1}). The calculated magnetic diameters (D_m) were in agreement with the apparent diameter. Moreover, a cytotoxicity study on canine fibroblasts showed an increase of cell viability for COS coated nanoparticles in comparison with pure Fe_3O_4 MNPs, with concentration dependence. To better explain the effect of the COS structure on the magnetic core other analyses are necessary, such as the internalization of NPs by the cells.

In addition, as a part of our investigations about the preparation of functionalized chitosan oligomer derivatives, the bibliographic study showed that new or improved properties of COS can be obtained by grafting various functional groups to COS backbone due to the existence of reactive hydroxyl and amino groups. Recently, importance has been given to synthesize functionalized COS by chemical modifications with the aim to improve the bioactivities of COS, while keeping intact the basic chemical properties. More studies could be found dealing with the synthesis of modified COS via *N*-substitution, less often through *O*-substitution and rarely through the aldehyde function of reducing-end units. Specifically, the reducing-end functionalization of COS has attracted our attention since it could preserve both the chemical nature of COS backbones and the inherent bioactivities of COS.

Thus, for **the second type of modification** we reported the synthesis of new COS-based building blocks functionalized at their reducing ends with various “clickable” chemical groups, such as alkene, alkyne, azide, hydrazide and thiol. Reducing-end derivatizations were performed by reaction of the COSamf aldehyde group with the amine group of anilines, hydrazides and *O*-hydroxylamines bearing different “clickable” groups. Note that the use of various reaction conditions (different temperature, time reaction and different equivalence of

added chemical groups) were testd and obtimized, in order to insure the success and complete condensations of COSamf with functionalized amine derivatives.

- ***Third:*** To illustrate the potential of these COS-based building blocks for the development of functional COS-based conjugates, we further investigated the synthesis of COS-PEG diblock copolymers. Specfically, in the first way we proposed to synthesis COS-PEG diblock copolymers based on the CuAAC click reaction using the terminal alkyne-functionalized COS building block and a commercial mPEG-azide. The coupling reaction was performed under similar CuAAC conditions ($CuSO_4$/sodium ascorbate) described by Guerry *et al.*[154] leading to the diblock copolymer with an overall mass yield of 72% after purification. However, it worth noting that the use of copper catalyst in the synthesis of COS-PEG diblocks could be a drawback, considering that (*i*) chitosan can present a strong affinity with copper ions [261] and (*ii*) the copper contamination in COS-based conjugates can limit their biomedical applications [262]. Consequently, in order to overcome this limitation, we have investigated another way for the synthesis of COS-PEG diblock copolymers free of copper ions. Thus, the synthesis of COS-*b*-PEG was carried out by hydrazide condensation of the COS building block with a commercial mPEG-NHS ester in 70% mass yield after purification. Chemical structures of copolymers were confirmed by ^{1}H NMR spectroscopy which indicated the expected resonances that are distinctive for each block

References

[1] Mourya VK, Inamdar NN, Choudhari YM. Chitooligosaccharides: Synthesis, characterization and applications. *Polymer Science Series A* **2011**;53:583-612.

[2] Rinaudo M. Chitin and chitosan: Properties and applications. *Progress in Polymer Science* **2006**;31:603-32.

[3] Domard A, Domard M. Chitosan: Structure-properties relationship and biomedical applications2001.

[4] Ramírez MÁ, Rodríguez AT, Alfonso L, Peniche C. Chitin and its derivatives as biopolymers with potential agricultural applications. *Biotecnología Aplicada* **2010**;27:270-6.

[5] Sorlier P, Denuzière A, Viton C, Domard A. Relation between the Degree of Acetylation and the Electrostatic Properties of Chitin and Chitosan. *Biomacromolecules* **2001**;2:765-72.

[6] Sorlier P, Viton C, Domard A. Relation between Solution Properties and Degree of Acetylation of Chitosan: Role of Aging. *Biomacromolecules* **2002**;3:1336-42.

[7] Boucard N, David L, Rochas C, Montembault A, Viton C, Domard A. Polyelectrolyte Microstructure in Chitosan Aqueous and Alcohol Solutions. *Biomacromolecules* **2007**;8:1209-17.

[8] Younes I, Rinaudo M. Chitin and Chitosan Preparation from Marine Sources. Structure, Properties and Applications. *Marine Drugs* **2015**;13:1133.

[9] Xia W, Liu P, Zhang J, Chen J. Biological activities of chitosan and chitooligosaccharides. *Food Hydrocolloids* **2011**;25:170-9.

[10] Das SN, Madhuprakash J, Sarma PVSRN, Purushotham P, Suma K, Manjeet K, et al. Biotechnological approaches for field applications of chitooligosaccharides (COS) to induce innate immunity in plants. *Critical Reviews in Biotechnology* **2015**;35:29-43.

[11] Tømmeraas K, Strand SP, Christensen BE, Smidsrød O, Vårum KM. Preparation and characterization of branched chitosans. *Carbohydrate Polymers* **2011**;83:1558-64.

[12] Qin C, Gao J, Wang L, Zeng L, Liu Y. Safety evaluation of short-term exposure to chitooligomers from enzymic preparation. *Food and Chemical Toxicology* **2006**;44:855-61.

[13] Rajapakse N, Kim M-M, Mendis E, Huang R, Kim S-K. Carboxylated chitooligosaccharides (CCOS) inhibit MMP-9 expression in human fibrosarcoma cells via down-regulation of AP-1. *Biochimica et Biophysica Acta (BBA) - General Subjects* **2006**;1760:1780-8.

[14] de Assis CF, Costa LS, Melo-Silveira RF, Oliveira RM, Pagnoncelli MGB, Rocha HAO, et al. Chitooligosaccharides antagonize the cytotoxic effect of glucosamine. *World Journal of Microbiology and Biotechnology* **2012**;28:1097-105.

[15] Avadi MR, Sadeghi AMM, Tahzibi A, Bayati K, Pouladzadeh M, Zohuriaan-Mehr MJ, et al. Diethylmethyl chitosan as an antimicrobial agent: Synthesis, characterization and antibacterial effects. *European Polymer Journal* **2004**;40:1355-61.

[16] Benhabiles MS, Salah R, Lounici H, Drouiche N, Goosen MFA, Mameri N. Antibacterial activity of chitin, chitosan and its oligomers prepared from shrimp shell waste. *Food Hydrocolloids* **2012**;29:48-56.

[17] Wang Y, Zhou P, Yu J, Pan X, Wang P, Lan W, et al. Antimicrobial effect of chitooligosaccharides produced by chitosanase from Pseudomonas CUY82007.

[18] Ueno K, Yamaguchi T, Sakairi N, Nishi N, Tokura S. Antimicrobial activity by fractionated chitosan oligomers. *Advances in Chitin Science* **1997**;2:156-61.

[19] Tayel AA, Moussa S, Opwis K, Knittel D, Schollmeyer E, Nickisch-Hartfiel A. Inhibition of microbial pathogens by fungal chitosan. *International Journal of Biological Macromolecules* **2010**;47:10-4.

[20] Li K, Xing R, Liu S, Qin Y, Yu H, Li P. Size and pH effects of chitooligomers on antibacterial activity against Staphylococcus aureus. *International Journal of Biological Macromolecules* **2014**;64:302-5.

[21] Hosseinnejad M, Jafari SM. Evaluation of different factors affecting antimicrobial properties of chitosan. *International Journal of Biological Macromolecules* **2016**;85:467-75.

[22] Choi B-K, Kim K-Y, Yoo Y-J, Oh S-J, Choi J-H, Kim C-Y. In vitro antimicrobial activity of a chitooligosaccharide mixture against Actinobacillusactinomycetemcomitans and Streptococcus mutans. *International Journal of Antimicrobial Agents* **2001**;18:553-7.

[23] Kim JY, Lee JK, Lee TS, Park WH. Synthesis of chitooligosaccharide derivative with quaternary ammonium group and its antimicrobial activity against Streptococcus mutans. *International Journal of Biological Macromolecules* **2003**;32:23-7.

[24] Li Z, Yang F, Yang R. Synthesis and characterization of chitosan derivatives with dual-antibacterial functional groups. *International Journal of Biological Macromolecules* **2015**;75:378-87.

[25] Oliveira EN, El Gueddari NE, Moerschbacher BM, Peter MG, Franco TT. Growth of Phytopathogenic Fungi in the Presence of Partially Acetylated Chitooligosaccharides. *Mycopathologia* **2008**;166:163-74.

[26] Kendra DF, Hadwiger LA. Characterization of the smallest chitosan oligomer that is maximally antifungal toFusarium solani and elicits pisatin formation inPisum sativum. *Experimental Mycology* **1984**;8:276-81.

[27] Wang Q, Zuo J-h, Wang Q, Na Y, Gao L-p. Inhibitory effect of chitosan on growth of the fungal phytopathogen, Sclerotinia sclerotiorum, and sclerotinia rot of carrot. *Journal of Integrative Agriculture* **2015**;14:691-7.

[28] Masuda S, Azuma K, Kurozumi S, Kiyose M, Osaki T, Tsuka T, et al. Anti-tumor properties of orally administered glucosamine and N-acetyl-d-glucosamine oligomers in a mouse model. *Carbohydrate Polymers* **2014**;111:783-7.

[29] Wu H, Aam BB, Wang W, Norberg AL, Sørlie M, Eijsink VGH, et al. Inhibition of angiogenesis by chitooligosaccharides with specific degrees of acetylation and polymerization. *Carbohydrate Polymers* **2012**;89:511-8.

[30] Liang T-W, Chen Y-J, Yen Y-H, Wang S-L. The antitumor activity of the hydrolysates of chitinous materials hydrolyzed by crude enzyme from Bacillus amyloliquefaciens V656. *Process Biochemistry* **2007**;42:527-34.

[31] Suzuki K, Mikami T, Okawa Y, Tokoro A, Suzuki S, Suzuki M. Antitumor effect of hexa-N-acetylchitohexaose and chitohexaose. *Carbohydrate Research* **1986**;151:403-8.

[32] Mattaveewong T, Wongkrasant P, Chanchai S, Pichyangkura R, Chatsudthipong V, Muanprasat C. Chitosan oligosaccharide suppresses tumor progression in a mouse model of colitis-associated colorectal cancer through AMPK activation and suppression of NF-κB and mTOR signaling. *Carbohydrate Polymers* **2016**;145:30-6.

[33] Zou P, Yuan S, Yang X, Zhai X, Wang J. Chitosan oligosaccharides with degree of polymerization 2–6 induces apoptosis in human colon carcinoma HCT116 cells. *Chemico-Biological Interactions* **2018**;279:129-35.

[34] Jeon YJ, Kim SK. Antitumor activity of chitosan oligosaccharides produced in ultrafiltration membrane reactor system2002.

[35] Day RB, Shibuya N, Minami E. Identification and characterization of two new members of the GRAS gene family in rice responsive to N-acetylchitooligosaccharide elicitor. *Biochimica et Biophysica Acta (BBA) - Gene Structure and Expression* **2003**;1625:261-8.

[36] Keen NT. Specific Elicitors of Plant Phytoalexin Production: Detenninants of Race Specificity in Pathogens? *Science* **1975**;187:74-5.

[37] McDowell JM, Dangl JL. Signal transduction in the plant immune response. *Trends in Biochemical Sciences* **2000**;25:79-82.

[38] A Hadwiger L, Ogawa T, Kuyama H. Chitosan polymer sizes effective in inducing phytoalexin accumulation and fungal suppression are verified with synthesized oligomers1993.

[39] de Jonge R, Peter van Esse H, Kombrink A, Shinya T, Desaki Y, Bours R, et al. Conserved Fungal LysM Effector Ecp6 Prevents Chitin-Triggered Immunity in Plants. *Science* **2010**;329:953-5.

[40] Akiyama K, Kawazu K, Kobayashi A. A novel method for chemo-enzymatic synthesis of elicitor-active chitosan oligomers and partially N-deacetylated chitin oligomers using N-acylated chitotrioses as substrates in a lysozyme-catalyzed transglycosylation reaction system. *Carbohydrate Research* **1995**;279:151-60.

[41] Carlos CJ, Johan M, Pierre C, Pierre VC. Size, acetylation and concentration of chitooligosaccharide elicitors determine the switch from defence involving PAL activation to cell death and water peroxide production in Arabidopsis cell suspensions. *Physiologia Plantarum* **2006**;127:44-56.

[42] Vander P, Vårum KM, Domard A, Eddine El Gueddari N, Moerschbacher BM. Comparison of the Ability of Partially N-Acetylated Chitosans and Chitooligosaccharides to Elicit Resistance Reactions in Wheat Leaves. *Plant Physiology* **1998**;118:1353-9.

[43] Park P-J, Je J-Y, Kim S-K. Angiotensin I Converting Enzyme (ACE) Inhibitory Activity of Hetero-Chitooligosaccharides Prepared from Partially Different Deacetylated Chitosans. *Journal of Agricultural and Food Chemistry* **2003**;51:4930-4.

[44] Leanderson P, Faresjö ÅO, Tagesson C. Green Tea Polyphenols Inhibit Oxidant-Induced DNA Strand Breakage in Cultured Lung Cells. *Free Radical Biology and Medicine* **1997**;23:235-42.

[45] Zhao D, Wang J, Tan L, Sun C, Dong J. Synthesis of N-furoyl chitosan and chito-oligosaccharides and evaluation of their antioxidant activity in vitro. *International Journal of Biological Macromolecules* **2013**;59:391-5.

[46] Li K, Liu S, Xing R, Qin Y, Li P. Preparation, characterization and antioxidant activity of two partially N-acetylated chitotrioses. *Carbohydrate Polymers* **2013**;92:1730-6.

[47] Chen A-S, Taguchi T, Sakai K, Kikuchi K, Wang M-W, Miwa I. Antioxidant Activities of Chitobiose and Chitotriose. *Biological and Pharmaceutical Bulletin* **2003**;26:1326-30.

[48] Li K, Xing R, Liu S, Li R, Qin Y, Meng X, et al. Separation of chito-oligomers with several degrees of polymerization and study of their antioxidant activity. *Carbohydrate Polymers* **2012**;88:896-903.

[49] dos Santos ALW, El Gueddari NE, Trombotto S, Moerschbacher BM. Partially Acetylated Chitosan Oligo- and Polymers Induce an Oxidative Burst in Suspension Cultured Cells of the Gymnosperm Araucaria angustifolia. *Biomacromolecules* **2008**;9:3411-5.

[50] Vo T-S, Ngo D-H, Bach LG, Ngo D-N, Kim S-K. The free radical scavenging and anti-inflammatory activities of gallate-chitooligosaccharides in human lung epithelial A549 cells. *Process Biochemistry* **2017**;54:188-94.

[51] Liang T-W, Chen W-T, Lin Z-H, Kuo Y-H, Dzung N, Wang S-L. An Amphiprotic Novel Chitosanase from Bacillus mycoides and Its Application in the Production of Chitooligomers with Their Antioxidant and Anti-Inflammatory Evaluation2016.

[52] Vo T-S, Kong C-S, Kim S-K. Inhibitory effects of chitooligosaccharides on degranulation and cytokine generation in rat basophilic leukemia RBL-2H3 cells. *Carbohydrate Polymers* **2011**;84:649-55.

[53] Yousef M, Pichyangkura R, Soodvilai S, Chatsudthipong V, Muanprasat C. Chitosan oligosaccharide as potential therapy of inflammatory bowel disease: Therapeutic efficacy and possible mechanisms of action. *Pharmacological Research* **2012**;66:66-79.

[54] Durán WN, Breslin JW, Sánchez FA. The NO cascade, eNOS location, and microvascular permeability. *Cardiovascular research* **2010**;87:254-61.

[55] Mei Y-x, Chen H-x, Zhang J, Zhang X-d, Liang Y-x. Protective effect of chitooligosaccharides against cyclophosphamide-induced immunosuppression in mice. *International Journal of Biological Macromolecules* **2013**;62:330-5.

[56] Zhang P, Liu W, Peng Y, Han B, Yang Y. Toll like receptor 4 (TLR4) mediates the stimulating activities of chitosan oligosaccharide on macrophages. *International Immunopharmacology* **2014**;23:254-61.

[57] M Kochkina Z, Chirkov S. [Effect of chitosan derivatives on the development of phage infection in cultured Bacillus thuringiensis]2000.

[58] Kochkina ZM, Chirkov SN. Influence of chitosan derivatives on the development of phage infection in theBacillus thuringiensis culture. *Microbiology* **2000**;69:217-9.

[59] Kim S-K, Rajapakse N. Enzymatic production and biological activities of chitosan oligosaccharides (COS): A review. *Carbohydrate Polymers* **2005**;62:357-68.

[60] Aam BB, Heggset EB, Norberg AL, Sørlie M, Vårum KM, Eijsink VG. Production of chitooligosaccharides and their potential applications in medicine. *Marine drugs* **2010**;8:1482-517.

[61] Zong H, Li K, Liu S, Song L, Xing R, Chen X, et al. Improvement in cadmium tolerance of edible rape (Brassica rapa L.) with exogenous application of chitooligosaccharide. *Chemosphere* **2017**;181:92-100.

[62] Xinyi XWZFH. Antimicrobial of Chitooligosaccharides and its Application to Food Preservation [J]. *JOURNAL OF WUXI UNIVERSITY OF LIGHT INDUSTRY* **1998**;4.

[63] Kim S-K, Kong C-S, Soon-Sun B, Kim J-A, Byul-Nim A. Cosmetic composition for preventing skin aging containing chitooligosaccharides. Google Patents; 2013.

[64] Muraki E. Partially N-acylated compound of chitooligosaccharide, salt thereof, and use thereof. Google Patents; 1997.

[65] J Tsai G, Y Wu Z, H Su W. Antibacterial Activity of a Chitooligosaccharide Mixture Prepared by Cellulase Digestion of Shrimp Chitosan and Its Application to Milk Preservation2000.

[66] Fan Fang L. Application of chitosan oligosaccharide in processing of individual quick frozen fish fillet CN1965706 (A) 2007-05-23.

[67] Seong HS, Kim JP, Ko W-S. Preparing Chito-Oligosaccharides as Antimicrobial Agents for Cotton1999.

[68] Seong H-S, Ko S-W, Song K-G. Antimicrobial Finish of Cotton Fabric with Chito-oligosaccharide (II)-Treatment on to Cotton Fabric by BTCA. *JOURNAL-KOREAN FIBER SOCIETY* **1998**;35:716-20.

[69] Hamed I, Özogul F, Regenstein JM. Industrial applications of crustacean by-products (chitin, chitosan, and chitooligosaccharides): A review. *Trends in Food Science & Technology* **2016**;48:40-50.

[70] Zhao X, Liu D, Yao K. Chitose composition for promoting medicine transfer through skin penetration and its use method CN1686559 (A)2005-10-26. **2005**.

[71] Ai Hui L, . Blood fat-lowering chewing tablet of housefly larvae chitooligosaccharides and method for making same CN1883306 (A) 2006-12-27 **2006**.

[72] Wang L. Application of water soluble chitosan in toothpaste and mouthwash CN1969801 (A) 2007-05-30 **2007**.

[73] Osorio-Madrazo A, David L, Trombotto S, Lucas J-M, Peniche-Covas C, Domard A. Kinetics Study of the Solid-State Acid Hydrolysis of Chitosan: Evolution of the Crystallinity and Macromolecular Structure. *Biomacromolecules* **2010**;11:1376-86.

[74] Vårum KM, Ottøy MH, Smidsrød O. Acid hydrolysis of chitosans. *Carbohydrate Polymers* **2001**;46:89-98.

[75] Horowitz ST, Roseman S, Blumenthal HJ. The Preparation of Glucosamine Oligosaccharides. I. Separation1,2. *Journal of the American Chemical Society* **1957**;79:5046-9.

[76] Trombotto S, Ladaviere C, Delolme F, Domard A. Chemical Preparation and Structural Characterization of a Homogeneous Series of Chitin/Chitosan Oligomers2008.

[77] Domard A, Cartier N. Glucosamine oligomers: 1. Preparation and characterization. *International Journal of Biological Macromolecules* **1989**;11:297-302.

[78] Jia Z, Shen D. Effect of reaction temperature and reaction time on the preparation of low-molecular-weight chitosan using phosphoric acid. *Carbohydrate Polymers* **2002**;49:393-6.

[79] Hasegawa M, Isogai A, Onabe F. Preparation of low-molecular-weight chitosan using phosphoric acid. *Carbohydrate Polymers* **1993**;20:279-83.

[80] Defaye J, Gadelle A, Pedersen C. A convenient access to β-(1 → 4)-linked 2-amino-2-deoxy-d-glucopyranosyl fluoride oligosaccharides and β-(1 → 4)-linked 2-amino-2-deoxy-d-glucopyranosyl oligosaccharides by fluorolysis and fluorohydrolysis of chitosan. *Carbohydrate Research* **1994**;261:267-77.

[81] Inaba T, Ohgushi T, Iga Y, Hasegawa E. Synthesis of 4-methylcoumarin-7-yloxy tetra-N-acetyl-.BETA.-chitotetraoside, a novel synthetic substrate for the fluorometric assay of lysozyme1984.

[82] Il'ina AV, Varlamov VP. Hydrolysis of Chitosan in Lactic Acid. *Applied Biochemistry and Microbiology* **2004**;40:300-3.

[83] Tømmeraas K, Vårum KM, Christensen BE, Smidsrød O. Preparation and characterisation of oligosaccharides produced by nitrous acid depolymerisation of chitosans. *Carbohydrate Research* **2001**;333:137-44.

[84] Bosso C, Defaye J, Domard A, Gadelle A, Pedersen C. The behavior of chitin towards anhydrous hydrogen fluoride. Preparation of β-(1→4)-linked 2-acetamido-2-deoxy-d-glucopyranosyl oligosaccharides. *Carbohydrate Research* **1986**;156:57-68.

[85] Hirano S, Kondo Y, Fujii K. Preparation of acetylated derivatives of modified chito-oligosaccharides by the depolymerisation of partially N-acetylated chitosan with nitrous acid. *Carbohydrate Research* **1985**;144:338-41.

[86] Allan GG, Peyron M. Molecular weight manipulation of chitosan II: prediction and control of extent of depolymerization by nitrous acid. *Carbohydrate Research* **1995**;277:273-82.

[87] Allan GG, Peyron M. Molecular weight manipulation of chitosan I: kinetics of depolymerization by nitrous acid. *Carbohydrate Research* **1995**;277:257-72.

[88] Einbu A, Grasdalen H, Vårum KM. Kinetics of hydrolysis of chitin/chitosan oligomers in concentrated hydrochloric acid. *Carbohydrate Research* **2007**;342:1055-62.

[89] Xia Z, Wu S, Chen J. Preparation of water soluble chitosan by hydrolysis using hydrogen peroxide. *International Journal of Biological Macromolecules* **2013**;59:242-5.

[90] Chang KLB, Tai M-C, Cheng F-H. Kinetics and Products of the Degradation of Chitosan by Hydrogen Peroxide. *Journal of Agricultural and Food Chemistry* **2001**;49:4845-51.

[91] Liaqat F, Eltem R. Chitooligosaccharides and their biological activities: A comprehensive review. *Carbohydrate Polymers* **2018**;184:243-59.

[92] Khoushab F, Yamabhai M. Chitin Research Revisited. *Marine Drugs* **2010**;8:1988.

[93] Aiba S-i. Preparation of N-acetylchitooligosaccharides by hydrolysis of chitosan with chitinase followed by N-acetylation. *Carbohydrate Research* **1994**;265:323-8.

[94] Usui T, Matsui H, Isobe K. Enzymic synthesis of useful chito-oligosaccharides utilizing transglycosylation by chitinolytic enzymes in a buffer containing ammonium sulfate. *Carbohydrate Research* **1990**;203:65-77.

[95] Wang S-L, Liu C-P, Liang T-W. Fermented and enzymatic production of chitin/chitosan oligosaccharides by extracellular chitinases from Bacillus cereus TKU027. *Carbohydrate Polymers* **2012**;90:1305-13.

[96] Mitsutomi M, Hata T, Kuwahara T. Purification and characterization of novel chitinases from Streptomyces griseus HUT 6037. *Journal of Fermentation and Bioengineering* **1995**;80:153-8.

[97] Tanabe T, Kawase T, Watanabe T, Uchida Y, Mitsutomi M. Purification and characterization of a 49-kDa chitinase from Streptomyces griseus HUT 6037. *Journal of Bioscience and Bioengineering* **2000**;89:27-32.

[98] Gao X-A, Ju W-T, Jung W-J, Park R-D. Purification and characterization of chitosanase from Bacillus cereus D-11. *Carbohydrate Polymers* **2008**;72:513-20.

[99] Somashekar D, Joseph R. Chitosanases — properties and applications: A review. *Bioresource Technology* **1996**;55:35-45.

[100] Thadathil N, Velappan SP. Recent developments in chitosanase research and its biotechnological applications: A review. *Food Chemistry* **2014**;150:392-9.

[101] Vårum KM, Kristiansen Holme H, Izume M, Torger Stokke B, Smidsrød O. Determination of enzymatic hydrolysis specificity of partially N-acetylated chitosans. *Biochimica et Biophysica Acta (BBA) - General Subjects* **1996**;1291:5-15.

[102] Monaghan RL, Eveleigh DE, Tewari RP, Reese ET. Chitosanase, a novel enzyme. *Nat New Biol* **1973**;245:78-80.

[103] Yang Y, Yu B. Recent advances in the synthesis of chitooligosaccharides and congeners. *Tetrahedron* **2014**;70:1023-46.

[104] Nordtveit RJ, Vårum KM, Smidsrød O. Degradation of partially N-acetylated chitosans with hen egg white and human lysozyme. *Carbohydrate Polymers* **1996**;29:163-7.

[105] Nordtveit RJ, Vårum KM, Smidsrød O. Degradation of fully water-soluble, partially N-acetylated chitosans with lysozyme. *Carbohydrate Polymers* **1994**;23:253-60.

[106] Verheul RJ, Amidi M, van Steenbergen MJ, van Riet E, Jiskoot W, Hennink WE. Influence of the degree of acetylation on the enzymatic degradation and in vitro biological properties of trimethylated chitosans. *Biomaterials* **2009**;30:3129-35.

[107] Zhang H, Du Y, Yu X, Mitsutomi M, Aiba S-i. Preparation of chitooligosaccharides from chitosan by a complex enzyme. *Carbohydrate Research* **1999**;320:257-60.

[108] Xie Y, Hu J, Wei Y, Hong X. Preparation of chitooligosaccharides by the enzymatic hydrolysis of chitosan. *Polymer Degradation and Stability* **2009**;94:1895-9.

[109] Qin C, Du Y, Xiao L, Li Z, Gao X. Enzymic preparation of water-soluble chitosan and their antitumor activity. *International Journal of Biological Macromolecules* **2002**;31:111-7.

[110] Muzzarelli RAA, Xia W, Tomasetti M, Ilari P. Depolymerization of chitosan and substituted chitosans with the aid of a wheat germ lipase preparation. *Enzyme and Microbial Technology* **1995**;17:541-5.

[111] Muzzarelli RAA, Tomasetti M, Ilari P. Deploymerization of chitosan with the aid of papain. *Enzyme and Microbial Technology* **1994**;16:110-4.

[112] Hai L, Bang Diep T, Nagasawa N, Yoshii F, Kume T. Radiation depolymerization of chitosan to prepare oligomers. *Nuclear Instruments and Methods in Physics Research Section B: Beam Interactions with Materials and Atoms* **2003**;208:466-70.

[113] Choi W-S, Ahn K-J, Lee D-W, Byun M-W, Park H-J. Preparation of chitosan oligomers by irradiation. *Polymer Degradation and Stability* **2002**;78:533-8.

[114] Xing R, Liu S, Yu H, Guo Z, Wang P, Li C, et al. Salt-assisted acid hydrolysis of chitosan to oligomers under microwave irradiation. *Carbohydrate Research* **2005**;340:2150-3.

[115] Tahtat D, Mahlous M, Benamer S, Nacer Khodja A, Larbi Youcef S. Effect of molecular weight on radiation chemical degradation yield of chain scission of γ-irradiated chitosan in solid state and in aqueous solution. *Radiation Physics and Chemistry* **2012**;81:659-65.

[116] San Juan A, Montembault A, Gillet D, Say JP, Rouif S, Bouet T, et al. Degradation of chitosan-based materials after different sterilization treatments2012.

[117] Chen RH, Chen JS. Changes of polydispersity and limiting molecular weight of ultrasound-treated chitosan. *Advances in Chitin Science* **2000**;4:361-6.

[118] Popa-Nita S, Lucas J-M, Ladavière C, David L, Domard A. Mechanisms Involved During the Ultrasonically Induced Depolymerization of Chitosan: Characterization and Control. *Biomacromolecules* **2009**;10:1203-11.

[119] Tokuyasu K, Ono H, Hayashi K, Mori Y. Reverse hydrolysis reaction of chitin deacetylase and enzymatic synthesis of β-d-GlcNAc-(1→4)-GlcN from chitobiose. *Carbohydrate Research* **1999**;322:26-31.

[120] Tokuyasu K, Ono H, Ohnishi-Kameyama M, Hayashi K, Mori Y. Deacetylation of chitin oligosaccharides of dp 2–4 by chitin deacetylase from Colletotrichum lindemuthianum. *Carbohydrate Research* **1997**;303:353-8.

[121] Samain E, Priem B. Method for producing oligopolysaccharides. Google Patents; 2013.

[122] Samain E, Drouillard S, Heyraud A, Driguez H, Geremia RA. Gram-scale synthesis of recombinant chitooligosaccharides in Escherichia coli. *Carbohydrate Research* **1997**;302:35-42.

[123] Chambon R, Despras G, Brossay A, Vauzeilles B, Urban D, Beau J-M, et al. Efficient chemoenzymatic synthesis of lipo-chitin oligosaccharides as plant growth promoters. *Green Chemistry* **2015**;17:3923-30.

[124] Usui T, Hayashi Y, Nanjo F, Sakai K, Ishido Y. Transglycosylation reaction of a chitinase purified from Nocardia orientalis. *Biochimica et Biophysica Acta (BBA) - General Subjects* **1987**;923:302-9.

[125] Aly MRE, Ibrahim E-SI, El Ashry ESH, Schmidt RR. Synthesis of chitotetraose and chitohexaose based on dimethylmaleoyl protection. *Carbohydrate Research* **2001**;331:129-42.

[126] Kuyama H, Nakahara Y, Nukada T, Ito Y, Nakahara Y, Ogawa T. Stereocontrolled synthesis of chitosan dodecamer. *Carbohydrate Research* **1993**;243:C1-C7.

[127] Schmitt F, Sinaÿ P. Synthèse de disaccharides à liaison (1→4) posseédant un résidu réducteur 2-acétamido-2-désoxy-D-glucopyranose: emploi de dérivés du 2-acétamido-1,6-anhydro-2-désoxy-β-D-glucopyranose. *Carbohydrate Research* **1973**;29:99-111.

[128] Nashed MA, Kiso M, Slife CW, Anderson L. Partially benzylated oxazoline derivatives of 2-acetamido-2-deoxy-D-glucopyranose as “standardized intermediates” for oligosaccharide synthesis. preparation of disaccharides having the sequences β-D-GlcpNAc(1→x)-D-Gal and β-D-GlcpNAc(1→4)-D-GlcNAc. *Carbohydrate Research* **1981**;90:71-82.

[129] Huang L, Wang Z, Li X, Ye X-s, Huang X. Iterative one-pot syntheses of chitotetroses. *Carbohydrate Research* **2006**;341:1669-79.

[130] Kusumoto S, Yamamoto K, Imoto M, Inage M, Tsujimoto M, Kotani S, et al. Chemical synthesis and biological activities of two disaccharide dipeptides corresponding to the repeating units of bacterial peptidoglycan1986.

[131] Kawada T, Yoneda Y. Selection of protecting groups and synthesis of a β-1,4-GlcNAc-β-1,4-GlcN unit2009.

[132] Ihara H, Hanashima S, Tsukamoto H, Yamaguchi Y, Taniguchi N, Ikeda Y. Difucosylation of chitooligosaccharides by eukaryote and prokaryote α1,6-fucosyltransferases. *Biochimica et Biophysica Acta (BBA) - General Subjects* **2013**;1830:4482-90.

[133] Issaree A. Synthesis of Hetero-chitooligosaccharides2008.

[134] Barroca-Aubry N, Pernet-Poil-Chevrier A, Domard A, Trombotto S. Towards a modular synthesis of well-defined chitooligosaccharides: synthesis of the four chitodisaccharides. *Carbohydrate Research* **2010**;345:1685-97.

[135] Hirano S, Yamaguchi R. N-acetylchitosan gel: A polyhydrate of chitin. *Biopolymers* **1976**;15:1685-91.

[136] Zou P, Li K, Liu S, Xing R, Qin Y, Yu H, et al. Effect of chitooligosaccharides with different degrees of acetylation on wheat seedlings under salt stress. *Carbohydrate Polymers* **2015**;126:62-9.

[137] Cabrera JC, Messiaen J, Cambier P, Van Cutsem P. Size, acetylation and concentration of chitooligosaccharide elicitors determine the switch from defence involving PAL activation to cell death and water peroxide production in Arabidopsis cell suspensions. *Physiologia Plantarum* **2006**;127:44-56.

[138] Abla M, Marmuse L, Delolme F, Vors J-P, Ladavière C, Trombotto S. Access to tetra-N-acetyl-chitopentaose by chemical N-acetylation of glucosamine pentamer. *Carbohydrate Polymers* **2013**;98:770-7.

[139] Tokuyasu K, Ono H, Mitsutomi M, Hayashi K, Mori Y. Synthesis of a chitosan tetramer derivative, β-d-GlcNAc-(1→4)-β-d-GlcNAc-(1→4)-β-d-GlcNAc-(1→4)-d-GlcN through a partial N-acetylation reaction by chitin deacetylase. *Carbohydrate Research* **2000**;325:211-5.

[140] Zhao Y, Park R-D, Muzzarelli RAA. Chitin deacetylases: properties and applications. *Marine drugs* **2010**;8:24-46.

[141] Aye KN, Karuppuswamy R, Ahamed T, Stevens WF. Peripheral enzymatic deacetylation of chitin and reprecipitated chitin particles. *Bioresource Technology* **2006**;97:577-82.

[142] Beaney PD, Gan Q, Magee TRA, Healy M, Lizardi-Mendoza J. Modification of chitin properties for enzymatic deacetylation. *Journal of Chemical Technology & Biotechnology* **2007**;82:165-73.

[143] Win N, Stevens W. Shrimp chitin as substrate for fungal chitin deacetylase. *Applied microbiology and biotechnology* **2001**;57:334-41.

[144] Wattjes J, Niehues A, Cord-Landwehr S, Hoßbach J, David L, Delair T, et al. Enzymatic Production and Enzymatic-Mass Spectrometric Fingerprinting Analysis of Chitosan Polymers with Different Nonrandom Patterns of Acetylation. *Journal of the American Chemical Society* **2019**;141:3137-45.

[145] Eom T-K, Senevirathne M, Kim S-K. Synthesis of phenolic acid conjugated chitooligosaccharides and evaluation of their antioxidant activity. *Environmental Toxicology and Pharmacology* **2012**;34:519-27.

[146] Ngo D-H, Qian Z-J, Ngo D-N, Vo T-S, Wijesekara I, Kim S-K. Gallyl chitooligosaccharides inhibit intracellular free radical-mediated oxidation. *Food Chemistry* **2011**;128:974-81.

[147] Je J-Y, Kim E-K, Ahn C-B, Moon S-H, Jeon B-T, Kim B, et al. Sulfated chitooligosaccharides as prolyl endopeptidase inhibitor. *International Journal of Biological Macromolecules* **2007**;41:529-33.

[148] Lu X, Guo H, Zhang Y. Protective effects of sulfated chitooligosaccharides against hydrogen peroxide-induced damage in MIN6 cells. *International Journal of Biological Macromolecules* **2012**;50:50-8.

[149] Trinh MDL, Dinh M-H, Ngo D-H, Tran D-K, Tran Q-T, Vo T-S, et al. Protection of 4-hydroxybenzyl-chitooligomers against inflammatory responses in Chang liver cells. *International Journal of Biological Macromolecules* **2014**;66:1-6.

[150] Maria Marzaioli A, Bedini E, Lanzetta R, Perino V, Parrilli M, De Castro C. Preparation and NMR characterization of glucosamine oligomers bearing an azide function using chitosan. *Carbohydrate Polymers* **2012**;90:847-52.

[151] Ngo D-N, Qian Z-J, Je J-Y, Kim M-M, Kim S-K. Aminoethyl chitooligosaccharides inhibit the activity of angiotensin converting enzyme. *Process Biochemistry* **2008**;43:119-23.

[152] Ngo D-N, Kim M-M, Kim S-K. Protective effects of aminoethyl-chitooligosaccharides against oxidative stress in mouse macrophage RAW 264.7 cells. *International Journal of Biological Macromolecules* **2012**;50:624-31.

[153] Ngo D-H, Ngo D-N, Vo T-S, Ryu B, Van Ta Q, Kim S-K. Protective effects of aminoethyl-chitooligosaccharides against oxidative stress and inflammation in murine microglial BV-2 cells. *Carbohydrate Polymers* **2012**;88:743-7.

[154] Guerry A, Bernard J, Samain E, Fleury E, Cottaz S, Halila S. Aniline-Catalyzed Reductive Amination as a Powerful Method for the Preparation of Reducing End-"Clickable" Chitooligosaccharides. *Bioconjugate Chemistry* **2013**;24:544-9.

[155] Pickenhahn VD, Grange M, De Crescenzo G, Lavertu M, Buschmann MD. Regioselective chitosan end-group activation: the triskelion approach. *RSC Advances* **2017**;7:18628-38.

[156] Pickenhahn VD, Darras V, Dziopa F, Biniecki K, De Crescenzo G, Lavertu M, et al. Regioselective thioacetylation of chitosan end-groups for nanoparticle gene delivery systems. *Chemical Science* **2015**;6:4650-64.

[157] Novoa-Carballal R, Müller AHE. Synthesis of polysaccharide-b-PEG block copolymers by oxime click. *Chemical Communications* **2012**;48:3781-3.

[158] Moussa A, Trombotto S. Octanoic Hydrazide-Linked Chitooligosaccharides-2,5-Anhydro-d-Mannofuranose. *Molbank* **2016**;2016:M904.

[159] Salim E, Ailincai D, Trombotto S. Chitooligosaccharide-2,5-anhydro-D-mannonic Acid. *Molbank* **2014**;2014:M832.

[160] Salim E, Galais A, Trombotto S. 4-(Hexyloxy)aniline-linked chitooligosaccharide-2,5-anhydro-D-mannofuranose. *Molbank* **2014**;2014:M815.

[161] Sugiyama H, Hisamichi K, Sakai K, Usui T, Ishiyama J-I, Kudo H, et al. The conformational study of chitin and chitosan oligomers in solution. *Bioorganic & Medicinal Chemistry* **2001**;9:211-6.

[162] El-Saharty YS, Bary AA. High-performance liquid chromatographic determination of neutraceuticals, glucosamine sulphate and chitosan, in raw materials and dosage forms. *Analytica Chimica Acta* **2002**;462:125-31.

[163] Crespo MOP, Martínez MV, Hernández JL, Lage Yusty MA. High-performance liquid chromatographic determination of chitin in the snow crab, Chionoecetes opilio. *Journal of Chromatography A* **2006**;1116:189-92.

[164] Liang Z, Leslie J, Adebowale A, Ashraf M, Eddington ND. Determination of the nutraceutical, glucosamine hydrochloride, in raw materials, dosage forms and plasma using pre-column derivatization with ultraviolet HPLC. *Journal of Pharmaceutical and Biomedical Analysis* **1999**;20:807-14.

[165] Shao Y, Alluri R, Mummert M, Koetter U, Lech S. A stability-indicating HPLC method for the determination of glucosamine in pharmaceutical formulations. *Journal of Pharmaceutical and Biomedical Analysis* **2004**;35:625-31.

[166] Hirai A, Odani H, Nakajima A. Determination of degree of deacetylation of chitosan by 1H NMR spectroscopy. *Polymer Bulletin* **1991**;26:87-94.

[167] Lee M-Y, Var F, Shin-ya Y, Kajiuchi T, Yang J-W. Optimum conditions for the precipitation of chitosan oligomers with DP 5–7 in concentrated hydrochloric acid at low temperature. *Process Biochemistry* **1999**;34:493-500.

[168] Kubota N, Eguchi Y. Facile preparation of water-soluble N-acetylated chitosan and molecular weight dependence of its water-solubility. *Polymer journal* **1997**;29:123.

[169] Zając A, Hanuza J, Wandas M, Dymińska L. Determination of N-acetylation degree in chitosan using Raman spectroscopy. *Spectrochimica Acta Part A: Molecular and Biomolecular Spectroscopy* **2015**;134:114-20.

[170] Jeong K-J, Song Y, Shin H-R, Kim JE, Kim J, Sun F, et al. In vivo study on the biocompatibility of chitosan–hydroxyapatite film depending on degree of deacetylation. *Journal of Biomedical Materials Research Part A* **2017**;105:1637-45.

[171] Mikhailov GP, Tuchkov SV, Lazarev VV, Kulish EI. Complexation of chitosan with acetic acid according to Fourier transform Raman spectroscopy data. *Russian Journal of Physical Chemistry A* **2014**;88:936-41.

[172] Xue C, Wilson LD. A structural study of self-assembled chitosan-based sponge materials. *Carbohydrate Polymers* **2019**;206:685-93.

[173] Thanou M, Verhoef JC, Junginger HE. Oral drug absorption enhancement by chitosan and its derivatives. *Advanced Drug Delivery Reviews* **2001**;52:117-26.

[174] Ilium L. Chitosan and Its Use as a Pharmaceutical Excipient. *Pharmaceutical Research* **1998**;15:1326-31.

[175] Wedmore I, McManus JG, Pusateri AE, Holcomb JB. A special report on the chitosan-based hemostatic dressing: Experience in current combat operations. *Journal of Trauma - Injury, Infection and Critical Care* **2006**;60:655-8.

[176] Fernandes JC, Borges M, Nascimento H, Bronze-da-Rocha E, Ramos OS, Pintado ME, et al. Cytotoxicity and genotoxicity of chitooligosaccharides upon lymphocytes. *International Journal of Biological Macromolecules* **2011**;49:433-8.

[177] Xu Q, Dou J, Wei P, Tan C, Yun X, Wu Y, et al. Chitooligosaccharides induce apoptosis of human hepatocellular carcinoma cells via up-regulation of Bax. *Carbohydrate Polymers* **2008**;71:509-14.

[178] Lv X, Liu Y, Song S, Tong C, Shi X, Zhao Y, et al. Influence of chitosan oligosaccharide on the gelling and wound healing properties of injectable hydrogels based on carboxymethyl chitosan/alginate polyelectrolyte complexes. *Carbohydrate Polymers* **2019**;205:312-21.

[179] Celio MR, Spreafico R, De Biasi S, Vitellaro-Zuccarello L. Perineuronal nets: past and present. *Trends in Neurosciences* **1998**;21:510-5.

[180] Yamaguchi Y. Lecticans: organizers of the brain extracellular matrix. *Cellular and Molecular Life Sciences CMLS* **2000**;57:276-89.

[181] Kwok J, Dick G, Wang D, Fawcett J. Extracellular Matrix and Perineuronal Nets in CNS Repair2011.

[182] Ylera B, Ertürk A, Hellal F, Nadrigny F, Hurtado A, Tahirovic S, et al. Chronically CNS-Injured Adult Sensory Neurons Gain Regenerative Competence upon a Lesion of Their Peripheral Axon. *Current Biology* **2009**;19:930-6.

[183] David S, Lacroix S. Molecular approaches to spinal cord repair. *Annual review of neuroscience* **2003**;26:411-40.

[184] Yang LJ, Lorenzini I, Vajn K, Mountney A, Schramm LP, Schnaar RL. Sialidase enhances spinal axon outgrowth in vivo. *Proceedings of the National Academy of Sciences* **2006**;103:11057-62.

[185] Schnell L, Schwab ME. Axonal regeneration in the rat spinal cord produced by an antibody against myelin-associated neurite growth inhibitors. *Nature* **1990**;343:269.

[186] Bradbury EJ, Moon LD, Popat RJ, King VR, Bennett GS, Patel PN, et al. Chondroitinase ABC promotes functional recovery after spinal cord injury. *Nature* **2002**;416:636.

[187] Bradbury EJ, Carter LM. Manipulating the glial scar: Chondroitinase ABC as a therapy for spinal cord injury. *Brain Research Bulletin* **2011**;84:306-16.

[188] Galtrey CM, Fawcett JW. The role of chondroitin sulfate proteoglycans in regeneration and plasticity in the central nervous system. *Brain Research Reviews* **2007**;54:1-18.

[189] Kwok JCF, Carulli D, Fawcett JW. In vitro modeling of perineuronal nets: hyaluronan synthase and link protein are necessary for their formation and integrity. *Journal of Neurochemistry* **2010**;114:1447-59.

[190] Barritt A, Davies M, Marchand F, Hartley R, Grist J, Yip P, et al. Chondroitinase ABC promotes sprouting of intact and injured spinal systems after spinal cord injury. *Journal of Neuroscience* **2006**;26:10856-67.

[191] Hurtado A, Cregg JM, Wang HB, Wendell DF, Oudega M, Gilbert RJ, et al. Robust CNS regeneration after complete spinal cord transection using aligned poly-l-lactic acid microfibers. *Biomaterials* **2011**;32:6068-79.

[192] Estrada V, Brazda N, Schmitz C, Heller S, Blazyca H, Martini R, et al. Long-lasting significant functional improvement in chronic severe spinal cord injury following scar resection and polyethylene glycol implantation. *Neurobiology of Disease* **2014**;67:165-79.

[193] Gnavi S, Barwig C, Freier T, Haastert-Talini K, Grothe C, Geuna S. Chapter One - The Use of Chitosan-Based Scaffolds to Enhance Regeneration in the Nervous System. In: Geuna S, Perroteau I, Tos P, Battiston B, editors. International Review of Neurobiology: Academic Press; 2013. p. 1-62.

[194] Kim H, Tator CH, Shoichet MS. Chitosan implants in the rat spinal cord: biocompatibility and biodegradation. *Journal of Biomedical Materials Research Part A* **2011**;97:395-404.

[195] Chedly J, Soares S, Montembault A, von Boxberg Y, Veron-Ravaille M, Mouffle C, et al. Physical chitosan microhydrogels as scaffolds for spinal cord injury restoration and axon regeneration. *Biomaterials* **2017**;138:91-107.

[196] Nothias F, Soares S, David L, Montembault A. Chitosan hydrogel for repairing nerve tissue. Google Patents; 2017.

[197] Schatz C, Viton C, Delair T, Pichot C, Domard A. Typical Physicochemical Behaviors of Chitosan in Aqueous Solution. *Biomacromolecules* **2003**;4:641-8.

[198] Gubin S, Koksharov Y, Khomutov G, Yurkov G. Magnetic nanoparticles: Preparation methods, structure and properties. *Uspekhi Khimii* **2005**;74:539-74.

[199] Murray CB, Norris DJ, Bawendi MG. Synthesis and characterization of nearly monodisperse CdE (E = sulfur, selenium, tellurium) semiconductor nanocrystallites. *Journal of the American Chemical Society* **1993**;115:8706-15.

[200] Jun Y-w, Huh Y-M, Choi J-s, Lee J-H, Song H-T, KimKim, et al. Nanoscale Size Effect of Magnetic Nanocrystals and Their Utilization for Cancer Diagnosis via Magnetic Resonance Imaging. *Journal of the American Chemical Society* **2005**;127:5732-3.

[201] Lu A-H, Salabas EL, Schüth F. Magnetic Nanoparticles: Synthesis, Protection, Functionalization, and Application. *Angewandte Chemie International Edition* **2007**;46:1222-44.

[202] Cardoso VF, Francesko A, Ribeiro C, Bañobre-López M, Martins P, Lanceros-Mendez S. Advances in Magnetic Nanoparticles for Biomedical Applications. *Advanced Healthcare Materials* **2017**;7:1700845.

[203] Yallapu MM, Othman SF, Curtis ET, Gupta BK, Jaggi M, Chauhan SC. Multi-functional magnetic nanoparticles for magnetic resonance imaging and cancer therapy. *Biomaterials* **2011**;32:1890-905.

[204] Ito A, Shinkai M, Honda H, Kobayashi T. Medical application of functionalized magnetic nanoparticles. *Journal of Bioscience and Bioengineering* **2005**;100:1-11.

[205] Saiyed Z, Telang S, Ramchand C. Application of magnetic techniques in the field of drug discovery and biomedicine. *BioMagnetic Research and Technology* **2003**;1:2.

[206] Wilhelm C, Gazeau F. Universal cell labelling with anionic magnetic nanoparticles. *Biomaterials* **2008**;29:3161-74.

[207] Hao R, Xing R, Xu Z, Hou Y, Gao S, Sun S. Synthesis, Functionalization, and Biomedical Applications of Multifunctional Magnetic Nanoparticles. *Advanced Materials* **2010**;22:2729-42.

[208] Ling D, Hyeon T. Chemical Design of Biocompatible Iron Oxide Nanoparticles for Medical Applications. *Small* **2012**;9:1450-66.

[209] Jun Y-w, Seo J-w, Cheon J. Nanoscaling Laws of Magnetic Nanoparticles and Their Applicabilities in Biomedical Sciences. *Accounts of Chemical Research* **2008**;41:179-89.

[210] Boxall C, Kelsall G, Zhang Z. Photoelectrophoresis of colloidal iron oxides. Part 2.-Magnetite (Fe3O4). *Journal of the Chemical Society, Faraday Transactions* **1996**;92:791-802.

[211] Wei Wu and Zhaohui Wu and Taekyung Yu and Changzhong Jiang and Woo-Sik K. Recent progress on magnetic iron oxide nanoparticles: synthesis, surface functional strategies and biomedical applications. *Science and Technology of Advanced Materials* **2015**;16:023501.

[212] Oldham JW. (R. T.) Shuey. Semiconducting ore minerals (Developments in Economic Geology, Vol. 4). Amsterdam and New York (Elsevier Sci. Publ. Co.), 1975. 415 pp., 55 figs. Price Dfl. 55.00 ($22.95). *Mineralogical Magazine* **1976**;40:656-.

[213] White AF, Peterson ML, Hochella MF. Electrochemistry and dissolution kinetics of magnetite and ilmenite. *Geochimica et Cosmochimica Acta* **1994**;58:1859-75.

[214] Xu C, Sun S. New forms of superparamagnetic nanoparticles for biomedical applications. *Advanced Drug Delivery Reviews* **2013**;65:732-43.

[215] Sharifi S, Seyednejad H, Laurent S, Atyabi F, Saei AA, Mahmoudi M. Superparamagnetic iron oxide nanoparticles for in vivo molecular and cellular imaging. *Contrast Media & Molecular Imaging* **2015**;10:329-55.

[216] Chatterjee K, Sarkar S, Jagajjanani Rao K, Paria S. Core/shell nanoparticles in biomedical applications. *Advances in Colloid and Interface Science* **2014**;209:8-39.

[217] Foglia S, Ledda M, Fioretti D, Iucci G, Papi M, Capellini G, et al. In vitro biocompatibility study of sub-5 nm silica-coated magnetic iron oxide fluorescent nanoparticles for potential biomedical application. *Scientific Reports* **2017**;7:46513.

[218] Sun M, Sun B, Liu Y, Shen Q-D, Jiang S. Dual-Color Fluorescence Imaging of Magnetic Nanoparticles in Live Cancer Cells Using Conjugated Polymer Probes. *Scientific Reports* **2016**;6:22368.

[219] Bourrinet P, Bengele HH, Bonnemain B, Dencausse A, Idee J-M, Jacobs PM, et al. Preclinical Safety and Pharmacokinetic Profile of Ferumoxtran-10, an Ultrasmall Superparamagnetic Iron Oxide Magnetic Resonance Contrast Agent. *Investigative Radiology* **2006**;41.

[220] Klotz M, Ayral A, Guizard C, Ménager C, Cabuil V. Silica Coating on Colloidal Maghemite Particles. *Journal of Colloid and Interface Science* **1999**;220:357-61.

[221] Wu M, Zhang YD, Hui S, Xiao TD, Ge S, Hines WA, et al. Magnetic properties of SiO2-coated Fe nanoparticles. *Journal of Applied Physics* **2002**;92:6809-12.

[222] Hyeon T. Chemical synthesis of magnetic nanoparticles. *Chemical Communications* **2003**;3:927-34.

[223] Peter MG. Applications and Environmental Aspects of Chitin and Chitosan. *Journal of Macromolecular Science, Part A* **1995**;32:629-40.

[224] Tsai G-J, Zhang S-L, Shieh P-L. Antimicrobial Activity of a Low-Molecular-Weight Chitosan Obtained from Cellulase Digestion of Chitosan. *Journal of Food Protection* **2004**;67:396-8.

[225] Guo Z, Xing R, Liu S, Zhong Z, Ji X, Wang L, et al. The influence of molecular weight of quaternized chitosan on antifungal activity. *Carbohydrate Polymers* **2008**;71:694-7.

[226] Huang J, Wang L, Zhong X, Li Y, Yang L, Mao H. Facile non-hydrothermal synthesis of oligosaccharide coated sub-5 nm magnetic iron oxide nanoparticles with dual MRI contrast enhancement effects. *Journal of Materials Chemistry B* **2014**;2:5344-51.

[227] Shukla S, Jadaun A, Arora V, Sinha RK, Biyani N, Jain VK. In vitro toxicity assessment of chitosan oligosaccharide coated iron oxide nanoparticles. *Toxicology Reports* **2015**;2:27-39.

[228] Le Thi TN, Nguyen TH, Hoang DQ, Tran TV, Nguyen NT, Nguyen DH. Development of new magnetic nanoparticles: Oligochitosan obtained by γ-rays and –coated Fe3O4 nanoparticles. *Applied Surface Science* **2017**;422:863-8.

[229] Huang Y, Gong J, Zhang Q, Hua M, Wu J. Synthesis and characterization of low molecular weight chitosan decorated Fe3O4 nanoparticles as T2 contrast agent. *Materials Chemistry and Physics* **2016**;180:122-7.

[230] Bae KH, Park M, Do MJ, Lee N, Ryu JH, Kim GW, et al. Chitosan Oligosaccharide-Stabilized Ferrimagnetic Iron Oxide Nanocubes for Magnetically Modulated Cancer Hyperthermia. *ACS Nano* **2012**;6:5266-73.

[231] Salim E, Ailincai D, Trombotto S. Chitooligosaccharide-2,5-anhydro-D-mannonic Acid2014.

[232] Vårum KM, Antohonsen MW, Grasdalen H, Smidsrød O. Determination of the degree of N-acetylation and the distribution of N-acetyl groups in partially N-deacetylated chitins (chitosans) by high-field n.m.r. spectroscopy. *Carbohydrate Research* **1991**;211:17-23.

[233] M. S. Handbuch der Elektrizität und des Magnetismus. Germany: Barth: Leipzig; 1921.

[234] de Britto D, Campana-Filho SP. A kinetic study on the thermal degradation of N,N,N-trimethylchitosan. *Polymer Degradation and Stability* **2004**;84:353-61.

[235] Focher B, Beltrame PL, Naggi A, Torri G. Alkaline N-deacetylation of chitin enhanced by flash treatments. Reaction kinetics and structure modifications. *Carbohydrate Polymers* **1990**;12:405-18.

[236] Focher B, Naggi A, Torri G, Cosani A, Terbojevich M. Chitosans from Euphausia superba. 2: Characterization of solid state structure. *Carbohydrate Polymers* **1992**;18:43-9.

[237] Waldron RD. Infrared Spectra of Ferrites. *Physical Review* **1955**;99:1727-35.

[238] Ma M, Zhang Y, Yu W, Shen H, Zhang H, Gu N. Preparation and characterization of magnetite nanoparticles coated by amino silane. *Colloids and Surfaces a-Physicochemical and Engineering Aspects* **2003**;212:219-26.

[239] Monazam ER, Breault RW, Siriwardane R. Kinetics of Magnetite (Fe3O4) Oxidation to Hematite (Fe2O3) in Air for Chemical Looping Combustion. *Industrial & Engineering Chemistry Research* **2014**;53:13320-8.

[240] Grimm S, Schultz M, Barth S, Muller R. Flame pyrolysis – a preparation route for ultrafine pure γ-Fe2O3 powders and the control of their particle size and properties. *Journal of Materials Science* **1997**;32:1083-92.

[241] Hunter RJ. Chapter 6 - Applications of the Zeta Potential. In: Hunter RJ, editor. Zeta Potential in Colloid Science: Academic Press; 1981. p. 219-57.

[242] Zamora-Mora V, Fernández-Gutiérrez M, González-Gómez Á, Sanz B, Román JS, Goya GF, et al. Chitosan nanoparticles for combined drug delivery and magnetic hyperthermia: From preparation to in vitro studies. *Carbohydrate Polymers* **2017**;157:361-70.

[243] Cornell RM, Schwertmann U. The Iron Oxides: Structure, Porperties, Reactions, Occurrences and Uses. Second ed. ed. Weinheim: Wiley-VCH; 2003.

[244] Kodama R. Magnetic nanoparticles. *Journal of Magnetism and Magnetic Materials* **1999**;200:359-72.

[245] Coey JMD. Noncollinear Spin Arrangement in Ultrafine Ferrimagnetic Crystallites. *Physical Review Letters* **1971**;27:1140-2.

[246] Mazo-Zuluaga J, Restrepo J, Mejía-López J. Effect of surface anisotropy on the magnetic properties of magnetite nanoparticles: A Heisenberg–Monte Carlo study. *Journal of Applied Physics* **2008**;103:113906.

[247] Oliveira PN, Bini RD, Dias GS, Alcouffe P, Santos IA, David L, et al. Magnetite nanoparticles with controlled sizes via thermal degradation of optimized PVA/Fe(III) complexes. *Journal of Magnetism and Magnetic Materials* **2018**;460:381-90.

[248] Unsoy G, Yalcin S, Khodadust R, Gunduz G, Gunduz U. Synthesis optimization and characterization of chitosan-coated iron oxide nanoparticles produced for biomedical applications. *Journal of Nanoparticle Research* **2012**;14:964.

[249] Bodker F, Morup S. Size dependence of the properties of hematite nanoparticles. *Europhysics Letters* **2000**;52:217-23.

[250] Li B, Jia D, Zhou Y, Hu Q, Cai W. In situ hybridization to chitosan/magnetite nanocomposite induced by the magnetic field. *Journal of Magnetism and Magnetic Materials* **2006**;306:223-7.

[251] Carpenter EE. Iron nanoparticles as potential magnetic carriers. *Journal of Magnetism and Magnetic Materials* **2001**;225:17-20.

[252] Hussain RF, Nouri AME, Oliver RTD. A new approach for measurement of cytotoxicity using colorimetric assay. *Journal of Immunological Methods* **1993**;160:89-96.

[253] Van Ta Q, Kim M-M, Kim S-K. Inhibitory Effect of Chitooligosaccharides on Matrix Metalloproteinase-9 in Human Fibrosarcoma Cells (HT1080). *Marine Biotechnology* **2006**;8:593-9.

[254] Mao S, Shuai X, Unger F, Simon M, Bi D, Kissel T. The depolymerization of chitosan: effects on physicochemical and biological properties. *International Journal of Pharmaceutics* **2004**;281:45-54.

[255] Jadhav SV, Kim BM, Lee HY, Im IC, Rokade AA, Park SS, et al. Induction heating and in vitro cytotoxicity studies of MnZnFe2O4 nanoparticles for self-controlled magnetic particle hyperthermia. *Journal of Alloys and Compounds* **2018**;745:282-91.

[256] Shahabadi N, Akbari A, Karampour F, Falsafi M. Cytotoxicity and antibacterial activities of new chemically synthesized magnetic nanoparticles containing eugenol. *Journal of Drug Delivery Science and Technology* **2019**;49:113-22.

[257] Yang N, Li W-H. Preparation of gold nanoparticles using chitosan oligosaccharide as a reducing and capping reagent and their in vitro cytotoxic effect on Human fibroblasts cells. *Materials Letters* **2015**;138:154-7.

[258] Jenkins GJS, Asadi R, Doak SH. Potential toxicity of superparamagnetic iron oxide nanoparticles (SPION) AU - Singh, Neenu. *Nano Reviews* **2010**;1:5358.

[259] Kumar V, Sharma N, Maitra SS. In vitro and in vivo toxicity assessment of nanoparticles. *International Nano Letters* **2017**;7:243-56.

[260] Mahmoudi M, Simchi A, Imani M, Shokrgozar MA, Milani AS, Häfeli UO, et al. A new approach for the in vitro identification of the cytotoxicity of superparamagnetic iron oxide nanoparticles. *Colloids and Surfaces B: Biointerfaces* **2010**;75:300-9.

[261] Rhazi M, Desbrières J, Tolaimate A, Rinaudo M, Vottero P, Alagui A. Contribution to the study of the complexation of copper by chitosan and oligomers. *Polymer* **2002**;43:1267-76.

[262] Kalia J, Raines RT. Advances in Bioconjugation. *Current organic chemistry* **2010**;14:138-47.

Annexes

1. Annex A: NMR spectrums of synthesized partially *N*-acetylated oligomers

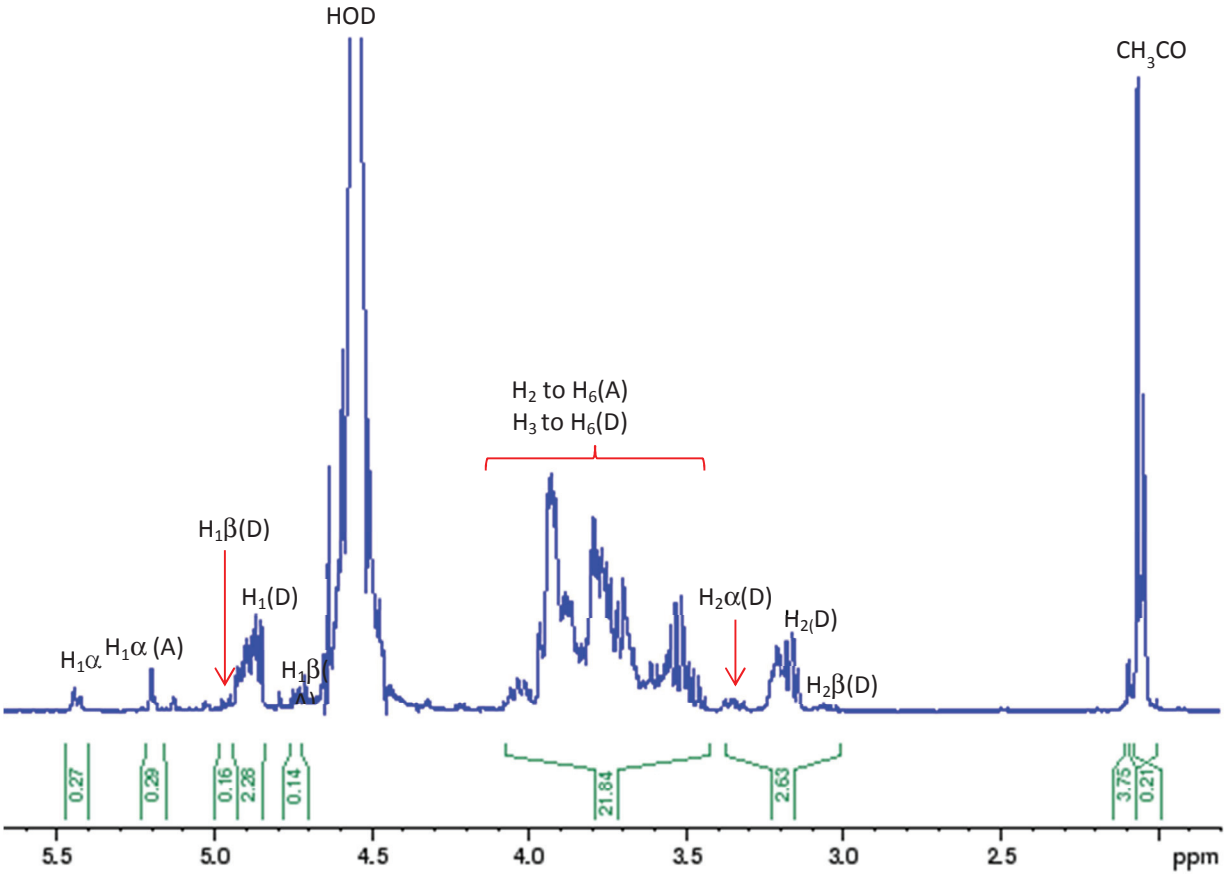

Figure 78: ^{1}H NMR spectrum (500 MHz, 48°C) of S2 (DA ~32 %) in D_2O.

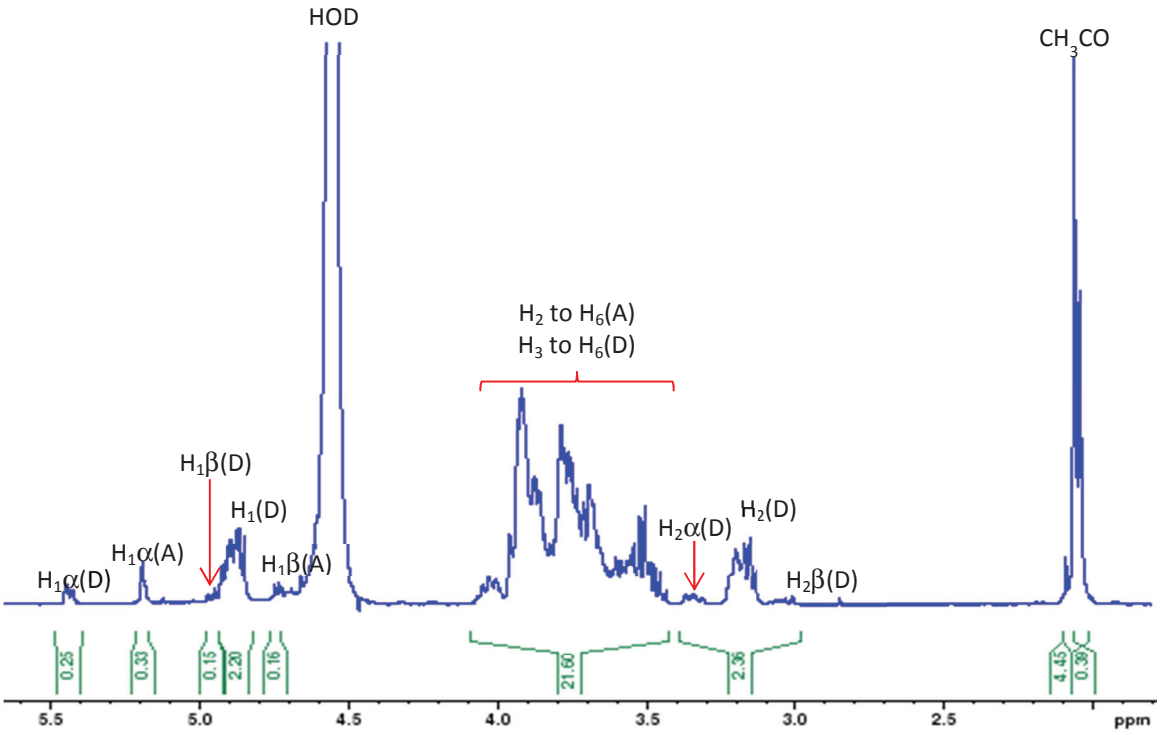

Figure 79: ^{1}H NMR spectrum (500 MHz, 48°C) of S3 (DA ~37 %) in D_2O.

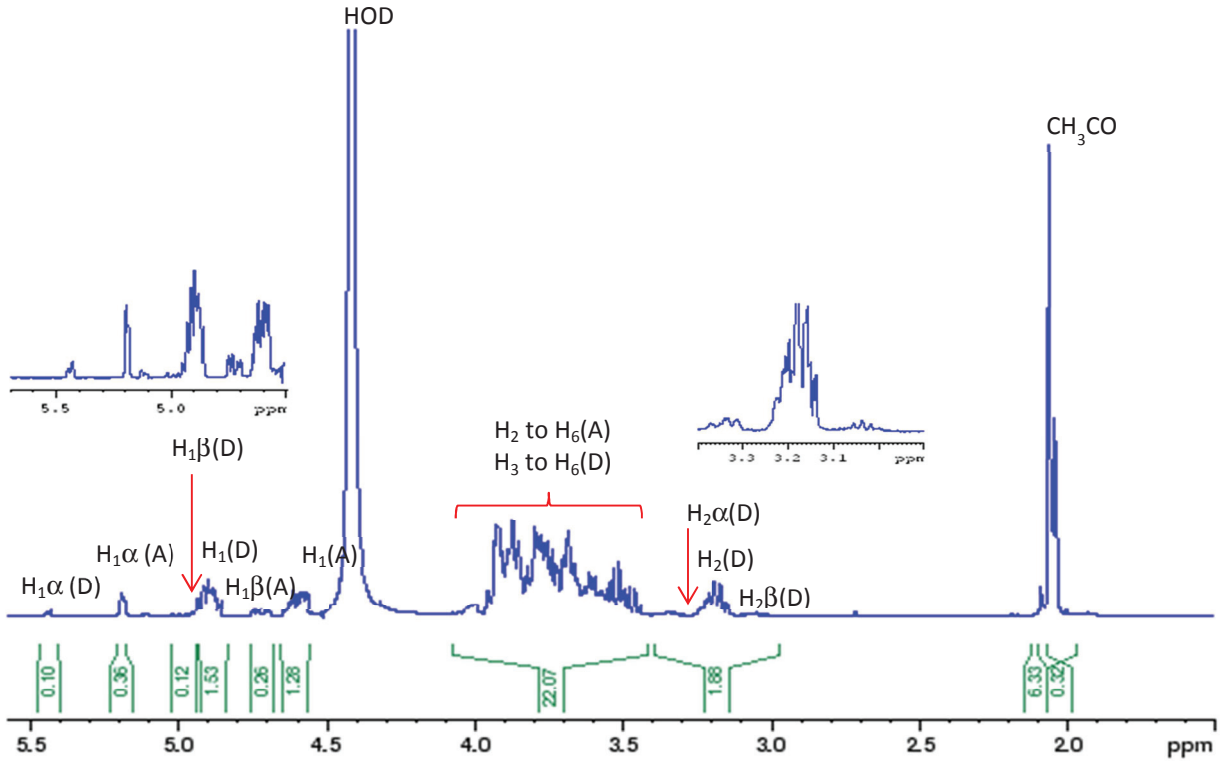

Figure 80: ^{1}H NMR spectrum (500 MHz, 50°C) of S4 (DA ~54 %) in D_2O.

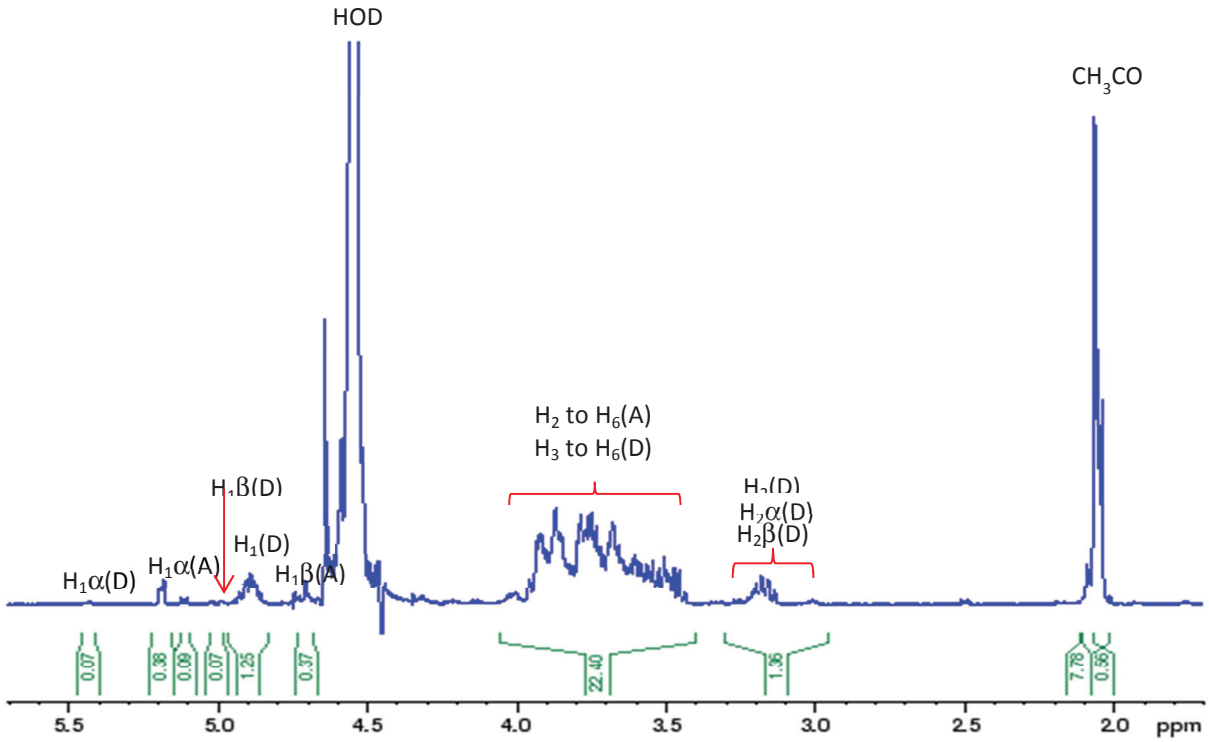

Figure 81: ^{1}H NMR spectrum (500 MHz, 48°C) of S5 (DA ~64 %) in D_2O.

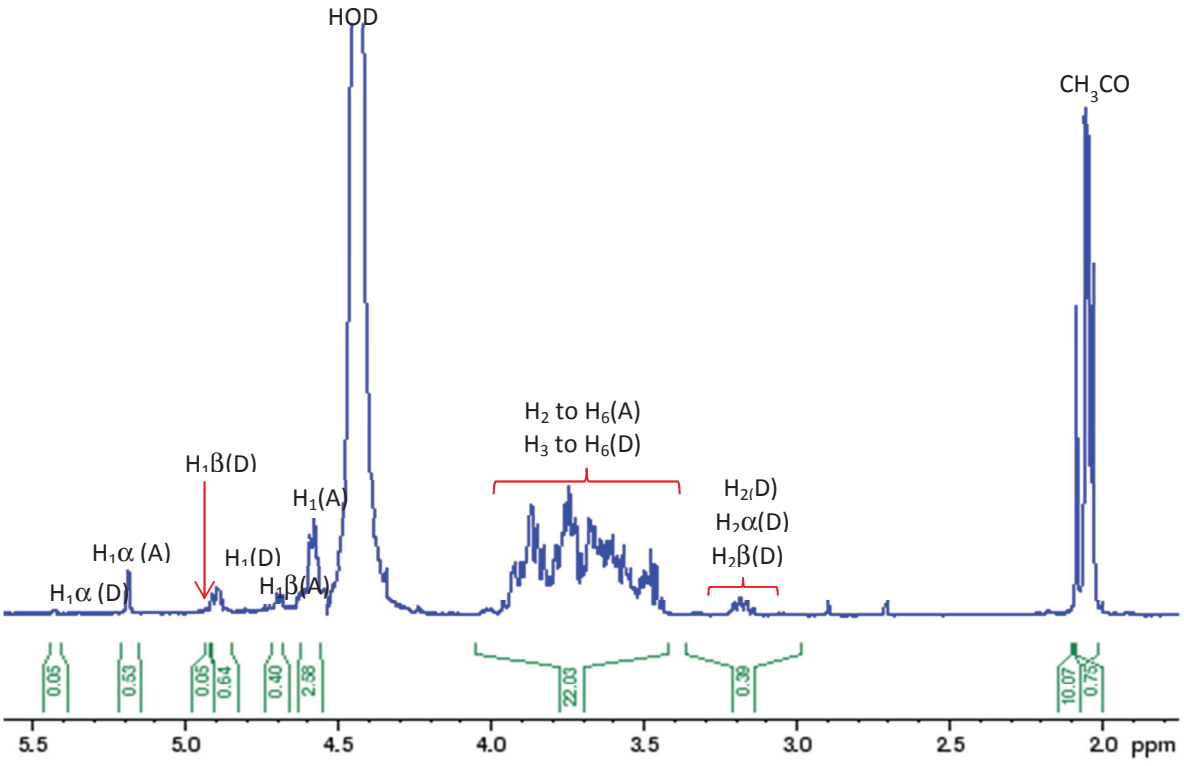

Figure 82: ^{1}H NMR spectrum (500 MHz, 50°C) of S6 (DA ~85 %) in D_2O.

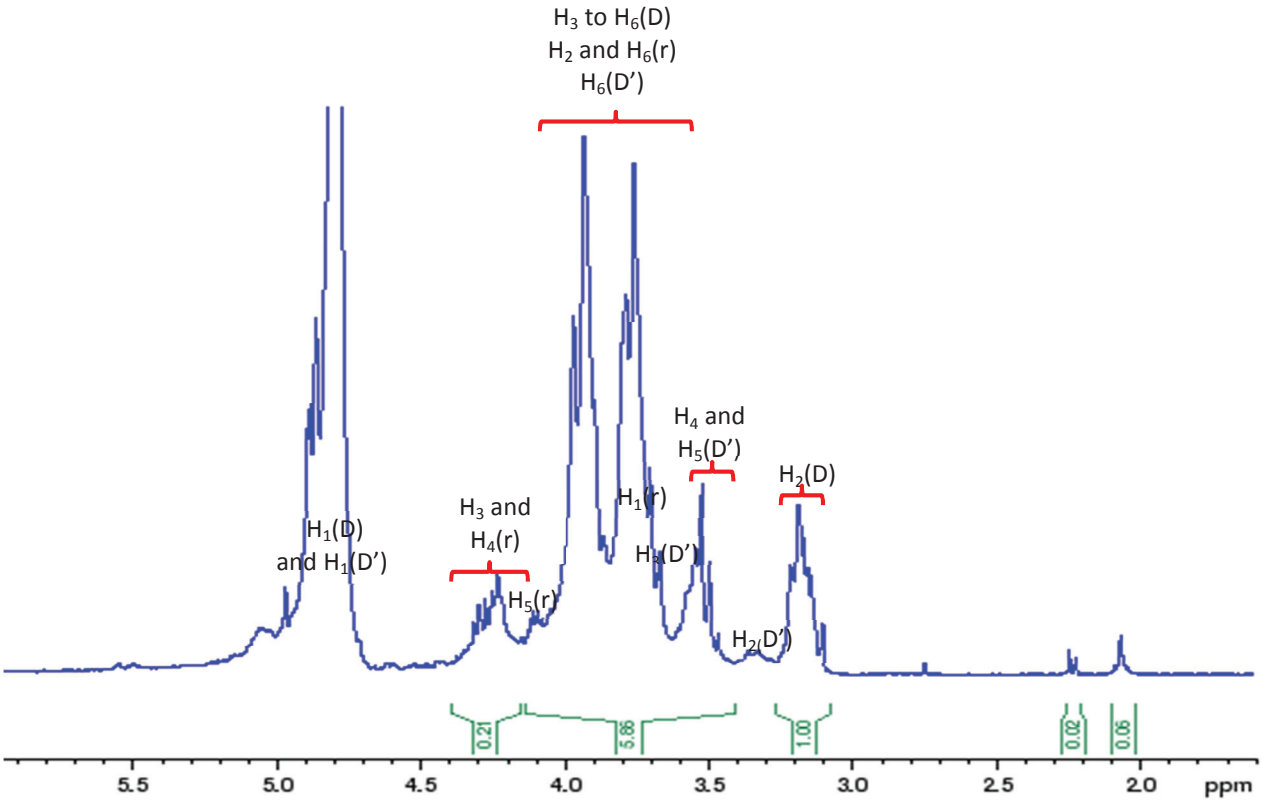

Figure 83: ^{1}H NMR spectrum (500 MHz, 50°C) of S7 (DP ~10, DA ~0 %) in D_2O.

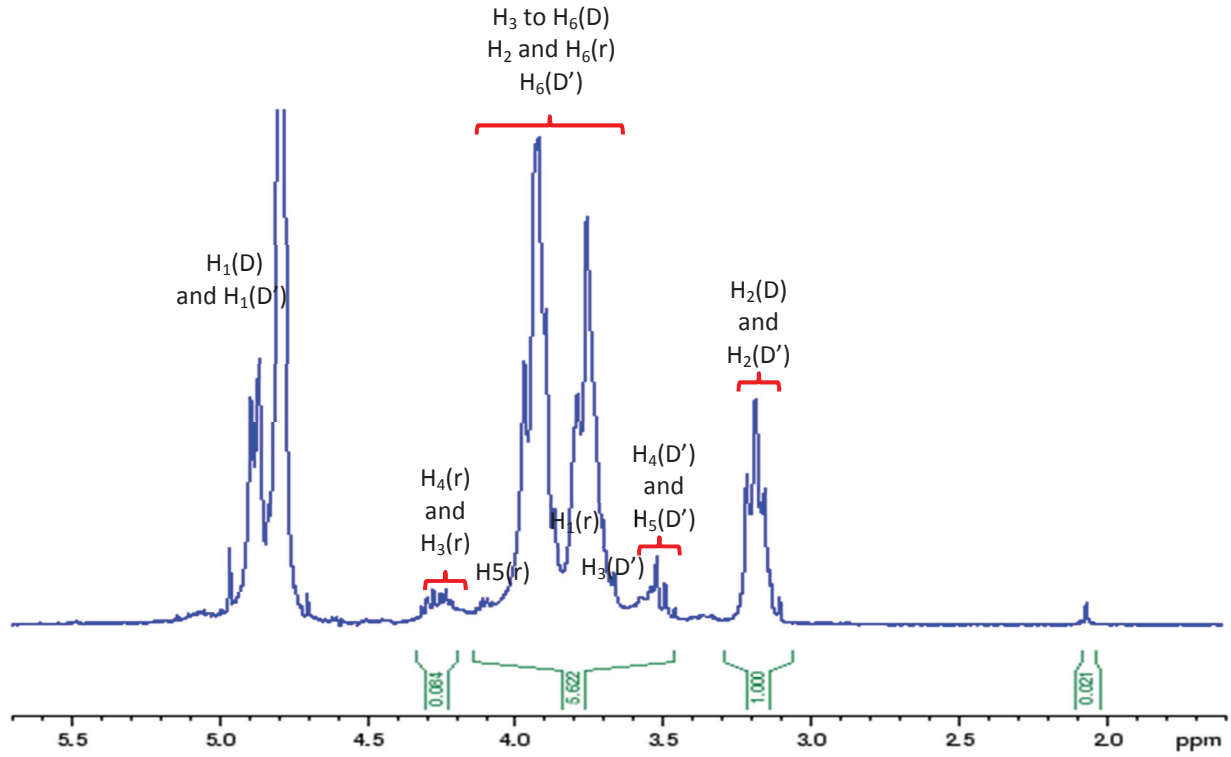

Figure 84: ^{1}H NMR spectrum (500 MHz, 50°C) of S8 (DP ~24, DA ~0 %) in D_2O.

2. Annexe B: Supporting Material for Paper 1

In situ synthesis of chito-oligosaccharide coated Fe_3O_4 nanoparticles, characterization and cytotoxicity evaluation for biomedical applications

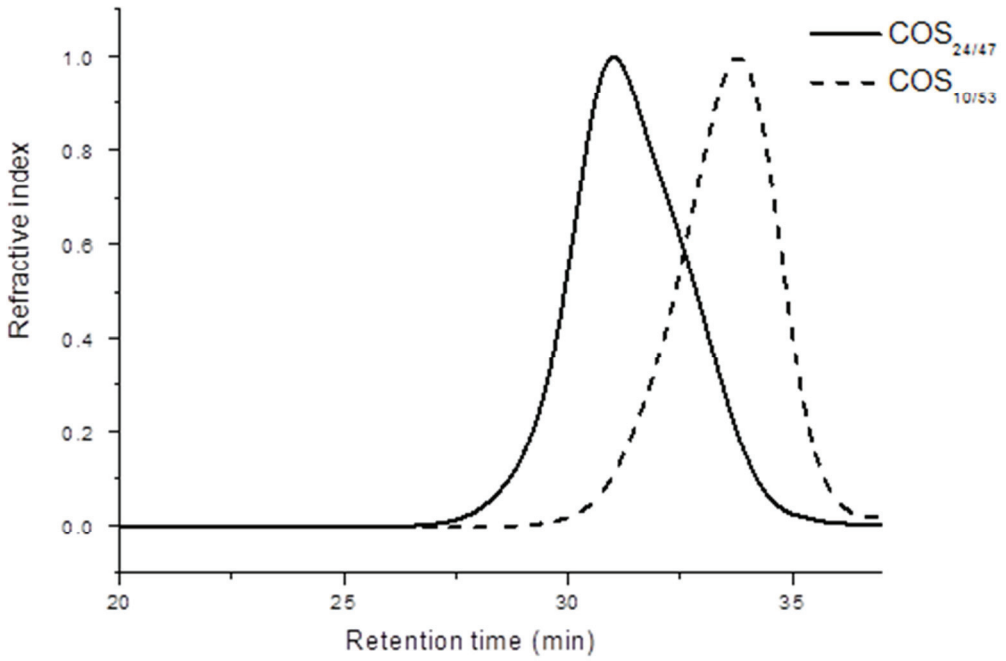

SMFigure 1 - Size exclusion chromatograms (AcOH (0.2 M)/$AcONH_4$ (0.15 M) buffer, pH 4.5) of $COS_{24/47}$ and $COS_{10/53}$.

The average DA of the different acetylated samples was determined by considering both signal areas of H2 protons of GlcN units ($I_{GlcN\text{-}H2}$) and acetyl protons of GlcNAc units (I_{CH3}) according to Equation 1. It was remarkable that the presence of acetic acid peaks was close to the signal of the acetyl groups. Of course this was taken into consideration when calculating the DA.

$$DA\ (\%) = \frac{\left(\frac{1}{3}\right) \times I_{CH_3}}{\left(\frac{1}{3}\right) I_{CH_3} + I_{GlcN-H2}} \times 100 \qquad \text{Eq. 1}$$

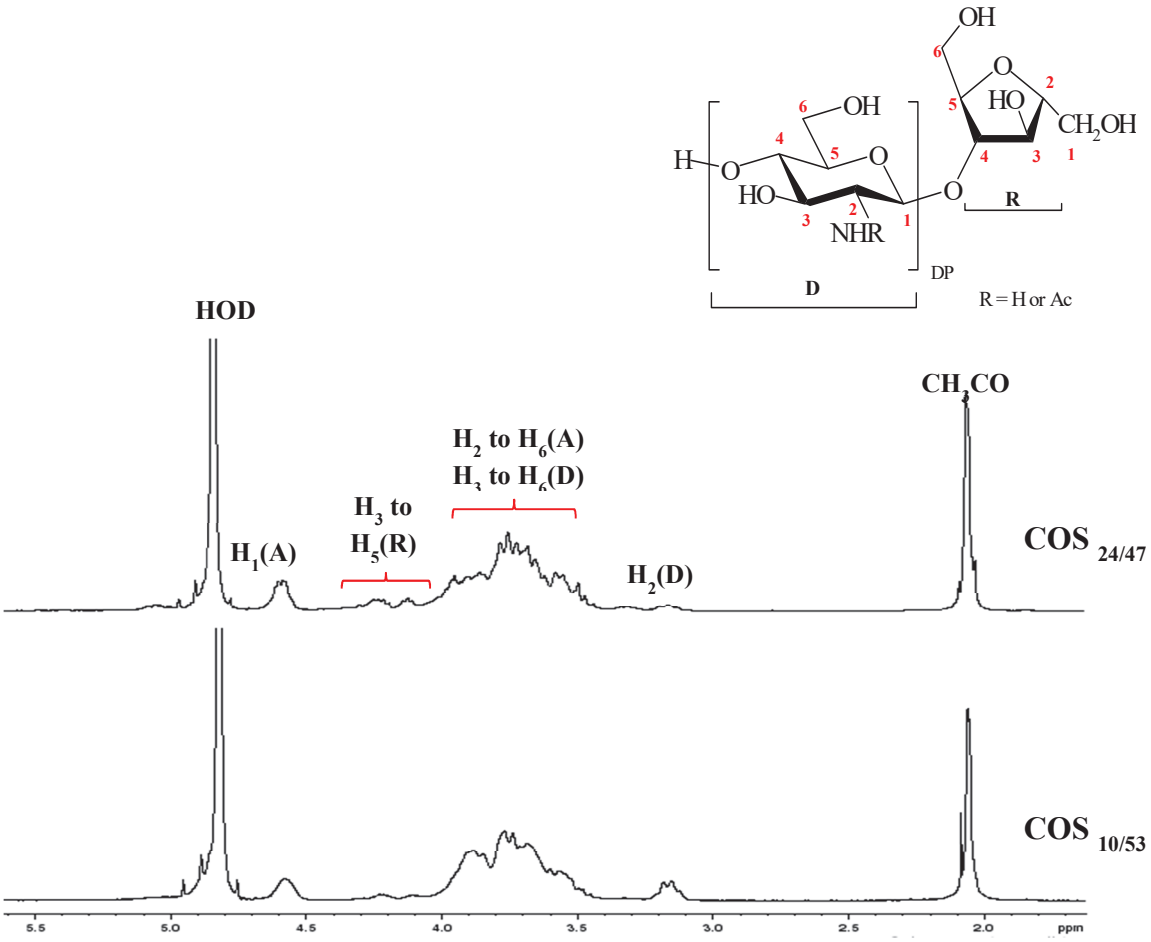

SMFigure 2 - ^{1}H NMR spectrum (500 MHz, 298 K) of $COS_{10/53}$ and $COS_{24/47}$ in D_2O and 5µl of HCl (D) for proton atoms of the GlcN unit, (A) for proton atoms of the GlcNAc unit and (R) for the proton atoms of the reduced amf unit.

The average DP for the acetylated oligomers, was calculated according to the number-average molar mass ($\overline{Mn}$) of the partially *N*-acetylated reduced chitooligosaccharides, the molar mass of the reduced amf unit ($M_{(reduced\ amf)}$ = 164 g/mol) and the molar mass of the GlcN repeating unit (M_0). However in this case M_0 depends on the DA, hence in Equation 2, M_0 includes the molar mass of the GlcN/GlcNAc unit ($M_{(GlcN)}$ = 161 and $M_{(GlcNAc)}$ = 203 g/mol). The results are demonstrated in Table 2.

$$\overline{DP} = \frac{\overline{Mn} - M_{(reduced\ amf)}}{M_{(GlcN)} \times \frac{(100 - DA)}{100} + M_{(GlcNAc)} \times \frac{DA}{100}} \qquad \text{Eq. 2}$$

Their characterization shows that their molar mass distribution Đ is rather narrow. The details for the calculations of $\overline{DP}$ and $\overline{DA}$ are given in Table 2.

Table 1 – Chito-oligosaccharides characteristics:

Samples $COS_{DP/DA}$	$\overline{Mw}$ [a] (kg/mol)	$\overline{Mn}$ [a] (kg/mol)	Đ [a]	$\overline{DP}$ [b]	$\overline{DA}$ [b]
$COS_{10/53}$	3.12	2.52	1.24	10±2	53
$COS_{24/47}$	6.49	4.81	1.35	24±2	47

(a) $\overline{Mw}$, $\overline{Mn}$, Đ and $\overline{DP_n}$ were determined by SEC-MALLS in ammonium acetate;
(b) The $\overline{DA}$ were determined by ^1H NMR in D_2O at 300 K.

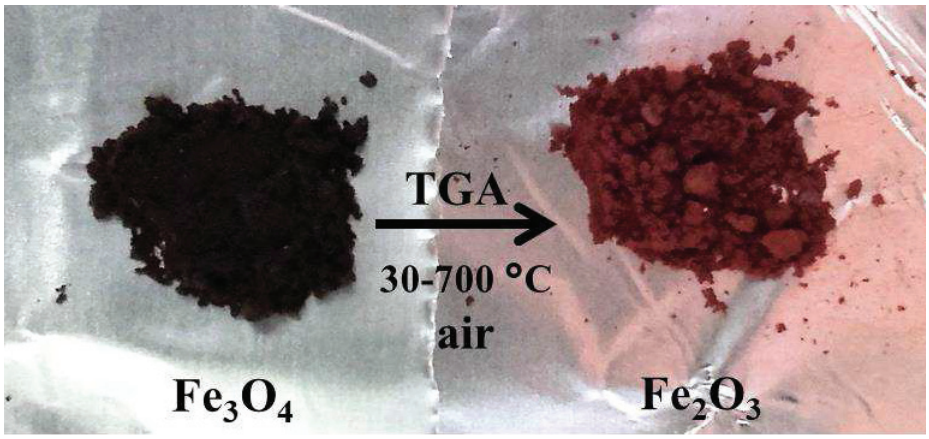

S.M. Figure 3 – Fe_3O_4 NPs (black)before pass for the TGA experiment, under air from 30 to 700 °C, and Fe_2O_3, final product (red)